Roman Geier, MSc BSc

Oxygen Effects on the Photo-Induced Radical Polymerization

DISSERTATION

zur Erlangung des akademischen Grades

Doktor der Naturwissenschaften

eingereicht an der

Technischen Universität Graz

Betreuer

Univ.-Prof. Mag.rer.nat. Dr.phil. Georg Gescheidt-Demner

Institut für Physikalische und Theoretische Chemie

Graz, November 2016

EIDESSTATTLICHE ERKLÄRUNG

Ich erkläre an Eides statt, dass ich die vorliegende Arbeit selbstständig verfasst, andere als die angegebenen Quellen/Hilfsmittel nicht benutzt, und die den benutzten Quellen wörtlich und inhaltlich entnommenen Stellen als solche kenntlich gemacht habe. Das in TUGRAZonline hochgeladene Textdokument ist mit der vorliegenden Dissertation identisch.

AFFIDAVIT

I declare that I have authored this thesis independently, that I have not used other than the declared sources/resources, and that I have explicitly indicated all material, which has been quoted either literally or by content from the sources used. The text document uploaded to TUGRAZonline is identical to the present doctoral thesis.

Datum	Unterschrift

Danksagung

Zu allererst möchte ich meinem Betreuer Prof. Georg Gescheidt-Demner, für die Möglichkeit zu der Mitarbeit an spannenden Forschungsprojekten, danken. Er war hierbei stets darauf bedacht, dass sein Team Freude an der Chemie hat und das die Arbeit auch Spaß macht. Ich möchte Ihm auch für die Zeit danken, welche er in mich investiert hat und für seine Geduld, wenn ich beim Schreiben etwas ausschweifend formulierte. Meine Arbeit am Institut war auch sehr geprägt von meinem Kollegen und Freund Dmytro, Dimi, Neshchadin. Ob wissenschaftliche oder technische Fragen, Dimi konnte diese fast immer beantworten und daneben hatten wir auch großartige Unterhaltungen über Gott und die Welt. Des Weiteren gebührt den Mitgliedern der Arbeitsgruppe Anna, Max, Edi, David, Yasmin, Maria, Miso und Christina Dank. Sie haben mir bei vielen Messungen oder wissenschaftlichen Problemen geholfen und waren ein wichtiger Bestandteil des sozialen Lebens. Die guten Seelen des Instituts, Hilde und Marion darf ich natürlich nicht vergessen. Sie nahmen mir teils lästige Verwaltungsaufgaben ab, halfen im Labor oder hatten mal ein offenes Ohr für verschiedenste Anliegen. Dank gilt auch Herrn Lang und Herrn Eisenkölbl für ihren technischen Support. Im Bereich der Lehre, welche mir große Freude bereitet hat, bedanke ich mich stellvertretend für die gute Zusammenarbeit bei Karl Gatterer, Anne-Marie Kelterer und Brigitte Bitschnau.

Für die projektübergreifende Arbeit möchte ich mich besonders bei Prof. Harald Stüger und Michael Haas bedanken. Das Germanium Projekt hat meine Dissertation enorm bereichert und es war spannend wieder direkt mit einem Studienkollegen zusammen zu arbeiten.

Seitens der Analytik danke ich Torsten Mayr, Josef Ehgartner und Marion Stampfer-Maric für die Unterstützung bei den Sauerstoffmessungen.

Private und dienstliche Angelegenheiten verschmolzen zum Teil. Während meiner Zeit auf der Uni habe ich viele Freunde gefunden, die mich teilweise das ganze Studium durch begleitet haben. Josef ist dafür mein bestes Beispiel. Ich danke ihm und meinen engen Freunden Florian, Clemens, Pez, und all jenen die mir nahe stehen für wundervolle gemeinsame Erfahrungen.

Meinen Eltern gilt ganz besonderer Dank. Sie haben mich das gesamte Studium hindurch unterstützt haben. Ohne sie wäre das nie möglich gewesen. Meine Familie war mir immer eine große Stütze und ich bin froh dass ich sie habe. Meine Schwester, mein Schwager, meine Oma und meine zahlreichen lebhaften Verwandten nehmen einen besonderen Platz in meinem Leben ein. Auch sie hatten einen großen Einfluss auf meine Arbeit.

Danke

Abstract

Photo-induced radical polymerization plays an important role in modern industrial applications. Various photoinitiators were developed to cater the different requirements. Type I initiators, on which the focus lies here, are usually more reactive than type II initiators, which is caused by a necessary bimolecular reaction of the later. Oxygen inhibition additionally leads to serious problems. Chemical and physical strategies were developed to minimize this effect. Several studies focus on the kinetic effect of oxygen inhibition but mechanistic approaches are rare.

This thesis focuses on two main parts; first, oxygen effects on initial stages of photo-induced radical polymerization and second, a new germanium based photoinitiator. The mechanistic investigation of oxygen effects is mainly based on CIDNP spectroscopy, supported by EPR, MS, NMR and kinetic simulations. The characterization of intermediates and follow-up products helped to develop ideas for oxygen dependent reaction mechanisms. There are significant correlations between the oxygen concentration, the photoinitiator type and decarboxylation.

I extended the mechanistic approach from the initiators to photo-induced radical polymerization processes. Oxygen dependent follow-up products of the initiators in the presence of butyl acrylate were detected. It was possible to observe double bond conversion depending on the oxygen concentration and to trap intermediate radicals. Additionally I determined addition rate constants and performed kinetic simulations of the suggested mechanisms.

The second part is related to a newly developed promising photoinitiator. Here I characterized its photoreactivity, polymerization ability and determined addition rate constants. In context of the established photoinitiators, the reactivity towards oxygen was tested and oxygen dependent products were characterized. This new germanium based initiator showed promising results, as it could theoretically form up to eight radicals.

Zusammenfassung

Lichtinduzierte radikalische Polymerisation spielt eine bedeutende Rolle in modernen industriellen Anwendungen. Unterschiedliche Photoinitiatoren wurden entwickelt um den mannigfaltigen Bedingungen gerecht zu werden. Typ I Initiatoren, auf welche ich mich hier konzentriere, sind im allgemeinen reaktiver als Typ II Initiatoren, was mit notwendigen bimolekularen Reaktionen zur Aktivierung des Initiators zusammen hängt. Ein wichtiger Aspekt bei Photopolymerisationen ist die Inhibierung durch Sauerstoff. Um diesem Problem entgegen zu wirken wurden physikalische und chemische Strategien entwickelt. Der kinetische Effekt der Sauerstoffinhibierung ist gut untersucht, jedoch sind mechanistische Studien rar.

Die vorliegende Arbeit gliedert sich in zwei Hauptteile. Den ersten Fokus lege ich auf Sauerstoffeffekte im Initiierungsschritt und der zweite Teil befasst sich mit einem neuen vielversprechenden germaniumbasierten Photoinitiator.

Die mechanistische Untersuchung der Sauerstoffinhibierung basierte vorwiegend auf CIDNP Spektroskopie, welche mit EPR, MS, NMR und kinetischen Simulationen ergänzt werden. Ich charakterisiere Zwischen- und Folgeprodukte und entwickle Vorschläge für sauerstoffabhängige Reaktionsmechanismen. Die Ergebnisse zeigen aussagenkräftige Korrelationen zwischen der Sauerstoffkonzentration, dem Initiatortyp und Decarboxylierungsreaktionen.

Ich habe den mechanistischen Ansatz von den Photoinitiierungsprozessen auf Photopolymerisationsprozesse ausgeweitet und untersuche die sauerstoffabhängige Bildung von Folgeprodukten in Anwesenheit von Butylacrylat. Es ist möglich die sauerstoffabhängige Umsetzung von Doppelbindungen zu beobachten. Intermediate konnten erfolgreich gefangen und charakterisiert werden. Zusätzlich war es erfolgreich Additions-Geschwindigkeitskonstanten zu bestimmen, welche die vorgeschlagenen Mechanismen mit kinetischen Simulationen bekräftigen.

Der zweite Schwerpunkt befasst sich mit der Charakterisierung eines neuen vielversprechenden germaniumbasierten Initiators. Ich habe die Photoreaktivität und die Fähigkeit zur Photopolymerisation geprüft. In diesem Zusammenhang wurden Geschwindigkeitskonstanten bestimmt und Polymertestkörper hergestellt. Die Effekte, Rund um die Sauerstoffinhibierung spielen auch hier eine wichtige Rolle und wurden eingehend untersucht. Dieser neue auf Germanium basierende Initiator zeigt, unteranderem durch die Möglichkeit der Bildung von bis zu acht Radikalen, vielversprechende Ergebnisse.

Content

1 General Introduction

Photochemistry covers a wide important field, from natural processes to industrial applications. There are numerous examples of photo-induced reactions that are important in nature. One of the most important is photosynthesis, which is a chlorophyll based energy conversion process. Not of minor importance is Vitamin D, which is essential for humans and is only produced when UVB light is present. Deep-water fishes, that use bioluminescence for hunting, are another example. In technical aspects photo chemistry is applied in several fields, from water treatment, organic synthesis to polymerization and many more.[1–3]

Photopolymerization was early applied to obtain polymer chains and since then this technique was steadily improved. Photopolymerization is nowadays the method of choice for all kinds of coatings. Photolithography is used for 3-D printing and in semiconductor industry. Even for medical purposes like in dentistry photochemistry is applied.[4–6]

Because of its advantages, the importance of photopolymerization is increasing. One advantage is the possible use of solvent-free formulations for coatings. This cuts production costs and is environmentally beneficial. Compared to thermally-initiated systems less energy is required and new LED technologies increase this benefit even more. Other advantages are a high spatial resolution and high curing speed.[7]

One of the main drawbacks of photo-induced radical polymerization is caused by oxygen inhibition. Oxygen can react with radicals and forms less active peroxides. Further oxygen quenches the excited state of the photoinitiator and singlet oxygen, which is highly reactive (i.e. it causes oxidative stress and can lead to cancer), might be formed.

This thesis consists of 6 chapters and starts with a general introduction. Chapter 2 provides information about the theoretical background and chapter 3 contains a description of all applied experimental techniques, methods and sample preparation and it is presenting experimental details. The present work focuses on two aspects; first the impact of oxygen on photoinitiators and on photopolymerization and second the characterization and evaluation of a new promising photoinitiator.

Chapter 4 presents the results of my studies on 2-hydroxy-2-methyl-1-phenylpropan-1-one, which is an industrially applied photoinitiator. The oxygen dependent reactivity and products of the photoinitiator and photoinitiating processes were studied. I developed oxygen dependent reaction mechanisms and simulated the obtained experimental data with a kinetic modelling program. The backbone of these results, are NMR and especially CIDNP based experiments.

Chapter 5 focuses on phenyl-bis-(2,4,6-trimethylbenzoyl) phosphine oxide, which is also an industrially applied photoinitiator. Additionally to mechanistic studies and product characterization like in chapter 4, I obtained oxygen dependent kinetic data. It was possible to differentiate between bulk effects, thermal diffusion and oxygen inhibition with live view thermal imaging. The part concerning thermal imaging was recently published.[8] The phosphorous containing initiator enabled us to apply ^{31}P-NMR and ^{31}P-CIDNP experiments.

Chapter 6 Here I characterized the photoinitiator abilities of tetramesitoylgermane. This promising photoinitiator has been synthesized in the Group of Prof. H. Stüger (TU Graz). The interesting mechanism of the novel photoinitiator shows radical formation and radical addition to monomers. The curing properties for various monomer formulations were tested and I studied the oxygen effects on this photoinitiator and compared the outcomes with the other investigated initiators. Parts of these results will be published soon.

2 Theoretical Background

2.1 Photoinitiators and Photo-Induced Radical Polymerization

For successful photo-induced radical polymerization efficient photoinitiators are required and developing new initiating systems and improving existing initiators are ongoing processes. Efficient photoinitiators must fulfill several criteria. They need to absorb at a desired wavelength with a high quantum yield and the active species formed upon photolysis (i.e. radicals) should show high reactivity towards monomers.[6,9]

In general, one differentiates between two types of photoinitiators. Norrish type I initiators undergo α or β homolytic cleavage and form directly two radicals. This unimolecular reaction is often considered to be faster than the bimolecular Norrish type II initiation process. Light at a reasonable wavelength for the α or β cleavage is required. The initiating radicals are mainly formed in the excited triplet state (T_1). The triplet state is reached via excitation of the initiator to the excited singlet state (S_1) followed by intersystem crossing (ISC). A sensitizer can be added in case the initiator does not absorb at a desired wavelength. In this case the sensitizer is excited to a triplet state and a radiationless energy transfer from the sensitizer to the initiator occurs.[6]

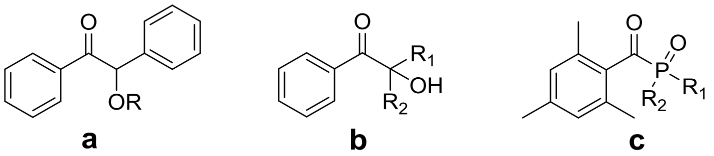

Scheme 1. Examples for typical Type I photoinitiators. a) benzoin derivatives, b) hydroxyalkylphenones and c) arylphosphine oxides.[10]

Depending on the substituent of the α carbon either α or β cleavage is preferred. When i.e. halogens are situated next, the bond cleaves at the β position.[11,12]

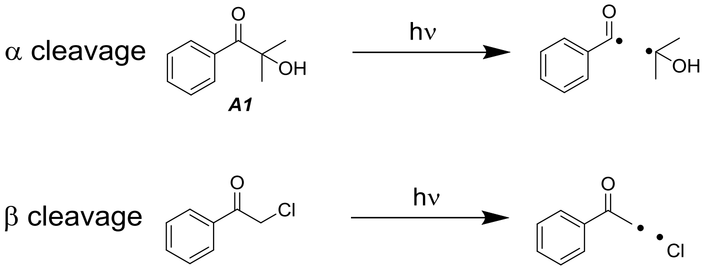

Scheme 2. Examples for an α and a β cleavage. α cleavage of an α-hydroxy ketone (2-hydroxy-2-methyl-1-phenylpropan-1-one) and β cleavage of 2-chloro-1-phenylethan-1-one.

In this present work I focused on initiators, which undergo α cleavage. The results for the α-hydroxy ketone, 2-hydroxy-2-methyl-1-phenylpropan-1-one ***A1***, which is displayed in **Scheme 2** and the bisacylphosphine oxide, phenyl-bis-(2,4,6-trimethylbenzoyl) phosphine oxide, which is a derivative of compound ***c*** in **Scheme 1**, are described here.

Type II initiators, as already mentioned undergo a bimolecular reaction. They require a hydrogen-atom source for activation. They can either directly abstract a hydrogen-atom or, more commonly involve a proton coupled electron transfer (PCET). Direct hydrogen-atom abstraction is observed i.e. for alcohols and ethers. Electron transfer reactions are common for secondary and tertiary amines.[13]

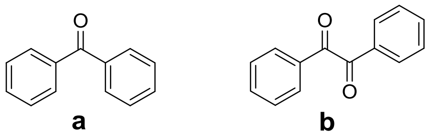

Scheme 3. Common Type II photoinitiators. a) benzophenone and b) dibenzoyl or benzil.[10]

Type II initiators can undergo two different initiation processes as displayed below. Both result in the formation of two uncharged radicals. The formed diphenylmethyl-ol radical tends to dimerize and generally the polymerization is initiated by the amine (co-initiator). A disadvantage of type II initiators is their reduced curing speed through the bimolecular process. At advanced polymerization state the diffusion is hindered and bimolecular reactions become less probable. Type II initiators require longer excited state lifetimes. This becomes problematic when oxygen is involved in competitive reactions.[13–17]

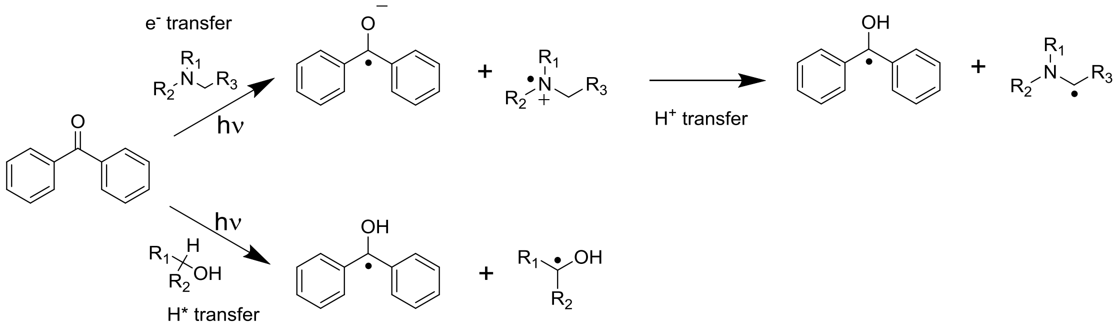

Scheme 4. Initiation process of benzophenone. With an amine first an electron transfer occurs, which is followed by a proton transfer. With alcohols direct hydrogen-atom abstraction takes place.

As mentioned before, these initiators are used for photo-induced radical polymerization in various industrial applications such as, coatings, electronics, 3-D printing, dentistry and many more. The photo-induced radical polymerization consists of 3 main steps; the excitation and cleavage of the initiator, the first radical addition to the monomer and the chain propagation. Moreover radical disproportionation and termination reactions occur.[18,19]

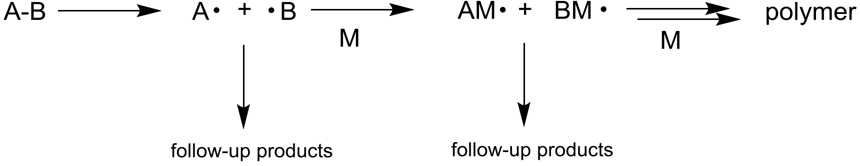

Scheme 5. General reaction scheme for photo-induced radical polymerization.

2.2 Oxygen Inhibition in Photo-Induced Radical Polymerization

Photo-induced radical polymerization with all its advantages and its wide field of applications has one serious drawback; inhibition by molecular oxygen. The inhibition causes incomplete curing, with tacky surfaces and in some cases the whole curing process fails.[15,20,21]

For easier handling and to reduce cost, industrial photopolymerization is often performed under atmospheric conditions. To reduce the impact of oxygen, alternative polymerization methods were developed. Thiolene systems and cationic polymerization of epoxides are less sensitive towards oxygen, but their application range is limited due the availability of various monomers. Often heterocyclic monomers i.e. oxirane and thietane are used. The release of the ring strain drives the reaction. Cationic epoxide polymerization has advantages in negative resist photopolymerization.[22–26] As radical photopolymerization cannot always be replaced by alternative methods, oxygen inhibition needs to be understood.

Oxygen inhibition is a complex process. **Scheme 6** represents general reaction pathways for photopolymerization, oxygen inhibition, oxygen scavenging and reinitiation processes.[27–29]

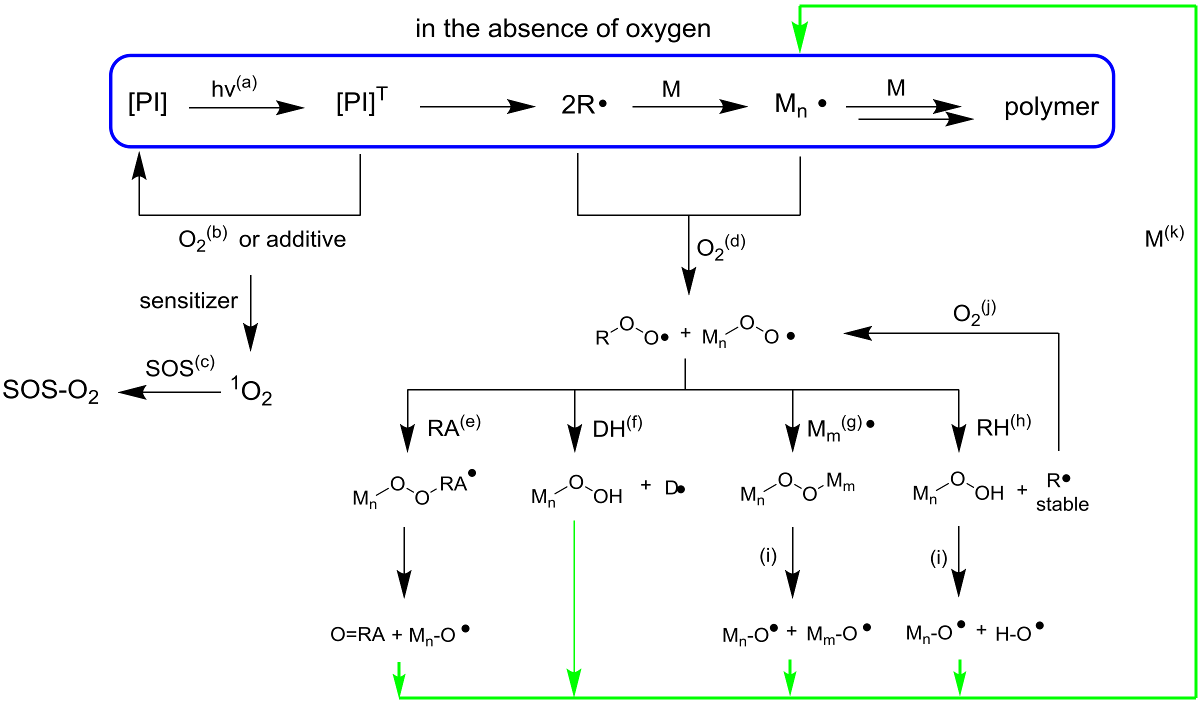

Scheme 6. Overview of radical photopolymerization in the absence and presence of oxygen. a) excitation of the initiator to the triplet state, b) oxygen dependent triplet quenching leads to singlet oxygen, c) reaction of singlet oxygen with a singlet oxygen scavenger. Reactive radicals R• initiate polymerization (M_n) via addition to monomer M and chain propagation leads to polymer. d) oxygen adds to radicals and forms less reactive peroxyl radicals. Reinitiation is possible by adding e) reducing agents RA and f) hydrogen-atom donors DH. i) peroxide decomposition of peroxides formed via termination reactions, i.e. with M_m• or hydrogen-atom abstraction from RH. k) newly via reinitiation processes formed radicals can proceed the polymerization.[29,30]

When oxygen is present two different inhibition processes occur. The oxygen ground state is a triplet, therefore it can effectively quench the excited triplet state of the photoinitiator and singlet oxygen is formed. Singlet oxygen is very reactive and can form further reactive oxygen species, which can lead to unwanted side products and incomplete curing. To avoid these effects, singlet oxygen scavengers can be added. The triplet quenching does not result in consumption of the initiator, which can be excited again. The second oxygen inhibiting process is the reaction of oxygen with initiator radicals. In this work I focus on this second case and its follow-up processes. Here, the initiator is consumed and peroxyl radicals are formed. Termination reactions can occur, and depending on the reaction conditions the predominantly formed peroxides can decompose. The addition of oxygen to carbon centered radicals is two to four orders of magnitudes faster than the radical addition to the monomer. Oxygen addition rates are reported to be significantly higher than 5 x10^8 M^{-1} s^{-1} and therefore are often within the diffusion controlled range.[31–37]

The formed peroxyl radicals are less reactive and do not react with the double bonds of acrylates. Therefore chain polymerization is inhibited. Oxygen is also able to react with monomer radicals and inhibit the reaction at this step.[31,32]

Crucial for oxygen inhibition is the concentration of dissolved oxygen (for acrylates it is in the order of 10^{-3} M) and the oxygen permeability of the resin. Depending on the resin type, the layer thickness of the coating and the concentration of the initiator inhomogeneous curing occurs.[38] Pigmented coatings and highly absorbing initiators lead to different radical concentrations within the layer. An additional effect for cross-linking systems is observed.[39] Cross-linking affects the propagation- and termination rate, which are both diffusion controlled processes. At low conversion the process is auto accelerated because of heat development. At higher conversion the more mobile monomer becomes sterically hindered and auto deceleration is observed.[40–42] When oxygen is present cross-linking becomes more complicated. Russell described mechanisms of termination and reinitiation processes for cross-linking systems.[43]

Decker and Jenkins calculated steady state oxygen concentrations in model resin systems. For their calculations they took the light intensity, the termination rate and the oxygen addition rate into account. They used formulations containing 2-5 wt. % of photoinitiator (2,2-dimethoxy-2-phenylacetophenone Irgacure 651) and acrylates. The outcome for typical acrylate termination rates is that polymerization only occurs for oxygen concentrations in the range of 10^{-6} M.[32] Bowman and Goodner obtain similar results and they developed prediction methods for double bond conversion in photopolymerization reactions and worked on oxygen diffusion.[44–46]

There are several strategies to avoid oxygen inhibition.[29,44,47,30,48] Physical barriers can be used to retain oxygen from the resins. Chemical strategies include compounds, which consume oxygen, scavenge singlet oxygen, reinitiate the reaction or are inert against oxygen. New technologies, like electron beam curing, are possible ways to eliminate oxygen inhibition. An excellent overview for the different strategies is provided by Ligon, Husár and Liska.[29]

There are several publications on the kinetic effects of oxygen on photopolymerization. Addition rate constants for various radicals towards oxygen were mainly determined by laser flash photolysis (LFP) or time resolved EPR.[32,34,49–56]

Kinetic oxygen inhibition effects have been widely studied but mechanistic effects at the molecular level are not well described. The formation of peroxyl radicals and the termination to peroxides are known, but further follow-up products, to my knowledge, have not been investigated so far.[34,57–60] In this thesis I want to determine mechanisms of oxygen dependent follow-up products. CIDNP- and NMR- results reveal intermediates and products. For the mechanistic determination the CIDNP effect is a powerful tool and therefore it is described in detail in the next section.

Oxygen inhibition is usually seen as an undesired effect, which needs to be eliminated. However there are applications developed, where the inhibitive effect is used. Grachev et al. describe molecular oxygen as a regulator in 3-D polymerization.[61] Another example is the catalyzed selective oxidation of hydrocarbons in photochemical reactions, which was recently reported by Sato et al.[62]

Our aim is to develop mechanisms for better understanding of oxygen inhibition and to gain knowledge to selectively use the inhibition effects.

2.3 Chemically Induced Dynamic Nuclear Polarization CIDNP

Paramagnetic compounds such as free-radicals cannot be observed directly by NMR but with the Chemically Induced Dynamic Nuclear Polarization effect a powerful magnetic resonance technique exists, which enables us to detect radical derived products and to obtain mechanistic information.[63,64]

To observe the effect fast radical reactions of radical pairs are required, which can either be started thermally or photo chemically. In radical pair reactions, unpaired electrons interact with nuclear spins and lead to polarization in the resulting NMR spectra. Polarization means that the overall spin distribution does no longer meet the requirement of the Boltzmann equilibrium. It derives from a non-Boltzmann distribution of the α or β spin populations. The preference of populating α or β spins is depending on the precursor and radical pair mechanism explains this effect. Because of the polarization no conventional NMR spectrum in respect to intensities of Zeeman transitions is observed. Instead strongly enhanced emission or absorption signals are obtained. In respect to chemical shifts the recorded spectra stay the same. Therefore signal assignment i.e. ^{1}H-CINDP experiments is identical as in ^{1}H-NMR experiments.

In CIDNP experiments we observe two different effects; the net effect and the multiplet effect. The net effect occurs, when all resonances of a multiplet have the same polarization (either enhanced emission or enhanced absorption). The multiplet effect is observed when different polarizations in the same multiplet occur.[65,66] Kaptein's rules allow predictions of polarizations and are a useful tool for qualitative interpretation of CIDNP spectra.[67]

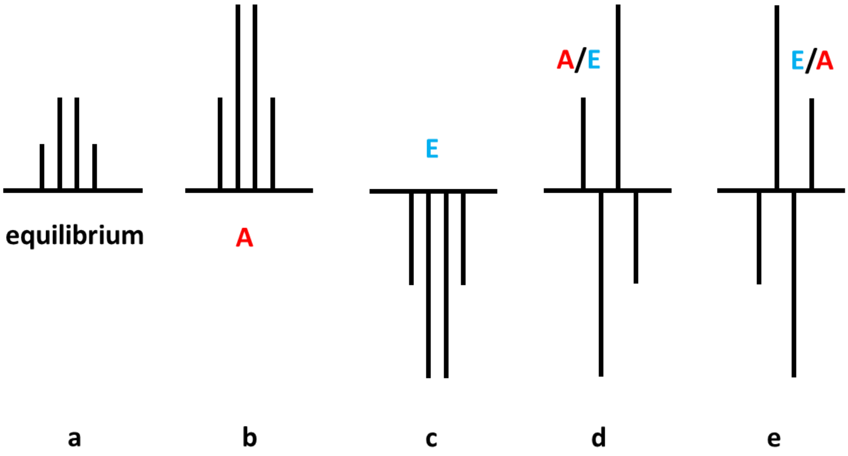

Figure 1. Possible CIDNP effects on a quadruplet. a) thermal equilibrium as observed in standard NMR experiments. b) net effect in Absorption. c) net effect in Emission. d) multiplet effect Absorption/Emission. e) multiplet effect in Emission/Absorption.

The explanation of these unusual NMR phenomena is provided by the Radical Pair Mechanism RPM. This theory covers most CIDNP observations, is well understood and described.[65,68–72] Additionally several books are available.[73–75]

The RPM is based on the idea of nuclear spin dependent recombination probabilities within a magnetic field H_0. When the precursor molecule R_1-R_2 is cleaved, electron spin correlated radicals R_1• and R_2• are formed. These electron spin correlated radicals are called radical pair. Radical pairs can be either formed thermally or photo chemically. Depending on the route of radical formation, radical pairs in the excited singlet or triplet are obtained (see **Scheme 7**).

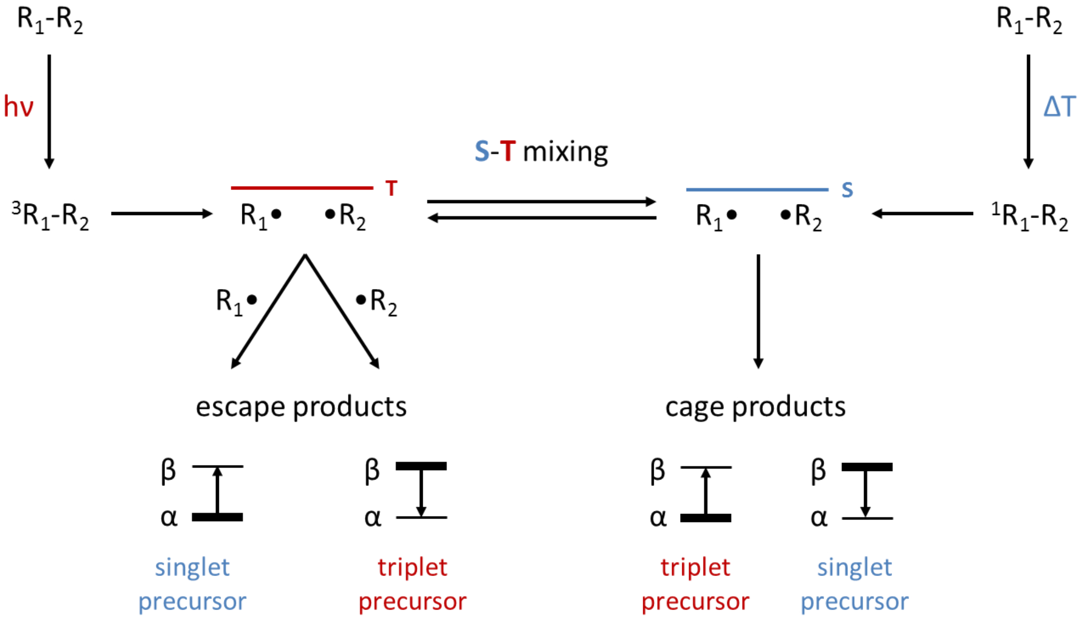

Scheme 7. Overview of required reactions to observe the CIDNP effect. Radical pairs are represented by radicals with an overbar. Overpopulation of spin states is represented by thick bars.

The radical pairs might undergo singlet-triplet mixing (S-T mixing). The last step consists of different subsequent reactions of singlet and triplet pairs, which form products observable by NMR. We differentiate between cage and escape products. Cage products are recombination products of the initial pair. Escape products are formed when the radicals escape the cage.

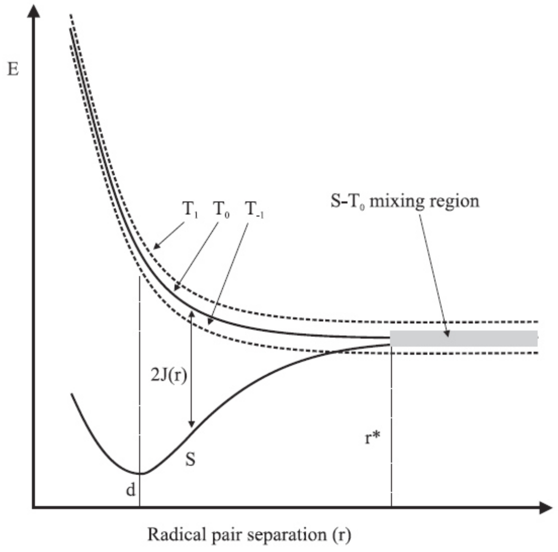

Figure 2. Energy levels in an external magnetic field as a function of radical pair distances.[77]

According to the Pauli principle recombinations are only allowed in the singlet state, therefore singlet-triplet mixing is required.

The rate of singlet-triplet mixing is dependent on the magnetic field H_0, the radical's *g* factor difference and the magnitude of the hyperfine coupling constant.

When a radical pair is formed in singlet state, it faces attractive forces for distances r < r* with an energy minimum at distance d. If the potential depth at d is larger than *k*T, then the radical spin states are trapped until the radicals reacted. Radicals in the triplet state face repulsive forces for distances r < r*. (**Figure 2**)

The singlet-triplet interconversion becomes possible for distances r > r* as the exchange interaction J(r) is small enough. As the distance increases, electron spins start to precess independently with different frequencies.[76] This process is illustrated by the vector representation in **Figure 3**.

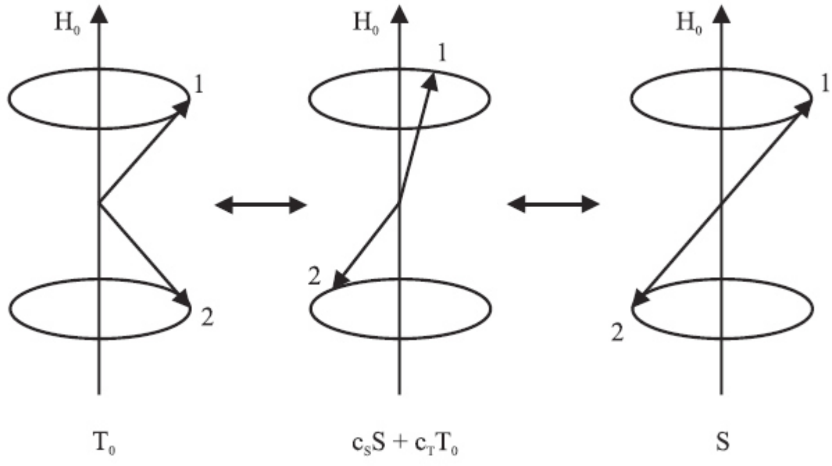

Figure 3. Vector representation for S-T_0 mixing of a triplet state derived radical pair shown for the electron spins 1 and 2 ($c_S + c_T = 1$). With kind permission from Neshchadin.[77]

The singlet-triplet mixing rate can be determined by the Lamor frequencies Δω difference of the two electron spins if two different radical species are formed. Faster singlet-triplet mixing happens with higher Δω values.

$$\Delta\omega = \omega_1 - \omega_2 = \frac{1}{2}\left[H_0 \Delta g \beta_e h^{-1} + \sum_{i=1}^{n} a_{1i} m_{1i} - \sum_{j=1}^{k} a_{2j} m_{2j}\right] \quad (1)^{a}$$

Equation 1 enables us to determine a value for singlet-triplet interconversion. The first term of the equation is derived from the spin-orbit interaction as the g factor is related to spin-orbit induced magnetic fields. The second and third term describe the electron-nuclear coupling.

---

[a] ω_1 and ω_2 are the Lamor frequencies of the unpaired electron spin of R_1• and R_2•. H_0 is the magnetic field strength, Δg is the *g* factor difference of the radicals, βe is the Bohr magneton, a_{1i} and a_{2j} are the hyperfine coupling constants and m_{1i} und m_{2j} are the magnetic quantum numbers.

Further contributions to the local field, which affects the radicals, derive from electron-spin interactions.

Based on **Equation 1** we can describe spin-selective reaction pathways displayed in **Scheme 7**. For simplification it can be assumed that the radical pair is formed in T_0 state, with only one radical carrying the magnetically active nucleus $|m_{1i}| = \frac{1}{2}$. Further we assume that Δ**g** and a_{1i} are both bigger than 0. These simplifications lead to two different Δω values, as two possible spin orientations, $m_{1i} = +\frac{1}{2}$ and $m_{1i} = -\frac{1}{2}$ exist.

$$\alpha, \qquad m_{1i} = +\frac{1}{2}, \qquad \Delta\omega_{+} = \frac{1}{2}\left[H_0 \Delta g \beta_e h^{-1} + \frac{1}{2} a_{1i}\right] \quad (2)$$

$$\beta, \qquad m_{1i} = -\frac{1}{2}, \qquad \Delta\omega_{-} = \frac{1}{2}\left[H_0 \Delta g \beta_e h^{-1} - \frac{1}{2} a_{1i}\right] \quad (3)$$

These equations simply relate singlet-triplet mixing to the nuclear spin orientation. The assumption that all contributions beside the spin orientation are constant causes higher Δω values for α spins.

A radical pair, which is formed in triplet state and possess an α spin is more likely to undergo triplet-singlet interconversion. Therefore we obtain an overpopulation of α spins in the singlet state and detect enhanced signals for the cage products. Radicals with β spin will stay longer in triplet state and therefore it is more likely that they diffuse apart and form diamagnetic escape products with an excess of β spins.

If the radicals are formed in the singlet state then radicals with α spin will obtain the triplet state faster and escape products will be overpopulated with α spins. Radicals with β spins will be more likely to stay in singlet state and therefore lead to cage products with excess β spins.

The mixing rate also influences the recombination probability to cage products. For photochemical applications fast mixing would lead to faster recombination.

To detect NMR signals, differences in spin population are required and CIDNP leads to overpopulation of spin states, which enhances the recorded signal intensities. The overpopulated state or polarization is obtained between 10^{-10} to 10^{-7} s and is therefore a rather fast process. Fortunately the polarization is preserved within the longitudinal relaxation time (for protons in small molecules ~ 0.5 – 10 s) and can be observed with ~0.5 – 4 µs radio frequency pulses.[78]

For this work CIDNP was the ideal method as I was able to follow photo induced reactions on a short time scale. An additional benefit was the detection of signals from small amounts of newly formed products. It was possible to obtain mechanistic information and additional kinetic data with time resolved CIDNP.

3 Experimental

To study the effects of oxygen on photoinitiation and photo-induced radical polymerization processes I used several analytical techniques. Structural determination and mechanistic aspects are the main focus of this present work. Various NMR experiments, especially CIDNP experiments led to the desired results. With NMR techniques it was possible to characterize starting materials, intermediates and final products. To confirm those results ESI-MS measurements were additionally applied. I obtained further insight into kinetics with LFP. To investigate further effects and to support the findings additional experiments included the use of oxygen sensors, time resolved EPR, UV-Vis, and kinetic simulations.

3.1 Materials and Methods

3.1.1 Materials

Acetonitrile d_3 from euriso-top® and deuterated- benzene, toluene and chloroform from Sigma-Aldrich were used. 2,2,6,6-Tetramethylpiperidin-1-yl)oxyl (TEMPO), 5,5-dimethyl-1-pyrroline-N-oxide (DMPO), *N*-*tert*-Butyl-α-phenylnitrone (PBN), triethylene glycol dimethacrylat (TEGDMA) and diurethane dimethacrylat (UDMA) were obtained from Sigma-Aldrich. Acetonitrile and toluene were from Roth. The photoinitiators 2-hydroxy-2-methyl-1-phenylpropan-1-one (Darocur™ 1173) and phenyl-bis-(2,4,6-trimethylbenzoyl) phosphine oxide (Irgacure™ 819) were from Ciba-Geigy, now part of BASF. Butyl acrylate, methyl methacrylate and styrene were obtained from Fluka. Argon 5.0 oxygen 3.5 and synthetic air 5.0 (79.5 % N_2 and 20.5 % O_2) were used from Messer. N_2 (g) was used from Airliquide via the house own gas supply system. With a MKS Instruments gas mixing device it was possible to obtain all desired defined gas mixtures.

3.1.2 Sample Preparation

I prepared stock solutions of the desired photoinitiator, the corresponding solvent and further additives such as butyl acrylate in 8 ml brown glass vials. The concentration range of the initiator and the solvent is adapted to each specific experiment. Precise compositions are mentioned in the results section.

3.1.3 NMR Experiments

^{1}H- ^{13}C- and ^{31}P NMR experiments were performed on a 200 MHz Bruker AC-200 FT-NMR spectrometer with a broadband multi nuclei probe head BBO 5 mm. 800 µl of the initiator solution were transferred into a 5 mm thin wall NMR tube. Then the tube was sealed with a septum. Bubbling for ~3 min with the desired gas mixtures adjusted the corresponding oxygen concentration. Afterwards I irradiated the samples with UV light from the Hamamatsu lamp. NMR spectra were recorded before and after irradiation. After irradiation, argon was flushed through oxygen containing samples and further NMR spectra were recorded. The additional argon flushing led to signal enhancement of samples, which previously reacted with oxygen.

3.1.4 CINDP Experiments

I recorded ^{1}H- and ^{31}P-CINDP spectra on a 200 MHz Bruker AVANCE DPX spectrometer. A custom-made 5 mm ^{1}H-CIDNP probe head and a custom-made multi nuclei CIDNP probe head were used.

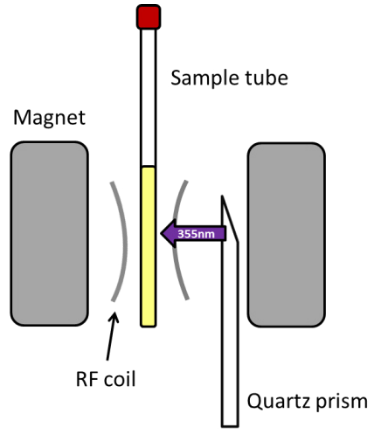

Figure 4. Schematic probehead arrangement in NMR magnet.

A Quantel Nd-YAG Brilliant Blue laser, which operates at 20 Hz and emits at 355 nm with ~80 mJ/pulse and a pulse length of ~8-10 ns, served as light source. The applied pulse sequence consisted out of presaturation followed by a laser pulse and a zg30 2 μs radio frequency detection pulse. Finally the free induction decay (FID) was recorded. Every pulse sequence was separated from the next by a delay time. Long time CIDNP experiments with multiple recorded spectra included an additional sample rotation after every 32 scans. This enhanced sample mixing and reduced probe bleaching. Experiments with additional rotation are indicated in the result section by the rotation number multiplied with the number of each cycles scans i.e. 4x32 scans with totally 128 recorded scans.

The sample preparation for CIDNP experiments was the same as for NMR experiments, but without irradiation or additional argon flushing.

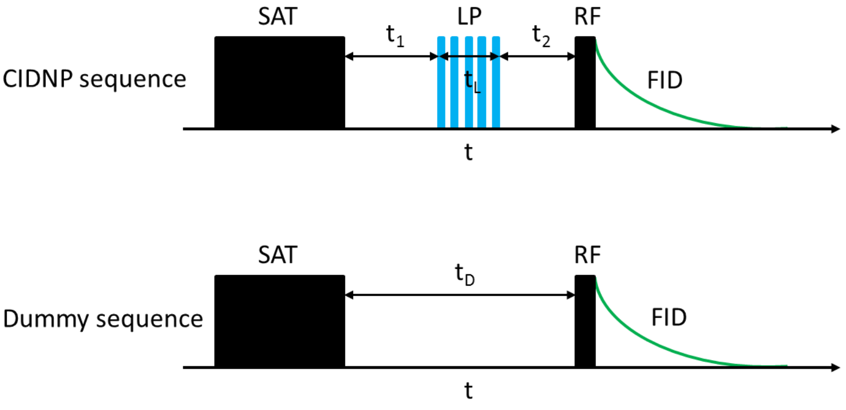

Figure 5. Typical CIDNP pulse sequences. The top trace shows the actual CIDNP pulse sequence, which starts with the presaturation SAT. This step is followed by adjustable delay time t_1 and subsequent laser pulses LP within the time t_L. An additional adjustable delay t_2 follows. For time resolved CDINP experiments spectra, with various delays t_2 are recorded. The delay is followed by a pseudo 90 degrees zg30 radio frequency detection pulse RF. Finally the free induction decay FID is acquired. The bottom traces shows the “Dummy” CIDNP pulse sequence. It is the same sequence but without laser pulses. Figure adapted from Neshchadin.[77]

3.1.5 UV-Vis Experiments

A TIDAS UV-Vis spectrometer from J&M Germany was used to record UV-Vis spectra and to determine the absorbance for LFP experiments. 1 cm x 1 cm quartz cuvettes were used.

3.1.6 LFP Experiments

For laser flash photolysis a LSK80 Laser Flash Photolysis Spectrometer from Applied Photophysics UK was used. The frequency tripled light of a pulsed Spitlight Compact 100 solid state Nd-YAG laser with an emitting wavelength of 355 nm from InnoLas Germany served as excitation source. The laser generates 8 ns pulses with an energy of 10 mJ/pulse.

I prepared stock solutions with toluene as solvent in 8 ml brown glass vials. The concertation of the photoinitiator was adjusted to an absorbance of ~0.3. For the determination of butyl acrylate addition rate constants the samples were deoxygenated by flushing with argon and a concentration range of acrylate from 0.05 M to 0.5 M was applied. To determine the oxygen addition rate constant oxygen mixtures between 1 % and 6 % were bubbled for 2 minutes through the sample. Transient absorption spectra were recorded in 1 cm x 1 cm quartz cuvettes, which can be sealed with septa. The decay was determined at the samples transient absorption maximum in a timescale of 20 µs.

3.1.7 EPR Experiments

Standard EPR experiments were recorded on a MiniScope MS 300 table EPR spectrometer from mt magnettech. The magnetic field ranged from 2000 – 4000 G with a modulation of 5 G. Samples were prepared in 1 ml with septa sealed colorless glass vials. Bubbling the samples for 3 minutes with the corresponding gas mixtures adjusted a desired oxygen concertation. The samples were irradiated with the Hamamatsu UV lamp. For EPR measurements the samples were transferred in glass capillaries and sealed.

3.1.8 TR-EPR

Time-resolved electron paramagnetic resonance (TR-EPR) spectra, using chemically induced dynamic polarization (CIDEP), were recorded with a Bruker ESP 300E X-band spectrometer with unmodulated static magnetic field and a LeCroy 9400 dual 125 MHz digital oscilloscope. For TR-EPR the desired magnetic field range is scanned and 100 accumulated EPR time responses are recorded.[79] An InnoLas SpitLight 400 Nd:YAG laser serves as a pulsed light source at 355 nm with ~ 10 ns pulses with a power of ~10 mJ/pulse. The oscilloscope is synchronized with the laser trigger and the whole setup is controlled by the tsc2 program developed by Dr. J. T. Toerring from Berlin Germany.

3.1.9 ESI-MS Experiments

A high resolution Q-Exactive Hybrid Quadrupole-Orbitrap mass spectrometer from Thermo Fischer was used for mass determination. Electrospray ionization (ESI) in negative mode, positive mode and positive mode with activation for the ionization was applied. In negative mode small amounts of formic acid were added.

3.1.10 Oxygen Measurement

The oxygen concentration in organic solvents was determined by using an oxygen sensor setup consisting out of a Firesting-Mini device and an oxygen trace sensor from PyroScience with a dihydroxy-aza-BODIPY dye as sensor material. The concentration measurements were performed in septum sealed NMR tubes with 10 mM initiator and the corresponding solvent. The oxygen concentration was adjusted with bubbling defined gas mixtures through the sample.

3.1.11 Thermal Imaging

Thermal imaging was done with a VarioCAm high resolution infrared camera by InfraTec Germany. Thermograms were recorded at a frequency of 10 Hz. For setup control and data evaluation IRBIS remote 3.0 software was used. 0.1 wt. % of the initiator was directly dissolved in butyl acrylate. 2 ml were filled in 5 mm thin wall NMR tubes and the oxygen concentration was adjusted by bubbling gas mixtures through it. The recording of the experiment began ~5 s before the reaction was initiated. The reaction was started by 10 s irradiation with the Hamamatsu UV lamp.

3.1.12 Kinetic Simulations

Copasi® was used for kinetic simulations. This is a freeware software and is developed by the COPASI project, an international collaboration between the Biocomplexity Institute of Virginia Tech, the University of Heidelberg and the University of Manchester.

2-hydroxy-2-methyl-1-phenylpropan-1-one

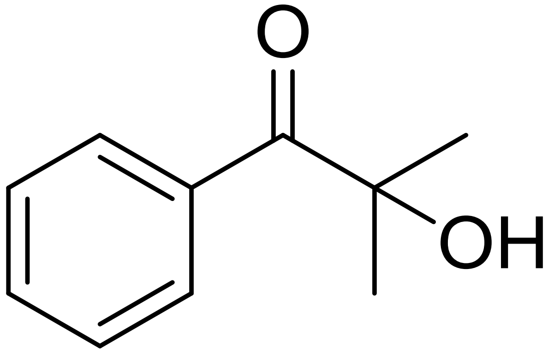

4 2-hydroxy-2-methyl-1-phenylpropan-1-one

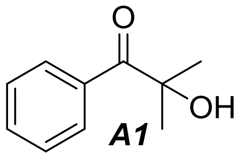

Scheme 8. 2-hydroxy-2-methyl-1-phenylpropan-1-one (A*1*) an α-hydroxy ketone.

2-hydroxy-2-methyl-1-phenylpropan-1-one (***A1***) an α-hydroxy ketone is used as a model compound in this part of the thesis. It is well studied and is commonly used as a standard type I photoinitiator. Its fragmentation upon irradiation to benzoyl- and propan-2-ol-2-yl radicals and the formation of recombination products is known. Various spectroscopic techniques provided an insight, into products formed in the dependence of oxygen and its kinetic behavior.

4.1 Results

This section presents the results of the investigation of the impact of oxygen on the α-hydroxy ketone ***A1***. Each subsection focuses on the results of the dedicated experiment. I start with the outcomes obtained from NMR experiments and continue with additional experimental techniques to support and strengthen these results. The discussion at the end compares and reviews this part.

4.1.1 ^{1}H-NMR Experiments

The following sections compare the results of compounds found after irradiating the photoinitiator depending on three factors; 1st a monomer, 2nd water and 3rd most important oxygen.

4.1.1.1 ^{1}H- NMR Experiments at Various Oxygen Concentrations

Spectra of non-irradiated photoinitiator solutions served as references. Irradiated photoinitiator samples, containing various amounts of oxygen led to additional products, which are reflected in the NMR spectra. **Figure 6** below illustrates typical ^{1}H-NMR spectra. The spectra of the oxygen containing samples show additional product signals, compared to oxygen-free samples.

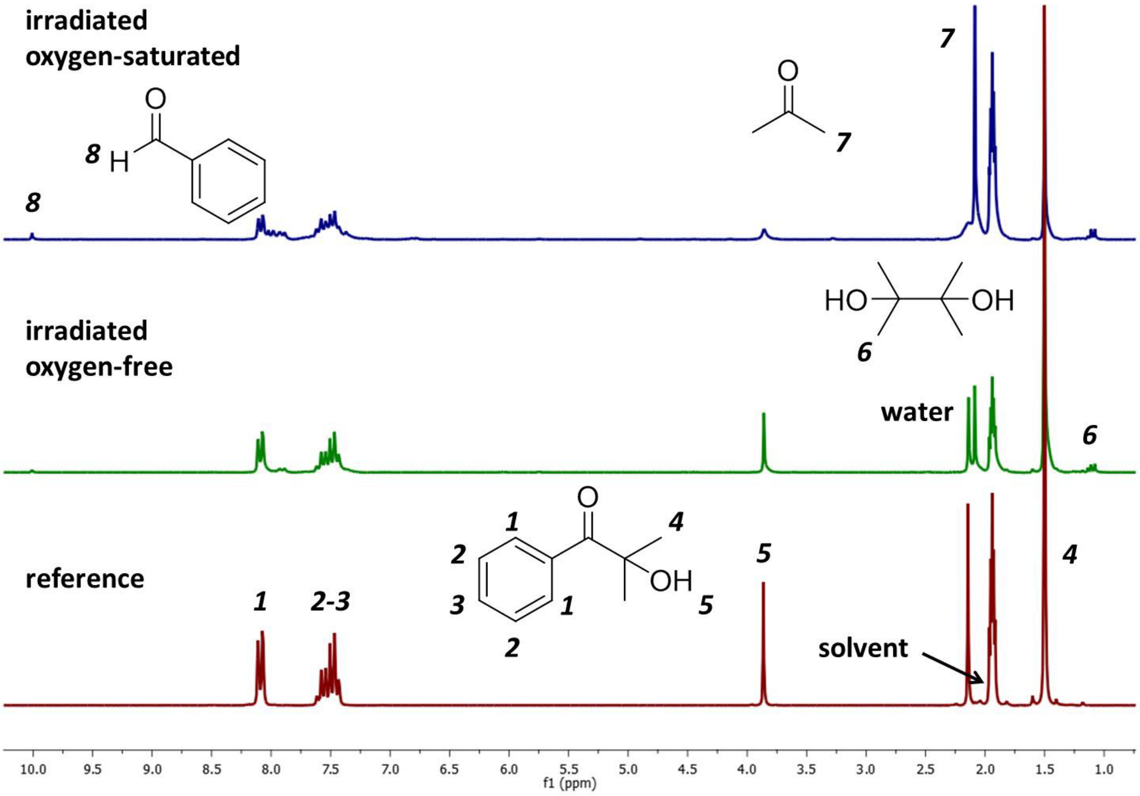

Figure 6. ^{1}H-NMR spectra of photoinitiator *A1* (10mM). The non-irradiated photoinitiator in acetonitrile is used as reference in the comparison of the oxygen-free and oxygen-saturated sample.

The irradiation with UV-light created radicals ***R1*** and ***R2***, which led to new products. ^{1}H-NMR spectra show these products but not the radicals. Radicals can be observed with ESR.

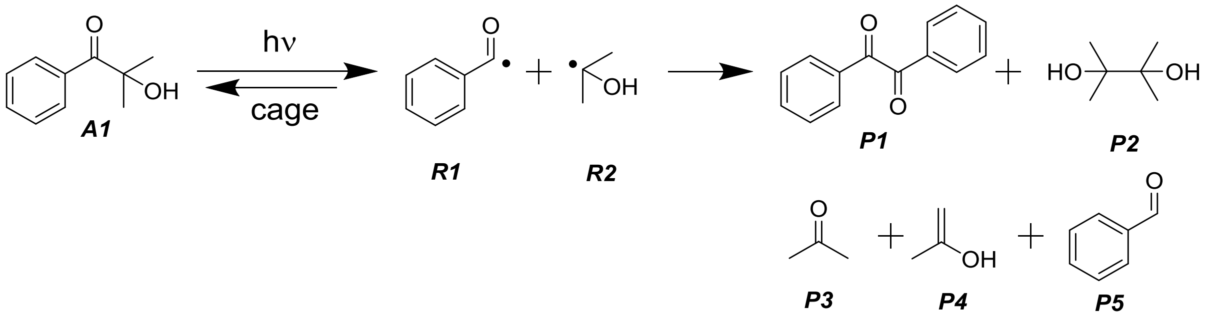

Scheme 9. Illustration of the light induced cleavage of the compound *A1*, formation of radicals and possible products of the radicals in the absence of oxygen.[80–82]

One of these new products is the expected pinacol ***P2***, which is presented in **Scheme 9** and is a recombination product of two propan-2-ol-2-yl ***R2*** radicals. Signal ***6*** at 1.1 ppm represents the protons of pinacols methyl groups. The spectra of the irradiated samples contain signals of the parent initiator ***A1***. Solely ^{1}H-NMR experiments cannot prove the formation of dibenzoyl ***P1***, as its signals overlap with the initiator within the aromatic region of the NMR spectrum.

Beside the recombination products, the experiments show evidence for new compounds such as acetone ***P3*** with its proton signals ***7*** at 2.1 ppm and benzaldehyde ***P5*** with the aldehyde proton ***8*** at 10.0 ppm. These products are well described.[80,82] A well-known hydrogen-atom abstraction reaction describes its formation. A benzoyl radical ***R1*** is able to abstract a hydrogen-atom from a propan-2-ol-2-yl radical ***R2*** to form benzaldehyde ***P5*** and the remaining acetone ***P3***.[27,83–85]

After irradiating the samples in the presence and in the absence of oxygen the compounds shown in **Scheme 10** can be observed.

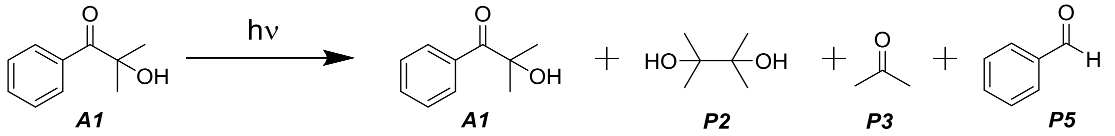

Scheme 10. Illustration of products, which are detected after irradiation of *A1*. Additionally to the initiator itself acetone, pinacol and benzaldehyde are formed.

On the first sight the oxygen-free and oxygen-saturated sample seem to behave similarly and the only eye-catching difference is the decrease of the water signal at 2.14 ppm. This is easily explained with the treatment of the samples. To obtain the desired oxygen concentration, the sample is bubbled with a mixture of nitrogen and oxygen. The oxygen is very dry and therefore reduces the amount of dissolved water in the solvent. The nitrogen on the other hand is relatively wet and the water signals do not decrease when the samples are treated with nitrogen. To prove if the effects derive from of oxygen or from water, additional experiments involved defined amounts of water. Those experiments are described in a further section.

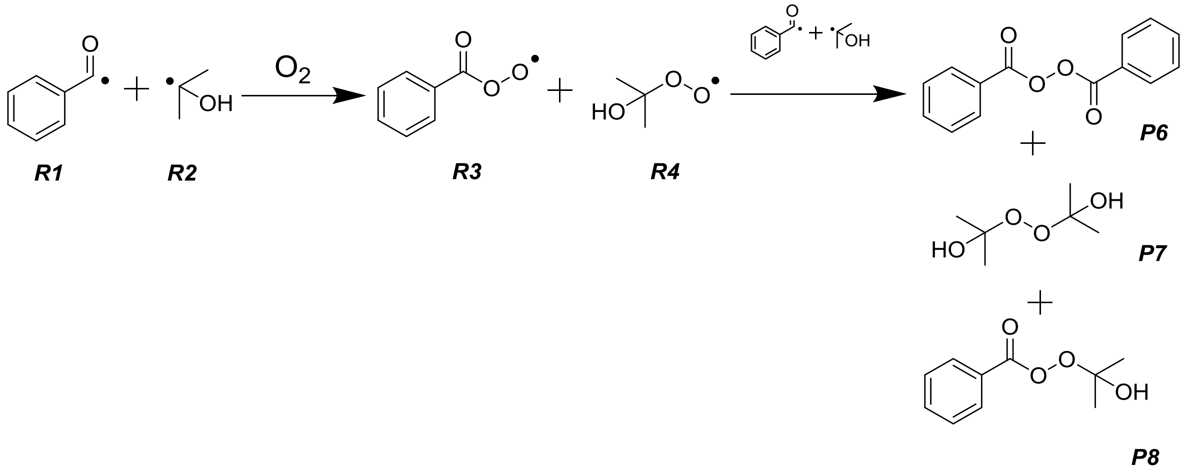

Scheme 11. Expected additional products formed of benzoyl *R1* and propan-2-ol-2-yl *R2* radicals in the presence of oxygen.

The rescaled aromatic region of the NMR spectrum reveals additional signals. **Figure 7** displays the additionally assigned peaks. Beside the typical signal of the aldehyde proton the aromatic proton signals ***9*** around 7.9 ppm confirm the formation of benzaldehyde ***P5***.

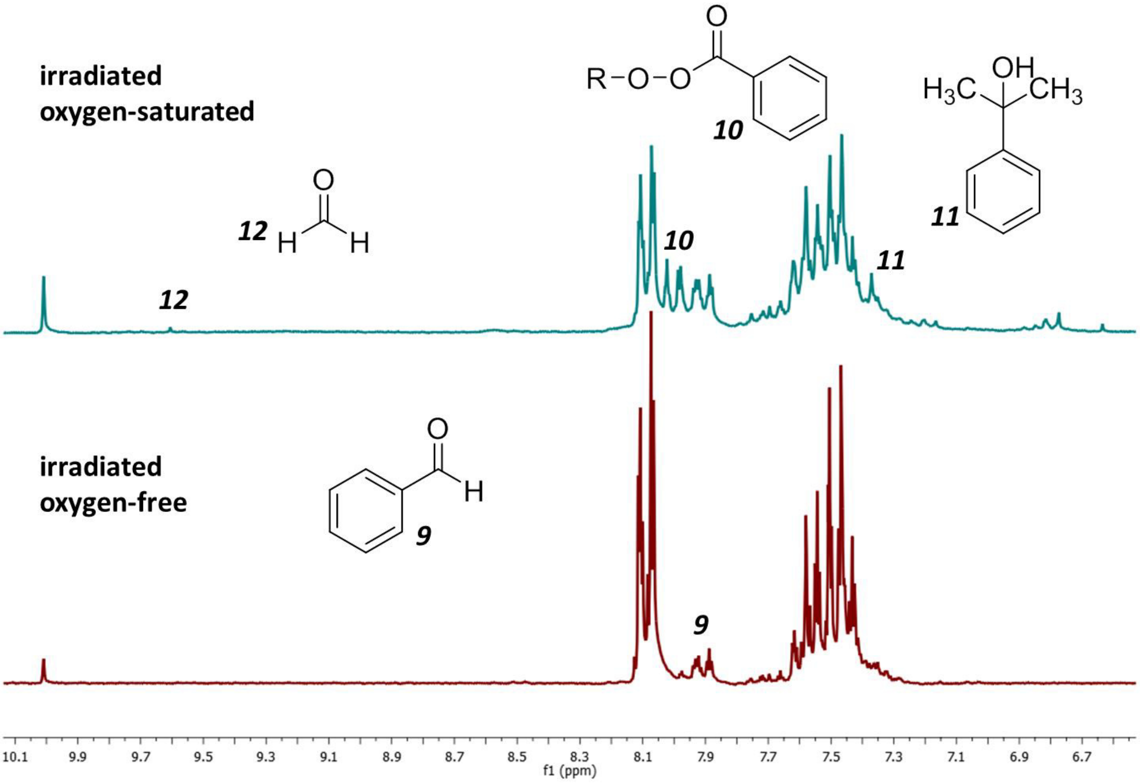

Figure 7. Detailed comparison of ^{1}H-NMR spectra. In the lower trace the irradiated, oxygen-free sample is displayed and in the upper trace, the irradiated oxygen-saturated sample. Differences are found in the aromatic region of the NMR spectrum.

Very interesting is the appearance of peak ***12*** at 9.6 ppm. Referring to literature and ^{1}H-NMR prediction tools this belongs to formaldehyde. Currently it is not clear how formaldehyde could be formed under these conditions, but reports about photochemical oxidations of olefins and intermediate carbonyls are published.[86] Signal ***10*** at 8.0 ppm probably belongs to a benzoyl peroxide. Unfortunately, according to literature and predicted values, further signals of benzoyl peroxides overlap with the signals of the initial compound ***A1***. The signal at 8.0 ppm is the only confirmed hint for the formation of benzoyl peroxide out of this experiment. Also this signal is only observable in the presence of oxygen. In the absence of oxygen peroxides cannot be formed and the corresponding spectra show no evidence for them. Additional ^{1}H-NMR experiments with dibenzoyl peroxide reveal signals in the corresponding area, that could match benzoyl based peroxides. However the aromatic signals of dibenzoyl peroxide are not necessarily identical with the also likely formed 2-hydroxypropan-2-yl-benzoperoxoate ***P8***.

Another compound worth to mention is 2-phenylpropan-2-ol ***P9***, its aromatic protons appear at 7.3 ppm and its methyl groups can be found at 1.25 ppm. The spectrum of the oxygen-free sample reveals traces of this compound, and the signal intensities enhances in the presence of oxygen. The formation of 2-phenylpropan-2-ol seems to depend on the concentration of oxygen, as the observed signal intensity is significantly higher in the oxygen-saturated sample, compared to the sample prepared under atmospheric conditions.

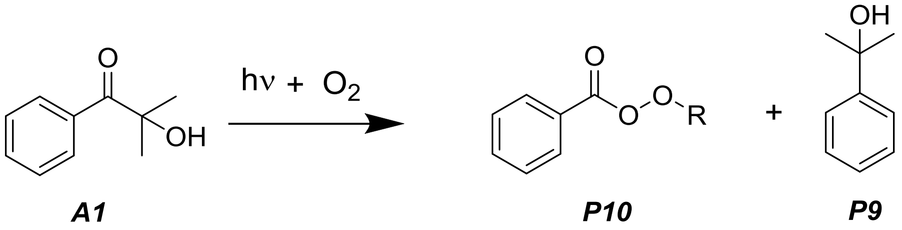

Scheme 12. Confirmed additional products formed from *A1* upon irradiation in the presence of oxygen. R is *R1* or *R2*.

Further signals at 6.7ppm 6.8 ppm and 6.9 ppm are recorded in the oxygen-saturated sample. Those signal fit to several possible compounds, such as phenol, benzoquinone and hydroperoxybenzene, but cannot be assigned unambiguously.

It is possible to analyze the products relative signal intensities in a semi quantitative way. The initial untreated initiator serves therefore as a reference. The reference is a basis to observe increases or decreases of signals in the dependence of the oxygen concentration. To compare each measurement, normalized, relative intensities based on the solvent are calculated. The analysis of the relative intensities derived from water signals, did not reveal significant differences compared to the solvent based calculations.

The initiator signal decreases after irradiation in dependence of the oxygen concentration. **Figure 8** plots the decay of the methyl groups' signal of the initiator ***A1***. The first point marks the starting concentration of the untreated initiator ***A1*** at a normalized, relative signal intensity of 2. The signals decrease after irradiation in dependence of the oxygen concentration. This trend is fitted by a single exponential function. Additionally the signal intensities, i.e. of the benzaldehyde ***P5*** proton, increase (displayed in **Figure 9**).

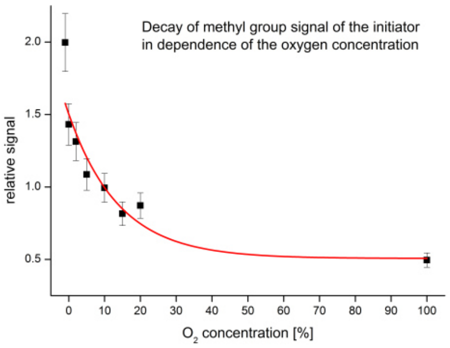

Figure 8. Decay of the initiators *A1* methyl group ^{1}H-NMR proton signal in dependence of the oxygen concentration

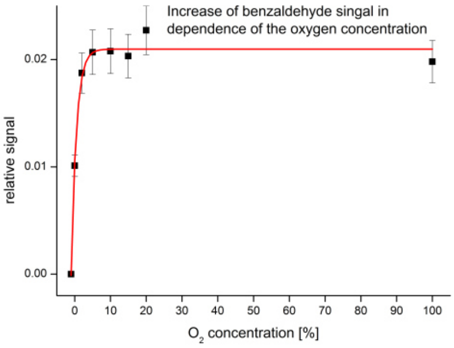

Figure 9. Increase of the benzaldehyde *P5* signal obtained from ^{1}H-NMR in dependence of the oxygen concentration

The irradiation with UV-light cleaves the α-bond of the initiator ***A1*** and radicals are formed. The radicals have several possibilities to react, indicated i.e. in **Scheme 9**. Examples are the recombination product ***P2*** and the parent photoinitiator ***A1***. The signals of ***P1*** overlap with ***A1*** in the aromatic region of the NMR spectrum, but ***A1*** can be characterized by its methyl groups.

In the absence of oxygen the back reaction to the parent initiator ***A1*** seems to be favored. About 75% of the initial signal intensity is found after irradiation. The signal intensity of ***A1s*** methyl groups is the basis for this estimation. When oxygen is present, only 25% of the initial signal is left. According to this the intensities of new formed products must increase. Through the presence of oxygen, the created radicals have another possible reaction partner and can form additional products.

The ^{1}H-NMR spectra of the irradiated oxygen containing photoinitiator provide hints for the formation of benzoyl peroxides (***P6*** and ***P8***). **Figure 8** shows a significant decrease of the initiator signals upon irradiation depending on the oxygen concentration. This is in line with the expected formation of peroxides ***P10***.

Worth to mention is the relative signal intensity of the products ***P2*** and ***P3*** in dependence of the oxygen concentration. Both have a maximum around 5% oxygen with a factor of 2 higher intensity compared to the oxygen-free and oxygen-saturated (100%) sample. The oxygen-free- and oxygen-saturated sample are within the same range. When small amounts of oxygen are present ***P2*** and ***P3*** seem to be formed in higher amounts. ***R1*** might form more stable benzoyl peroxides; therefore smaller amounts of ***R1*** are available to react with ***R2***.

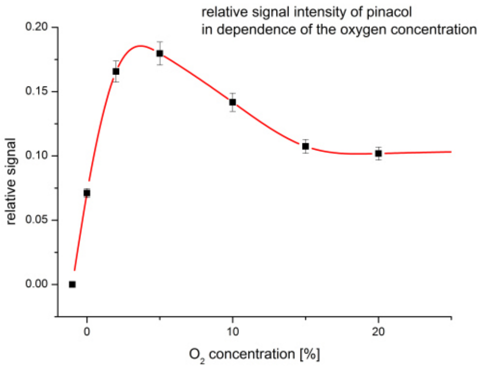

Figure 10. Relative ^{1}H-NMR signal intensity of pinacol *P2* depending on the oxygen concentration.

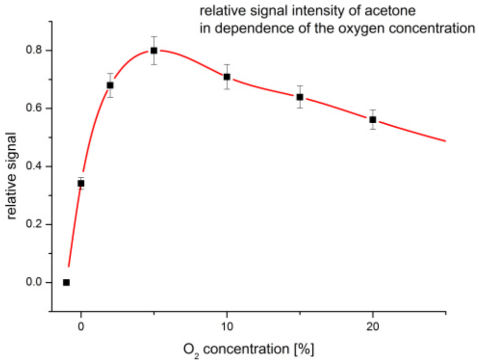

Figure 11. Relative ^{1}H-NMR signal intensity of acetone *P3* depending on the oxygen concentration

4.1.1.2 ^{1}H-NMR Experiments in the Presence of Butyl Acrylate

In order to observe oxygen effects not only at the photoinitiation step but also on the polymerization, experiments in the presence of monomers were performed. The most promising and best to follow monomer was butyl acrylate. This monomer gives well resolved ^{1}H-NMR signals, which are not overlapping with ***A1***.

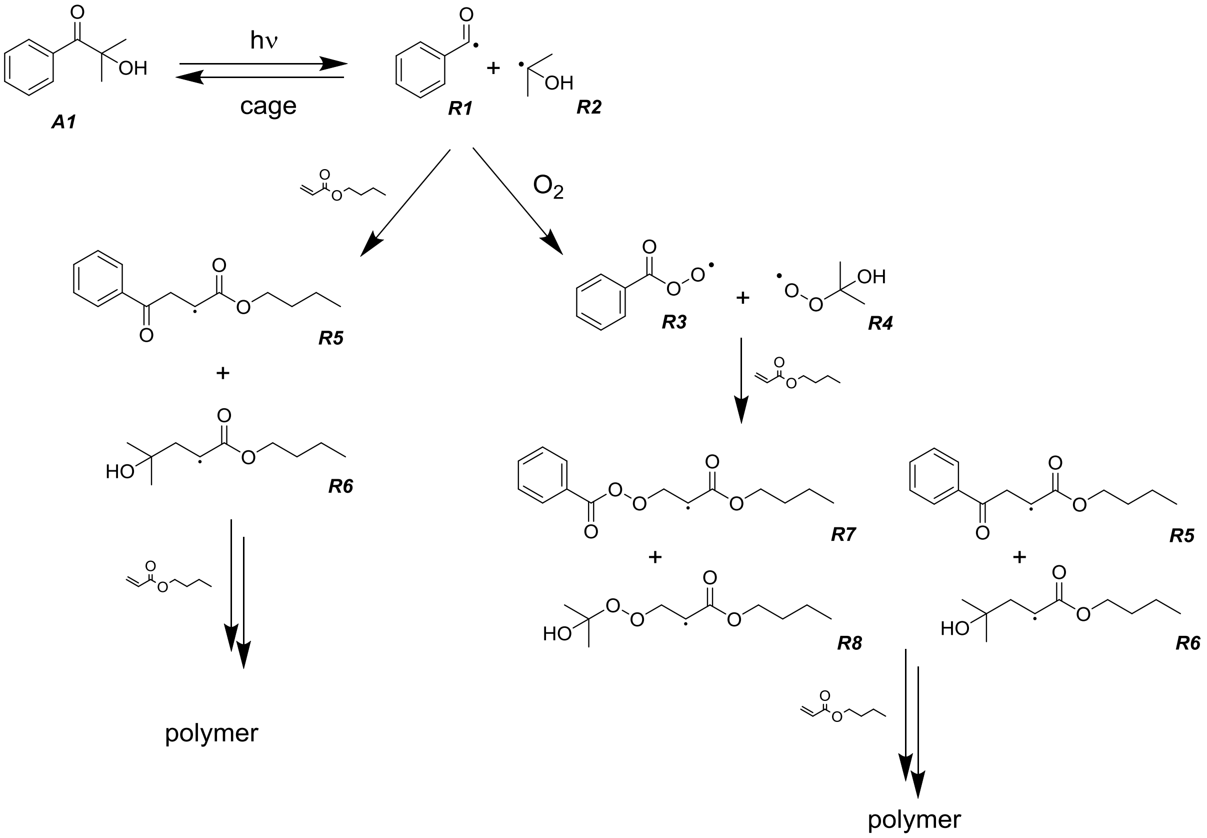

Scheme 13. Expected additional compounds after irradiation of the *A1* with butyl acrylate in the presence and absence of oxygen. Note; for simplification radical recombination products and products formed through hydrogen-atom abstraction are not shown here they are displayed in Scheme 9-12.

The scheme above shows expected additional products out of the photoinitiated reaction of ***A1*** and butyl acrylate in the absence and presence of oxygen. In the absence of oxygen the additions of ***R1*** and ***R2*** radicals to butyl acrylate are expected. This addition will initiate a chain reaction and will lead to the formation of a polymer. The ^{1}H-NMR experiments provide information about the first addition step.

It is expected that radicals react with oxygen first to form peroxyl radicals ***R3*** and ***R4***. Peroxyl radicals are known to be less reactive but here the results show that the first addition is possible.

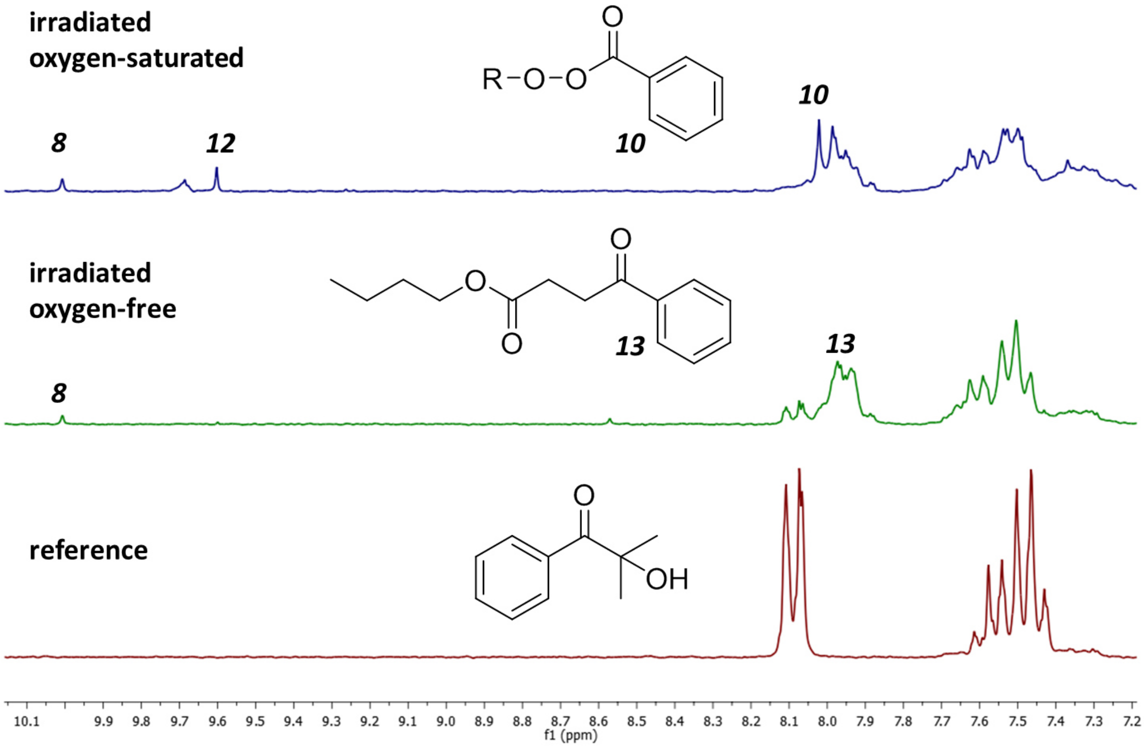

Figure 12.. ^{1}H-NMR spectra of *A1* (10mM) and butyl acrylate (100 mM) after 3 minutes of UV irradiation in the aromatic area. On the bottom trace the spectrum of the non-irradiated initiator (reference) is displayed. The middle trace shows the spectrum of the irradiated oxygen-free sample and the spectrum on top represents the oxygen-saturated sample.

After irradiation all samples contain the proton signal ***8*** of benzaldehyde. The spectrum of the oxygen-free sample shows the new peak ***13*** at 8.0 ppm and an unassigned signal at 8.6 ppm, while signal intensity of the initiator decreased. Signal ***13*** belongs to the growing chain of the polymer ***P11***, consisting out of the benzoyl ***R1*** part of the initiator and at least one molecule of butyl acrylate. In the presence of oxygen this signal is visible but less developed. In this case the benzoyl peroxide ***P10*** with signal ***10*** seems to be dominant. After irradiation, signals of the initiator are not observed. Signal ***12*** at 9.6 ppm, which could indicate formaldehyde and another new signal at 9.7 ppm, which is only observed in the presence of oxygen, appear in the spectra.

There are more differences in the aliphatic range of the NMR spectra, which are displayed in **Figure 13**. The methyl ***4*** signal of the reference spectrum decreases after irradiation in dependence of the oxygen concentration. In the monomer free system signal ***4*** can be observed after irradiation of the oxygen-saturated sample, but this is not possible when monomer is present. The spectrum of the oxygen-saturated sample shows no signal of the initiators methyl groups ***4***, which means that the back reaction is not favored and other pathways are preferred.

The spectrum of the oxygen-free sample shows a significant lower intensity of the initiators methyl protons signals. In the absence of oxygen additional reaction pathways are missing and the back reaction is more likely to happen. Signal ***5*** represents the hydroxyl group proton of the initiator ***A1*** and it behaves same as signal ***4***. The hydroxyl group signals of newly formed species are shifted to a lower field and the signals overlap with signals ***14*** and ***20***. Therefore the hydroxyl groups cannot be distinguished anymore.

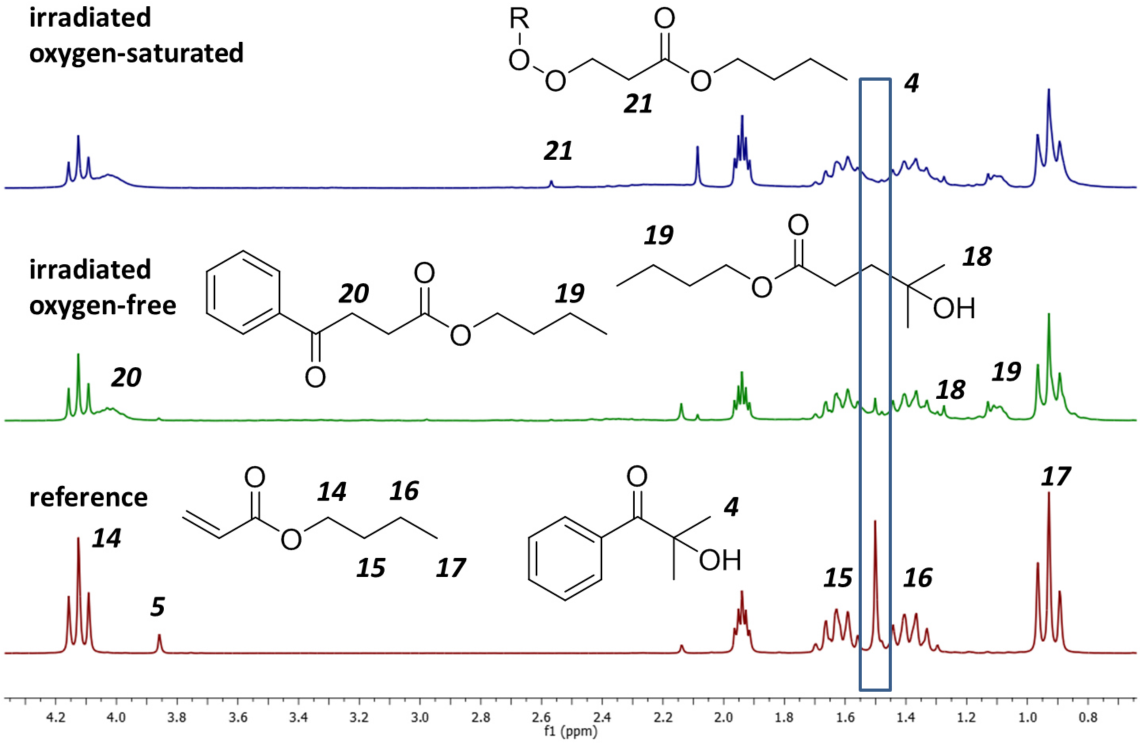

Figure 13. ^{1}H-NMR spectra of *A1* (10mM) and butyl acrylate (100 mM) after 3 minutes of UV irradiation in the aliphatic range.

Acetone ***P3*** is under these conditions one of the major products and the formation of it is preferred in the oxygen-saturated sample. A broad band ***20*** around 4 ppm indicates double bond conversion into newly formed single bonds. Another clue for the double bond conversion is the shift to the higher field of the initial multiplet ***16*** to the new band ***19***. Signal ***18*** represents the proton of a hydroxyl group. This hydroxyl group belongs to compound ***P12*** and it is formed through the addition of ***R2*** to butyl acrylate, which is displayed in **Figure 13.** ***P12*** and pinacol ***P2*** are here the only compounds, which contain hydroxyl groups.

Signal ***21*** at 2.5 ppm probably belongs to the methylene group of the peroxide ***P13***, which is displayed in **Figure 13.** The benzoyl peroxide ***P10*** is visible in the aromatic region of the NMR spectrum. These combined results support the formation of butyl-3-(benzoylperoxy)-propanoate ***P13***.

Scheme 14 displays the new products, which are formed through the addition of butyl acrylate in the absence or presence of oxygen. For simplification of the graph, the already described products i.e. benzaldehyde and acetone are omitted here.

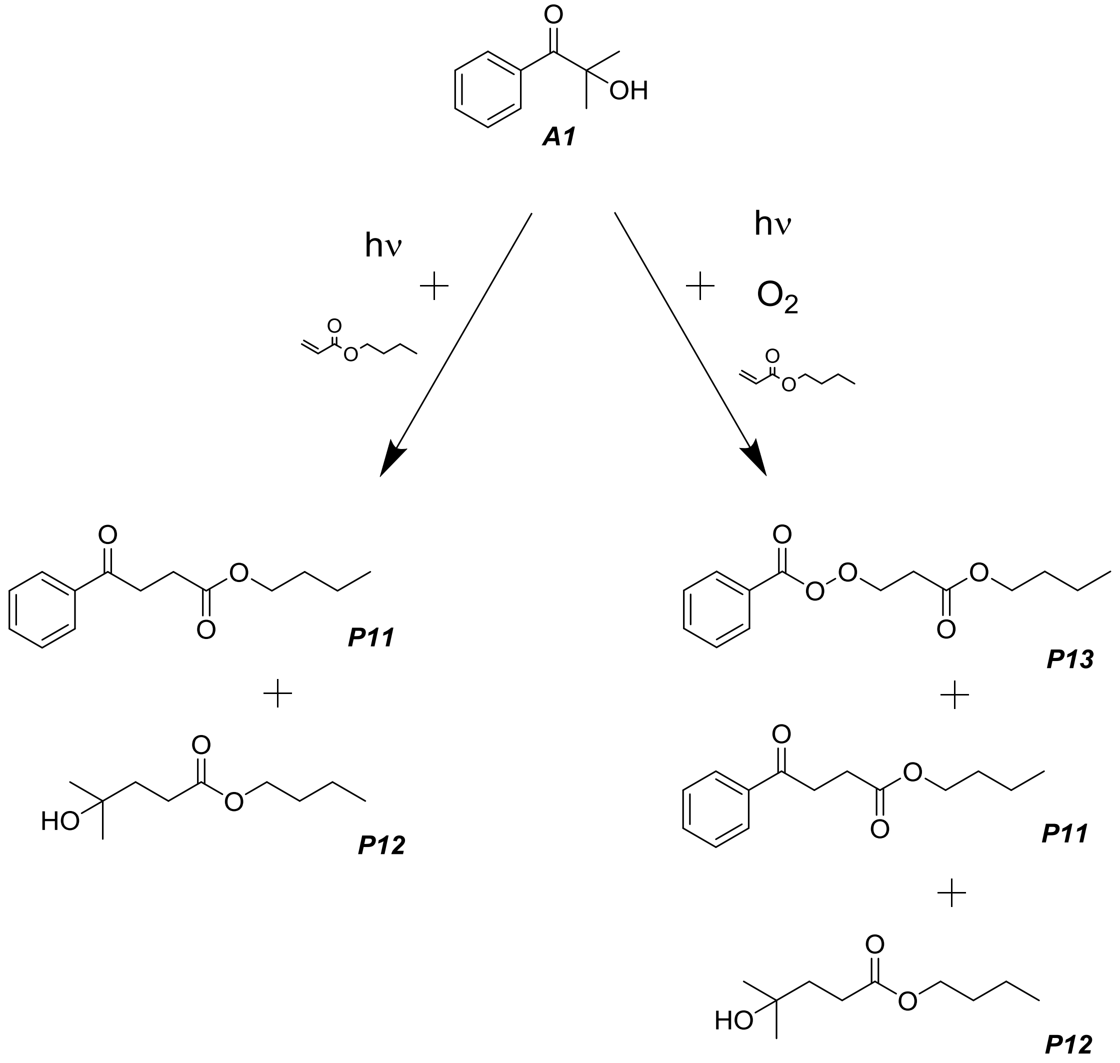

Scheme 14. Illustration of by ^{1}H-NMR experiments confirmed newly found products, when butyl acrylate is added. In the absence of oxygen the addition products of *R1* and *R2* to butyl acrylate are detected. In the presence of oxygen I find strong indications for the formation of butyl-3-(benzoylperoxy)-propanoate *P13* as well as the addition products *P11* and *P12*.

These NMR measurements indicate that oxygen is consumed during a light induced curing process, by the formation of peroxides. Oxygen measurements, which quantify the consumption, are presented in section 4.1.7.

Worth to mention is the bulk behavior of the NMR samples containing butyl acrylate in a concentration of 100 mM. After irradiation and in the absence of oxygen this sample slowly cured and became solid, while samples containing atmospheric amounts of oxygen became highly viscous. Oxygen-saturated samples did not seem to cure, as no changes in the viscosity were observed, although NMR experiments indicated minor double bond conversion. The double bond conversion in the presence of oxygen is mainly caused by the first addition of a radical to butyl acrylate; there is no evidence for further chain propagation.

4.1.1.3 ^{1}H-NMR Experiments in Dependence of Water

The miscibility of acetonitrile with water leads to water peaks in the ^{1}H-NMR spectra. To clarify if effects are caused by water or by oxygen, spectra with defined amounts of water were recorded in the absence and presence of oxygen. The samples were “dry”, or contained 1 M, 4 M, or 20 vol. % water and 10 mM ***A1***.

The dry and 1 M water containing samples show no differences beside the water peak. In respect to the oxygen concentration the same products are found and the minor amounts of water do not influence the results. The sample with 4 M water does not show any product fragmentation and the water peaks shifted to 3.0 ppm. The addition of water causes some kind of resonance interference. The existing signals broaden and contain additional resonances. With 20 vol. % water added those phenomena become more pronounced and the water peak moves to 3.5 ppm and an additional broad signal at 6.0 ppm appears.

The water concentration of untreated samples is far below 1 M and these results indicate that minor amounts of water do not affect the reactions. Same results are observed for experiments where butyl acrylate is added.

4.1.2 ^{13}C-NMR Experiments

In addition to ^{1}H-NMR experiments I performed ^{13}C-NMR measurements to confirm the results gained from the ^{1}H-NMR investigations. The chemical shifts of e.g. benzoyl peroxides and the polymerization products of butyl acrylate, tend to overlap. This makes the structure elucidation extremely difficult and sometimes impossible. ^{13}C-NMR has the benefit of a bigger range of chemical shifts, which enables to determine additional structures.

4.1.2.1 ^{13}C-NMR Experiments in Dependence of Oxygen

First let us recall the main expected products (**Scheme 15**) after irradiation of ***A1***. To simplify the scheme only the additional found products in the presence of oxygen are displayed.

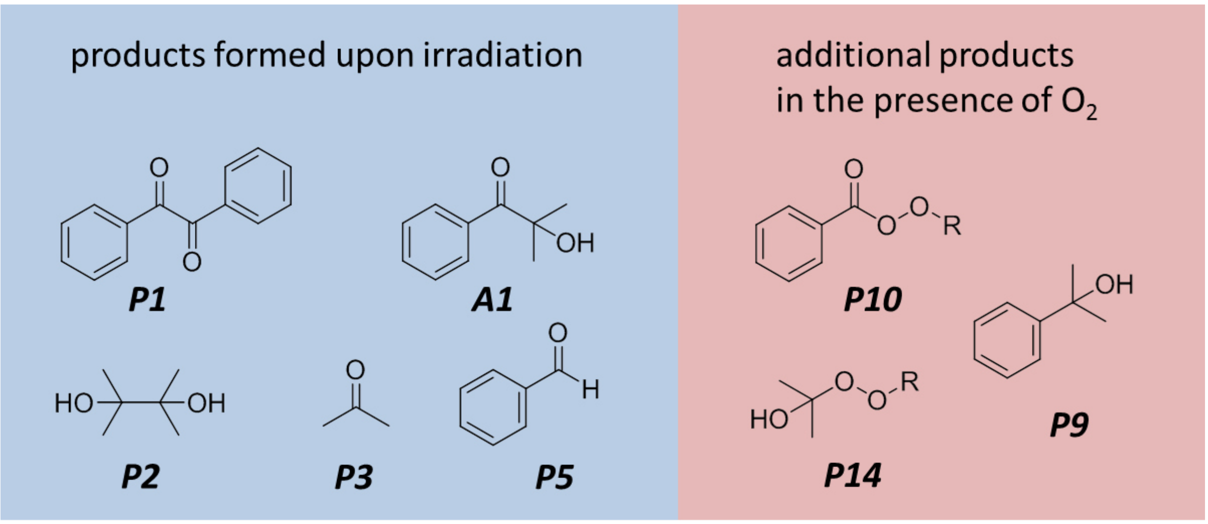

Scheme 15. Products formed upon irradiation of *A1* (blue background). Additional products, which are formed in the presence of oxygen, are indicated by the red background.

The interpretation of the aliphatic region of the spectra is difficult as the chemical shift differences are not big and through multiplet splitting of the methyl groups peak overlaps occur. In principle acetone should be found around 30 ppm. At this shift a signal is visible, but it is possible that it belongs to a multiplet originating from the parent initiator.

On the other hand in the aromatic region of the spectra shift differences are significant and signals, which depend on the oxygen concentration, can be observed. **Figure 14** displays this desired part of the spectra. The broad peak ***a*** at 205.5 ppm belongs to the carbonyl carbon of ***A1*** and, when the sample is irradiated additionally to the carbonyl carbon of acetone ***P3***. The intensity of this signal increases after irradiation as acetone is formed. The signal of the carbonyl carbon of other possible created products such as ***P1*** and ***P5*** should also be in the same area.

In the non-irradiated reference spectrum, the assignment of ***A1's*** aromatic signals (***b-g***) is possible. The carbon ***b***, which is the closest to the carbonyl group has the highest shift and is found at 136.1 ppm. This carbon is of particular interest, because the chemical shift depends significantly on the group, which is attached to the carbonyl.

Interesting to mention is peak ***h***, which belongs to ***P1***. This signal appears in the untreated reference sample as well as in the oxygen-free irradiated sample. The presence in the reference sample indicates slight decomposition of ***A1*** during sample preparation. Compared to ^{1}H-NMR experiments the signals of ***P1*** and ***A1*** can be distinguished in ^{13}C-NMR spectra. After irradiation the intensity of ***h*** increases, this indicates the additional formation of ***P1***. Another hint for some decomposition is the finding of propanol in ^{1}H-NMR spectra.

In the oxygen-free irradiated spectrum signal ***i*** at 129.4 ppm represents the meta protons of ***P1***. This signal appears in the reference spectrum only as a shoulder. As ***d*** declines ***i*** becomes visible as an independent peak.

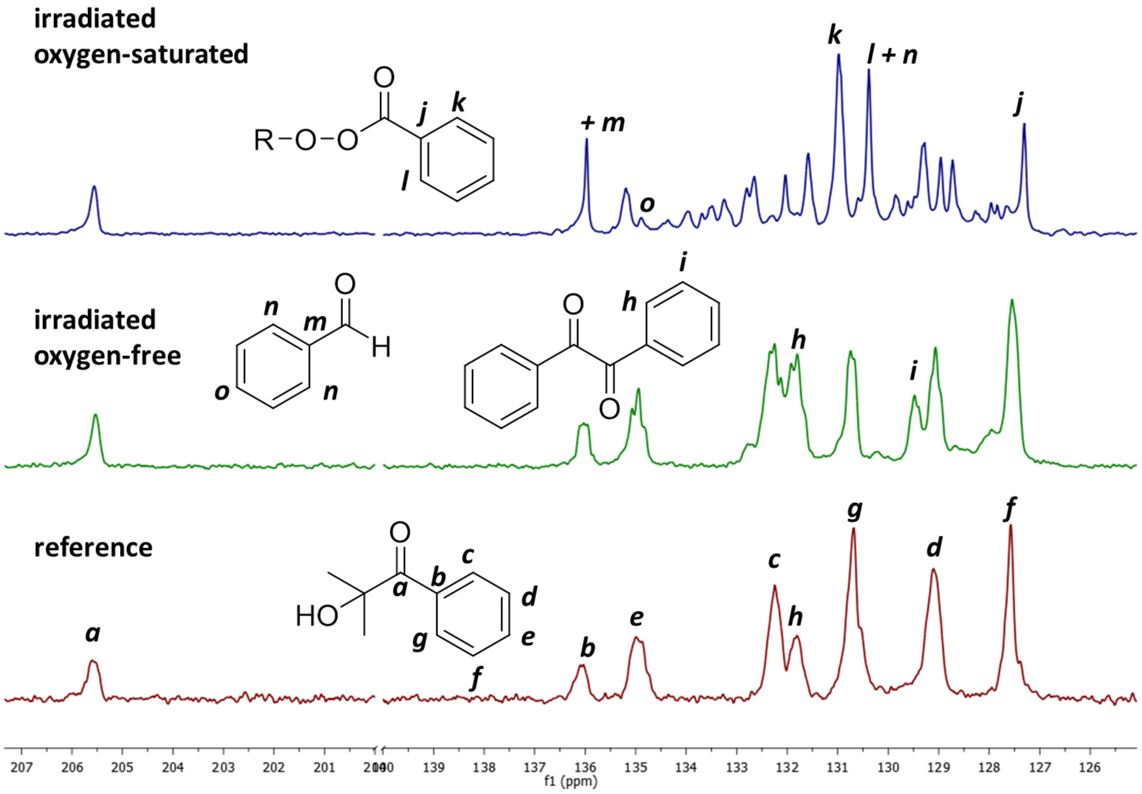

Figure 14. Aromatic area of ^{13}C-NMR spectra of *A1* (1M) after irradiation in dependence of oxygen. The bottom trace displays the spectrum of the non-irradiated photoinitiator. The middle trace shows the spectrum of the oxygen-free irradiated sample and the upper trace displays the spectrum of the oxygen-saturated sample.

Peaks ***j***, ***k*** and ***l*** strongly indicate that peroxide ***P10*** is formed in the presence of oxygen. ***k*** at 130.9 ppm is neither observed in the spectrum of the oxygen-free sample nor overlapping with any other peak. Compared to the corresponding carbon ***c*** at 132.2 ppm of the initiator, the signal of ***k*** is significantly shifted to a higher field. Signal ***j*** at 127.2 ppm is not overlapping with signal ***f*** from the parent initiator at 127.6 ppm.

^{13}C-NMR experiments confirm the formation of benzaldehyde ***P5*** by e.g. signal ***m*** at 135.9 ppm in the oxygen-saturated sample. In the absence of oxygen the broad peak ***b*** of the initiator overlaps with the aldehyde signal ***m***. After irradiation and in the absence of oxygen signals of the parent compound ***A1*** are left, which cover the signal ***m*** from ***P5***. A good indication for two or more overlapping peaks, including the signal of ***P5*** is the shape of the initiator signal ***b***. After irradiation of the oxygen-free sample, this broad peak has no longer a maximum and a plateau is observable instead. In the oxygen-saturated sample peak ***m*** of the benzaldehyde appears in a pointed shape.

After irradiation of the oxygen-free sample I can only assign ***P1***, as ***P5*** overlaps with existing broad signals. The oxygen-saturated sample once more provides information about formed benzoyl peroxides ***P10*** and benzaldehyde ***P5***. Worth to mention is, that the signals of the initiator are not detectable in the spectrum of the oxygen-saturated sample. This is also observed in the aliphatic region of the spectrum and is in line with the findings from the ^{1}H-NMR experiments.

Further experiments, with chloroform as solvent, show comparable results, but chloroform is not the ideal solvent for this system as the solvent peaks overlap with tertiary carbon signals.

4.1.2.2 ^{13}C-NMR Experiments in Dependence of Oxygen with Butyl Acrylate

Signal ***p*** at 166.4 ppm represents the carbonyl carbon of butyl acrylate. This signal is an excellent indicator for the polymerization, as it shifts to lower fields when the double bond is converted. In the absence of oxygen the benzoyl radical ***R1*** attacks the double bond and the addition product ***P11*** can be determined via the new signal of the carbonyl carbon ***s*** around 175.4 ppm. Another hint for the addition of ***R1*** to butyl acrylate is signal ***t*** at 137.1 ppm, which is also shifted to a lower field. In the presence of oxygen neither of these peaks is observable. Signal ***p*** is after irradiation and in the presence of oxygen still visible. This indicates that no double bond conversion occurred in the oxygen-saturated sample.

In the presence of oxygen signal ***j*** indicates the formation of benzoyl peroxides ***P10***, but the determination of the exact species is not possible here.

Further assignments are not possible within the aromatic area of the spectra, as butyl acrylate partly overlaps with other signals and polymerization creates a huge amount of different molecules.

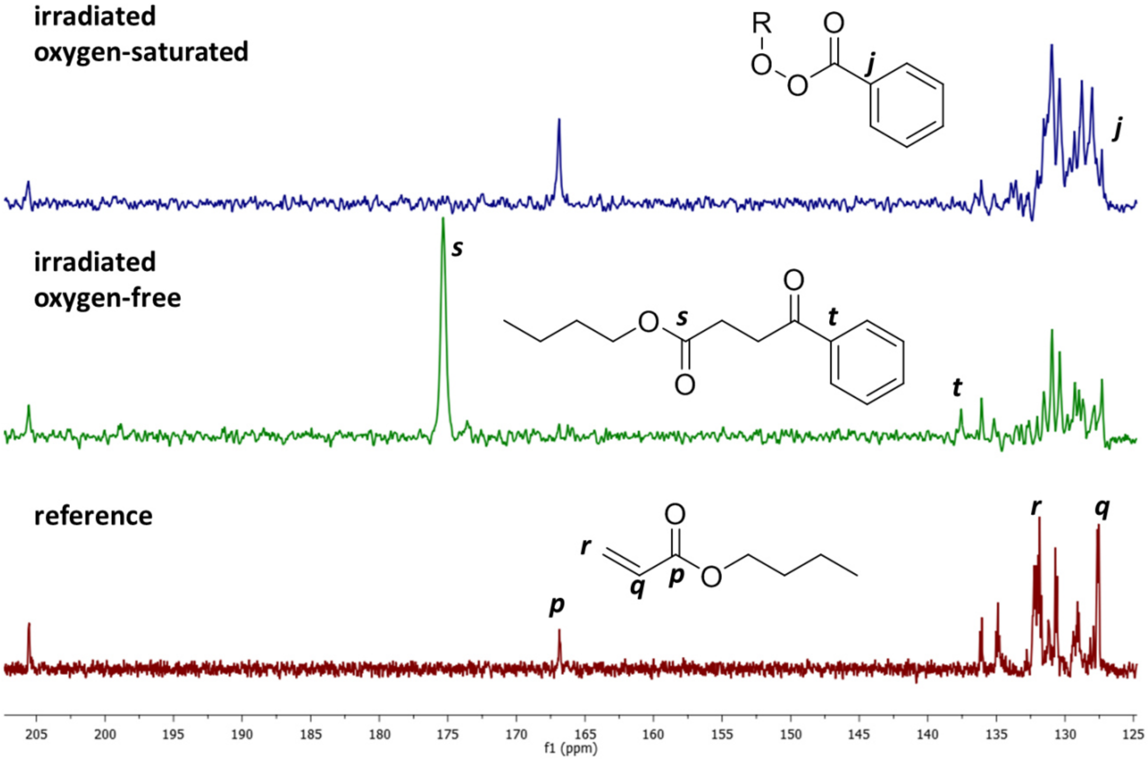

Figure 15. ^{13}**C-NMR of** ***A1*** **(100 mM) with butyl acrylate (400 mM) in the aromatic region of the NMR spectrum. On the lower trace the spectrum of the non-irradiated initiator with butyl acrylate is shown. The middle and the upper trace display the spectra of the irradiated oxygen-free and oxygen containing sample.**

This experiment shows that oxygen-saturated samples do not significantly polymerize. The spectra of atmospheric oxygen containing samples provided evidence of double bond conversion and samples with more than 400 mM butyl acrylate cured.

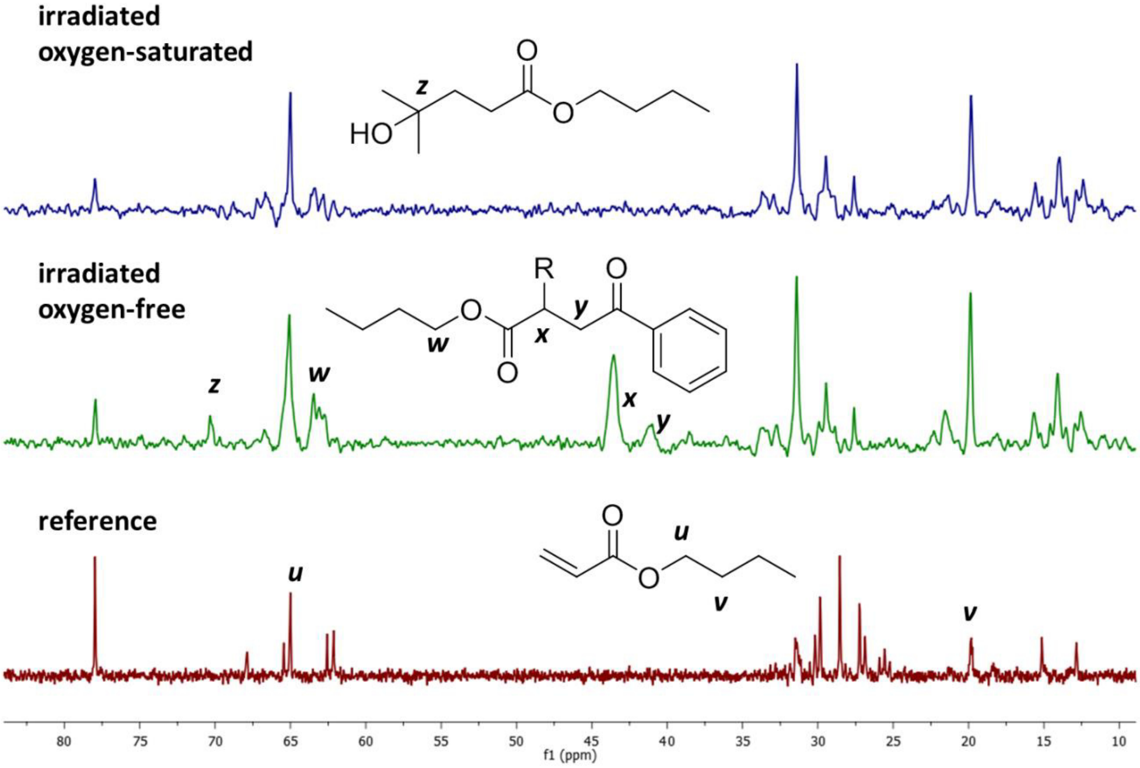

Figure 16. ^{13}C-NMR spectra of *A1* (100 mM) with butyl acrylate (400 mM) in dependence of the oxygen concentration in the aliphatic area. The lower trace shows the spectrum of the non-irradiated initiator with butyl acrylate. The middle and the upper trace display the spectra of the irradiated oxygen-free and oxygen containing sample.

Butyl acrylates impurities, which probably derive from oxidation processes, are detected in the aliphatic region of the spectra. Irradiation of the oxygen-free sample leads to double bond conversion, which can be followed by the new signals ***x*** and ***y***. ***x*** at 43.6 ppm indicates the presence of at least a dimer and the corresponding monomer has a signal around 32 ppm. Peaks in this area are recorded, but overlaps with products ***P2*** and ***P3*** occur.

Peak *z* at 70.4 ppm is detectable only in the oxygen-free sample. It corresponds to the tertiary carbon of ***R2*** attached to butyl acrylate. This indicates that both fragments of ***A1***, ***R1*** and ***R2*** are able to initiate the polymerization.

^{13}C-NMR experiments show that double bond conversion is possible in the absence of oxygen and in the presence of atmospheric oxygen amounts. Oxygen-saturated samples provided no evidence for double bond conversion. On the other hand, these measurements confirm the formation of benzoyl peroxides in the presence of oxygen.

4.1.3 CIDNP Experiments

One of the huge advantages of CIDNP is the signal suppression of analytes, which have no radical precursor. In principle solvent peaks or signals of starting material should not be visible. Signal overlapping is an evident problem in standard ^{1}H-NMR experiments, but with CIDNP it should not be an issue.

Well resolved spectra allow proper peak assignment of main- and minor products. A strength of this technique is the detection of short lived intermediates such as prop-1-en-2-ol ***P4***. Others like 2-peroxypropan-2-ol ***P14*** species can be confirmed, but most important for mechanistic approaches is that only products with direct radical precursors are observed.

4.1.3.1 ^{1}H-CIDNP of A1 in Dependence of Oxygen

The results of these experiments provide information about products, which are formed 2 µs after the sample is excited by a laser pulse. The line broadening effect of oxygen causes interpretation problems of oxygen-saturated samples.

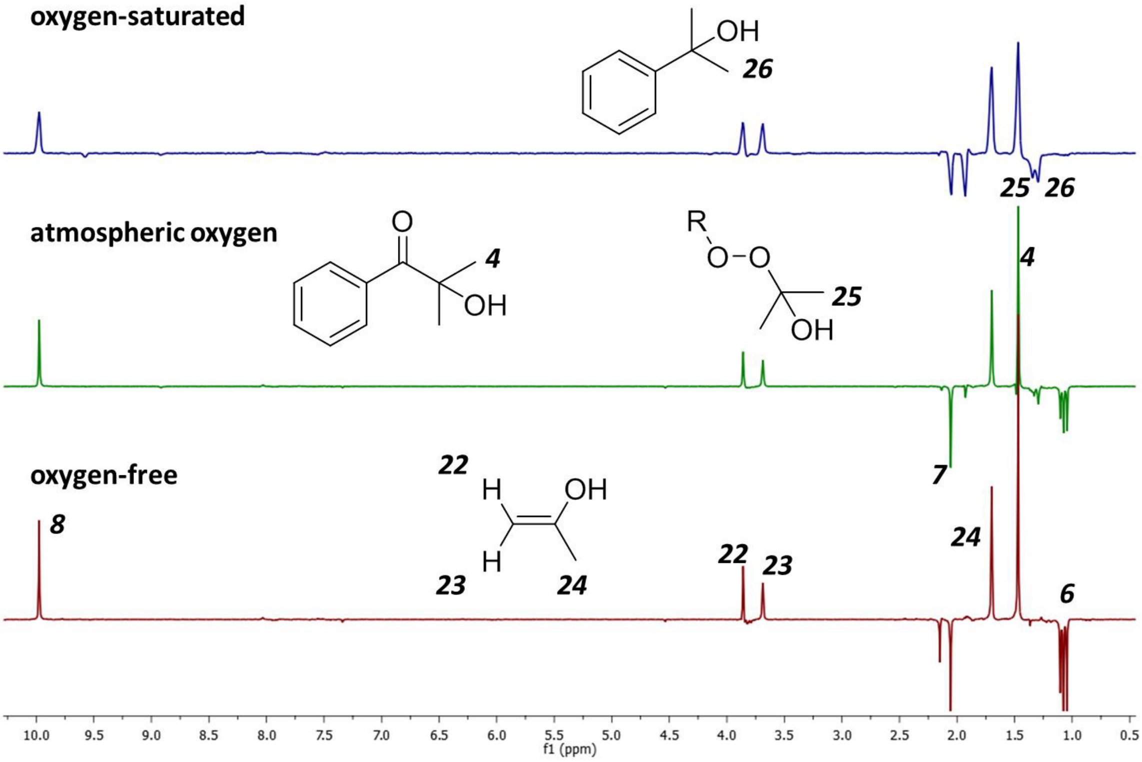

Figure 17. ^{1}H-CIDNP spectra of *A1* (10 mM) in dependence of oxygen (32 scans). The bottom trace shows the oxygen-free ^{1}H-CIDNP spectrum obtained from *A1*. The middle trace displays the spectrum of the sample containing atmospheric oxygen concentrations, while the top trace represents the oxygen-saturated sample.

Comparing these spectra, with the standard ^{1}H-NMR spectra after irradiation, reveals new signals as well as changes in the intensity. The signal of benzaldehyde ***8*** is pronounced and in enhanced absorption, as well as the signal of ***A1s*** methylene groups ***4***. Product signals, belonging to the parent initiator, confirm the cage reaction. These results correspond to already published data.[80]

The protons ***6*** in enhanced emission represent pinacol ***P2*** and its signal intensity decreases in dependence of the oxygen concentration. In the oxygen-saturated sample only traces of ***P2*** are left.

New, compared to the ^{1}H-NMR, are the signals ***22***, ***23*** and ***24***, which belong to prop-1-en-2-ol ***P4***. ^{1}H-NMR experiments show no evidence for this compound, as the equilibrium of the keto-enol tautomerization is on the side of acetone ***P3***, which is identified as peak ***7***. ***P4*** and ***P3*** are found in the presence and absence of oxygen.

The Peaks at 2.1 ppm represent water in the oxygen-free sample. This signal decreases in the presence of oxygen, as the sample is flushed with dry gas. The oxygen-free samples contained more water, because the used nitrogen was wet. To clarify, if the observed effects are caused by water or oxygen, I added 50 mM water to oxygen-free and oxygen-saturated samples and additionally a dry oxygen-free sample was prepared by using argon. The result of this experiment was that traces of water do not cause different spectra. Therefore, the observed effects are caused by oxygen.

Signal ***25*** at 1.29 ppm in oxygen containing samples belongs to a species of ***P14***. Further, ***P9*** with signal ***26*** at 1.35 ppm is only observed in the presence of oxygen. The weak peak at 9.6 ppm in the oxygen-saturated sample is again a hint for the formation of formaldehyde.

4.1.3.2 ^{1}H-Time-Resolved-CIDNP in Dependence of Oxygen

TR-CIDNP was performed to obtain information about reaction kinetics. The delay between the laser-pulse and the recording of the spectrum was in the range from 0 µs to 25 µs.

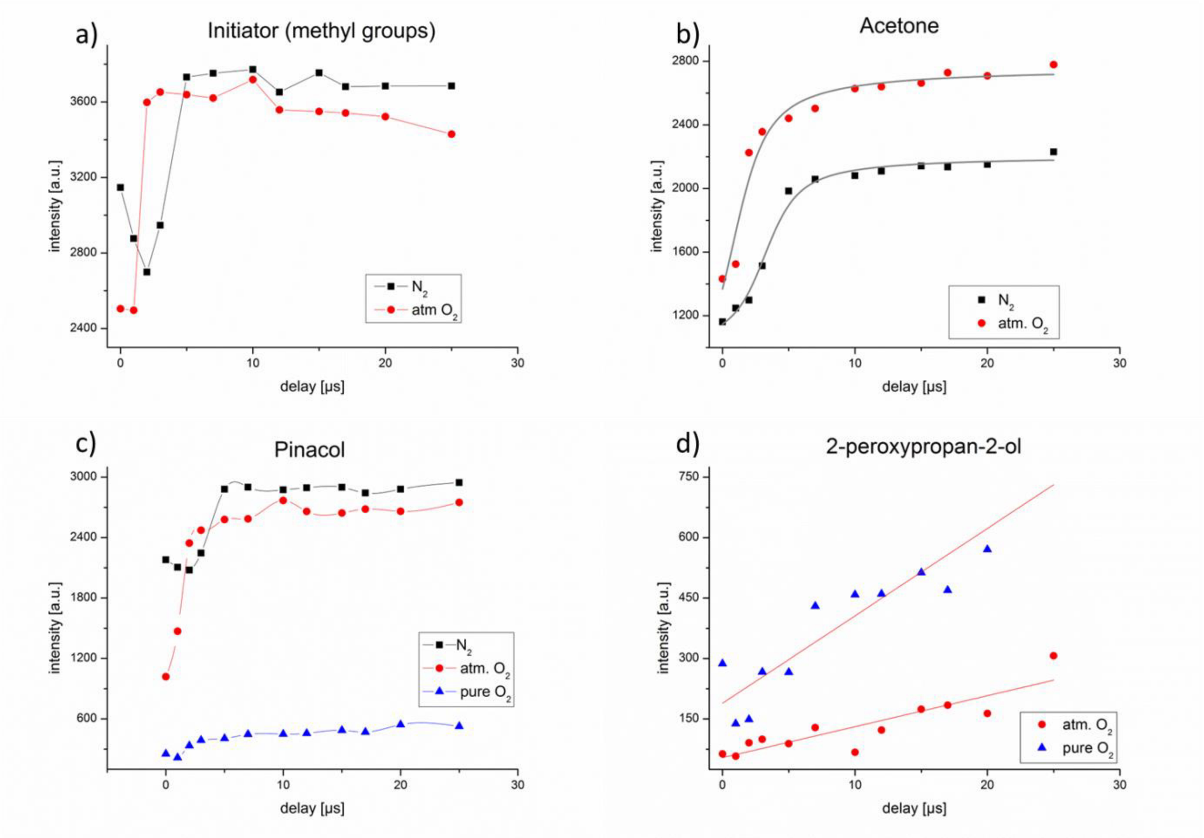

Figure 18. ^{1}H-CIDNP signal intensities in dependence of the delay time of, a) the methyl groups of *A1* b) acetone *P3* c) pinacol *P2* d) 2-peroxypropan-2-ol *P14*.

The signal of the methyl group of the initiator shows a dependence on oxygen. When no oxygen is present, the methyl signal decays from 0 µs to 2 µs delay and rapidly increases from 2 µs to 5µs. After 5 µs a stable plateau is reached. The signal intensity of the sample containing oxygen is the same after 0 µs and 1 µs delay. After 1 µs the intensity increases immediately and reaches a slowly decreasing maximum. ^{1}H-NMR experiments after irradiation show, that this signal is biggest in the absence of oxygen. The results, displayed in **Figure 18a**, indicate the same, as the initial signal slightly decays in the presence of oxygen.

The signals attributed to acetone show a different picture. Oxygen enhances the signal intensity of ***P3*** and it is formed earlier in higher amounts. After 2 µs in the presence of oxygen an almost doubled signal intensity of acetone is observed, while in the oxygen-free sample the intensity only increased by around 10 %. After the equilibrium is reached, the oxygen containing sample has a 25 % higher acetone signal intensity, than the oxygen-free sample. This result fits to ^{1}H-NMR experiments, which show that more acetone is formed in the presence of oxygen.

Signals of pinacol ***P2*** on the other hand behave opposite. The increase of the signal intensity by increasing the delay is biggest in the absence of oxygen. The oxygen-free and atmospheric samples behave, except for the first 3 µs, similar. I measure extremely reduced ***P2*** signal intensities in the oxygen-saturated sample. The signal intensity of ***P2*** from the oxygen-saturated sample differs by a factor of approximately 10, compared to the oxygen-free sample.

Interesting is the formation of 2-peroxypropan-2-ol ***P14***. This cannot be detected in oxygen-free samples and the signal intensities depend on the oxygen concentration. More oxygen leads to higher signal intensities of the peroxides and that increase over time. The relatively low signal intensity is an issue. The signal intensity of the parent initiator is approximately 10 times higher, than the intensity of the peroxide. When oxygen is present, the formation of acetone ***P3*** is preferred; therefore less ***R2*** is available to react with oxygen to form ***P14***.

The signals of 2-phenylpropan-2-ol ***P9*** show similar results as ***P14***, which are only detected in the presence of oxygen and the signal intensities, are highest in the oxygen-saturated samples. The signal intensities of the sample under atmospheric conditions decrease up to 15 µs delay and then increase again. Within the delay times of 0-25 µs the signal intensities are approximately on the same level. The oxygen-saturated sample shows significantly increased signal intensities at longer delays. These results fit to ^{1}H-NMR measurements, where oxygen-saturated samples provide the highest signal intensities.

The results for prop-1-en-2-ol ***P4*** are comparable with ***P2***. The development of the signal intensities of the oxygen-free and the atmospheric oxygen sample are similar. The oxygen-saturated sample gives always lower signal intensities.

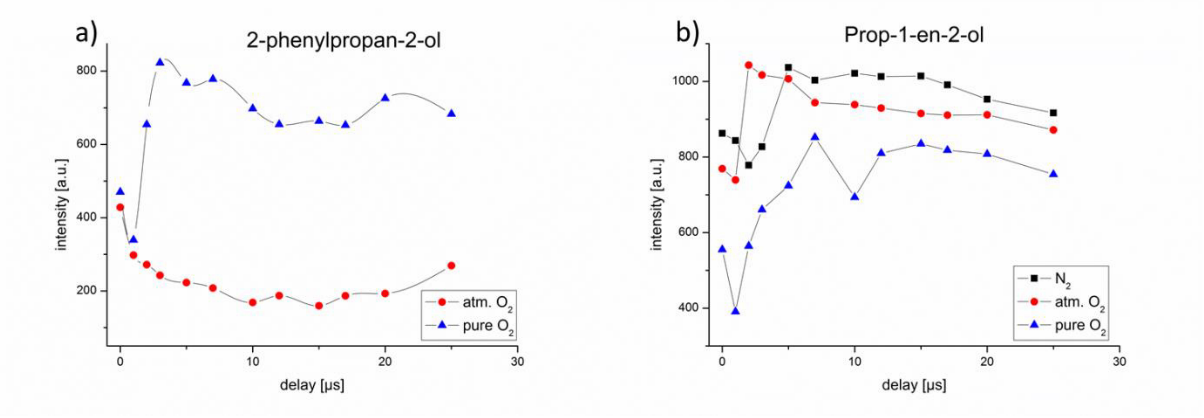

Figure 19. ^{1}H-CIDNP signal intensities of samples containing different oxygen concentrations in dependence of the delay time of a) 2-phenylpropan-2-ol *P9* and b) prop-1-en-2-ol *P4*.

4.1.3.3 ^{1}H CIDNP of A1 with Butyl Acrylate in Dependence of Oxygen

The spectra in **Figure 20** are similar to those without butyl acrylate and all the expected signals from the initiator and its follow up products are present.

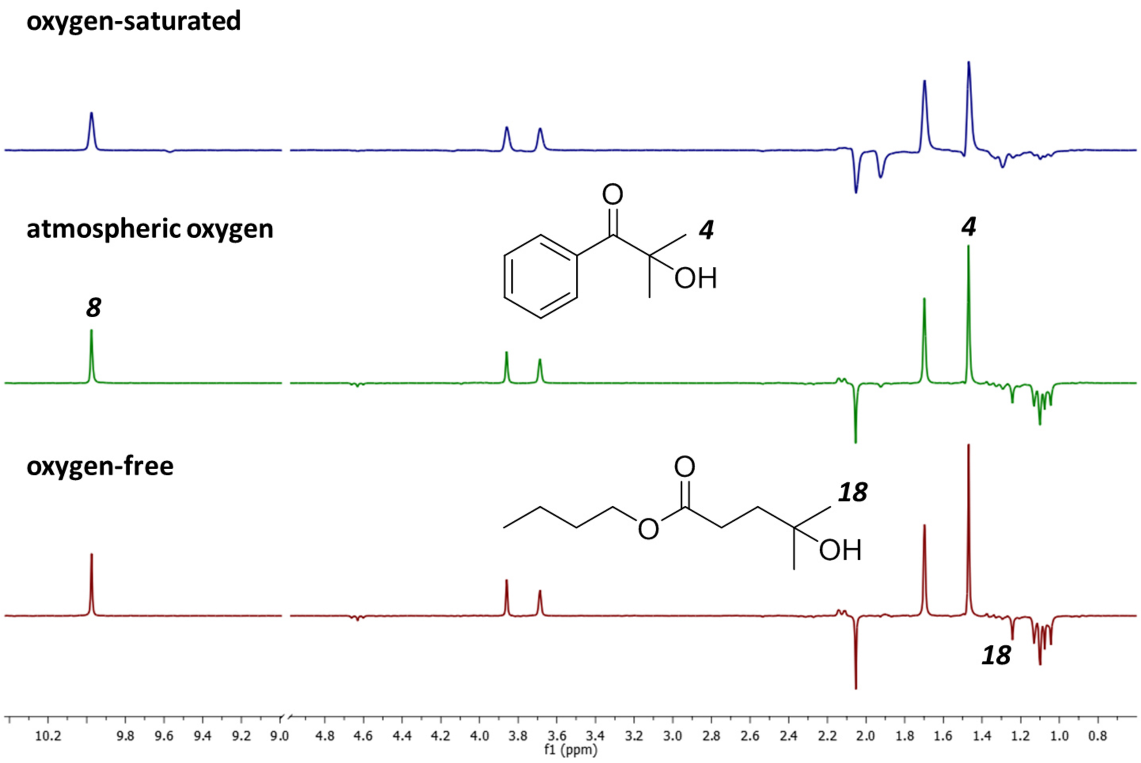

Figure 20. ^{1}H-CIDNP spectra of *A1* (10 mM) with butyl acrylate (100 mM) and various oxygen concentrations (32 scans). The bottom spectrum represents the oxygen-free sample, while the middle trace displays the spectrum of the sample containing atmospheric oxygen. The top trace shows the spectrum of the oxygen-saturated sample.

In the aromatic region of the NMR spectrum, weak additional resonances appear, that belong to benzoyl groups and the double bond of butyl acrylate. These signals indicate the addition of the benzoyl radicals ***R1*** to the double bond of butyl acrylate. Additionally, in the oxygen-saturated sample, signal traces appear, which fit to formaldehyde. This might be a hint that formaldehyde is also formed via a radical mechanism. I observed this signal also in the irradiated ^{1}H-NMR spectra of ***A1*** in the presence of oxygen.

Worth to mention is peak ***18*** at 1.25 ppm in the spectra of the oxygen-free sample and the sample with atmospheric oxygen. It belongs to butyl 4-hydroxy-4-methylpentanoate ***P12*** and this molecule is formed after the addition of ***R2*** to butyl acrylate. This new signal does not overlap with others i.e. ***P2***, which is observed around 1.1 ppm.

The peaks in the spectrum of the oxygen-saturated sample are broadened and the signal ***18*** of ***P12*** is not visible, but again there is evidence for ***P14*** via the peak at 1.29 ppm.

4.1.3.4 ^{1}H-CIDNP Experiments of A1 with Butyl Acrylate in Dependence of Oxygen after Irradiation

^{1}H-NMR experiments showed that after irradiation the initiator is decomposed and in dependence of the oxygen concentrations the signal intensities of ***A1*** decrease. Samples containing lower oxygen concentrations should therefore still contain initiator, which could be activated.

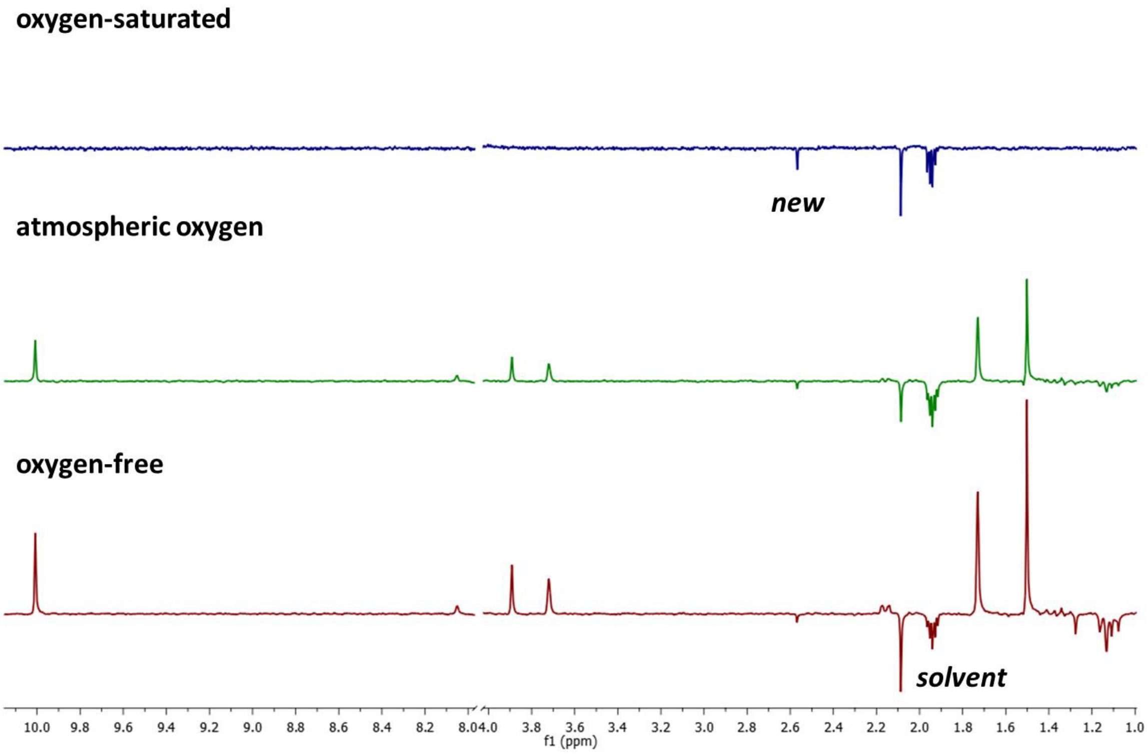

Figure 21. ^{1}H-CIDNP spectra of *A1* and butyl acrylate after UV irradiation and in dependece of the oxygen concentration (32 scans). The bottom trace shows the oxygen-free ^{1}H-CIDNP spectrum. The middle trace displays the spectrum of the sample containing atmospheric oxygen concentration while the top trace represents the oxygen-saturated sample.

The spectra recorded after irradiation, in absence of oxygen and under atmospheric conditions, are similar to the corresponding ^{1}H-CIDNP spectra of the non-irradiated samples. A difference is the strong signal of the solvent. Acetonitrile provides a quintet at 1.94 ppm and the solvent signal is in all three spectra pronounced compared to CINDP experiments of non-irradiated samples.

Additionally, the spectra show a new peak at 2.57 ppm. This peak could belong to poly butyl acrylate or to an oxygen species attached to butyl acrylate.

The enhanced signal at 8.05 ppm, which belongs to an aromatic compound, is interesting. This signal intensity increased significantly, compared to previous ^{1}H-CIDNP experiments.

The preceding irradiation leads to benzaldehyde ***P5***, which is not inert and can be decomposed by light. A possible product of the decomposition is benzene, which could explain the additional signal in the aromatic area of the spectrum.

The spectrum of the oxygen-saturated sample shows only 3 different signals, which represent acetonitrile, acetone and a not assigned product. The signal intensity of the new peak at 2.57 ppm is more pronounced in the presence of oxygen, than in the absence of oxygen.

4.1.4 Spin Trap- and Experiments in the Presence of TEMPO

The initiator ***A1*** was irradiated with UV light in the absence and presence of oxygen and the created radicals were spin trapped. Spin trap experiments included EPR and NMR measurements with *N*-*tert*-Butyl-α-phenylnitrone (PBN) and 5,5-dimethyl-1-pyrroline-N-oxide (DMPO). Additionally, (2,2,6,6-Tetramethylpiperidin-1-yl)oxyl (TEMPO) reacted with the created radicals to form diamagnetic products, which are characterized with ^{1}H-NMR and ^{13}C-NMR experiments.

4.1.4.1 EPR Measurements

Several samples of ***A1*** mixed with different ratios of *N*-*tert*-Butyl-α-phenylnitrone (PBN) were irradiated with the Hamamatsu UV-lamp in the absence and presence of oxygen for 1 minute and subsequently EPR spectra were recorded. PBN is a common spin trap agent and the detection of benzoyl derived radicals is expected; these are displayed in the following scheme. Literature states that PBN does not react with ***R2***.[87]

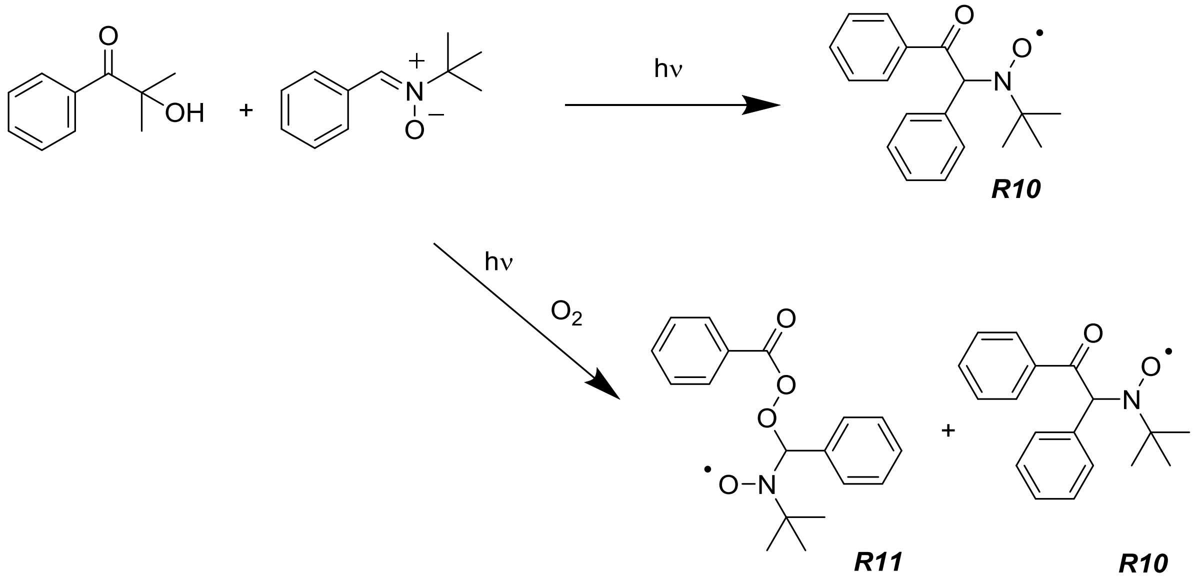

Scheme 16. Expected spin trapped species upon irradiation and follow-up reaction of *A1* with PBN in the absence and presence of oxygen. In the absence of oxygen the trapped product *R10* is expected. In the presence of oxygen benzoyl peroxide *R3* might be trapped.

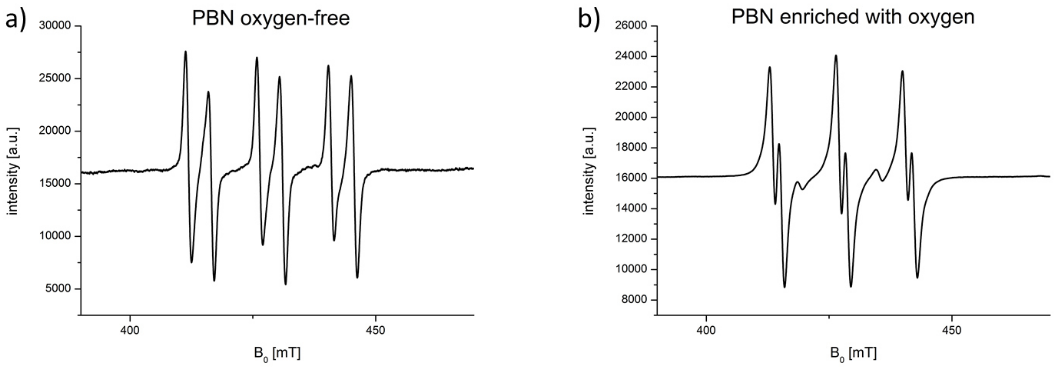

Figure 22 EPR spectrum of a) oxygen-free sample with *A1* (25 mM) with PBN (50 mM) and b) oxygen-saturated sample with *A1* (25 mM) with PBN (50 mM) in acetonitrile.

In the absence of oxygen the EPR hyperfine splitting constants are a_N= 14.51 G and a_H= 4.62 G. These results correspond excellent to the values for ***R10***, published by G. Hutchings et al.[87] and are matching well to other data.[54,88–90] The EPR spectrum in the absence of oxygen reveals no further radicals; this fits to our expectations, as ***R2*** does not react with PBN.[87]

The spectrum of the oxygen-saturated sample reveals lower hyperfine splitting constants with a_N= 13.56 G and a_H= 1.93 G. Hutchings suggests for similar values benzoyloxy radicals.[87,91] According to the NIEH spin trap database oxygen centered radicals like benzoyloxy are likely. I expect similar hyperfine splitting's for the trapped ***R3***. EPR data clearly indicate an oxygen centered radical, which is supported by NMR results. The EPR spectrum contains hints for a second radical, which is most likely ***R10***.

Additionally to PBN, experiments were performed with DMPO, which is able to trap ***R1*** and ***R2***.[92] A possible disadvantage is the formation of DMPO dimers.

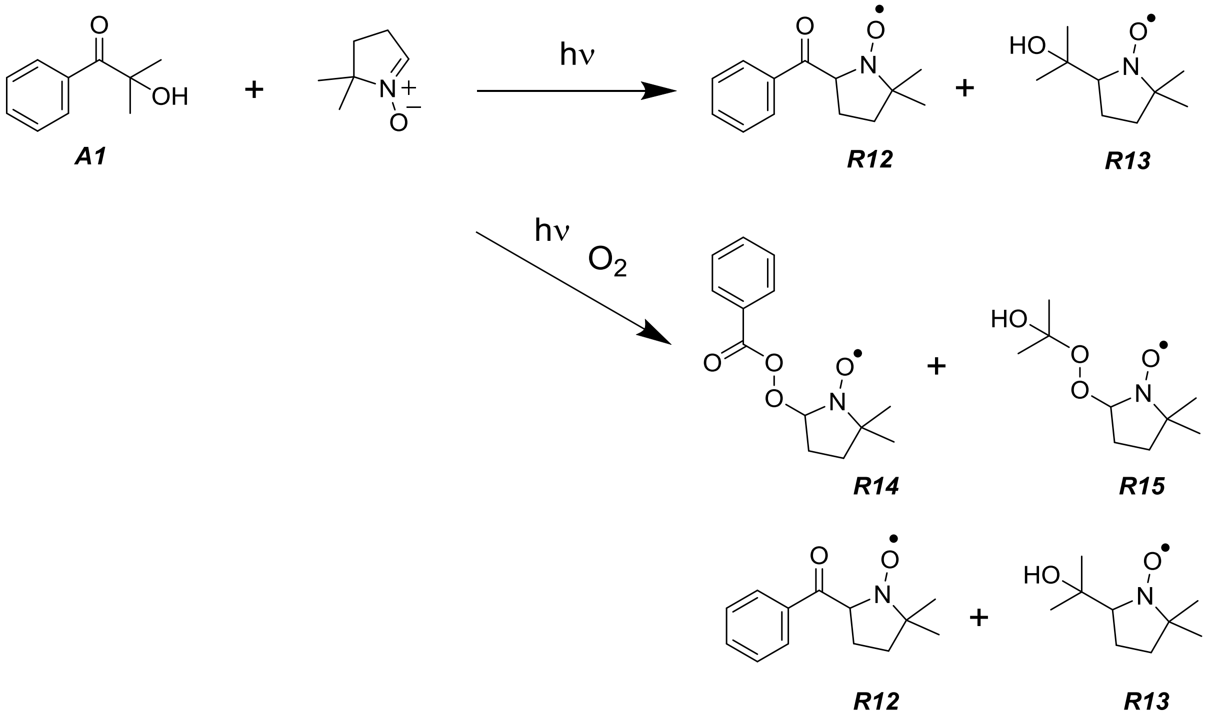

Scheme 17. Expected spin trapped species upon irradiation and follow-up reaction of *A1* with DMPO in the absence and presence of oxygen. In the absence of oxygen *R1* and *R2* will be trapped. In the presence of oxygen additionally the corresponding peroxides *R3* and *R4* can be trapped.

The spectrum of the oxygen-free sample indicates the formation of several radicals. In the range from 350 to 380 mT the spectrum has a similarity to the commonly formed DMPO dimer. Water within the sample could have led to additional radicals, which were not expected.

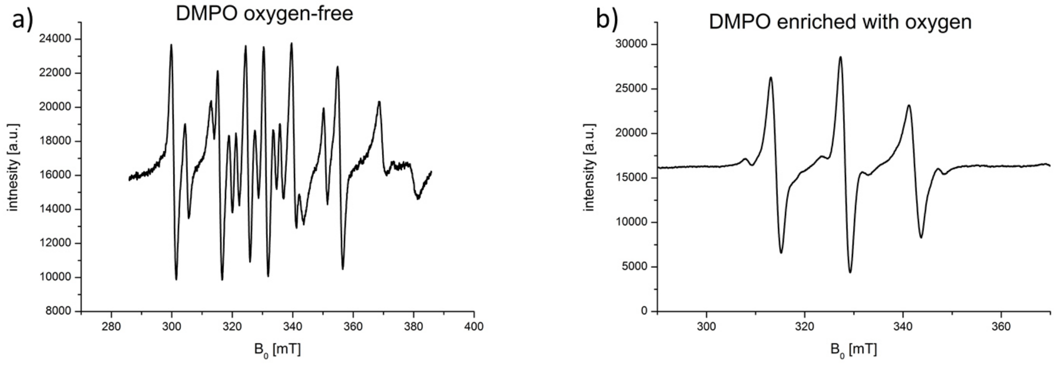

Figure 23 EPR spectrum of a) oxygen-free *A1* sample (25 mM) with DMPO (50 mM) and b) oxygen-saturated *A1* sample (25 mM) with DMPO (50 mM) in acetonitrile.

The spectrum of the oxygen-saturated sample shows a pronounced triplet. The hyperfine splitting of this signal is a_N= 14.25 G. An additional weak signal has an approximate hyperfine splitting of a_N= 15.5 G.

The main signal fits to oxygen centered radicals ***R14*** and ***R15***, as well as to the DMPO dimer. The additional signal indicates a carbon centered radical. For the hyperfine splitting of a_N 15.5 G a phenyl radical is suggested.[92,93] Phenyl radicals can be obtained via decarbonylation and decarboxylation reactions.

4.1.4.2 NMR Spin Trap Experiments

^{1}H- and ^{13}C-NMR experiments of the samples followed subsequently the EPR measurements. The spin trapped radicals themselves should not be visible in the NMR experiments. With NMR measurements paramagnetic substances cannot be detected and they lead to severe line broadening. However, hydrogen-atom abstraction or follow-up reaction may yield diamagnetic products.

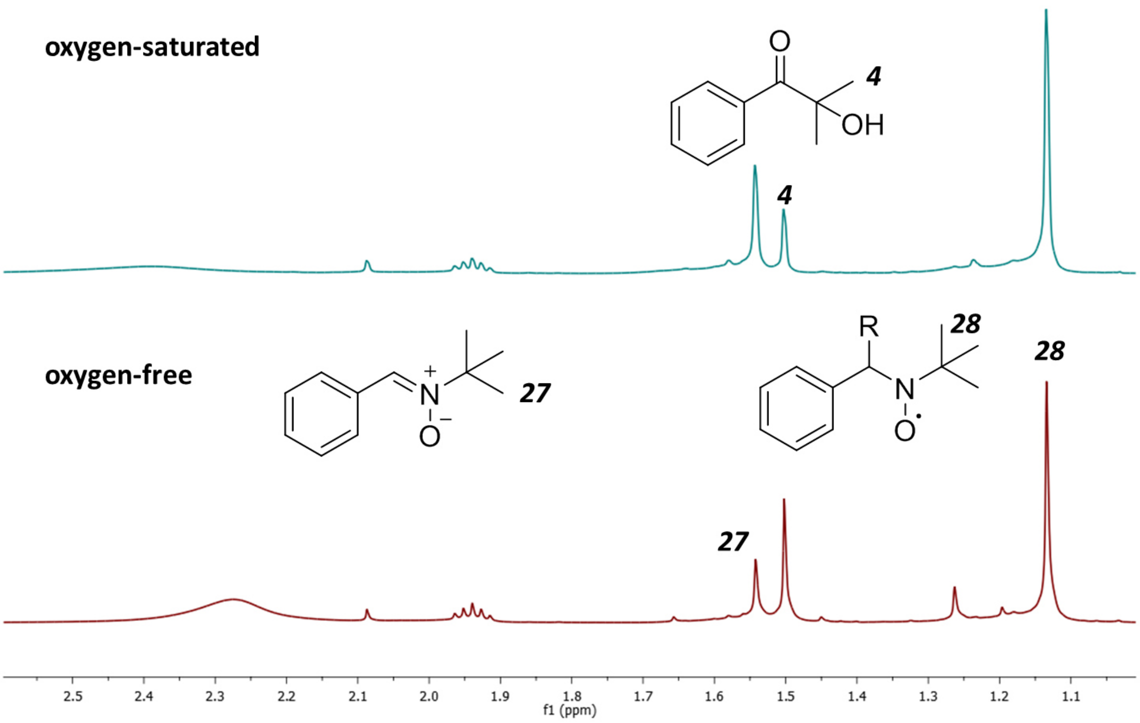

Figure 24. ^{1}H-NMR of irradiated *A1* (25 mM) with PBN (50 mM) in presence and absence of oxygen. The lower trace represents the oxygen-free sample and the upper trace the oxygen-saturated sample. Line broadening through remaining radicals is observed in both spectra.

Both samples contain signals representing benzaldehyde, acetone and the initiator. In the presence of oxygen once more the intensity of the initiator decreases after irradiation. The samples have usually a dark brown color, therefore the penetration of light is reduced and not every initiator molecule cleaves. Also the formed radical can recombine to the initial compound. The methyl groups of PBN ***27*** are detected at 1.54 ppm and the protons of the double bond are observed at 8.3 ppm.

A radical attacks the double bond and through conversion to a single bond the methyl groups of PBN are shifted to a higher field and provide a peak ***28*** at 1.13 ppm. Concerning these methyl groups no difference is observed if oxygen is present or not. The double bond conversion of PBN is responsible for the shift of the methyl groups ***28***.

I also recorded ^{13}C-NMR spectra of the spin trap samples containing PBN and DMPO. The ^{13}C-NMR spectra of the oxygen-free samples and the oxygen containing samples show no difference. Only the spin trap (PBN and DMPO) and ***A1*** are visible there and no further products are observed. The ^{1}H-NMR experiments with DMPO on the other hand revealed differences in dependence of the oxygen concentration

In the absence of oxygen benzaldehyde signals appear, that cannot be found in the oxygen-saturated sample. The spectrum of the oxygen-saturated sample reveals a signal at 9.66 ppm, additionally two triplets ***33*** at 2.44 ppm and ***32*** at 2.24 ppm and a further peak ***31*** at 1.55 ppm. These signals belong to the newly formed 4-methyl-4-nitropentanal ***P15***.

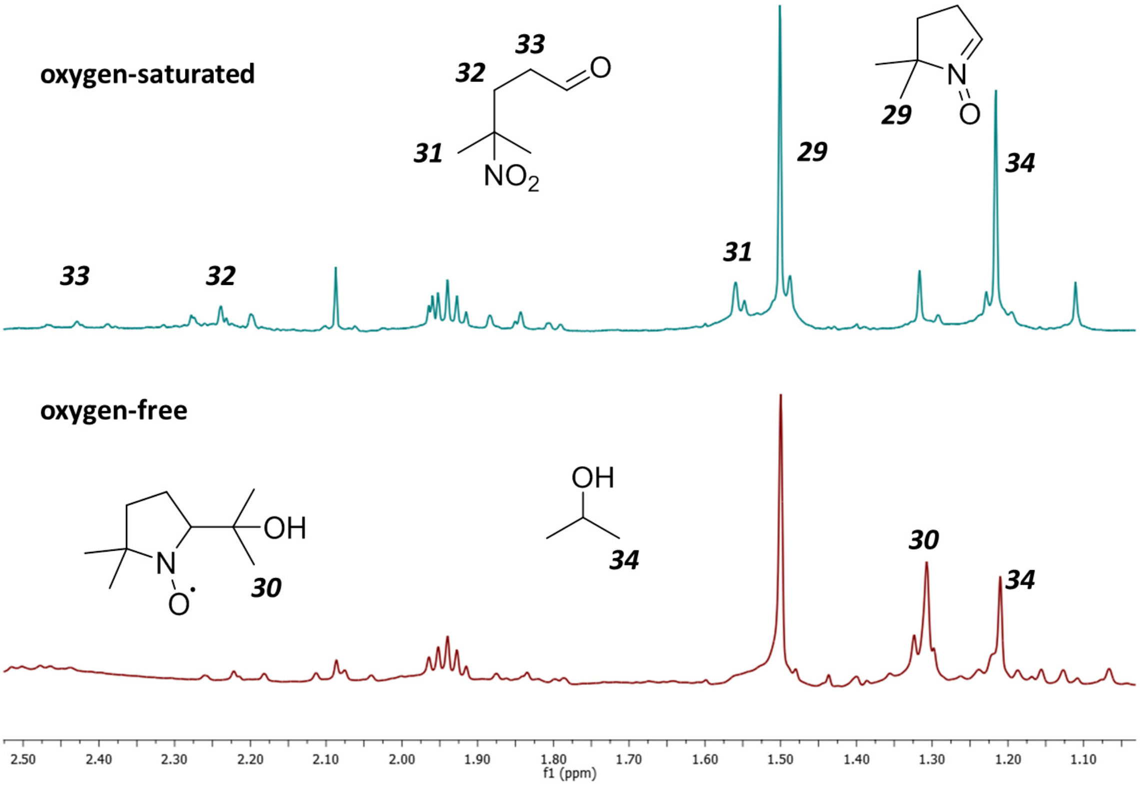

Figure 25. **^{1}H-NMR of irradiated *A1* (25 mM) with DMPO (50 mM) in presence and absence of oxygen. The spectrum of the oxygen-free sample is shown on the bottom and the spectrum of the oxygen-saturated sample is displayed on top.**

Signal ***30*** represents the trapped product of ***R2*** and DMPO. This signal is far more pronounced in the absence of oxygen, than in the presence of oxygen. Acetone is formed in the presence of oxygen in significant amounts, while in the oxygen-free sample only traces are detected. Peak ***34*** indicates the formation of significant amounts of isopropanol ***P17*** in the oxygen-saturated sample, while the amount is significantly decreased in the oxygen-free sample.

The multiplets at 2.22 ppm and 2.07 ppm, which are found in the absence of oxygen, correspond to DMPO's CH_2-groups.

The aromatic region of the NMR spectrum reveals in both samples additional signals at 8.05 ppm and 8.0 ppm. These signals fit to the addition product of ***R1*** to DMPO, as well as benzoyl peroxide.

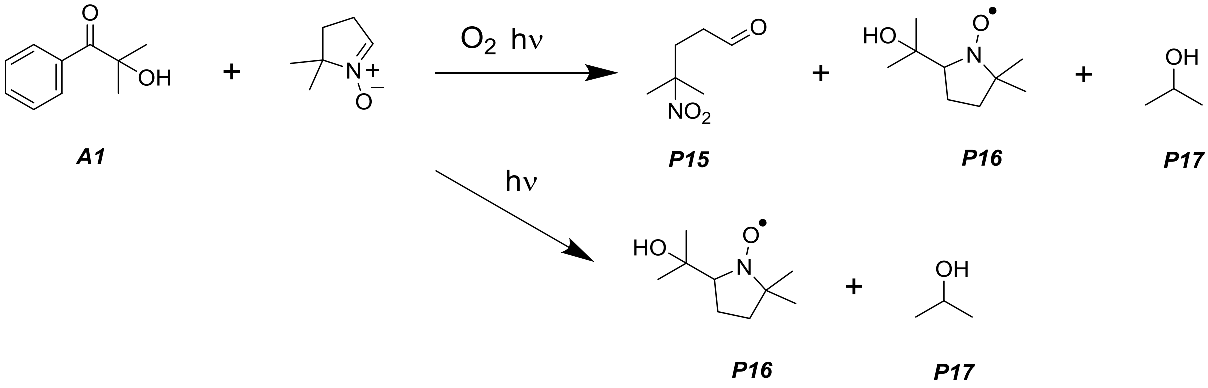

Scheme 18. Additional confirmed products detected by ^{1}H-NMR after the reaction of *A1* with DMPO in the presence and absence of oxygen.

P15 is a decomposition product of DMPO in the presence of oxygen, which indicates that DMPO is not the ideal spin trap for oxygen-saturated samples.

4.1.4.3 TEMPO trapped NMR Experiments

Similar to spin traps, TEMPO should act as a radical scavenger in oxygen dependent ^{1}H- and ^{13}C-NMR experiments of ***A1***.

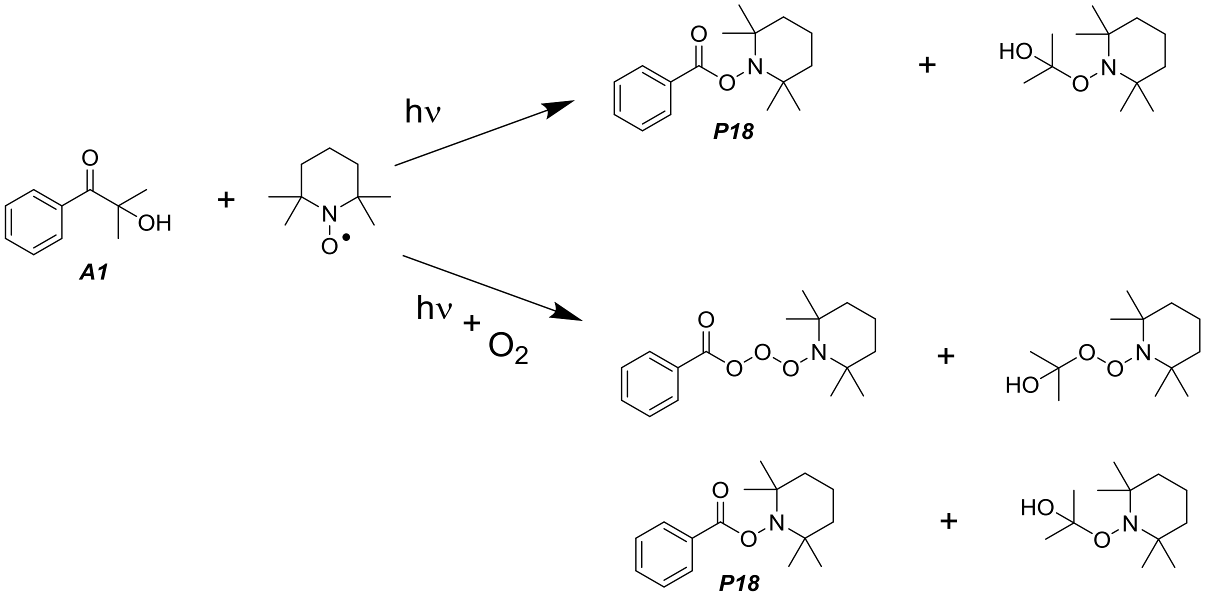

Scheme 19. Additional expected products by using TEMPO as a radical scavenger in the absence and presence of light upon UV irradiation of *A1*.

TEMPO is an additional reaction partner of the formed radicals and the main expected products are displayed in **Scheme 19**. The expectations were not fully met, as NMR experiments led to partly different interesting results.

The reference spectrum shows only signals belonging to the initiator even though TEMPO is present. TEMPO is a stable free-radical and therefore not visible in NMR and the presence of radicals causes line broadening. This effect occurs as radicals reduce the relaxation time.

After irradiation, both samples contain benzaldehyde, which is determined by the typical peaks at 10.0 ppm and 7.9 ppm. The spectra show strong acetone signal intensities with approximately doubled signal intensity in the oxygen-saturated sample, compared to the oxygen-free sample. This has two reasons; First the presence of oxygen. Oxygen-saturated samples without TEMPO have by 50-70 % increased acetone signal intensities, compared to oxygen-free samples. Second; TEMPO seems to support the acetone formation as it is able to abstract a hydrogen-atom.[94,95]

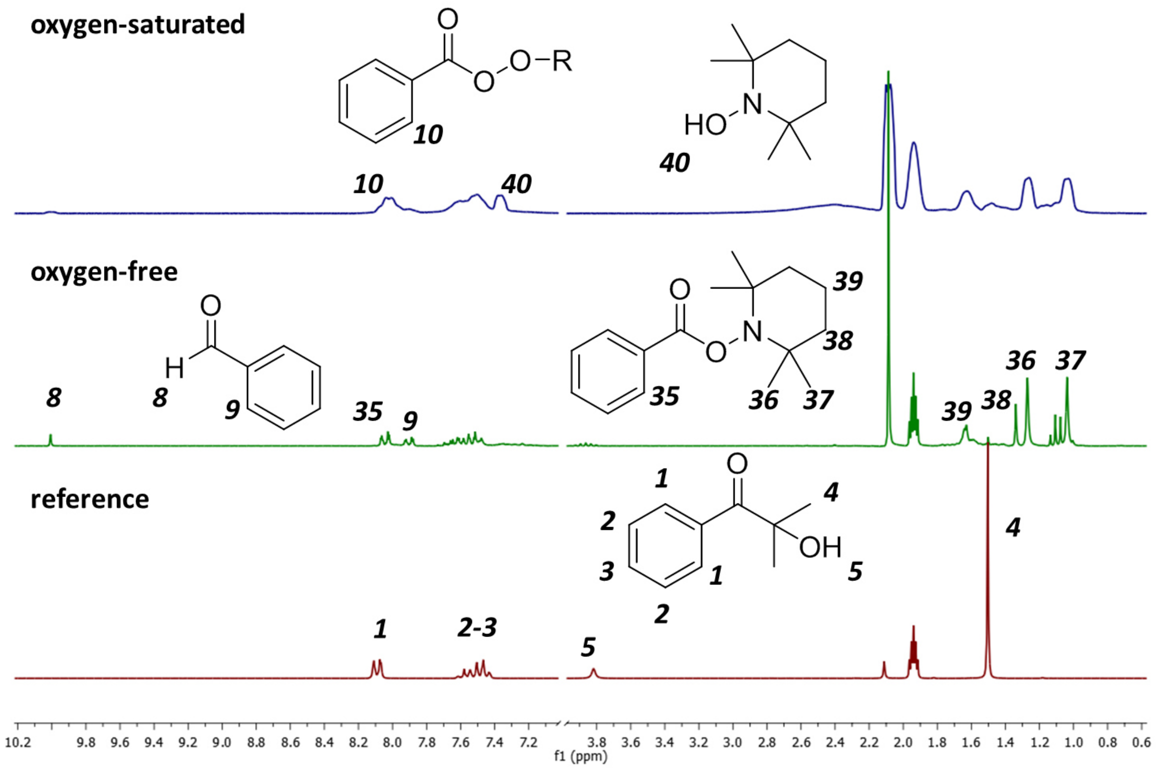

Figure 26. **^{1}H-NMR spectra of *A1* (10 mM) with TEMPO (20 mM) in the presence and absence of oxygen. The lower trace displays the non-irradiated sample and serves as reference. The middle spectrum shows the oxygen-free sample after irradiation and the spectrum on top represents the oxygen-saturated sample after irradiation.**

The spectrum of the oxygen-free sample shows again pinacol ***P2*** signals. After irradiation and in the presence of TEMPO, signals of the initiator are not found. This indicates that the back reaction is less favored in the presence of TEMPO. TEMPO seems to be more reactive towards ***A1***, than the spin traps PBN and DMPO. The long irradiation time ensures the cleavage of the initiator. Bleaching of the sample occurs as TEMPO is consumed.

In the oxygen-free sample signals are present, which belong to 2,2,6,6-tetramethylpiperidin-1-yl benzoate ***P18***. This is the termination product of ***R1*** and TEMPO. The aromatic signal ***35*** at 8.05 ppm of this compound is up field shifted, compared to the initiator. The aliphatic signals ***36-39*** belong to the TEMPO derived part of ***P18***. These signals are not influenced by the group, which adds to TEMPO's oxygen. Predictions suggest that signal ***36*** and ***37*** have the same shift, but conformation effects lead to the observed splitting. The integrals of both signals are the same. The signal ratios of the assigned peaks fit to TEMPO derived products. Signals ***36*** and ***38*** from the TEMPO substituent overlap in the oxygen-saturated sample, through line broadening.

2,2,6,6-tetramethylpiperidin-1-ol ***P19*** is a new product, which is formed in the presence of oxygen. Signal ***40*** at 7.35 ppm belongs to its hydroxy group and in the absence of oxygen only traces of this signal can be found.

The spectrum of the oxygen-saturated sample reveals a signal at 8.0 ppm belonging to a benzoyl peroxide ***P10***. The results from ^{1}H-NMR experiments are insufficient to determine the precise structure of the peroxide; therefore further ^{13}C-NMR experiments were performed.

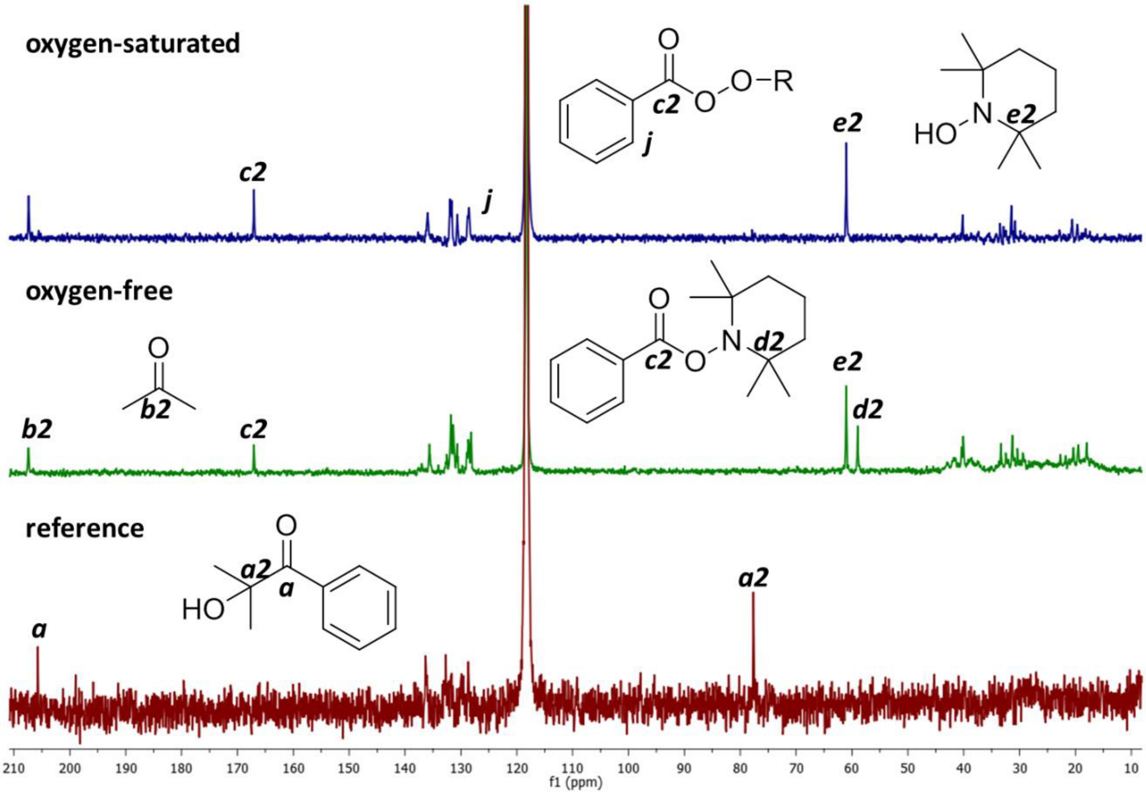

Figure 27. ^{13}C-NMR spectra of *A1* (100 mM) with TEMPO (200 mM) in the presence and absence of oxygen. The lower trace displays the non-irradiated sample. The middle spectrum shows the oxygen-free sample the spectrum on top represents the oxygen-saturated sample, both after irradiation.

Signal ***a*** and ***a2*** in the non-irradiated reference spectrum belong to the parent initiator. After irradiation these signals disappear, which indicates that follow-up reactions are preferred, and this finding is in line with the ^{1}H-NMR results.

In the absence and in the presence of oxygen the carbonyl carbon of acetone provides a signal at 207.4 ppm. There is an additional carbonyl signal ***c2*** at 167.0 ppm. This signal fits to ***P18*** and to ***P10***. In the absence of oxygen the assignment to ***P18*** is supported by the quaternary carbon ***d2*** at 58.9 ppm. This signal is not detected in the presence of oxygen. Therefore it is more likely that signal ***c2***, in the presence of oxygen, belongs to ***P10***. The formation of peroxides is also indicated by ^{1}H-NMR experiments.

Signal ***e2*** at 61.0 ppm peak represents the quaternary carbon of ***P19*** and is found in both samples, but in the oxygen-saturated sample it is more pronounced.

The combination of the ^{1}H- and ^{13}C-NMR results, provide strong evidences, that the products displayed in **Scheme 20** are formed.

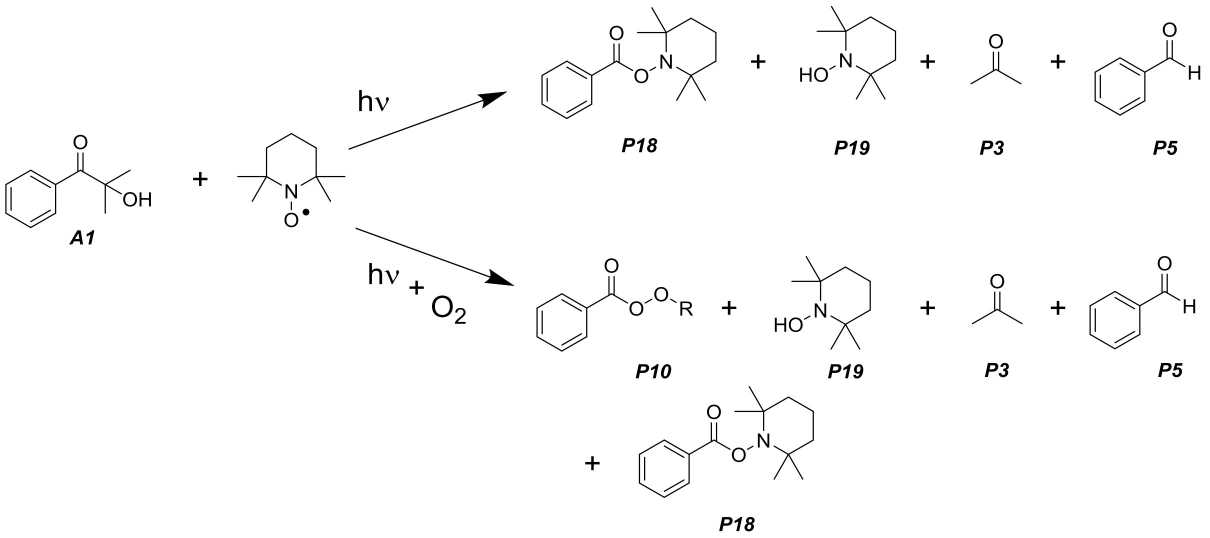

Scheme 20. Overview of products, which I detect in ^{1}H- and ^{13}C-NMR spectra after irradiation of *A1* with TEMPO in the presence or absence of oxygen.

In accordance with the expectations, TEMPO scavenges ***R1***, in the absence of oxygen. In the presence of oxygen signals representing ***P10*** appear, but its reaction with TEMPO cannot be confirmed.

There is no evidence that TEMPO scavenges ***R2*** ,but it abstracts hydrogen-atoms.[94,95] This additional hydrogen-atom abstraction leads to a significant higher amount of acetone, which is represented in the high intensities of the acetone signals.

4.1.5 Mass Spectrometry

NMR based structure elucidation of similar products is not always possible. Therefore, and to confirm NMR results high resolution mass spectrometry experiments with matrix assisted laser desorption ionization (MALDI) and electro spray ionization (ESI) were performed. For the mass analysis MALDI uses time of flight (MALDI-TOF) and ESI uses an orbitrap.

Sample preparation is the same as for post irradiation NMR experiments. The samples contain acetonitrile as solvent, 10 mM initiator and defined amounts of oxygen. Additional probes included each one of the following compounds: butyl acrylate, TEMPO, PBN or DMPO.

The MALDI-TOF experiments were not successful. The ionization source is not suitable for photo active compounds. There is no oxygen dependent difference and mainly decomposition products are observed. Additional polymerization experiments followed by MALDI-TOF-MS should minimize the decomposition problem.

10 mM initiator were directly dissolved in methyl methacrylate and irradiated for 10 s in the absence or presence of oxygen. This procedure leads to polymer dissolved in monomer. After the addition of n-hexane the polymer precipitated. The filtered and dried polymer was then dissolved in acetonitrile and analyzed by MALDI-TOF-MS.

Both samples, oxygen-free and oxygen-saturated, formed polymer, but the mass analysis revealed no differences. This indicates that in the presence of oxygen part of the initiator reacts with oxygen and the other part with the monomer. The distribution between them depends on the addition rate constants.

ESI-MS experiments on the other hand worked very well. Here I put the focus on the initiator itself and prepared 10 mM initiator probes in acetonitrile in the absence or in the presence of oxygen.

ESI-MS measurements were carried out in the negative, the positive and the positive mode with activation. Formic acid was added as puffer. The positively charged pseudo molecule ions are formed by protonation or with ammonium. The negative ions are formed either by deprotonation or by addition of an electron.

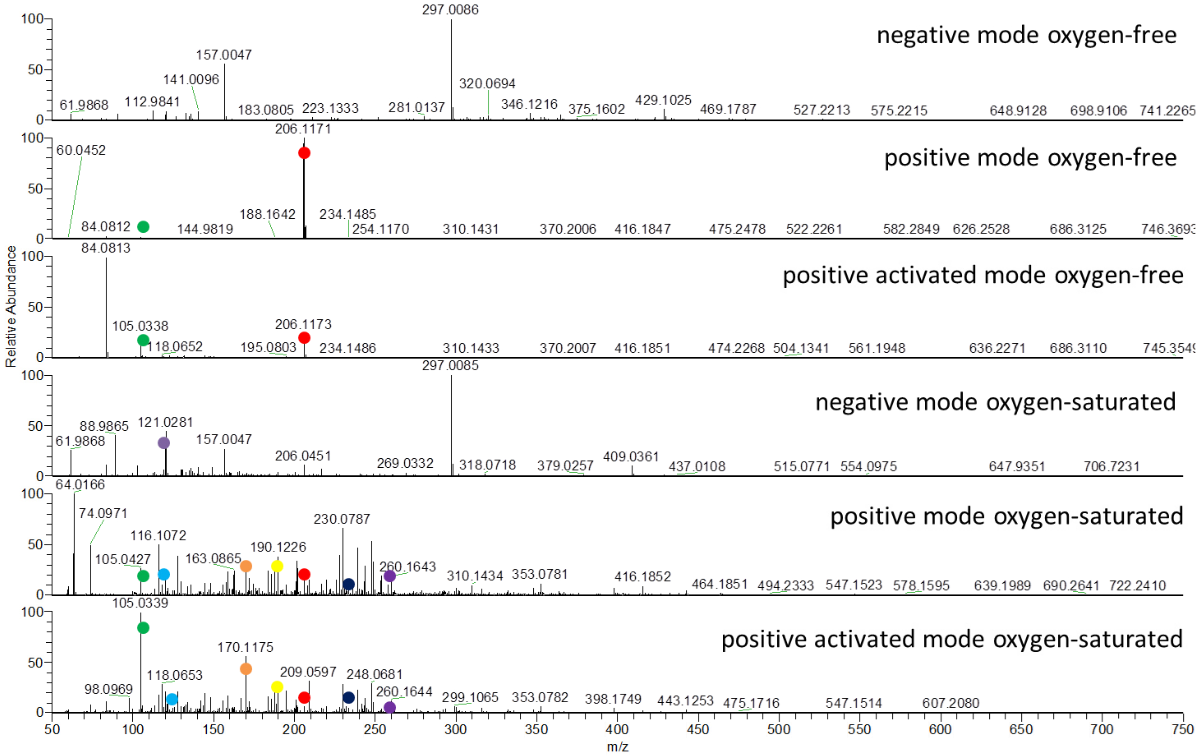

Figure 28. ESI-MS results of *A1* after irradiation. The lower three traces represent the oxygen-saturated sample. The upper three traces display the spectra of the oxygen-free sample. For each sample experiments in the negative, the positive and the positive activated mode were performed. Assigned signals are marked and the structures are displayed in Scheme 21.

The negative mode leads to fewer fragmentation products, than the positive. In the absence of oxygen fewer signals, than in the presence of oxygen appear. In the negative mode the most dominant peaks are at m/z 141, 157 and 297. Those signals are probably caused by matrix effects as I detect the identical signals in the BAPO spectra (see chapter 5 section 5.1.7).

The most interesting signal in the negative mode is found at m/z 121. This signal belongs to benzoate and is found in large abundance in the presence of oxygen. The spectrum of the positive mode contains the corresponding signal at m/z 122.

The peak with the highest abundance in the positive mode and in the absence of oxygen appears at m/z 206 (red). This peak corresponds to the initiator ionized with ammonium. The positive mode spectrum in the presence of oxygen contains the same signal, but in a much lower quantity. This fits to the NMR findings, of the decrease of initiator signal intensities, when the oxygen concentration is increased.

The signal at m/z 105 (green), which belongs to the benzoyl cation, has a higher abundance in the presence of oxygen, than in the absence of oxygen. This species is most likely derived from benzaldehyde. This result supports the previously discussed oxygen dependent NMR findings of benzaldehyde.

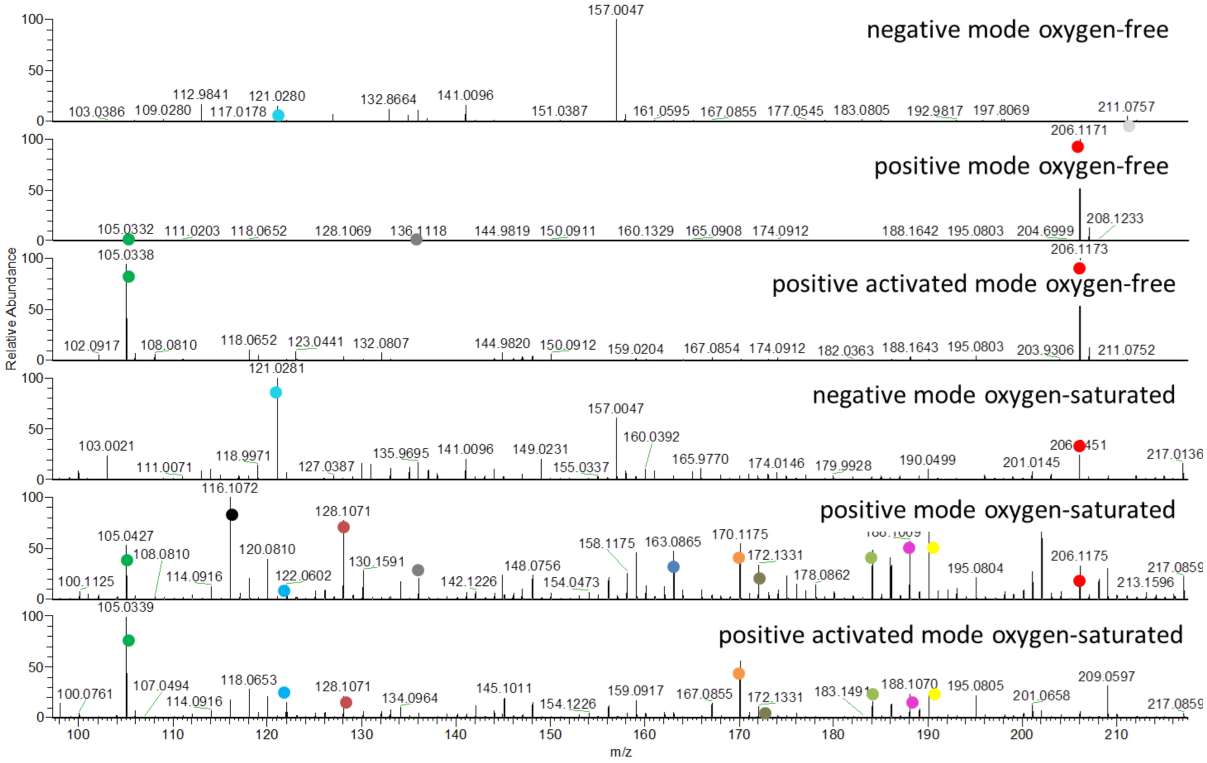

Figure 29. Enlarged section of the ESI-MS results of *A1* after irradiation. The lower three traces represent the oxygen-saturated sample. The upper three traces display the spectra of the oxygen-free sample. For each sample experiments in the negative, the positive and the positive activated mode were performed. Assigned signals are marked and the structures are displayed in Scheme 21.

In the presence of oxygen the signal at m/z 128 represents hydroperoxybenzene with ammonium. To form this compound intermediate phenyl radicals are required. Additional hints for phenyl radical intermediates are 1-1’-biphenyl (m/z 172), benzophenone (m/z 183) and oxydibenzene (m/z 188). The formation of hydroperoxybenzene fits to the post irradiation ^{1}H-NMR spectra in the presence of oxygen, where corresponding signals at 6.8 ppm and 6.9 ppm are found.

The additional peroxide species, 2(phenylperoxy)propan-2-ol, has a peak at m/z 170. NMR experiments revealed only the formation of ***P14***, but here the exact species was determined. The signal at m/z 260 confirms the already by NMR experiments indicated formation of dibenzoylperoxide ***P1***.

The interesting peak at m/z 136 belongs to 2-phenylpropan-2-ol ***P9***, which was observed in traces in ^{1}H-NMR spectra. Comparable to NMR measurements the signal intensities of this compound are increased in the presence of oxygen.

The signal at m/z 116 represents cyclohexanone and it has higher abundance the presence of oxygen, than in the absence of oxygen. Only in the presence of oxygen 3-oxo-3-phenylpropanenitrile at m/z 163 is found, which seems to be a product of the solvent and ***R1***.

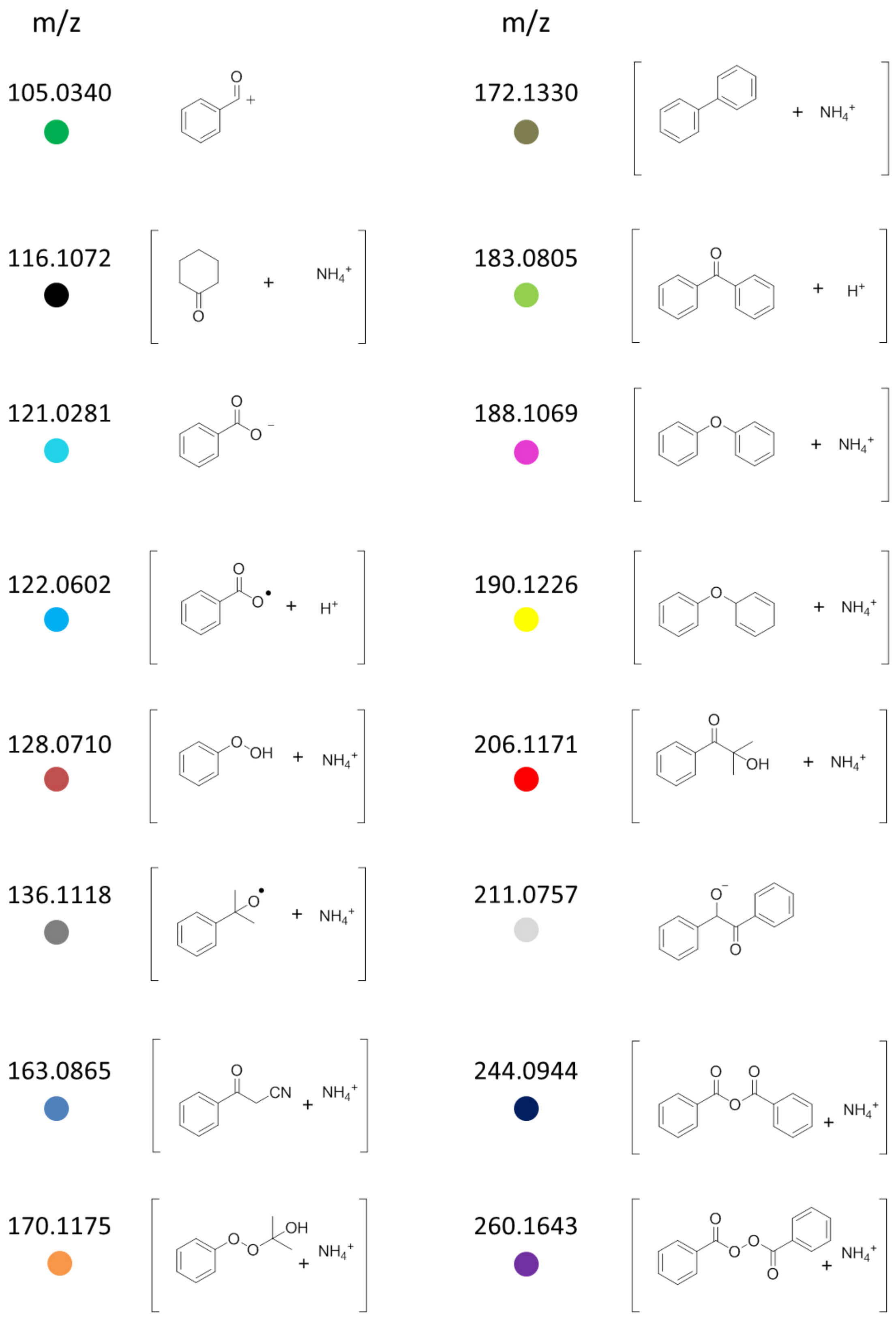

Scheme 21. Overview of the marks indicated in the MS traces of Figure 28 and Figure 29 and their structure assignment. Compounds in brackets represent pseudo molecules with ammonium or a proton.

4.1.6 Kinetic Simulations with Copasi®

Kinetic simulations with published data help to understand possible reaction mechanisms and to estimate amounts of formed products. For simple reactions with few parameters the results are fitting very well to experimental data. Oxygen containing reaction systems are rather complex and therefore simplification is required. Here I show the impact of oxygen on the initiation step and on a model polymerization.

The following reaction scheme with the rate constants displayed in **Table 1** represents the basis of the simulations.

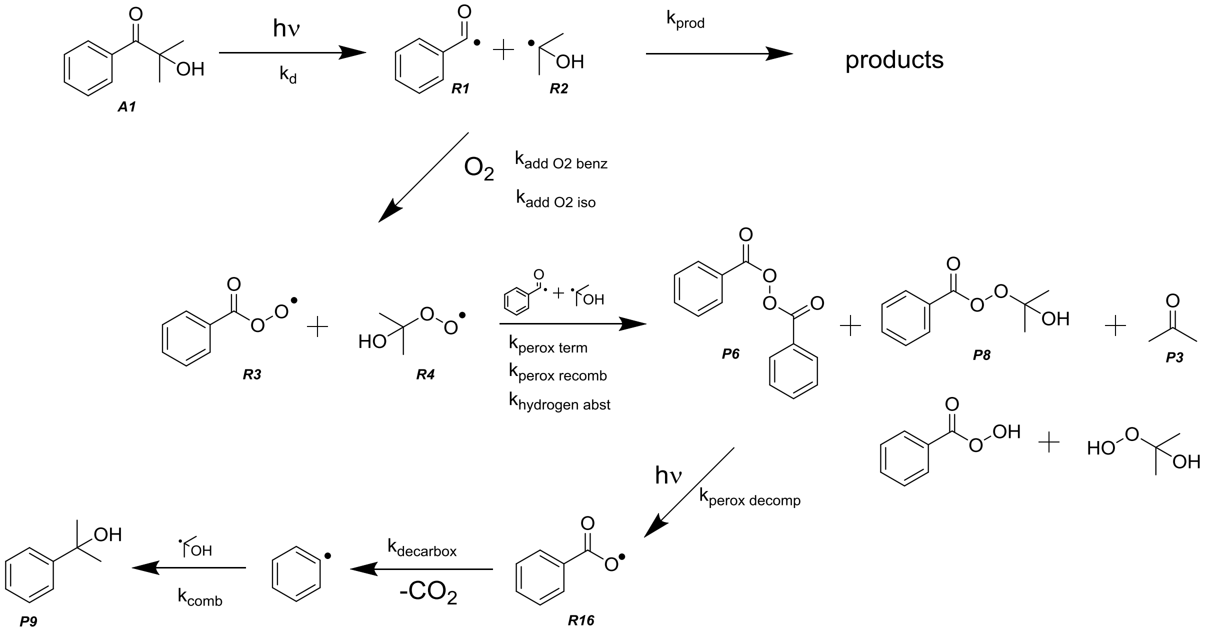

Scheme 22. Overview of reaction steps used for kinetic simulations. In the absence of oxygen only the initiator, the intermediate radicals and the products are modelled. In the presence of oxygen, oxygen addition is added. Peroxyl radical reactions are estimated with peroxyl radical recombination and -termination and an additional hydrogen-atom abstraction. The simulation displayed in Figure 30d includes a peroxide decomposition term. In this model light induced decomposition succeeds peroxide formation, followed by decarboxylation and finally the formation of 2-phenylpropan-2-ol *P9*.

Table 1. rate constants used for simulations.

rate constant	value	unit	reference	rate constant	value	unit	reference
k_d	8.3×10^5	s^{-1}	96,34,97	$k_{hydrogen\ abstr}$	1.8×10^7	$M^{-1}\ s^{-1}$	96,98,29,99,100
k_{prod}	$\sim 2 \times 10^7$	$M^{-1}\ s^{-1}$	34,97,53	$k_{perox\ term}$	$\sim 6 \times 10^7$	$M^{-1}\ s^{-1}$	101,60,61
$k_{add\ O_2\ benz}$	3.0×10^9	$M^{-1}\ s^{-1}$	34,102,29,44	$k_{perox\ decomp}$	1.0×10^5	s^{-1}	103,101,104,61
$k_{add\ O_2\ iso}$	6.6×10^9	$M^{-1}\ s^{-1}$	34,102,29,44	$k_{decarbox}$	1.0×10^4	s^{-1}	105,106,103
$k_{add\ BA\ benz}$	2.5×10^5	$M^{-1}\ s^{-1}$	34,102,29	k_{comb}	$\sim 2 \times 10^7$	$M^{-1}\ s^{-1}$	100,107
$k_{add\ BA\ iso}$	1.3×10^7	$M^{-1}\ s^{-1}$	34,102,29	k_{prop}	1000	$M^{-1}\ s^{-1}$	108,45,60,61

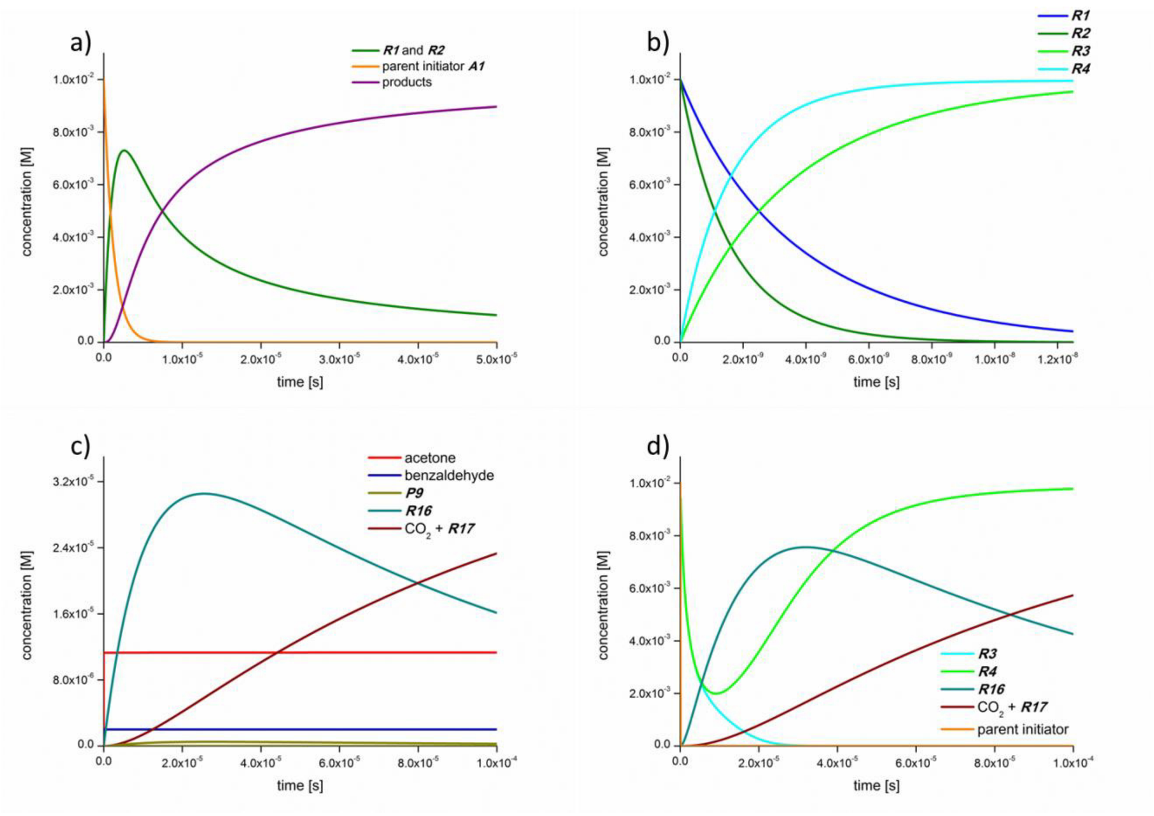

Figure 30. Kinetic simulations of *A1*. Concentration vs. time plots with various parameters and different selected compounds. a) decomposition of the initiator, the formation of benzoyl *R1* and propan-2-ol-2-yl *R2* radicals, and the formation of products in the absence of oxygen. b) decay of *R1* and *R2* and formation of benzoperoxyl *R3* and propan-2-ol-2-peroxyl *R4* through the addition of oxygen. c) Selected compounds after first addition of oxygen to *R1* and *R2*. d) Inclusion of a peroxide decomposition term. Initiator concentration is 0.01 M and the oxygen concentration in simulation a is 0 M and is 0.1 M in b, c and d.

Figure 30a shows the concentration decay of the initiator upon irradiation. The graph is a simplified concentration vs. time plot, which includes three different processes; First decomposition of the initiator; Second formation of intermediate radicals and third product formation. Through the decomposition of the initiator, ***R1*** and ***R2*** are formed. These radicals can react in various ways and form products like acetone, benzaldehyde and radical recombination products (**Scheme 22**).

In the presence of oxygen the time scale changes massively as the addition rates of oxygen to ***R1*** and ***R2*** are about two orders of magnitudes higher than the product formation out of the radicals. In the presence of oxygen the life time of the free-radicals is at the ns scale. **Figure 30b** displays the addition of oxygen to ***R1*** and ***R2***, where we can see that the addition of oxygen to ***R2*** is approximately two times faster, than the addition of oxygen to ***R1***.

The simulations become complex, when a focus is put on follow-up products. The simulation displayed in **Figure 30c** includes peroxyl radical termination and decomposition reactions. In this simulation the concentration of ***R16*** decreases and the concentrations of the phenyl radical ***R17*** and CO_2 increase. This model leads to traces of ***P9*** and an additional hydrogen-atom abstraction reaction causes the amount of acetone to rise.

The simulation displayed in **Figure 30d** contains an additional peroxide decomposition step, causing higher amounts of ***R2***, which can be available for other reactions. The maximum transient concentration of ***R16*** is only 30 µM in the simulation displayed in **Figure 30c** and here it is about 8 mM.

The simulations show that a huge diversity of products can be formed upon irradiation and in the presence of oxygen, but only traces of them are obtained, if no peroxide decomposition is included. The NMR and mass spectrometry experiments revealed that some products like acetone are formed in higher amounts in the presence of oxygen, which fits to simulations were peroxide decomposition was included.

Additional simulations included the decarbonylation of benzoyl radicals, with the rate of approximately of ~ 1 s^{-1}. The decarbonylation is orders of magnitudes slower than other reactions in the simulations and therefore this process is not observed.[109,110,111] However the quantitative decarbonylation is possible in the presence of a catalytic converters, but those were not applied in this system.[112]

The addition of initiator radicals to monomer in the absence and presence of oxygen is also very interesting. The simulations show a strong influence of the oxygen concentration. The following scheme represents the reactions, which were used for the simulations. The applied rate constants are summarized in **Table 1**. I chose the propagation rate constant for the polymerization k_{prop}= 1000 M^{-1} s^{-1} as literature values are between a couple of hundreds and several thousand M^{-1} s^{-1} depending on the system. [45,60,108,113]

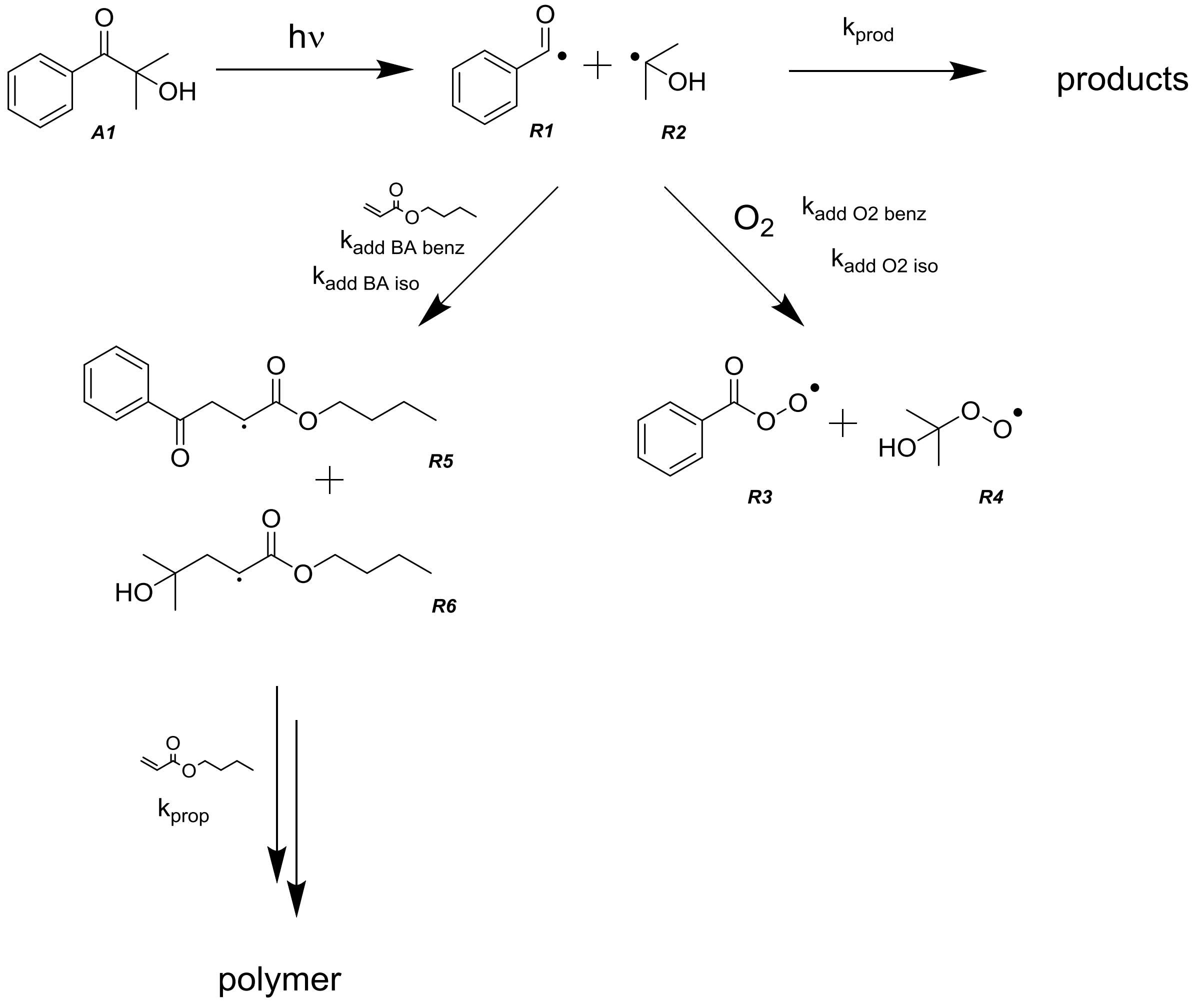

Scheme 23. Overview of reactions used for the simulations. Starting with the light induced cleavage of the initiator, this is followed by product formation of *R1* and *R2*. Addition of the radicals to the monomer and propagation reactions. In the presence of oxygen addition of oxygen *R1* and *R2*.

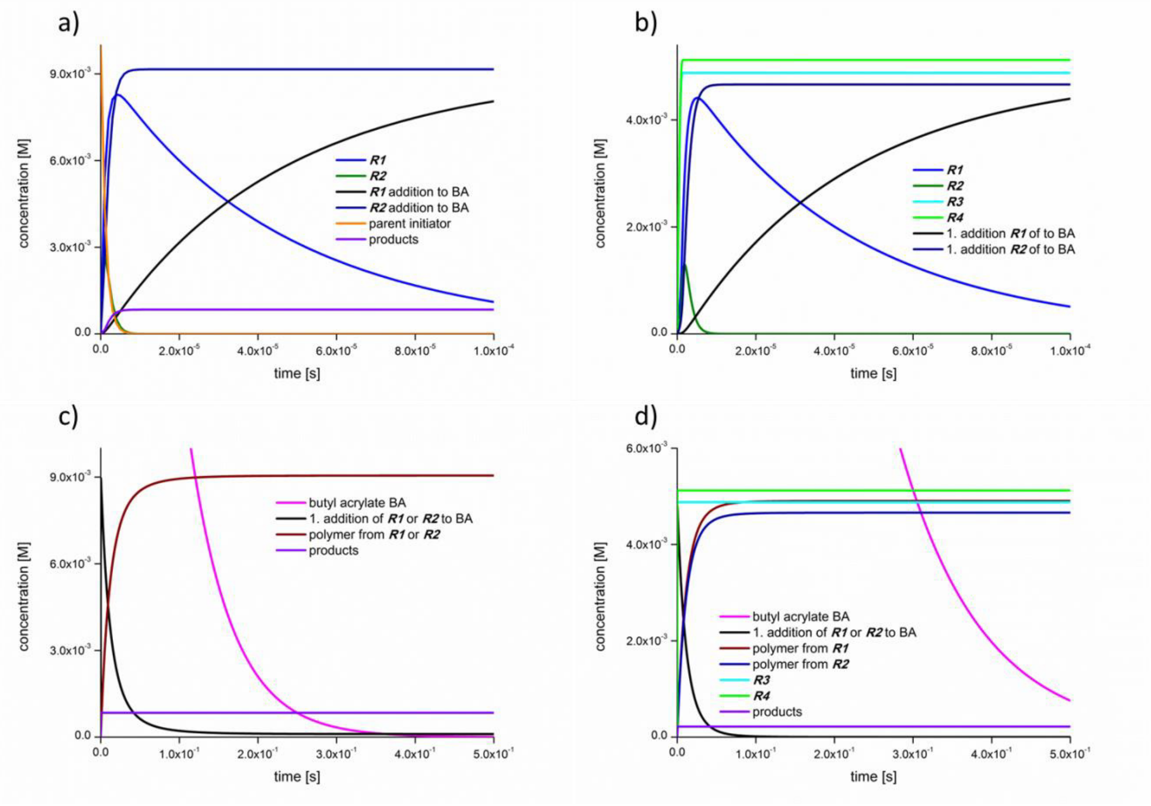

Figure 31. Kinetic simulations of the reaction of *A1* with butyl acrylate in the absence and presence of oxygen. 0.01 M of the initiator are used; 0.1 M of butyl acrylate and 0.01 M of oxygen when present. a) shows the first addition of benzoyl *R1* and propan-2-ol-2-yl *R2* radical to butyl acrylate in the absence of oxygen. b) displays the first addition of *R1* and *R2* to butyl acrylate in the presence of oxygen. c) represents the propagation reaction for the formation of poly butyl acrylate in the absence of oxygen. d) shows the formation of polymer in the presence of oxygen.

In the absence of oxygen fast addition of ***R2*** to butyl acrylate and the by two orders of magnitudes slower addition of ***R1*** to the monomer occur. The concentration of the initiator decreases, while follow-up products are formed.

The addition rate of ***R1*** to oxygen is approximately four and the addition rate of ***R2*** to oxygen is approximately two orders of magnitudes higher, compared to the addition rates to butyl acrylate. These reactions were simulated with two oxygen concentrations, 10 mM and 100 mM respectively. The simulation with 100 mM oxygen contains mainly peroxyl radicals and only traces of first addition products.

I chose 10 mM oxygen, because at this concentration the ratio between initiator and oxygen is 1:1 and the ratio between initiator derived radicals and oxygen is 2:1. Additionally the concentration of 10 mM oxygen corresponds with the oxygen saturation of acetonitrile under 1 atm oxygen partial pressure, which is comparable to the oxygen-saturated samples in this thesis.[114,115] The simulations with 10 mM oxygen fit very well to the experimental results of samples under atmospheric conditions.

The simulation containing 10 mM oxygen is displayed in **Figure 31b** and shows bigger amounts of additional products. First mainly the peroxyl radicals are formed until the oxygen is consumed and then ***R1*** and ***R2*** attack primarily the monomer.

About 50 % of the initiator reacted with oxygen, while the rest formed addition products with the acrylate or formed benzaldehyde and acetone. ***R2*** reacts faster with both oxygen and monomer, than ***R1*** does.

In the absence of oxygen an additional propagation step enables to follow the simulated polymerization. The polymerization stops after ~ 0.4 s when the butyl acrylate is consumed and the resulting polymer is formed by equal amounts of ***R1*** and ***R2***.

In the presence of 10 mM oxygen the first main products are again peroxyl radicals ***R3*** and ***R4***. The first addition and then the polymerization succeed the consumption of oxygen. The polymerization stops ~ 0.8 s after initiation, which is ~ 0.4 s later, than in the absence of oxygen. There is a difference in the amount of polymer created from ***R1*** and ***R2*** in the presence of oxygen. The slower ***R1*** initiates more poly butyl acrylate chains than the faster ***R2***, because ***R2*** reacts faster with oxygen and therefore a higher amount is already consumed before it can initiate the polymerization.

No polymerization occurs in the presence of 100 mM oxygen and the main products are ***R3*** and ***R4*** and only traces of additional products. The oxygen concentration decreases during this simulation to 80 mM.

The simulations fit to my experimental data, as in the absence of oxygen double bond conversion occurred and in the presence of higher amounts butyl acrylate even full curing. The results are the same in the presence of atmospheric amounts of oxygen and in the absence of oxygen, except the additional peroxide based products in the presence of oxygen. Oxygen-saturated samples on the other hand showed no double bond conversion or polymerization. This also corresponds with published simulations on the oxygen inhibition on methyl methacrylate polymerizations.[49]

4.1.7 Oxygen Measurement

I measured the oxygen concentration in deuterated acetonitrile with an optical oxygen sensor. The output of the sensor is a function of the partial pressure, which can be converted into molar values by applying Henry's law with the corresponding Henry coefficient k_H^{px}= 203.8 x 10^6 Pa. [115,116]

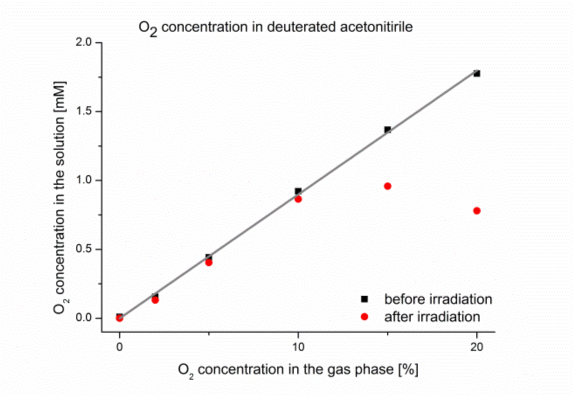

Figure 32. Oxygen concentration in deuterated acetonitrile with *A1* (10 mM) before and after irradiation.

Figure 32 displays the molar oxygen concentration in deuterated acetonitrile as a function of the oxygen partial pressure in the gas phase. The x-axis represents the oxygen concentration in vol. % of the gas phase, while the y-axis shows the calculated molar values in the liquid phase. The used oxygen sensor works well in the range from 0 to 20 vol. % oxygen. Above 20 vol. % the sensor becomes inaccurate.

After irradiation the oxygen concentration at lower given oxygen concentrations decreases for about 10 % and at higher concentrations up to 56 %. At higher concentrations oxygen consumption is observed too, but accurate values cannot be given as it is outside of the sensors operation range.

1.8 mM oxygen are dissolved in deuterated acetonitrile under atmospheric conditions, which is similar to published data of oxygen solubility in acetonitrile.[115,116,117] The slight difference to published data can be caused by the use of deuterated solvent.

4.2 Discussion

2-hydroxy-2-methyl-1-phenyl-propan-1-one ***A1*** is a well-studied photoinitiator, which I used as a model compound to study oxygen effects on photoinitiation processes. CIDNP results show products formed via a radical pathway, while NMR experiments provide additional information about further reaction products. Mass spectrometry experiments confirmed NMR results and additional expected species were detected with them.

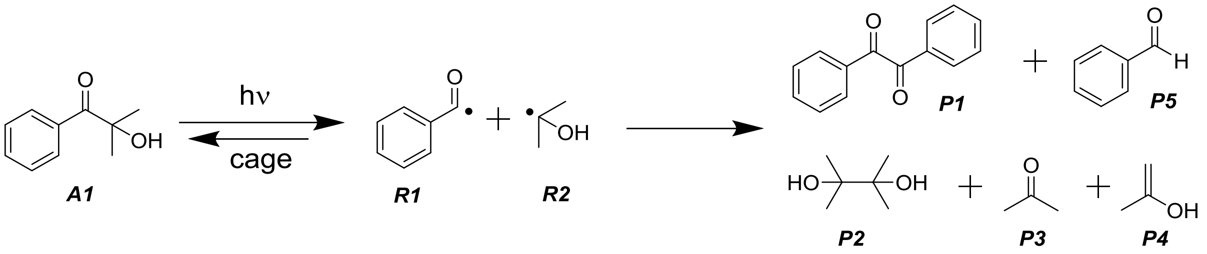

Scheme 24. Overview of products formed in the absence of oxygen. I can confirm these products by NMR ^{1}H-CIDNP and mass spectrometry.

The results for ***A1*** in the absence of oxygen correspond with published data.[30,97,118] CIDNP experiments revealed the expected products displayed in **Scheme 24**. The recombination of benzoyl radicals ***R1*** to dibenzoyl ***P1*** was not detected with CIDNP, but this product was proven by ^{13}C-NMR and confirmed by ESI-MS. Propen-2-ol ***P4*** on the other hand is only found in CIDNP spectra, as acetone is the preferred tautomeric form.

Through the formation of new products in the presence of oxygen, also the compound ratios changed. In the presence of oxygen the signal intensities of acetone increase and the signal intensities belonging to the parent initiator decrease.

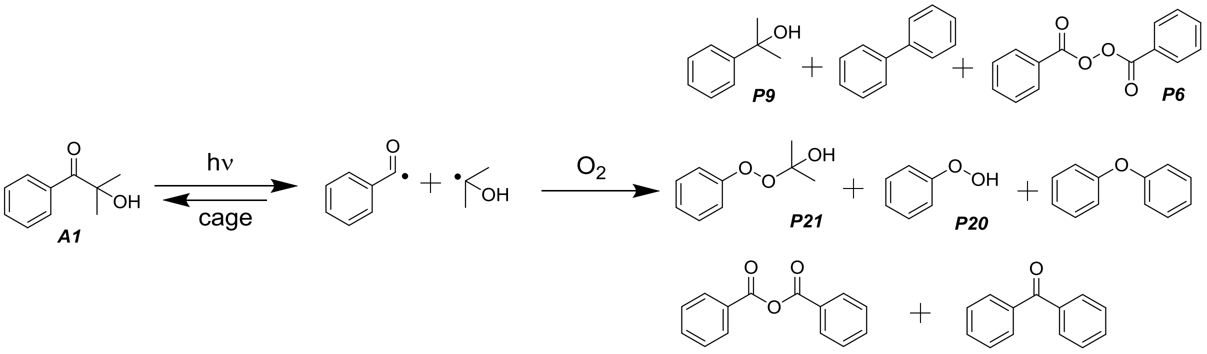

Scheme 25 Additional products formed in the presence of oxygen.

The ^{1}H-NMR signals for ***P9*** significantly increase in the presence of oxygen and this compound is also detected with mass spectrometry. The large signal intensity in the presence of oxygen indicates a different pathway for the formation of ***P9***. The benzoyl radical can undergo a decarbonylation, which is reported but also stated to be rather unlikely. The rate for benzoyl decarbonylation is in the order of 1 s^{-1}, while the decarboxylation rate of ***R16*** is about four orders of magnitudes faster.[111,110,109] When oxygen is present the corresponding peroxyl radicals ***R3*** and ***R4*** are formed. Those can recombine with other radicals or abstract a proton to form hydroperoxides.

Under UV light peroxides, like dibenzoyl peroxide ***P6***, decompose and in this system the benzoyloxy radical ***R16*** is created. This radical undergoes a decarboxylation, leading to the phenyl radical.[87,105,119,33] Following the suggested pathway displayed in **Scheme 26** benzoic acid could be formed via a hydrogen-atom abstraction. Because of signal overlapping the determination of benzoic acid by NMR is not possible. ESI-MS results show benzoate but it is not known if it is present in the sample or if it is formed through the ionization.

The intermediate phenyl radical is also difficult to observe, however Hutchings et al. reported that they trapped the phenyl radical with PBN as well as ***R16***.[87] The detection of the phenyl radical was not successful and as our system differs from Hutchings, I might have observed ***R3*** instead of ***R16***. They state the hyperfine coupling constant a_H= 1.8 G while, my result for the PBN trapped species is a_H= 1.93 G.

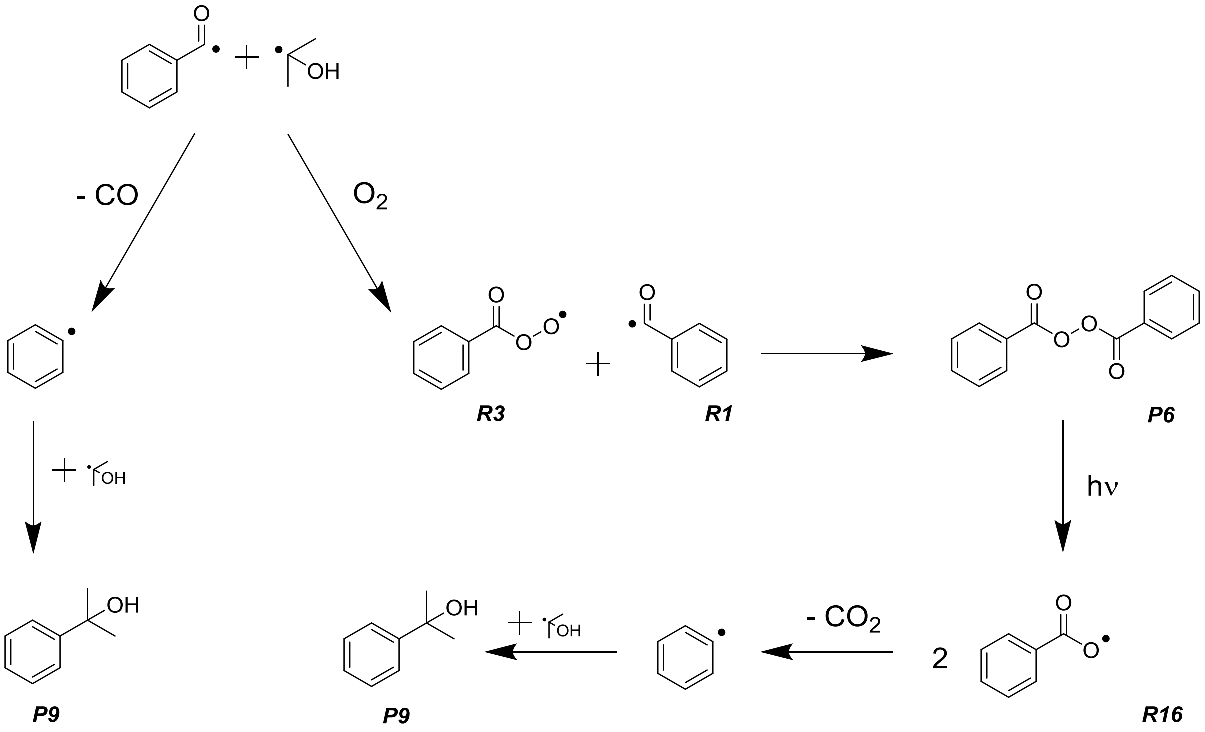

Scheme 26. Suggested pathway of the formation of 2-phenylpropan-2-ol *P9* in the presence and absence of oxygen.

The suggested pathway offers in the presence of oxygen an additional way for the formation of ***P9***. The multiple steps, which are necessary to obtain the product, make this route unlikely on the first sight, compared to the route in the absence of oxygen, as there are only two steps, but the different rates for decarbonylation and for decarboxylation result in an essential difference.

In the absence of oxygen the rate determining, very slow decarbonylation is followed by the fast addition of ***R2***.

In the presence of oxygen, first the very fast oxygen addition occurs, which is succeeded by the fast recombination to ***P6***. The decomposition of ***P6*** upon UV irradiation is comparable with the decomposition rate of the parent initiator. The following decarboxylation is also very fast and the last reaction step is the same as in the absence of oxygen.

The kinetic simulations revealed that the suggested pathway in the presence of oxygen is possible. The simulation in the absence of oxygen and including the decarbonylation term shows no evidence for the formation of ***P9***.

ESI-MS experiments support the suggested pathway, as in the presence of oxygen ***P6*** and even more important additional follow-up products are detected. The mass spectra show signals belonging to benzoate and further phenyl based compounds, like 1-1'-diphenyl and hydroperoxybenzene ***P20***.

Worth to mention is 2-(phenylperoxy)propan-2-ol ***P21***, this is another phenyl based product, which was detected by ESI-MS in oxygen-saturated samples.

Kinetic simulations, NMR- and ESI-MS experiments support the suggested pathway for the formation of ***P9*** in the presence of oxygen. The decomposition of dibenzoylperoxide ***P6*** leads to reactive radicals, which can form ***P9*** after decarboxylation and reaction with ***R2***.

There are hints, that an oxygen quenched initiation process can be restarted by the decomposition of ***P6***. This reinitiation process is already discussed, as one possibility to overcome oxygen inhibition. [61,29, 30,58]

It was possible to follow the oxygen dependent double bond conversion with ^{1}H- and ^{13}C-NMR experiments. Bowman et al state that the average oxygen concentration in acrylates under atmospheric conditions is about 10^{-3} M, and further Decker et al. reported that polymerization occurs only if the oxygen concentration is below ~4 x 10^{-6} M. [44,33,38] The oxygen concentration in acetonitrile under atmospheric conditions is about 1.8 x 10^{-3} M. With this amount of dissolved oxygen and in contrast to these publications, my results indicate double bond conversion. For oxygen-saturated samples no polymerization is observed. Bowman worked with acrylates in bulk while I worked in diluted solution and obtain only small oligomers.[44]

Under atmospheric conditions the addition of ***R1*** and ***R2*** to butyl acrylate and the ongoing polymerization occur. Additionally peroxides are formed, which are the main products in oxygen-saturated samples.

Oxygen is consumed, through the formation of peroxides and the largest consumption in % is observed under atmospheric conditions. Under these conditions polymerization is possible, as sufficient amounts of ***R1*** and ***R2*** are still available, which is supported by the kinetic simulations and the oxygen measurements. Oxygen-saturated samples on the other side do not polymerize, as they contain oxygen in excess, which mainly leads to the formation of peroxides and their follow-up products.

One of these products is the already described dibenzoylperoxide ***P6***, which is also used as a photo initiator. ^{1}H-NMR spectra of samples containing oxygen reveal the addition products of oxygen containing species to butyl acrylate. These signals could derive either from ***R3*** or ***R16***, which are not distinguishable in ^{1}H-NMR spectra. ***R16***, which is formed upon decomposition of ***P6*** is known to add to butyl acrylate.

The experiments under atmospheric conditions showed that ***R1*** addition to butyl acrylate occurs more often than the addition of ***R16*** to the monomer, as the ^{1}H-NMR signal intensities for benzoyl ***R1*** addition products are higher. In our system ***R16*** is produced via several steps, which are displayed in **Scheme 26** and the simulation of this system fits to my NMR results.

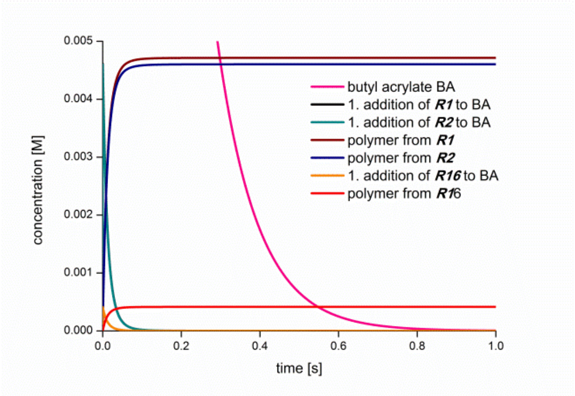

Figure 33. Kinetic simulation of a photo induced polymerization in the presence of oxygen. 10 mM *A1*, 10 mM O_2 and 100 mM butyl acrylate. This simulation includes peroxide decomposition and reinitiation via benzo oxyl, indicated in Scheme 26.

The simulation in **Figure 33** displays the polymerization products based on the initiator. Almost equal amounts of polymer derive from ***R1*** and ***R2***, and only a small fraction from ***R16***.

Reinitiation in the presence of oxygen via peroxide decomposition plays a minor role and for this process the oxygen concentration is crucial. With 10 mM initiator and 10 mM oxygen the polymerization is possible. Simulations with 100 mM oxygen showed no polymers.

To conclude, experiments and simulations showed comparable results for polymerization processes. In the absence of oxygen the determination of curing products and few side products was successful. In the presence of atmospheric oxygen amounts polymerization is still observable and additional side products, like peroxides and ***P9*** are detected. Oxygen-saturated samples show only peroxides and additional side products.

phenyl-bis-(2,4,6-trimethylbenzoyl) phosphine oxide

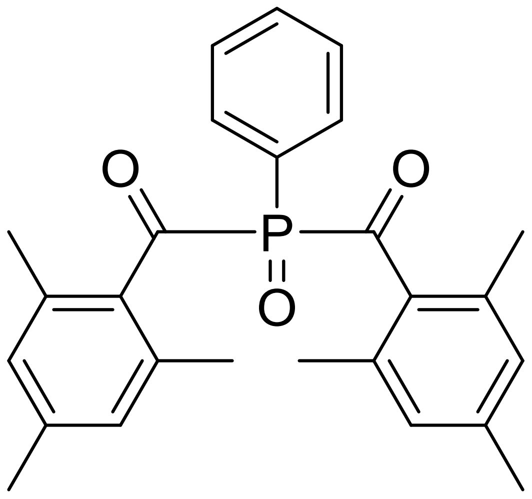

5 phenyl-bis-(2,4,6-trimethylbenzoyl) phosphine oxide

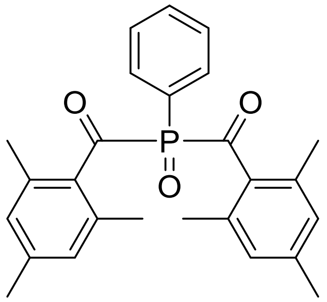

Scheme 27. phenyl-bis-(2,4,6-trimethylbenzoyl) phosphine oxide (BAPO).

The bisacylphosphine oxide phenyl-bis-(2,4,6-trimethylbenzoyl) phosphine oxide (BAPO) is also known as Irgacure 819®. This BAPO is an efficient type I photoinitiator, which is used in various industrial applications. It has an absorption maximum around 380 nm, which makes it an ideal initiator for highly pigmented solutions in outdoor applications like paintings. Additionally, this BAPO cures under sun light and photo bleaches.

It is also used for, higher cross linked polymers, various types of coatings, like gel coatings and for the formation of composites.[10]

Also scientifically BAPO is well described and spectroscopic and kinetic reference data exist. Multiple studies were performed by Nicholas Turro and his research group. [53,120,121,122] My working group used this BAPO frequently. [82,123,124]

5.1 Results

Here I performed various ^{1}H- ^{13}C- and ^{31}P-NMR experiments, studying the initiator in the presence and absence of oxygen and monomer upon irradiation. In the presence and absence of oxygen TEMPO scavenged the formed radicals and the obtained products were characterized with NMR experiments.

^{1}H- and ^{31}P- CIDNP experiments support mechanistic approaches of the oxygen influence and these results are confirmed by additional ESI-MS measurements.

With an oxygen sensor and controlled partial pressures, it was possible to determine, the oxygen concentrations in the solutions.

LFP measurements resulted in the determination of monomer and oxygen addition rate constants. These rate constants were used to create kinetic models with Copasi®.

Additionally, I followed oxygen dependent radical photo polymerizations with a high resolution thermal camera. With this technique, a live view of polymerizations and differentiation between thermal effects, bulk diffusion and oxygen inhibition is possible.

5.1.1 ^{1}H-NMR Experiments

5.1.1.1 ^{1}H-NMR Experiments at Various Oxygen Concentrations

The treatment of BAPO samples is the same as for ***A1*** based samples, which includes the ^{1}H-NMR experiments before and after irradiation in the presence or absence of defined oxygen concentrations. The observable changes within the spectra are tremendous and displayed in **Figure 34** below.

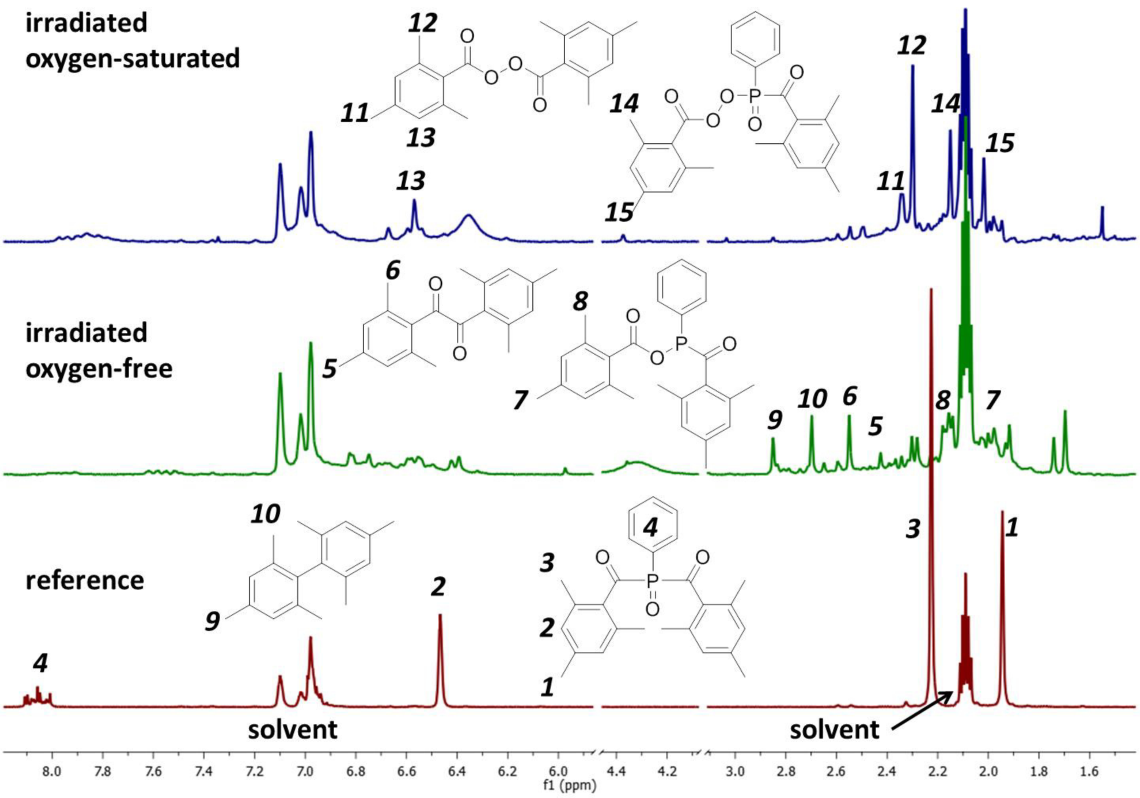

Figure 34. ^{1}H-NMR of BAPO 10 mM (32 scans in toluene). At the bottom trace the spectrum of the non-irradiated initiator in the absence of oxygen is displayed. The middle spectrum represents the irradiated sample without oxygen and the top trace displays the irradiated sample in the presence of oxygen.

Before irradiation the spectrum of the initiator is well resolved and it is possible to assign all peaks, without the problem of solvent derived signal overlap. In addition to the chemical shifts, the integrals of peaks ***1***, ***2*** and ***3*** fit perfectly to the structure.

The signals of the initiator disappear, when the sample is irradiated. Another aspect, that the oxygen-free and the oxygen-saturated sample have in common, is their fragmentation into many different follow-up products.

The spectrum of the oxygen-free irradiated sample reveals the three different species ***P'1***, ***P'3*** and ***P'4***. Peaks ***5*** at 2.54 ppm and ***6*** at 2.42 ppm belong to dimesitoyl ***P'1***. The reduced photoinitiator ***P'3*** is identified via peaks ***7*** and ***8*** at 2.01 ppm and 2.16 ppm respectively. This reduction is commonly known and best observed in ^{1}H-CIDNP- and especially in ^{31}P-CIDNP experiments.

The signals ***9*** and ***10*** at 2.85 ppm and 2.69 ppm are of particular interest, as they are dependent on the oxygen concentration and they represent 2,2',4,4',6,6'-hexamethyl-1,1'-biphenyl ***P'4***. In the absence of oxygen these peaks are clearly visible, while in the presence of oxygen only traces of these signals are found. Protons of ***P'4***s methyl groups are shifted significantly to a lower field than those of ***P'1***. Also in case of ***P'4*** the protons of the para methyl group are shifted to lower fields, compared to the ortho methyl groups.

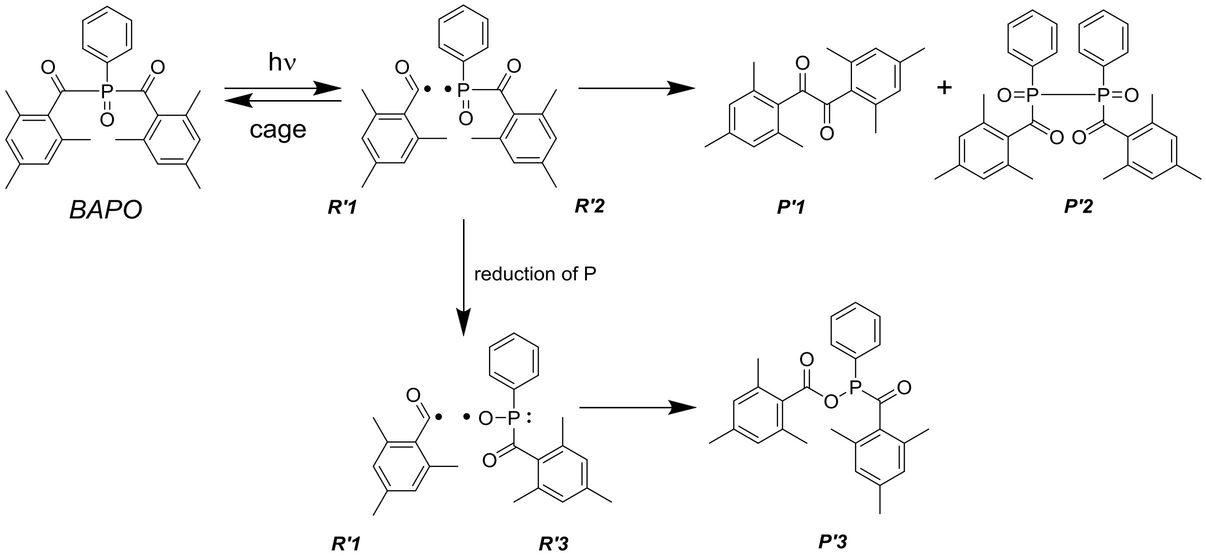

Scheme 28. Illustration of bond cleavage and radical formation of BAPO upon irradiation with UV light in the absence of oxygen. Recombination to the initiator is indicated with the "cage" step. Recombination products of the radicals are displayed in the top reaction step. The phosphinoyl radical can be reduced, which leads to compound *P'3*.

The scheme above illustrates the first reactions of BAPO upon irradiation. The ^{1}H-NMR experiments were based on 3 minutes of irradiation, therefore the cleavage of BAPO's both mesitoyl groups is expected and compounds ***P'2*** and ***P'3*** are interpreted as intermediates.

The formation of ***P'4*** should include a decarbonylation or a decarboxylation step. From ***A1*** we know that decarboxylation processes are preferred. A possible mechanism could include compound ***P'3*** and is indicated in **Scheme 29** below.

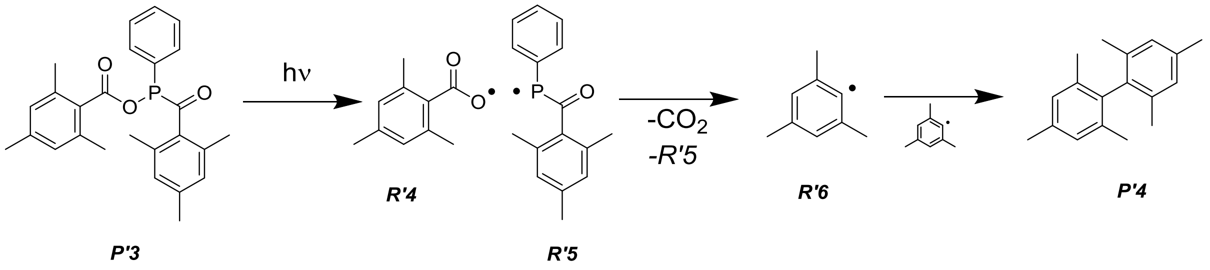

Scheme 29. Possible way for the formation of 2,2',4,4',6,6'-hexamethyl-1,1'-biphenyl *P'4* via compound *P'3*. After cleavage of *P'3 R'4* is formed this undergoes decarboxylation and leads to mesitoyl radicals *R'6*. Two *R'6* recombine to *P'4*.

Further assignments, in the spectra recorded after irradiation and in the absence of oxygen, cannot be done without speculation. In principle ***R'6***, formed after decarbonylation or decarboxylation, could attach to ***R'5*** or ***R'2***. This might explain in the absence of oxygen the signals at 1.74 ppm and 1.70 ppm, but prediction tools and reference samples are limited and therefore I cannot confirm a compound were ***R'6*** is attached to phosphorus.

Through product fragmentation and signal overlap, assignments in the aromatic region of the NMR spectrum are difficult. After irradiation both samples do not contain signals of the initiators aromatic protons ***2***. Peak overlaps, especially in the aromatic region of the spectrum, are a serious problem in the presence and absence of oxygen peak, but in the presence of oxygen one pronounced peak ***13*** at 6.59 ppm appears. This signal belongs to a mesitoyl peroxide species, which can be determined as dimesitoyl peroxide ***P'5***, through its para ***11*** and ortho ***12*** methyl groups' protons at 2.34 ppm and at 2.30 ppm respectively.

An additional signal, that has a similar shift like compound ***P'3***, is 2,4,6-trimethylbenzoic phenyl(2,4,6-trimethylbenzoyl)phosphinic peroxyanhydride ***P'6***, which is formed in the presence of oxygen. For this product further hints are provided by signal ***14*** at 2.15 ppm and signal ***15*** at 2.02 ppm.

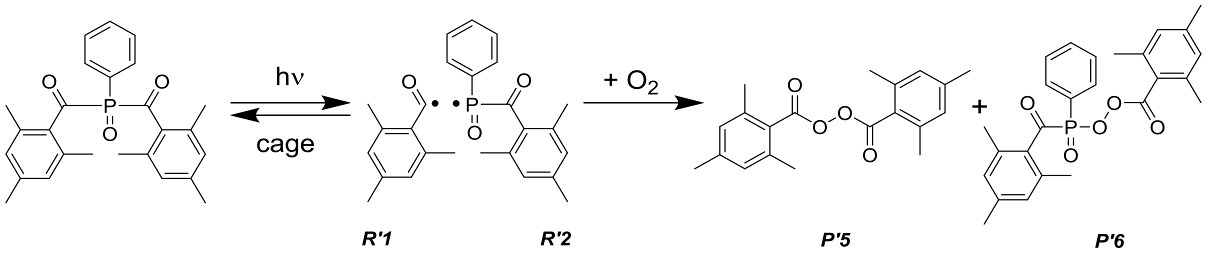

Scheme 30. Confirmed products found after irradiation with UV light in the presence of oxygen. Dimesitoyl peroxide *P'5* and compound *P'6* are detected while signals of the initiator disappear.

The para methyl group, which belongs to compound ***P'6*** and the para methyl group from compound ***P'3*** have a slightly different chemical shift (2.15 ppm and 2.16 ppm respectively). Distinguishing between these two signals is difficult; therefore additional ^{13}C- and ^{31}P-NMR data are required.

Upon irradiation in the absence of oxygen an additional broad peak appears at 4.3 ppm. This peak moves to lower fields, when the oxygen concentration increases and in the oxygen-saturated sample it is observed around 6.3 ppm. This broad signal indicates fast exchangeable protons, which probably derive from by degradation formed phosphorous based acids.

The repetition of this experiment with acetonitrile as a solvent shows the typical signal of 2,4,6-trimeethylbenzaldehyde ***P'7*** around 10 ppm. The aldehyde is formed, through hydrogen-atom abstraction of ***R'1***, which is not possible in toluene, as neither the solvent nor the initiator has abstractable hydrogen-atoms. The water in acetonitrile acts as a hydrogen-atom donor, which enables the formation of the aldehyde.

In acetonitrile a strongly pronounced broad peak shifts to a lower field, when the oxygen concentration is increased. The signal intensity of these fast exchangeable protons is higher in acetonitrile, than in toluene and the chemical shift is different. In the absence of oxygen the peak is observed around 3 ppm and it shifts to around 5 ppm in the oxygen-saturated sample. The increased intensity of this signal in a water containing solvent is an indication for the formation of an acid.

Both experiments led to the same results in respect to product fragmentation behavior, beside the detection of the aldehyde and the increased intensity of the broad peak.

5.1.1.2 ^{1}H-NMR Experiments with Butyl Acrylate

The ^{1}H-NMR experiments with addition of monomer, before and after the irradiation are similar to the experiments based on ***A1***. In order to keep the product fragmentation low, the samples (10 mM initiator and 100 mM butyl acrylate in benzene) were exposed with 64 1 µs laser pulses.

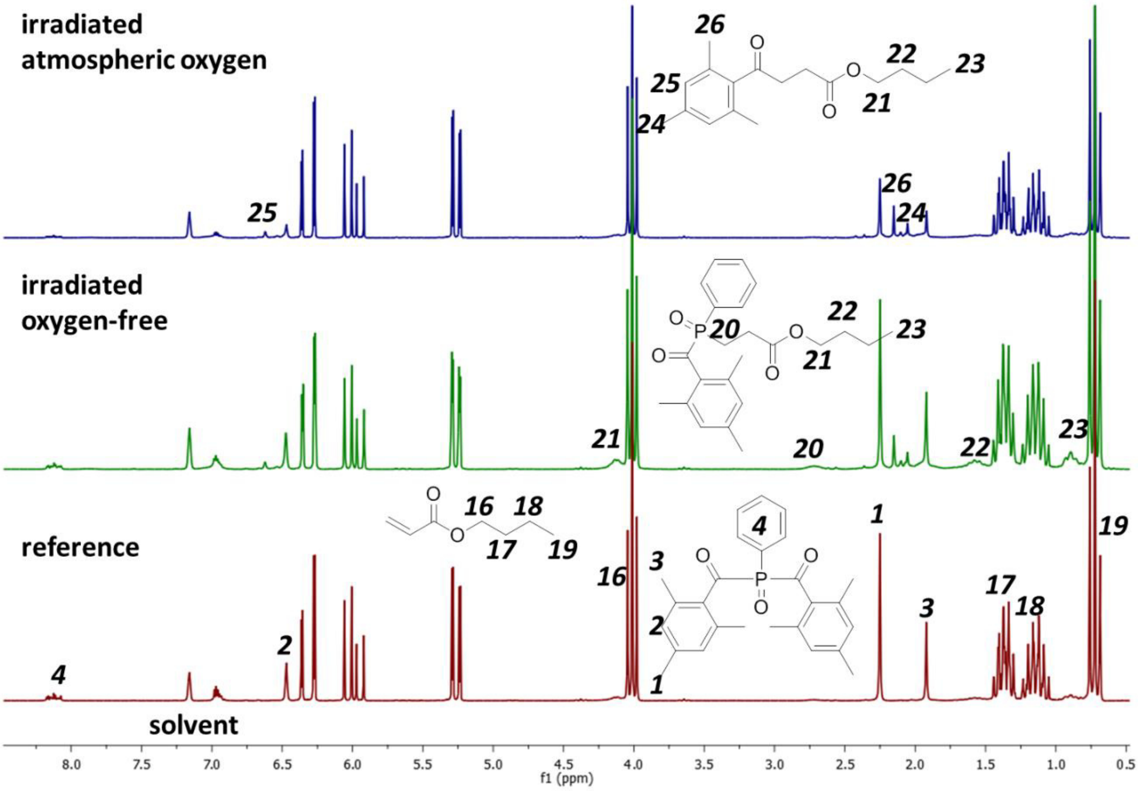

Figure 35. ^{1}H-NMR spectra of BAPO 10 mM and butyl acrylate 4 mM before and after irradiation, in absence and presence of oxygen (32 scans in benzene). The bottom trace represents the non-irradiated oxygen-free sample and serves as reference. The middle spectrum belongs to the irradiated oxygen-free sample and the top spectrum to the corresponding oxygen containing sample.

The signal assignment of the well resolved reference spectrum is easily possible. The use of benzene causes slightly shifted signals, compared to the experiments performed in toluene. The aromatic region of the NMR spectrum shows signals belonging to butyl acrylates double bond protons, but for my purposes the signals of the butyl chain are more important, as they are excellent indirect indicators for double bond conversion.

After irradiation of the oxygen-free sample the signal at 10.6 ppm, which represents the aldehyde proton of 2,4,6-trimeethylbenzaldehyde ***P'7***, appears. Peaks ***21***, ***22*** and ***23*** belong to the protons of the butyl chain of the "polymerized" acrylate. These signals indicate the double bond conversion through addition of either ***R'1*** or ***R'2***, but the differentiation, which radical attacked is not possible with this technique.

I am able to follow the addition of ***R'2*** to the monomer via signal ***20***. Through the radical addition these two protons are in close proximity to phosphorous, which leads to a broad peak around 2.7 ppm, but when a mesitoyl radical ***R'1*** adds the protons are observed at 3.28 ppm.

The additional signals ***24*** at 2.06 ppm and ***26*** at 2.15 ppm represent the protons of the para and ortho methyl groups of ***R'1***, which is attached to the acrylate. The aromatic protons ***25*** of this product have a signal at 6.62 ppm.

In case of the oxygen-free sample three main products, the two addition products of either ***R'1*** or ***R'2*** with butyl acrylate and ***P'7***, can be found. This experiment does not provide evidence for other recombination products of the radicals. Further the integral of the broad peak ***20*** indicates that ***R'2*** adds more efficient to the monomer.

The behavior in the presence of oxygen is similar. With atmospheric oxygen concentrations the addition products of ***R'1*** and ***R'2*** to the acrylate are detected but the signal intensities are much lower, than in the absence of oxygen. In the presence of oxygen double bond conversion decreases and the mesitoyl peroxide ***P'8*** is detected in small amounts. Oxygen saturated samples show no evidence for double bond conversion, only ***P'7*** and ***P'8*** are found.

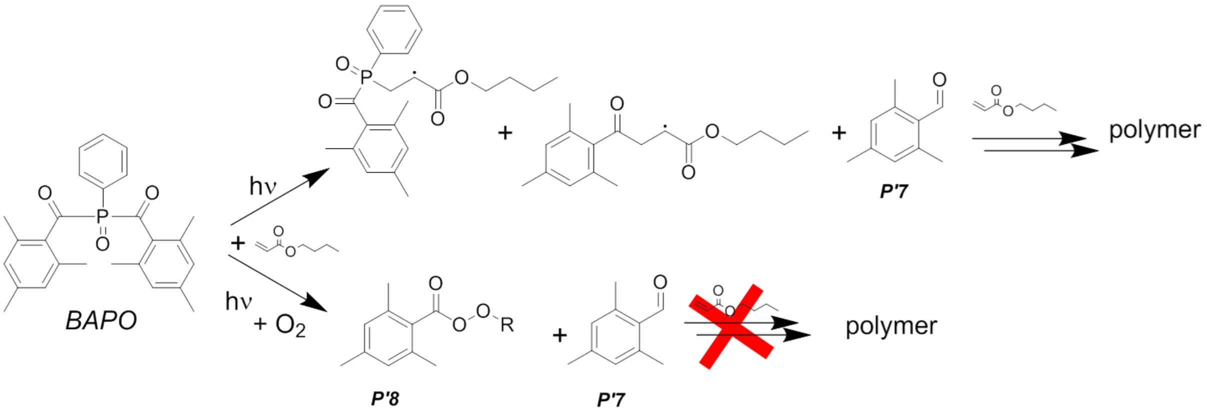

Scheme 31. Products found with ^{1}H-NMR experiments after irradiation of BAPO in the absence and presence of oxygen.

The scheme above sums up the results of these experiments, with the oxygen dependent addition of ***R'1*** and ***R'2*** to butyl acrylate as a main finding. The signal intensities representing the addition of ***R'1*** and ***R'2*** to the acrylate decrease, when higher amounts of oxygen are present. Oxygen-saturated samples showed no radical addition to the monomer. Hydrogen-atom abstraction leads to the formations of 2,4,6-trimeethylbenzaldehyde ***P'7***. In the presence of oxygen the main products are ***P'7*** and the corresponding peroxides. It is possible to follow double bond conversion and curing processes in the dependence of the oxygen concentration.

5.1.1.3 ^{1}H-NMR Experiments in Dependence of Water

After irradiation of the photoinitiator, broad peaks appear, that most likely belong to a phosphorous derived acid. Measurements in toluene and also in acetonitrile show these signals. In acetonitrile these signals were more pronounced, as the solvent contains some water and therefore easy exchangeable protons are available. As explained before with ***A1***, water has some influence on the process. Therefore ^{1}H-NMR experiments with defined amounts of were performed.

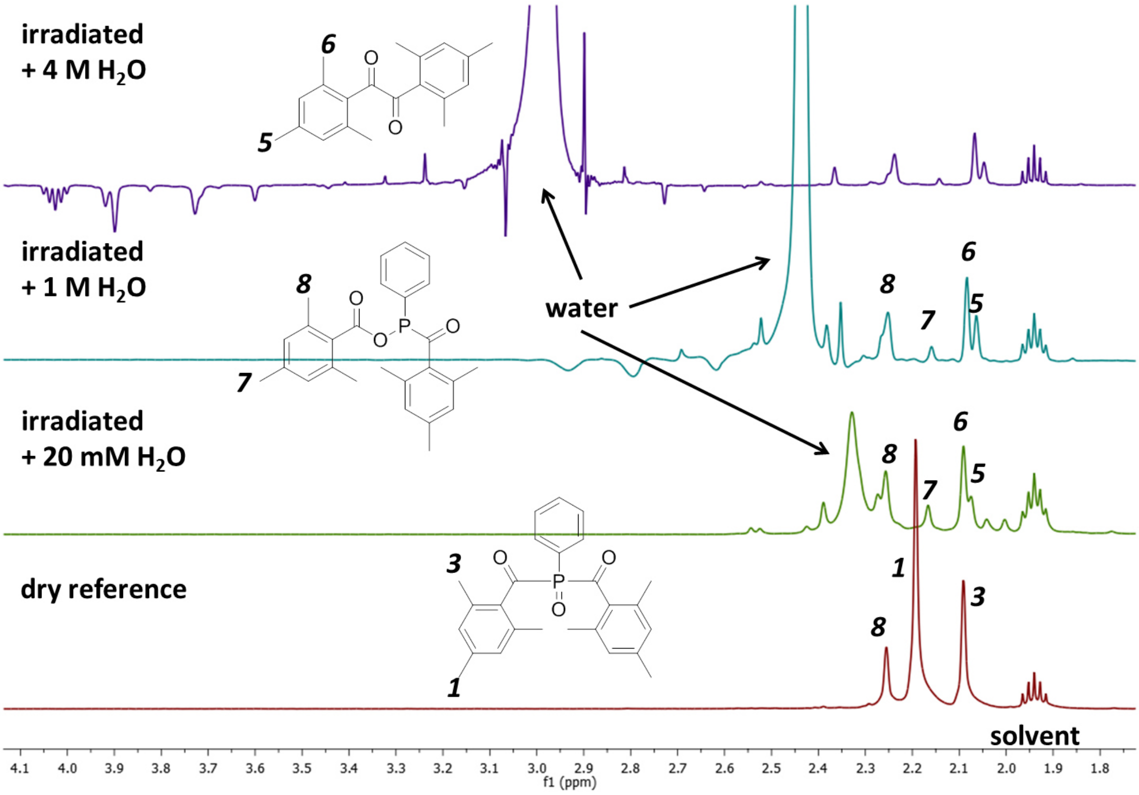

Figure 36. ^{1}H-NMR spectra of BAPO with various amounts of water after irradiation (acetonitrile, 32 scans, 10 mM BAPO). The bottom spectrum shows the untreated BAPO in dry acetonitrile. The spectra above represent irradiated samples with 20 mM, 1 M and 4 M of water.

The reference spectrum displays the peaks of the initiator in the aliphatic range. Signal ***8*** belongs to the reduced form of the initiator ***P'3***. To suppress huge product fragmentation the irradiation time was reduced to 30 s. After the short irradiation all samples lead to the same fragmentation pattern, as after longer irradiation times. The initiator is decomposed and the man products ***P'1*** and ***P'3*** and the side product ***P'7*** are formed.

The water peak shifts to lower fields and signals of the analytes are slightly shifted to higher fields, when the water content is enlarged. Beside the slight shift, a general peak broadening and the increase of artefacts at higher water concentrations, no effects on the products are observed.

5.1.2 ^{13}C-NMR Experiments

The ^{13}C-NMR experiments with ***A1*** revealed additional useful information, as it was possible to confirm the formation of peroxides and to observe the addition of benzoyl ***R1*** and propan-2-ol-2-yl ***R2*** radicals to butyl acrylate. The carbonylic carbon of the acrylate was ideal to follow the double bond conversion. Here the aim is to determine the exact structures of the formed peroxides and to follow double bond conversion.

In order to obtain well resolved spectra, to reduce product fragmentation and to minimize overlaps with the solvent, it was necessary to reduce the irradiation time to 30 s and to use chloroform.

5.1.2.1 ^{13}C-NMR Experiments in Dependence of Oxygen

The ^{1}H-NMR experiments revealed that dimesitoyl ***P'1*** is formed in the absence of oxygen and that the initiator is partly reduced to ***P'3***. In the presence of oxygen mesitoyl peroxides ***P'8*** are detected but it is not possible to determine the exact structure of the peroxide with this experiment. It is likely that dimesitoyl peroxide ***P'5*** is formed.

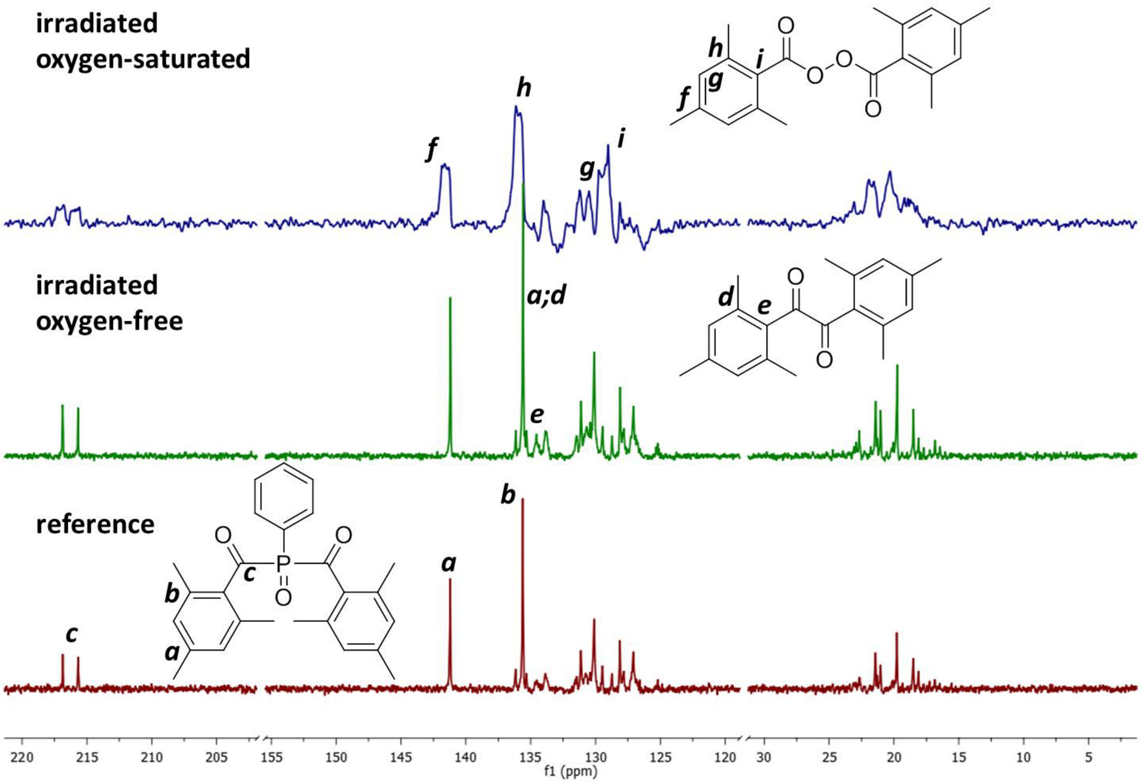

Figure 37. ^{13}C-NMR spectra of BAPO in dependence of the oxygen concentration after irradiation (chloroform 4096 scans, 100 mM BAPO). The bottom traces represents the non-irradiated reference sample in the absence of oxygen. The middle spectrum belongs to the oxygen-free irradiated sample and the top spectrum to the oxygen-saturated irradiated sample.

The reference spectrum contains the two signals of the carbonylic carbons of BAPO, one at 215.8 ppm and the other at 216.8 ppm. Signal ***a*** belongs to the para carbon of the mesitoyl with a shift of 141.2 ppm and signal ***b*** to the ortho carbons with 135.6 ppm.

After irradiation in the absence of oxygen the additional signals ***d*** and ***e*** are detected. ***d*** overlaps with signal ***a*** from the initiator and is recognized by a shoulder. Both new signals fit to ***P'1***. The oxygen-free sample shows no further products, although additional products are likely. Signals of the reduced form of the initiator ***P'3*** probably overlap with the signals of the parent compound.

In the presence of oxygen peak broadening occurs and new signals, which represent dimesitoyl peroxide ***P'5***, are found. Signals ***f*** at 141.9 ppm and ***h*** 136.1 ppm are low field shifted compared to the corresponding parent para and ortho carbons ***a*** and ***b***. Additional signals are ***g*** and ***i***. ***g*** represents the meta carbons at 130.6 ppm and ***i*** the ipso carbon at 129.0 ppm. All aromatic carbons of ***P'5*** can be assigned here, but the methyl groups on the other hand are not strongly influenced by the oxygen addition and therefore it is not possible to observe a different chemical shift for them.

Further assignments in the spectrum of the oxygen-saturated sample are not feasible due to bad resolution and signal overlaps.

The ^{13}C experiments create strong indications, that ***P'5*** is the main peroxide species, which is formed upon irradiation of BAPO.

5.1.2.2 ^{13}C-NMR Experiments in Dependence of Oxygen with Butyl Acrylate

These ^{13}C-NMR spectra are excellently resolved, compared to those containing only the initiator, especially when the sample was saturated with oxygen. Of special interest is the aromatic region of these NMR experiments. The signal at 166.0 ppm represents the carbonylic carbon ***j*** of butyl acrylate. As described already in chapter 4, the carbonyl signal of the acrylate shifts to lower fields, when the double bond is converted into a single bond.

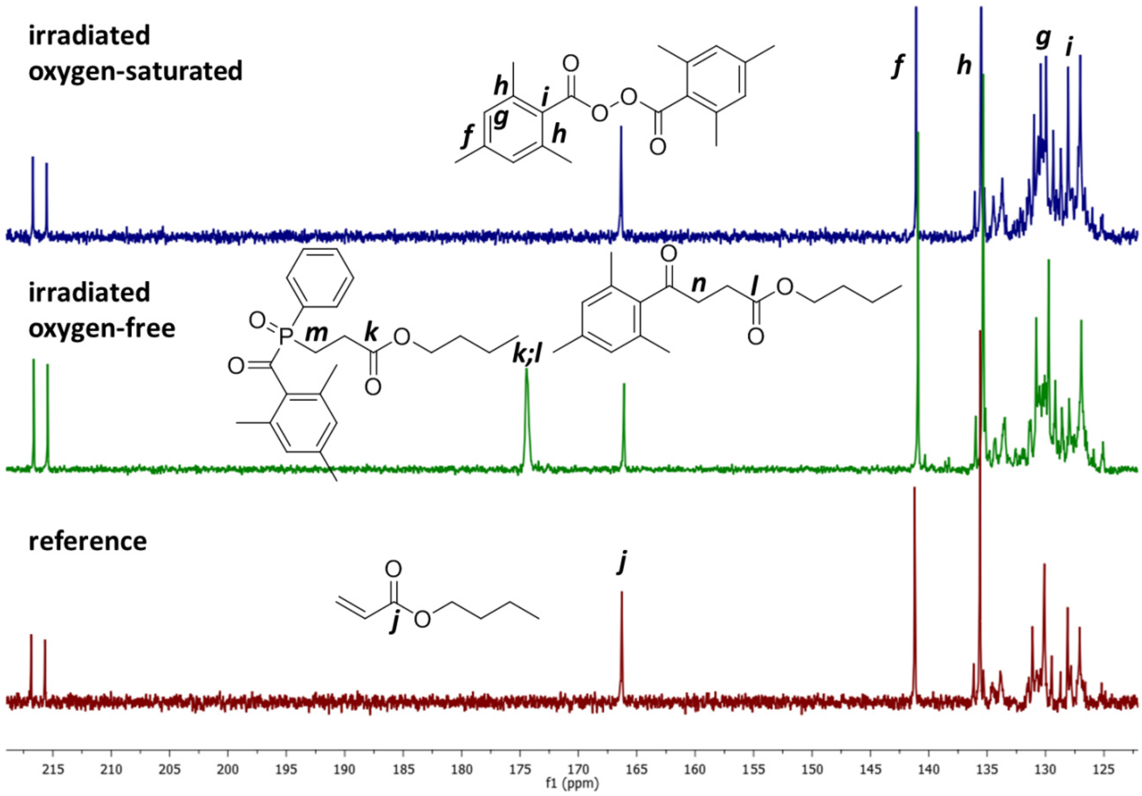

Figure 38. ^{13}C-NMR spectra of BAPO 100 mM in dependence of the oxygen concentration after irradiation with butyl acrylate 400 mM (chloroform 4096 scans).On the lower trace the reference sample consisting out of BAPO and butyl acrylate is displayed. The middle spectrum represents the oxygen-free irradiated sample and the top spectrum the oxygen-saturated sample.

After 30 s of irradiation signal ***j*** is still detected, but related to butyl acrylate an additional peak ***k;l*** at 174.4 ppm is found, which belongs to ***R'1*** or ***R'2*** attached to the acrylate. Only from this signal it is not feasible to distinguish, which radical attacked the acrylate, but the signals in the aliphatic region of the spectrum contain further information. The addition of ***R'1*** to the monomer results in a signal at 41.2 ppm and the addition of ***R'2*** leads to a peak at 18.9 ppm.

In accordance with the ^{1}H-NMR results I can confirm the addition of ***R'1*** and ***R'2*** to butyl acrylate. However ^{13}C-NMR experiments are not feasible to obtain information about the addition probability of the radical species.

In the presence of oxygen ^{13}C-NMR experiments do not reveal double bond conversion, which is indicated by the change of butyl acrylates carbonylic carbon shift (signal ***j***). For butyl acrylate no changes are observed. The initiator based side products are the same, as in the ^{13}C spectrum of BAPO in the presence of oxygen. This spectrum is better resolved and again it is possible to assign the additional signals to ***P'5***.

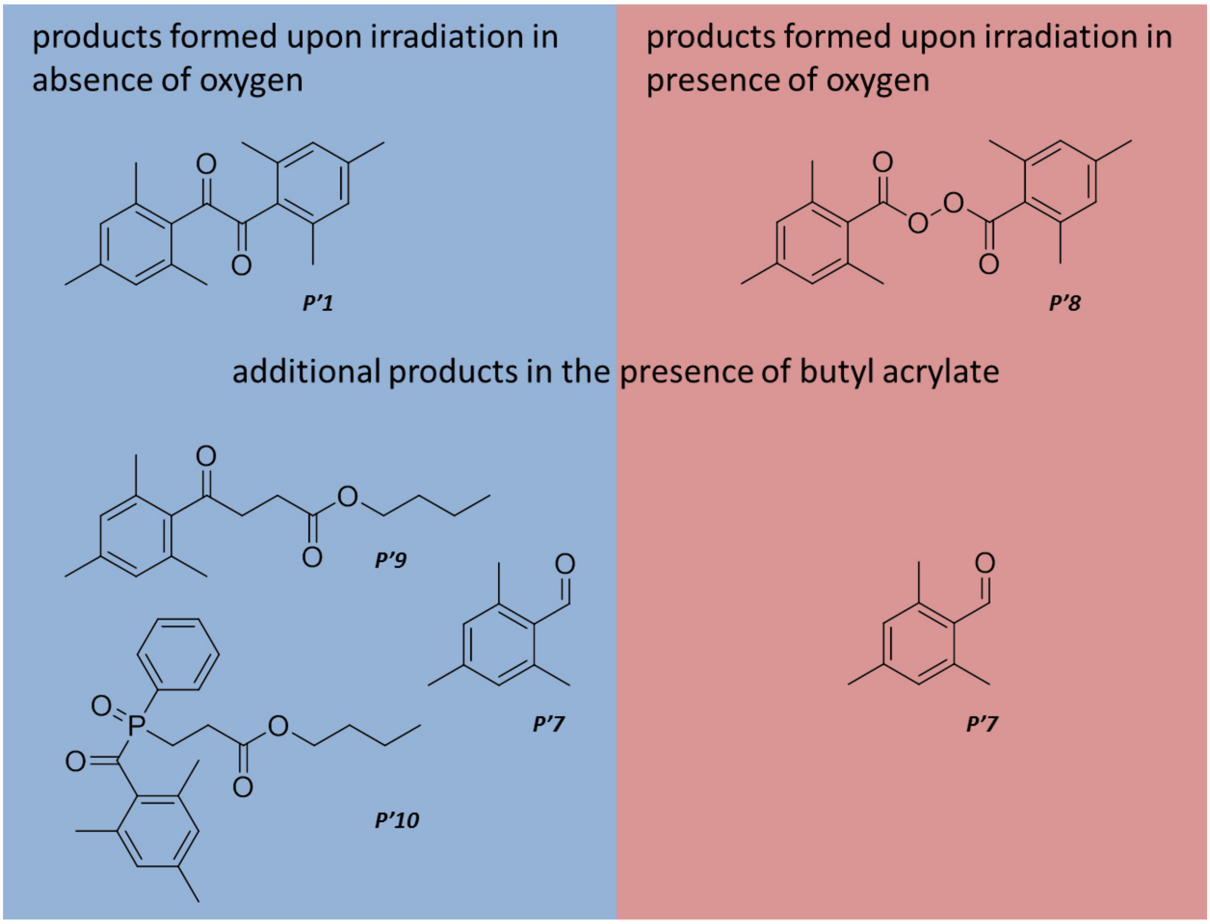

Scheme 32. Overview of products, which are confirmed by ^{13}C-NMR measurements. In the left blue field products are displayed, which are formed in the absence of oxygen. In the presence of butyl acrylate the addition products to the monomer and 2,4,6-trimeethylbenzaldehyde are formed. The right red field represents the products that I detect in the presence of oxygen.

With ^{13}C-NMR experiments it was possible to observe the addition of ***R'1*** and ***R'2*** to the monomer in the absence of oxygen. In oxygen-saturated samples only the parent initiator, ***P'7*** and ***P'8*** were found.

5.1.3 ³¹P-NMR Experiments

BAPO is dedicated for ^{31}P-NMR experiments, as the shift of BAPO's single phosphorus strongly depends on its chemical surrounding and therefore should provide further information about reaction products. However this method faces difficulties as references and predictions are limited.

The ^{31}P-NMR irradiation experiments with BAPO are the same as with ^{1}H- and ^{13}C-NMR. It was necessary to adjust concentrations and irradiation times to obtain proper results. 10 mM initiator and 3 minutes of irradiation lead only to a rough baseline. As the other NMR experiments showed already and mass spectrometry will show soon, BAPO tends to form many different products and therefore the signal intensities of each fragment are low.

I obtained best results with 50 mM initiator and 60 s of irradiation. Lower irradiation times are not useful, as then only the parent initiator is observed.

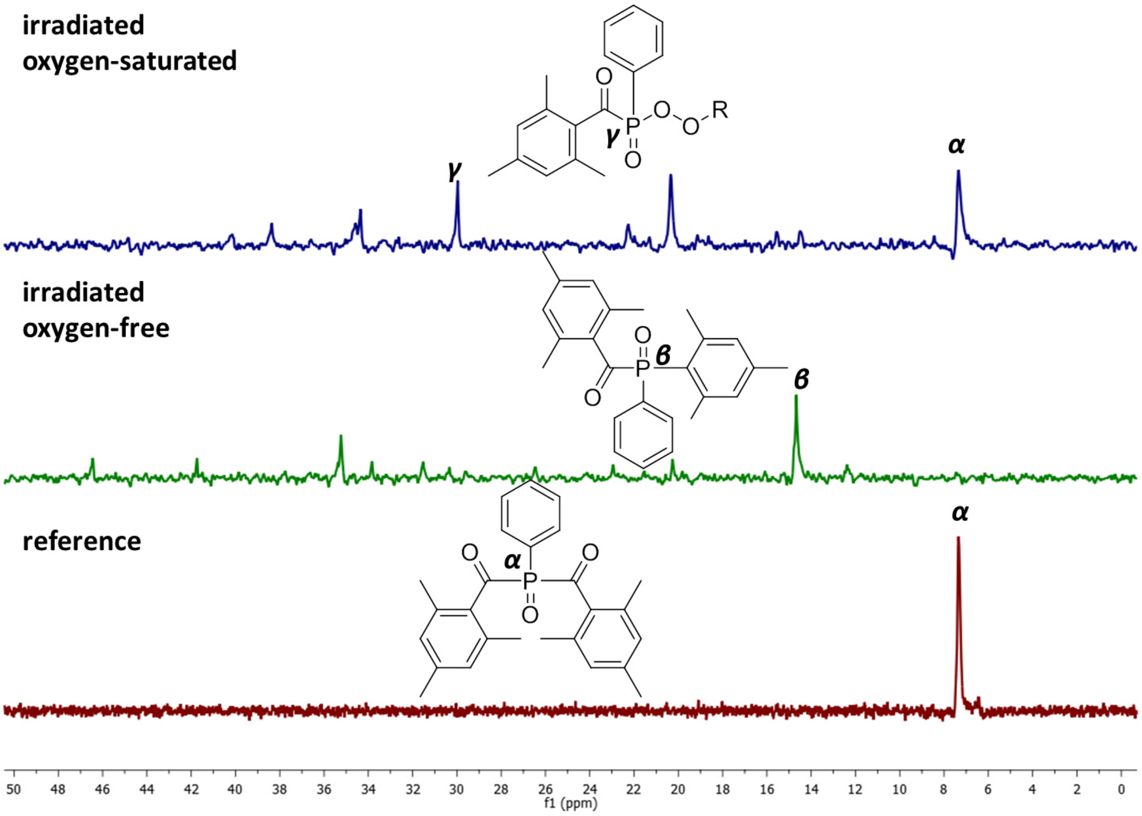

Figure 39. ^{31}P-NMR of BAPO 50 mM in dependence of oxygen (toluene, 64 scans). The bottom traces shows the spectrum of the BAPO with its typical peak at 7.35 ppm. The middle trace represents the oxygen-free irradiated sample and the top trace the oxygen-saturated irradiated sample. R can be *R'1* or *R'2*.

The reference spectrum displays one peak ***α*** at 7.35 ppm, which belongs to BAPO. After irradiation of the oxygen-free sample the signal of the parent initiator disappeared, which corresponds with the ^{1}H-NMR results. Signal ***β*** at 14.2 ppm possibly belongs to the mono acyl phosphine oxide ***P'11***. The formation of ***P'11*** is not contradicting with in ^{1}H-NMR spectra observed ***P'4***. Both compounds require the 2,4,6-trimethyl phenyl radical ***R'6*** as an intermediate, which can be formed via decarbonylation or decarboxylation.

In the presence of oxygen the signal of the initiator and several additional signals appear. It is possible to assign signal γ at 30.0 ppm to a phosphinoyl peroxide ***P'12***, which is either attached to ***R'1*** or ***R'2***.

Further signals, in the absence and presence of oxygen, should belong to P-P bonded compounds, but from these data it is not feasible to determine their structures. Although the chemical shift change from 5- to 3-bonded phosphorus is tremendous, the reduction is not observed here. I observed these changes in ^{31}P-CIDNP experiments and described the results in section 5.1.5.

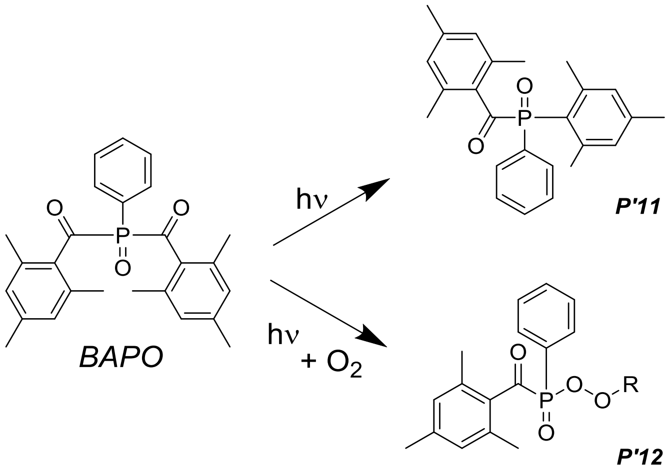

Scheme 33. Additional products observed in ^{31}P-NMR experiments in the presence and absence of oxygen. R can be *R'1* or *R'2*.

These experiments were carried out also in the presence of butyl acrylate with irradiation times between 5 s and 3 min. These conditions led to many different products and the signal intensities of most of these products are low and can hardly be distinguished from the baseline. In the absence of oxygen a broad peak from ~23-29 ppm is observed, which fits to the expected signal of the addition product ***P'10*** from ***R'2*** and butyl acrylate. The sample under atmospheric conditions leads to the same result. The oxygen-saturated sample shows only a rough baseline with no resolved peaks.

5.1.4 ^{1}H-CIDNP Experiments

^{1}H-NMR experiments revealed several products, which are formed upon irradiation. Partially signals overlap with the solvent and signal intensities can be low. Here I take advantage of the CINDP effect, which reduces interferences with the solvent, leads to signal enhancement and provides mechanistic information.

5.1.4.1 ^{1}H-CIDNP Experiments of BAPO in Dependence of Oxygen

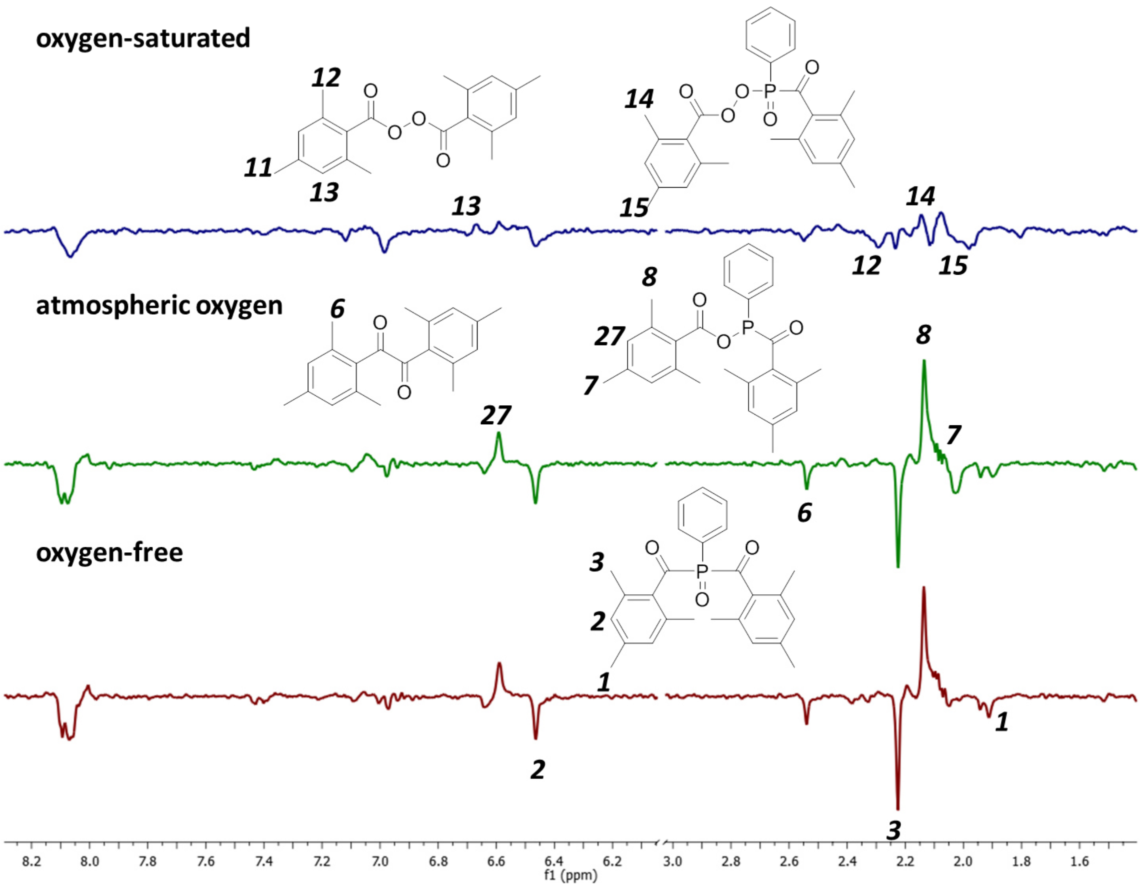

Figure 40. **^{1}H-CIDNP spectra of BAPO 10mM and various oxygen concentrations (toluene 4x32 scans). The bottom trace represents the oxygen-free sample. The middle trace shows the spectrum of BAPO under atmospheric conditions and the top spectrum represents the oxygen-saturated sample.**

The ^{1}H-CIDNP spectra of the oxygen-free sample and the sample under atmospheric conditions are similar. When small amounts of oxygen are present peak broadening occurs and traces of additional signals are found. The differences become more pronounced when the oxygen concentration increases.

The spectrum in the absence of oxygen reveals three different products. The pronounced signals ***1***,***2*** and ***3*** represent the cage product. The reduced product ***P'3*** of the initiator is observable via signals ***7***, ***8*** and ***27***. Here it is feasible to assign signal ***27*** at 6.59 ppm to the aromatic hydrogen-atoms of this compound. Also the recombination product dimesitoyl ***P'1*** is clearly visible in **Figure 40**.

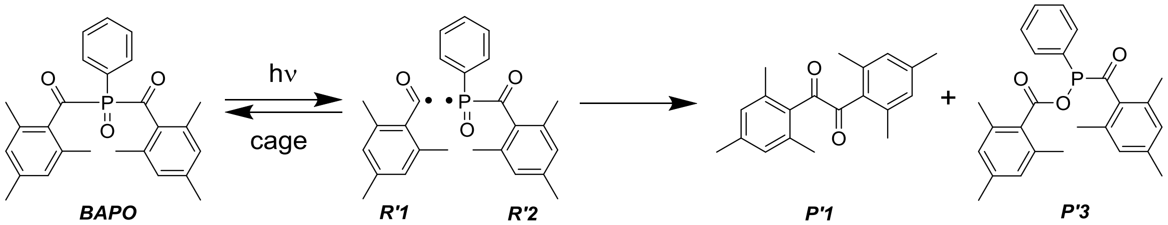

Scheme 34. Products found with ^{1}H-CIDNP in the absence of oxygen.

The ^{1}H-CIDNP spectra in the presence of oxygen show signals belonging to the initiator and to additional oxygen dependent products. Comparable to ^{1}H-NMR experiments it is possible to assign the signals to dimesitoyl peroxide ***P'5*** and to compound ***P'6***. The oxygen-saturated sample faces the problems of low signal intensities and severe peak broadening. However the ^{1}H-CIDNP results support the formation of ***P'5*** and ***P'6***.

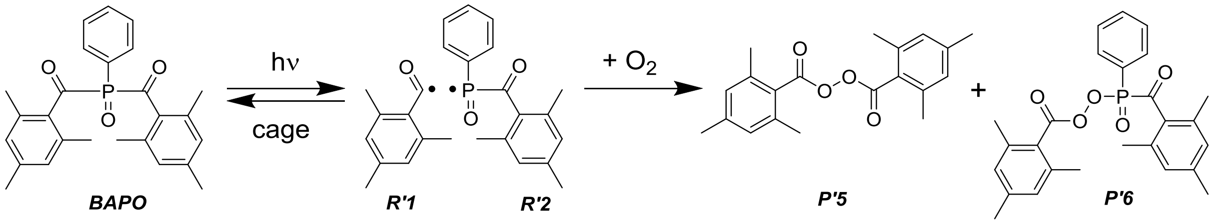

Scheme 35. Additional products detected in the presence of oxygen.

Here it is not possible to detect the recombination product ***P'2***, consisting out of two phosphinoyl radicals ***R'2***, with a P-P bond. ^{31}P-CIDNP is the most useful method to distinguish between different phosphorus species and the results are described in section 5.1.5.

5.1.4.2 ^{1}H-CIDNP Experiments of BAPO with Butyl Acrylate in Dependence of Oxygen

The ^{1}H-NMR experiments were useful to follow double bond conversion and here further information for the radical attack to the double bond is obtained.

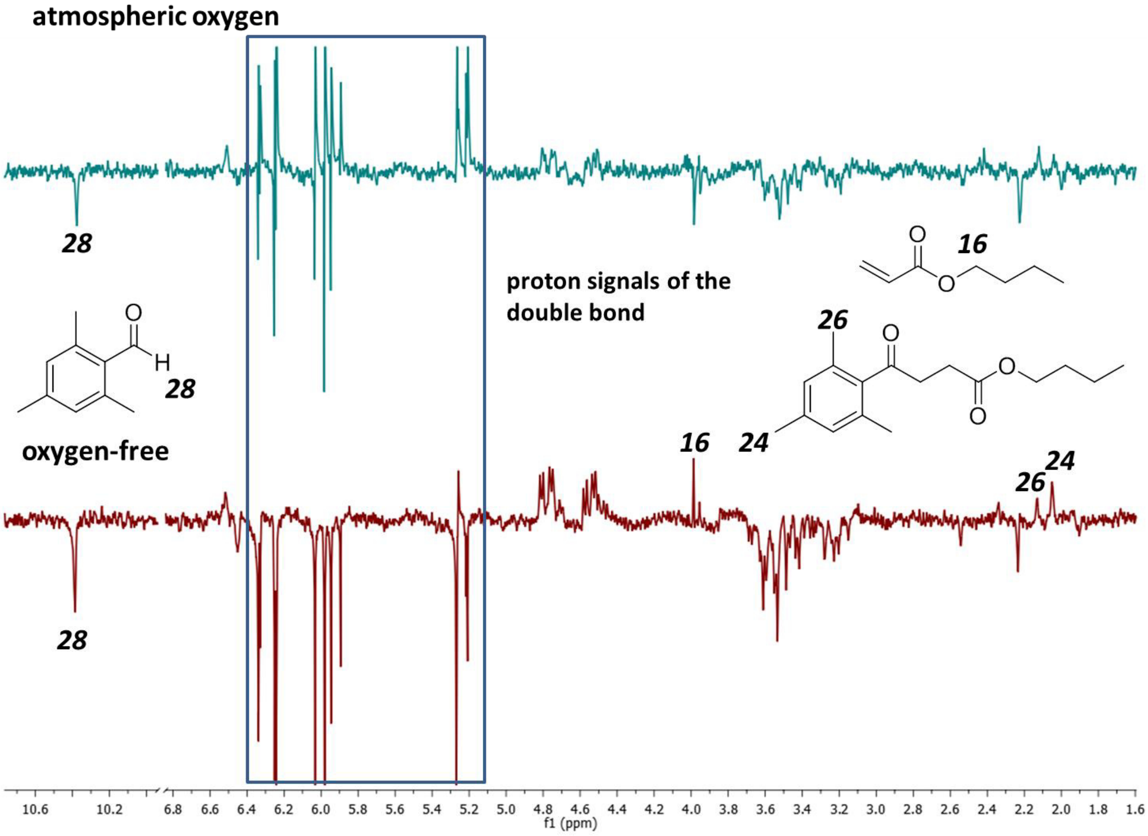

Figure 41. ^{1}H-CINDP spectra of BAPO 10 mM and butyl acrylate 100 mM in dependence of the oxygen concentration (toluene 32 scans). The lower spectrum belongs to the oxygen-free sample and the upper spectrum to the sample under atmospheric conditions.

The dummy scans show the insufficient presaturation through the high amount of butyl acrylate. After subtraction of the dummy scan, spectra with large signal intensities of butyl acrylates double bond protons are obtained, which could indicate radical polymerization and double bond conversion. Additionally signals ***24*** and ***26*** represent the addition product ***P'9*** of ***R'1*** and the acrylate. These are the same signals, which were observed in ^{1}H-NMR experiments. It is possible to detect dimesitoyl ***P'1*** and additionally 2,4,6-trimeethylbenzaldehyde ***P'7*** with signal ***28*** at 10.3 ppm.

In the presence of atmospheric oxygen concentrations the signal intensities are reduced and oxygen-saturated samples show only a rough baseline with some polarization of the acrylate through the insufficient presaturation.

5.1.4.3 ^{1}H-CIDNP Experiments of BAPO in Dependence of Oxygen and Water

In order to observe water effects, ^{1}H-CIDNP spectra of samples with defined amounts of water were recorded. ^{1}H-NMR experiments showed that water leads to slight shifts of the signals, but the products keep the same. These experiments lead to matching results, as the detected cage and escape products are the same in the water-free reference sample.

In the presence of water intense signals appear, which shift to lower field when the water concentration increases. The shift of the water signals is in line with the ^{1}H-NMR results. In the presence of water it is possible to observe the same cage and escape products, but partially signals overlap.

From this experiment I can conclude that traces of water, which are present in the solvents do not interfere with the system. High amounts of water should be avoided.

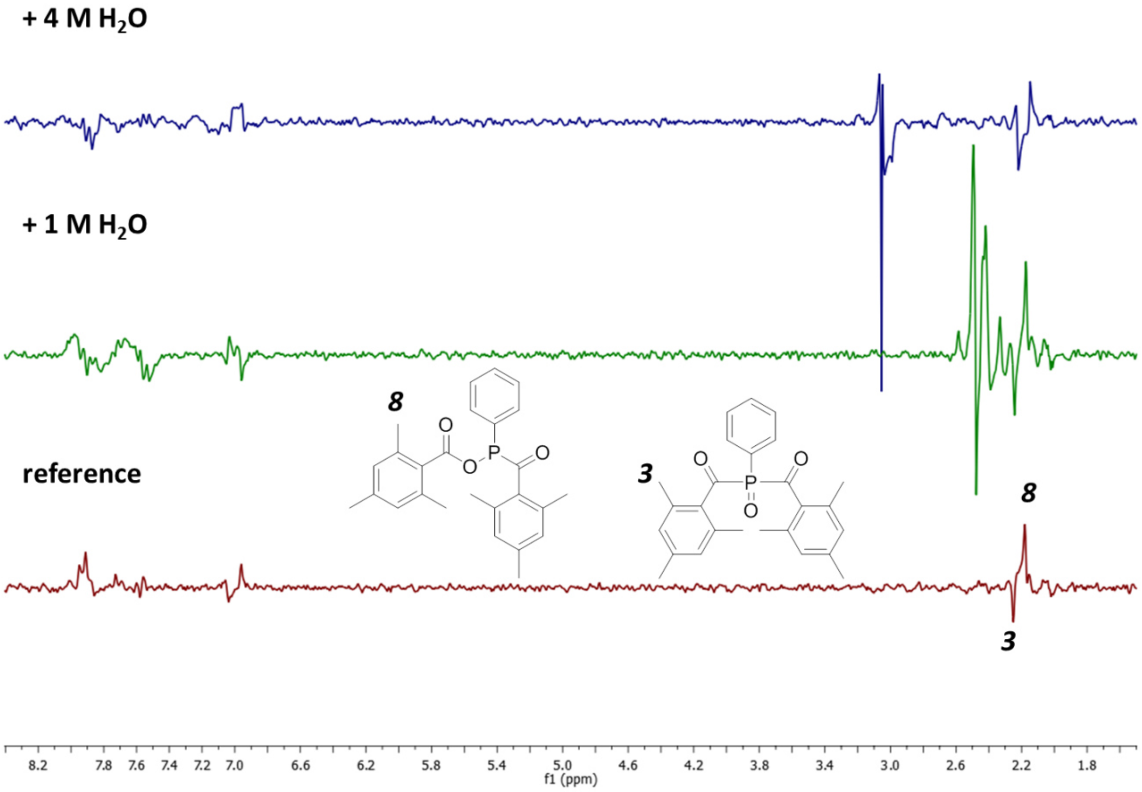

Figure 42. ^{1}H-CIDNP spectra of BAPO 10 mM and various water concentrations (acetonitrile, 32 scans). The bottom trace represents a water-free sample and serves as reference. The middle trace shows the spectrum of BAPO with 1 M water and the top spectrum represents the sample with 4 M water.

5.1.5 ^{31}P-CIDNP Experiments

^{31}P-NMR experiments were only partial successful, as the fragmentation of BAPO and the reduced signal to noise ratio caused problems. The ^{31}P-CINDP experiments ensure to observe products formed via a radial mechanism on a short time scale and with enhanced signal intensities.

5.1.5.1 ^{31}P-CIDNP Experiments of BAPO in Dependence of Oxygen

In the absence of oxygen I obtain the same results as Urszula Kolczak described in her PhD thesis.[125,118] The spectra show additionally to the cage product, the phosphorus containing escape products. Signals ***ζ*** at 22.71 ppm and 24.74 ppm indicate the formation of a P-P bond and belong to compound ***P'2***.

Compound ***P'3*** was already successfully determined with ^{1}H-NMR and ^{1}H-CIDNP experiments and here it is possible to identify it via signal ***η*** at 96.87 ppm. Additionally the doublets of signal ***ε*** at 108.40 ppm and 106.8 ppm and doublet ***δ*** at 16.37 ppm and 15.06 ppm represent the escape product ***P'13*** formed out of ***R'2*** and reduced ***R'2***.

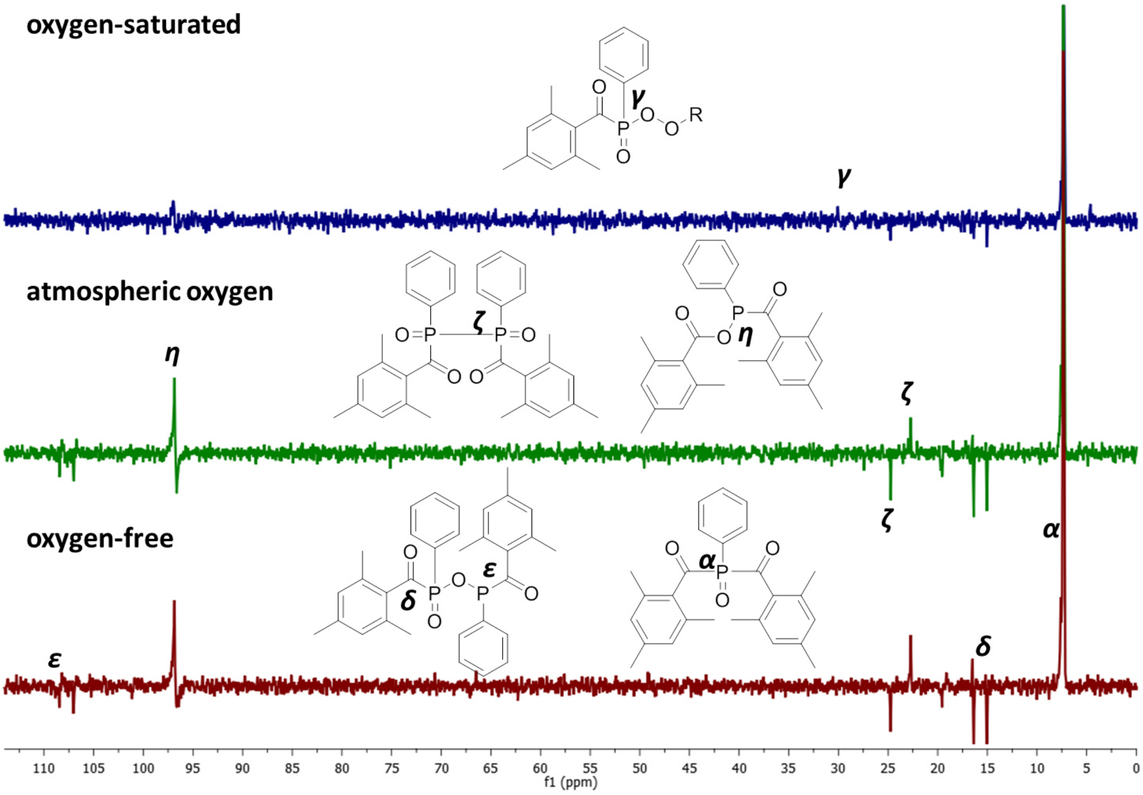

Figure 43. ^{31}P-CIDNP spectra of BAPO 10 mM and various oxygen concentrations (toluene, 4x32 scans). The bottom spectrum represents the oxygen-free sample and the middle spectrum the sample under atmospheric conditions. The top trace shows the spectrum of the oxygen-saturated sample. R is *R'1* or *R'2*.

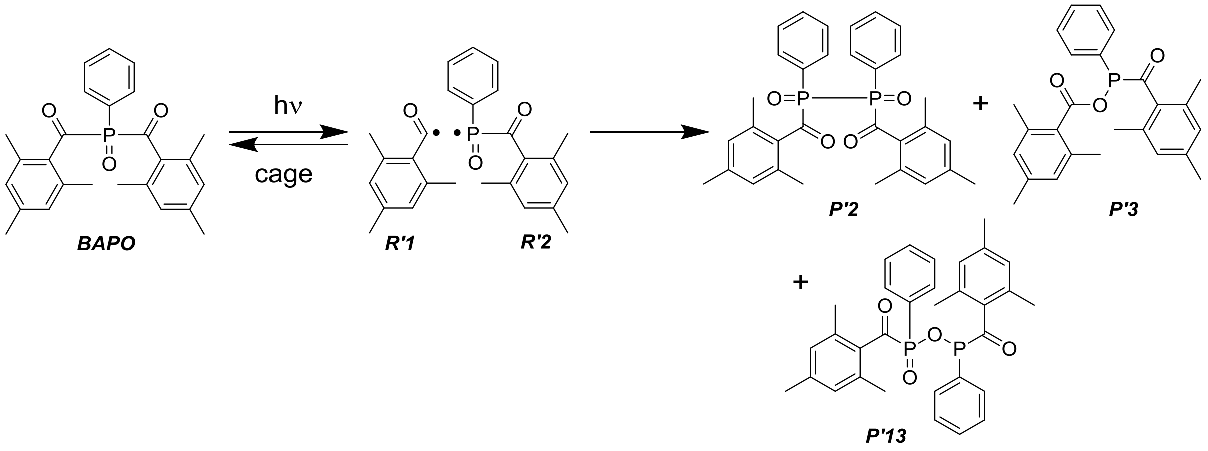

Scheme 36. Cage and escape products confirmed with 31P-CIDNP experiments in the absence of oxygen.

In the presence of oxygen similar effects as in ^{1}H-CIDNP experiments occur, including significant decrease of signal intensities. The main product in the presence of oxygen is the parent initiator and the same signals as in the absence of oxygen are detected.

In the spectrum of the oxygen saturated-sample, like in ^{31}P-NMR experiments, signal ***γ*** at 30.20 ppm belongs to the peroxide ***P'12***, with R being either ***R'1*** or ***R'2***. With ^{1}H-CIDNP measurements it is possible to detect the peroxide ***P'6***, which is ***P'12*** with the substituent ***R'1***. Unfortunately I cannot distinguish between the two species here as both species should have the same phosphorus shift. As phosphinoyl peroxides are not very stable it is only possible to observe them in CIDNP- and after short time irradiation in NMR experiments. With long irradiation times no corresponding signals in NMR spectra appear.

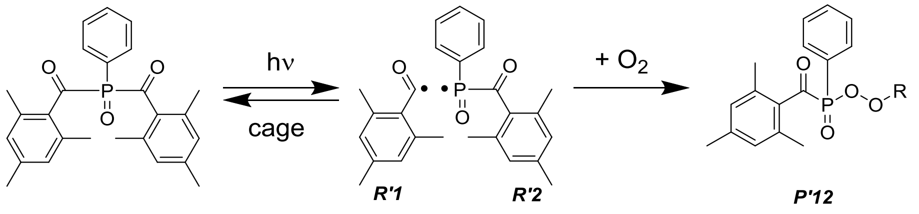

Scheme 37. Additional escape product found with ^{31}P-CIDNP in the presence of oxygen. R is *R'1* or *R'2*.

5.1.5.2 ^{31}P-CIDNP Experiments of BAPO and Butyl Acrylate in Dependence of Oxygen

Compared to ^{1}H-CIDNP here the big advantage is that only phosphorus containing compounds are visible and that NMR signal interferences from not saturated butyl acrylate are not an issue.

In the presence of butyl acrylate the ^{31}P-CIDNP spectra differ from the spectra recorded in the absence of monomer, as it is not possible to observe the recombination product ***P'13***. The spectra show the cage- and the escape product ***P'3***. The signals ζ at 22.71 ppm and 24.40 ppm belong to ***P'2*** and the second signal is slightly shifted to a higher field compared to the ^{31}P-CIDNP measurement without butyl acrylate. In the absence of oxygen and under atmospheric conditions this peak has a shoulder and compared to the second peak belonging to compound ***P'2*** it has a higher signal intensity. Therefore I assume that the signal at 24.40 ppm is overlapping with an additional compound.

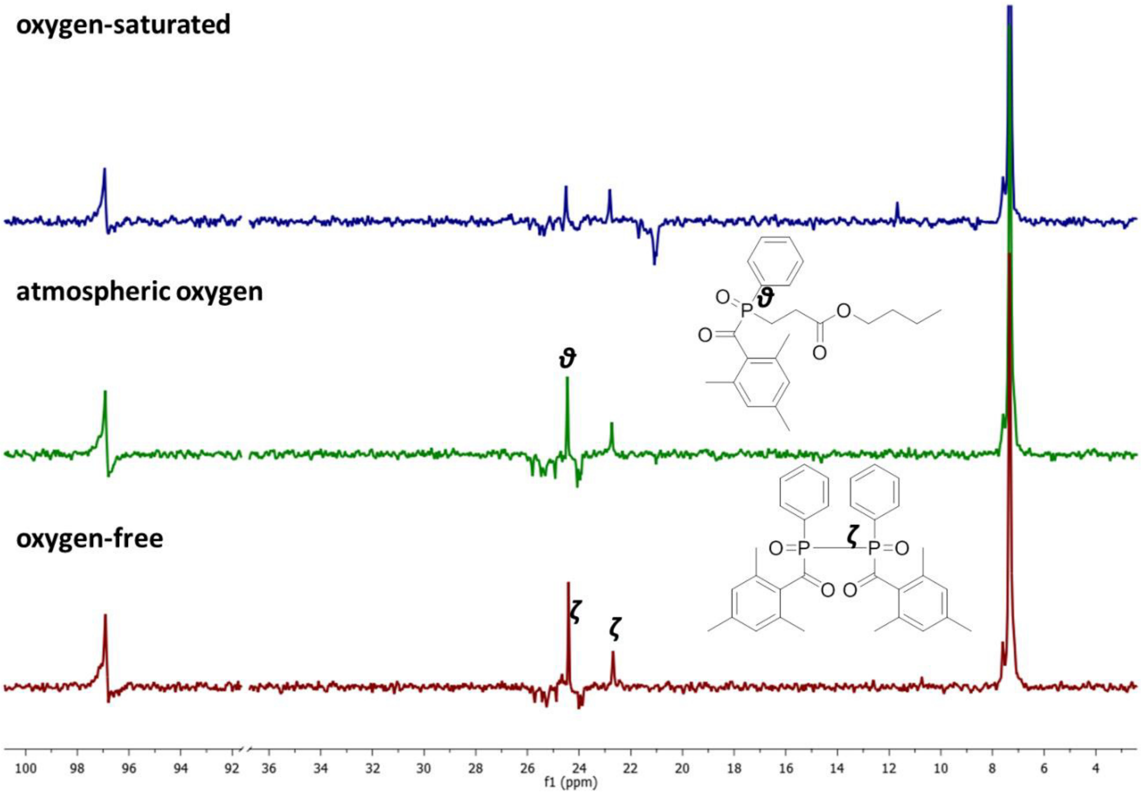

Figure 44. ^{31}P-CIDNP spectra of BAPO 10 mM with butyl acrylate 100 mM and various oxygen concentrations (toluene, 4x32 scans). The bottom trace shows the spectrum of the oxygen-free sample. The middle spectrum represents the sample under atmospheric conditions and the top spectrum the oxygen-saturated sample.

Predictions and reference data indicate, that the overlapping signal at 24.40 ppm belongs to the addition product ***P'10*** of ***R'2*** to butyl acrylate. This assumption is supported by the observation in the oxygen-saturated sample. There the two ζ signals have the same intensity and the second peak has a shift of 24.48 ppm. The spectrum of the oxygen-free sample shows at the same shift a signal with a shoulder. This indicates that ***R'2*** in oxygen-saturated samples does not react with the acrylate, which is supported by the previous findings, that in oxygen-saturated samples double bond conversion does not occur.

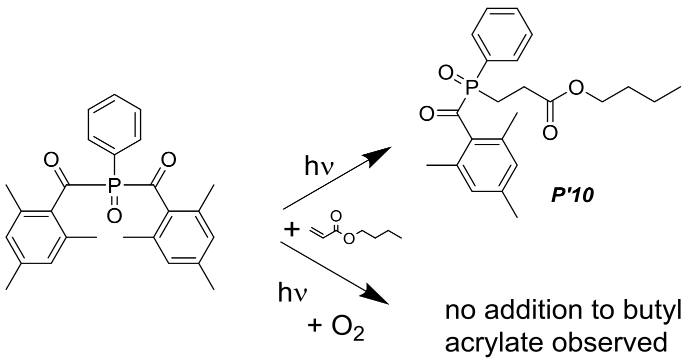

Scheme 38. Additional reaction products found with ^{31}P-CIDNP experiments in the presence of butyl acrylate.

5.1.6 Radical Trapping with TEMPO

TEMPO can be applied as a radical scavenger and is therefore added to the photoinitiator solutions. The results show that TEMPO reacts with the radicals, which are formed upon irradiation and yields by ^{1}H- ^{13}C- and ^{31}P-NMR experiments observable compounds.

5.1.6.1 ^{1}H-NMR Experiments with TEMPO at Various Oxygen Concentrations

In the reference spectrum only the initiator and the solvent are visible, as TEMPO is paramagnetic. After irradiation the spectrum of the oxygen-free sample contains broad new peaks and the signals of the parent initiator disappear. TEMPO's protons provide signals in the range from 1.0 ppm to 1.5 ppm; due to the broad and overlapping signals a precise assignment is not possible.

These TEMPO signals also belong to a newly found compound, which is the reaction product of TEMPO and ***R'1***. The signals at 2.30 ppm (***28***), 2.48 ppm (***30***) and 6.64 ppm (***29***) indicate the formation of ***P'14*** 2,6-tetramethylpiperidin-1-yl 2,4,6-trimethylbenzoate. The peak shapes point to possibly overlapping signals but further structure determination is not feasible. The reaction between ***R'2*** and TEMPO is likely but not observable with ^{1}H-NMR.

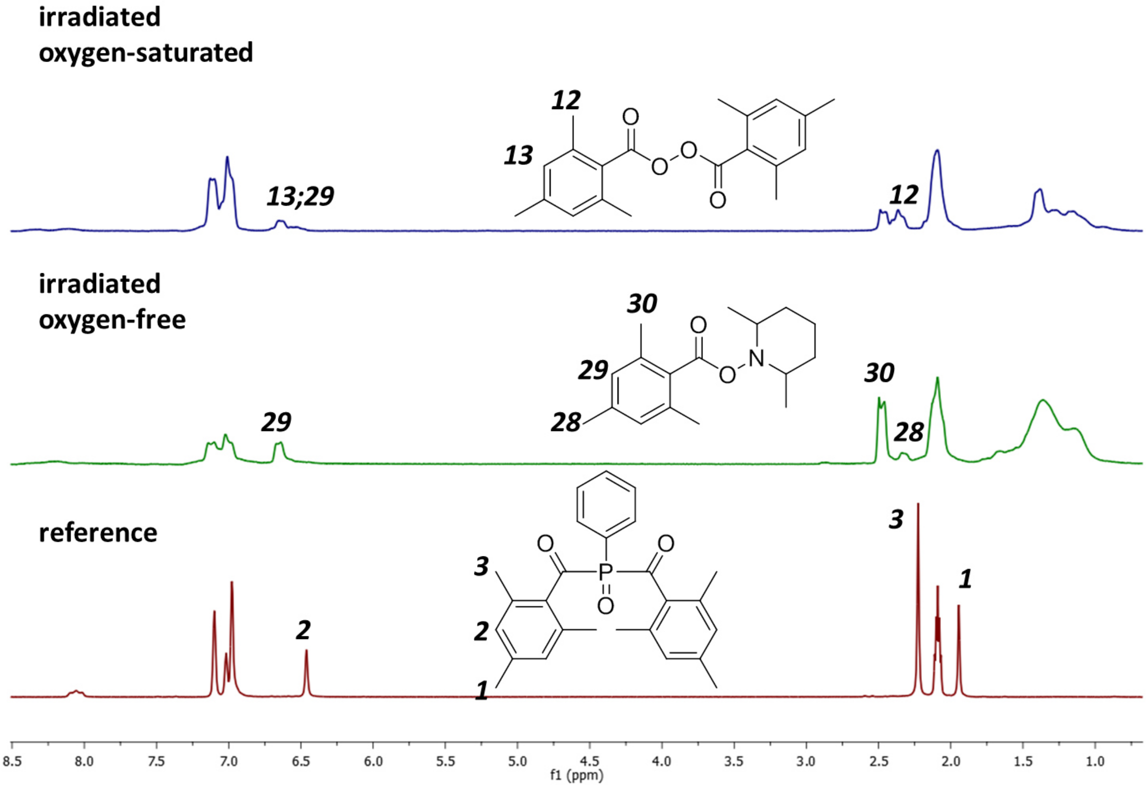

Figure 45. ^{1}H-NMR spectra of BAPO 10 mM and TEMPO 20 mM at various oxygen concentrations, before and after irradiation (32 scans in toluene). The bottom spectrum represents the non-irradiated sample. The middle trace shows the spectrum of the oxygen-free irradiated sample and the top spectrum the oxygen-saturated sample.

In the presence of oxygen signals belonging to ***P'14*** are detected. These signals overlap partially with the signals belonging to dimesitoyl peroxide ***P'8***. It is possible to assign the peroxide through a substituent effect, which strongly influences the para methyl group of the mesitoyl ***R'1***. When ***R'1*** reacts with TEMPO the protons of the para methyl are shifted to a higher field than the ortho methyl group protons. In the absence of oxygen shifts and relative intensities of peaks ***28*** and ***30*** indicate this behavior. In the presence of oxygen these two peaks have similar intensities. This is because for ***P'8*** the shift of para methyl protons is higher than the shift of the ortho methyl protons. Here I find the para signals at the same value as the ortho signals of ***P'14*** and vice versa.

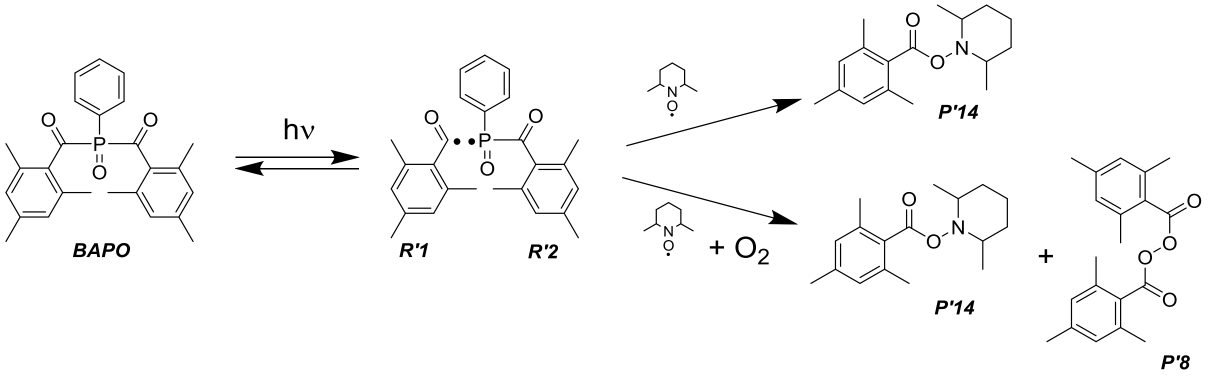

Scheme 39. With ^{1}H-NMR experiments observed reaction products of BAPO and TEMPO in the absence and presence of oxygen.

With ^{1}H-NMR experiments, in the absence and presence of oxygen, it is possible to detect the reaction product of ***R'1*** and TEMPO. In the presence of oxygen ***P'8*** is additionally observed. On the other hand there is no evidence for the possible reaction product of the mesitoyl peroxide radical ***R'7*** and TEMPO.

5.1.6.2 ^{13}C-NMR Experiments with TEMPO at Various Oxygen Concentrations

Here I present data that support the findings from ^{1}H-NMR experiments. The reaction of ***R'1*** and TEMPO is best followed by the carbonyl carbon signal, as signal ***c*** of BAPO is detected around 210 ppm and the carbonyl signal ***r*** (168.56 ppm) of the reaction product 2,6-tetramethylpiperidin-1-yl 2,4,6-trimethylbenzoate ***P'14*** has a significantly different shift. The shift of the aromatic carbons ***p*** and ***q*** support this, as well as signal ***s*** at 60.05 ppm. This signal belongs to the carbons in position 2 and 6 of TEMPO. The ^{13}C-NMR spectra in the absence and presence of oxygen show all signals of this compound.

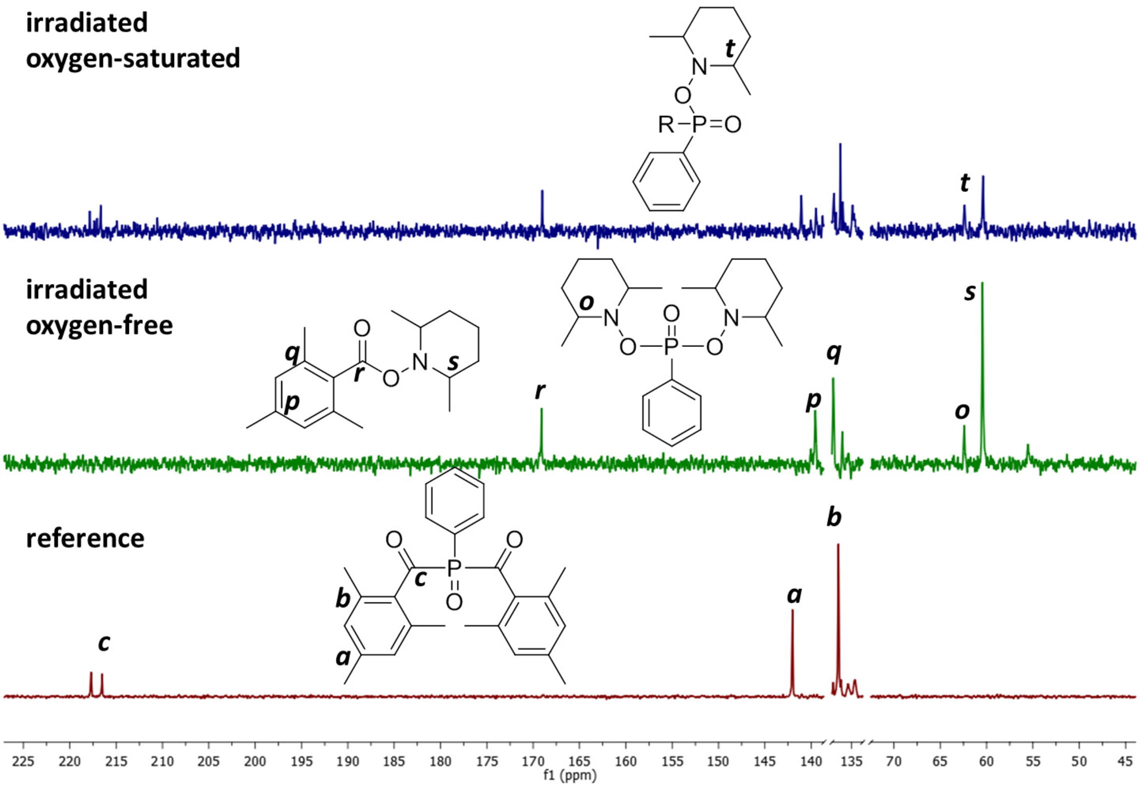

Figure 46. ^{13}C-NMR spectra of BAPO 10 mM and TEMPO 20 mM at various oxygen concentrations, before and after irradiation(4096 scans in toluene). The bottom spectrum represents the non-irradiated sample. The middle trace shows the spectrum of the oxygen-free irradiated sample and the top spectrum the oxygen-saturated sample. R: *R'1*, *R'2* or *R'7*.

Signal ***o*** is of particular interest, as it indicates that phosphorus is bound to TEMPO, which results in a shift to lower field. BAPO has two mesitoyl substituents and both can cleave. If one mesitoyl is still attached to the phosphorus the carbonyl carbon of the mesitoyl substituent should provide a signal around 210 ppm. In the absence of oxygen this carbonyl signal is not observed. Therefore it is likely that compound ***P'15*** is formed.

In the presence of oxygen signals representing ***P'15*** are observed. Additionally signal ***t*** indicates that TEMPO is attached to ***R'2*** but here it is not possible to distinguish between phosphinoyl, which is attached to one or two TEMPO units. In the presence of oxygen carbonyl signals still appear around 210 ppm. There are multiple possible explanations: parts of the parent initiator are still existing, dimesitoyl peroxide ***P’8*** or similar mesitoyl peroxides are formed and TEMPO replaced only one of BAPOs mesitoyl substituent groups.

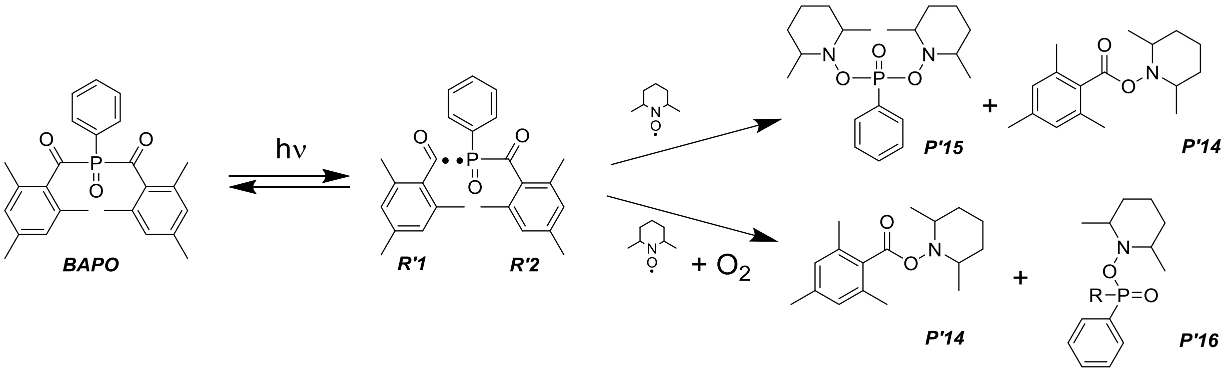

Scheme 40. With ^{13}C-NMR experiments observed reaction products of BAPO and TEMPO in the absence and presence of oxygen. R: *R’1*, *R’2* or *R’7*.

The formation ***P’14*** in the absence and presence of oxygen is corresponding with the results obtained from the ^{1}H-NMR experiments. Additionally with these experiments and in the absence of oxygen it was possible to observe compound ***P’15***.

5.1.6.3 ^{31}P-NMR Experiments with TEMPO at Various Oxygen Concentrations

I repeated the same radical scavenging experiment and recorded ^{31}P-NMR spectra. The non-irradiated reference spectrum contains signals of the parent initiator. Irradiation causes severe product fragmentation and only small signal intensities of the formed products are detected. The spectrum of the oxygen containing sample shows traces of the parent initiator and in the absence of oxygen these signals are not found.

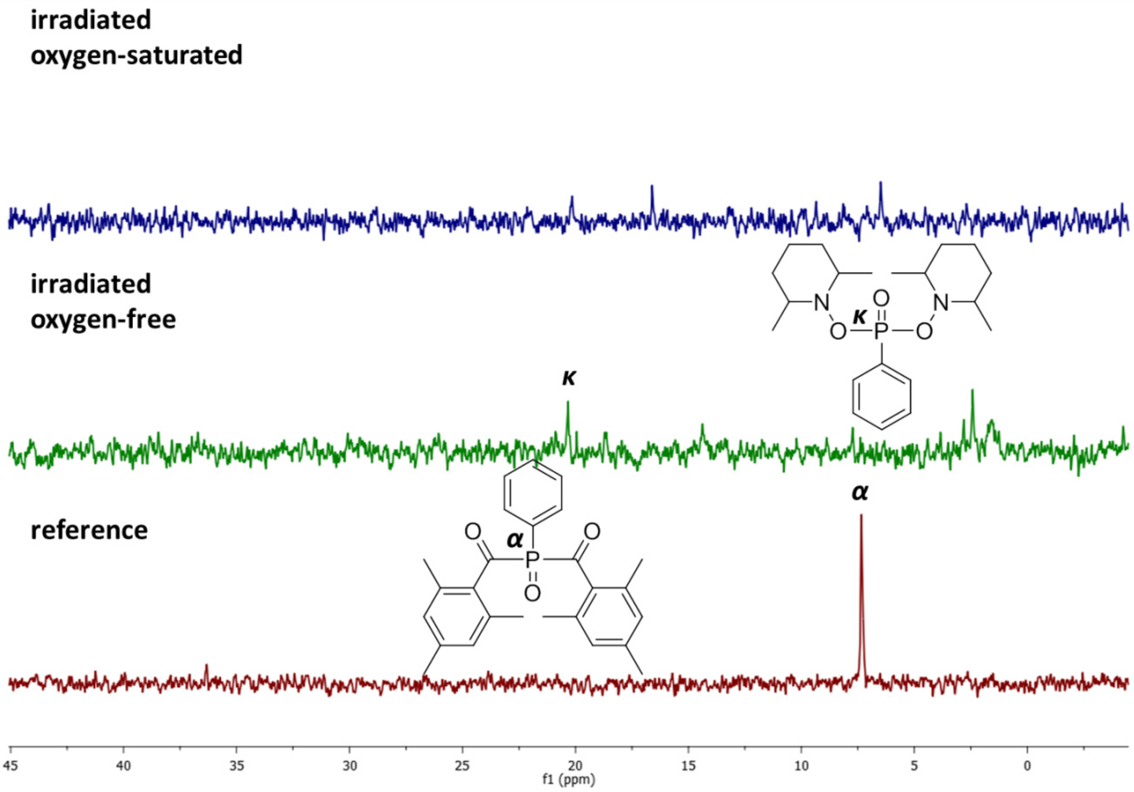

Figure 47. **^{31}P-NMR of BAPO 10 mM and TEMPO 20 mM (256 scans in toluene). On the bottom trace the spectrum of the non-irradiated sample in the absence of oxygen is displayed. The middle spectrum represents the irradiated sample without oxygen and the top trace displays the irradiated sample in the presence of oxygen.**

The promising signal ***κ*** has a shift of 20.20 ppm and is found in both samples, but in the absence of oxygen it has higher signal intensity. ACD/labs® and MestReNova® prediction tools calculate a phosphorus signal of compound ***P'15*** around 17 ppm with an error of 5 ppm. Signal ***κ*** is within the predicted regime and I expect that phosphorus, which has two TEMPO units as substituents, is shifted to lower fields compared to the signal of the parent initiator, therefore the assumption that ***κ*** represents compound ***P'15*** is feasible.

5.1.7 Mass Spectrometry

ESI-MS experiments were performed to obtain additional information about formed products and to support NMR results with an independent method. NMR experiments indicated already significant product fragmentation of the initiator upon irradiation and the ESI-MS results show the product fragmentation much better. Many different signals appear in the observed range from m/z 50 to m/z 750. The assigned signals are color-coded in the displayed graphs and the structures are shown at the end of this section in **Scheme 41**.

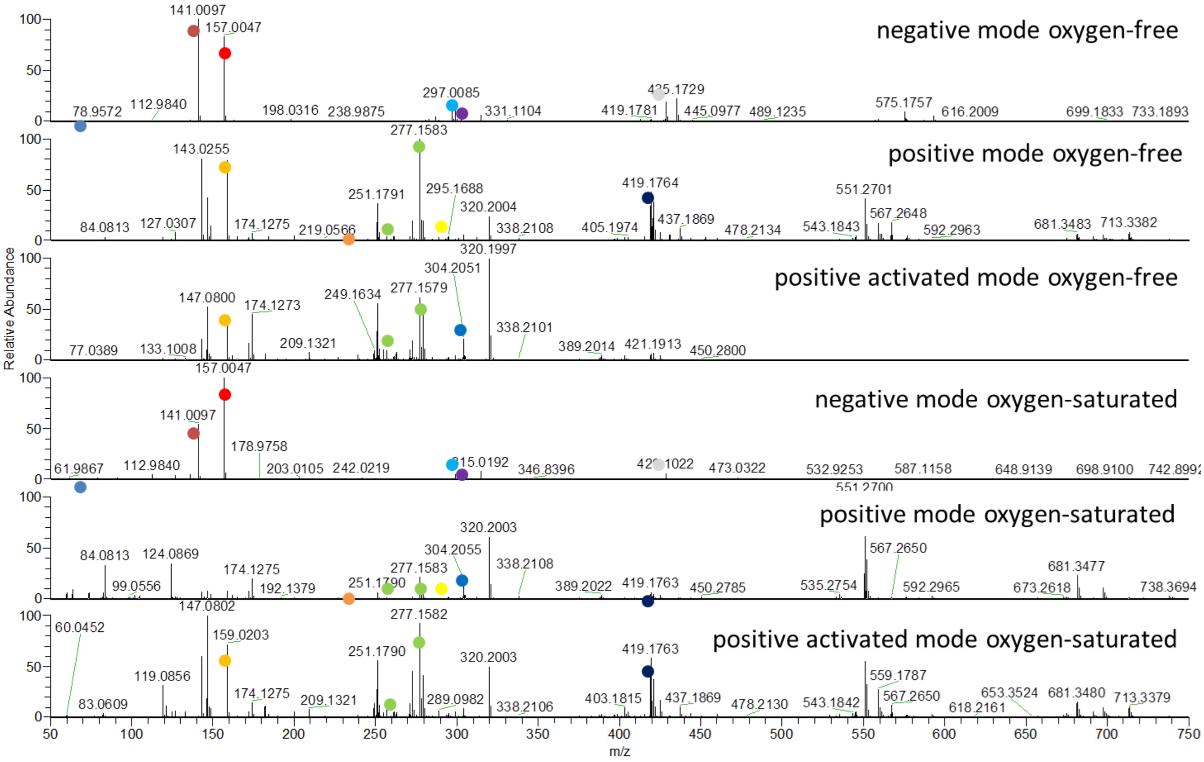

Figure 48. ESI-MS results of BAPO 10 mM after irradiation. The lower three traces represent the oxygen-saturated sample. The upper three traces display the spectra of the oxygen-free sample. For each sample experiments in the negative, the positive and the positive activated mode were performed. Assigned signals are color-coded and the structures are displayed in Scheme 41.

The differences between oxygen containing and oxygen-free samples are not significant, as the same pseudo molecules and comparable relative abundances are obtained. After irradiation the spectra of both samples contain a signal at m/z 419, which belongs to the protonated form of the initiator.

These results indicate the formation of several phosphorus based acids, which fits to the observation of fast exchanging proton signals in ^{1}H-NMR. The signal at m/z 78.9 represents traces of the deprotonated form of phosphenic acid. The spectra indicate high abundances of phenylphosphinic acid in the negative mode (signal at m/z 141) and in the positive mode (signal at m/z 143). Additionally the peaks of phenylphosphonic acid appear at m/z 157 and 159.

The signal at m/z 147 represents the mesitoyl fragment and the corresponding aldehyde ***P'7*** is observed at m/z 149. The recombination product dimesitoyl ***P'1*** provides a signal at m/z 295. With ***A1*** I observed dibenzoyl peroxide ***P6*** but here, against the expectation, it was not possible to detect the corresponding peroxide ***P'8***.

Similar to ***A1*** 2,4,6-trimethyl phenyl substituents containing products are detected. The formation of 2,4,6-trimethyl phenyl supports decarbonylation and decarboxylation mechanisms. For example I detect 2,2',4,4',6,6'-hexamethyl-1,1'-biphenyl ***P’4*** at m/z 239.

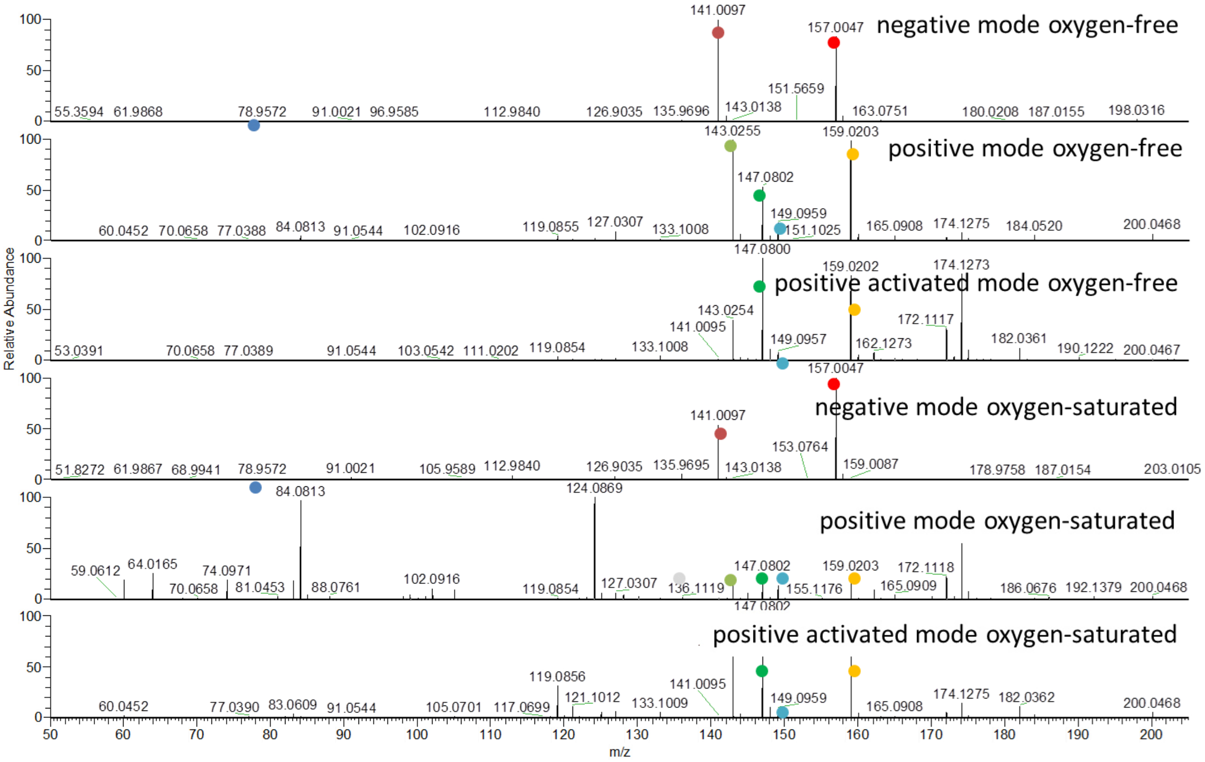

Figure 49. Enlarged section of the ESI-MS results of BAPO 10 mM after irradiation. The lower three traces represent the oxygen-saturated sample. The upper three traces display the spectra of the oxygen-free sample. For each sample experiments in the negative, the positive and the positive activated mode were performed. Assigned signals are color-coded and the structures are displayed in Scheme 41.

The enlarged sections of the ESI-MS graphs indicate some differences between oxygen containing and oxygen-free samples. It appears that phosphorus derived acids and mesitoyl fragments are found in higher abundance when oxygen is absent. It is not feasible to assign the peaks at m/z 84 and m/z 124, which are predominantly formed in the presence of oxygen.

Additional pseudo molecules containing two phosphorus atoms and phosphorus based peroxides appear. These molecules and substructures support my NMR results.

m/z		m/z	
78.9572 ●	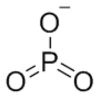	159.0202 ●	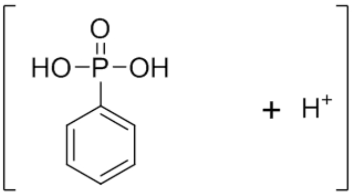
141.0097 ●	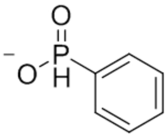	239.0980 ●	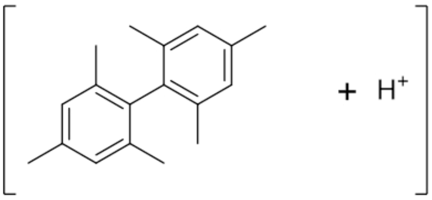
143.0255 ●	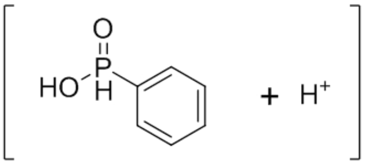	255.0928 ●	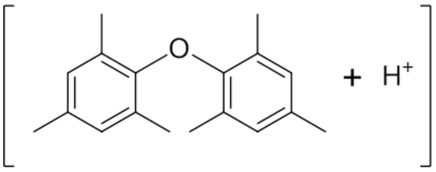
147.0802 ●	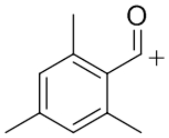	295.1688 ●	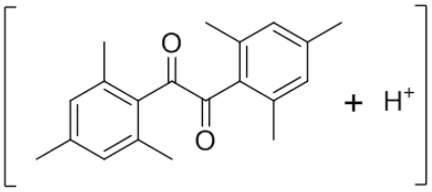
149.0959 ●	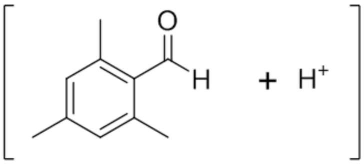	297.0085 ●	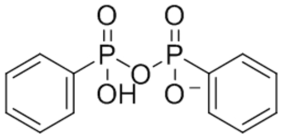
157.0047 ●	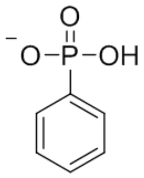	303.0790 ●	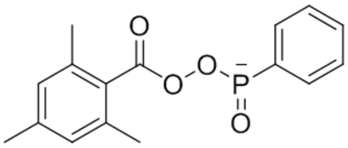

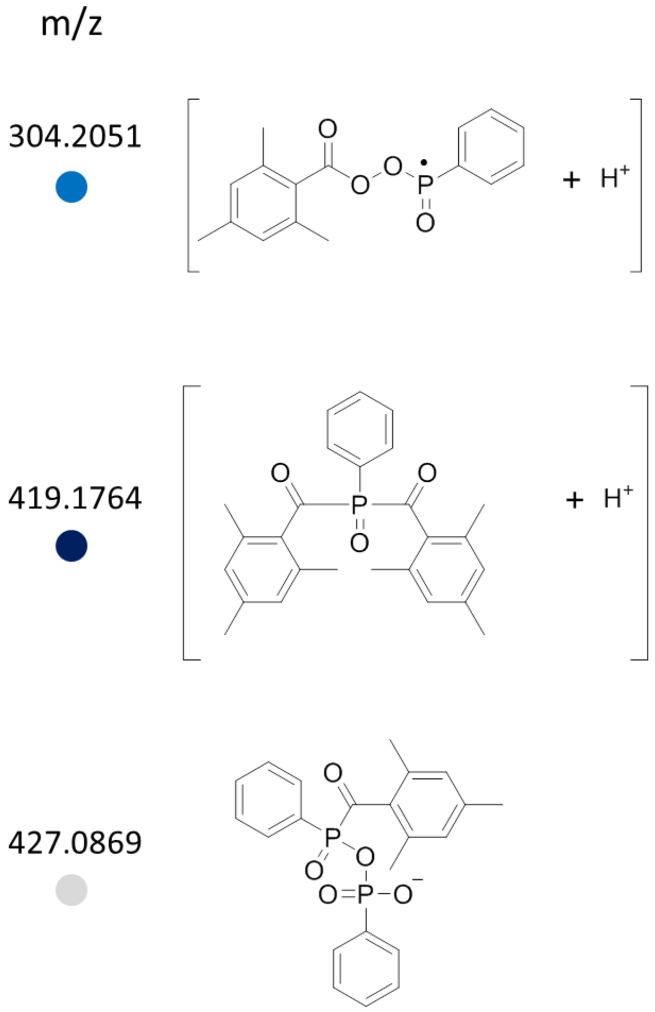

Scheme 41. Overview of the marks indicated in the MS traces of Figure 48 and Figure 49 and their structure assignment. Compounds in brackets represent pseudo molecules with ammonium or a proton.

5.1.8 Oxygen Measurement

I measured the oxygen concentration in deuterated toluene before and after the irradiation of BAPO. The used optical sensor is designed for determining low oxygen concentrations and works best in the range from 0-20 % oxygen under normal conditions.

From the measured partial pressure I calculated the actual molar concentration via Henry's law. k_H^{px}= 110.6 x 10^6 Pa was used for the calculations.[126,127,128]

Figure 50 displays the molar oxygen concentration in the solvent as a function of the oxygen partial pressure in % under normal conditions. The application of Henry's law leads to linear functions, which imply that the oxygen sensor is within its operation range. Upon irradiation the oxygen concentrations decrease. From NMR and ESI-MS experiments we know that peroxides are formed in the presence of oxygen and therefore oxygen is consumed. The results from α-hydroxy ketone ***A1*** show the same effect but for BAPO it is more pronounced. The oxygen concentrations of the irradiated BAPO samples can also be fitted linearly. I can explain the stronger pronounced oxygen consumption with BAPO's possibility to undergo additional cleavages. The cleavage in the first step usually leads to ***R'1*** and ***R'2*** and both radicals can react with oxygen. The phosphinoyl radical ***R'2*** after the first cleavage is a MAPO derivative and therefore the second mesitoyl group can be removed. In principle BAPO leads up to 4 radicals, which are able to react with oxygen, instead of two radicals derived from ***A1***.

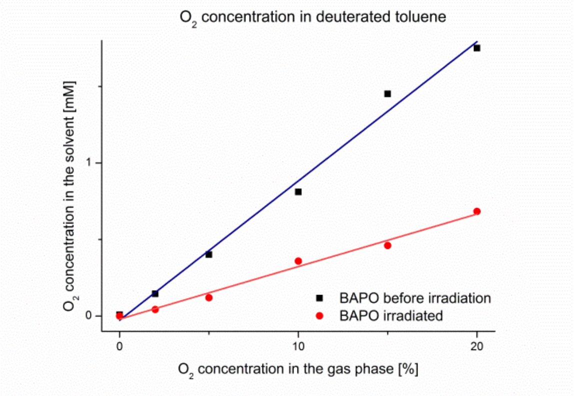

Figure 50. Oxygen concentration in deuterated toluene with BAPO 10 mM before and after irradiation.

In samples under atmospheric conditions 1.75 mM oxygen are dissolved in toluene. After irradiation only 0.68 mM oxygen are detected, which means that ~61 % were consumed. Lower oxygen concentrations lead to similar values and they are presented in **Figure 51**.

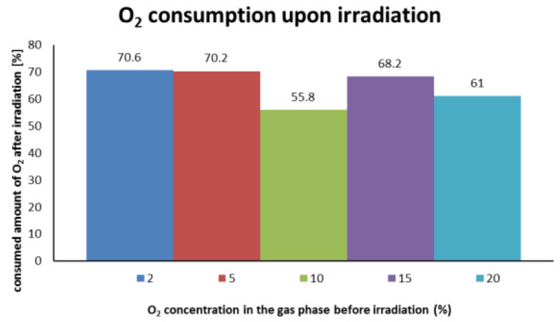

Figure 51. Percentage of the consumed oxygen concentrations after irradiation.

5.1.9 Laser Flash Photolysis

The addition rate constants for ***R'1*** and ***R'2*** to butyl acrylate are known, but most values were determined in acetonitrile. I used toluene and for this solvent lower addition rate constants compared to acetonitrile are reported.[51,129]

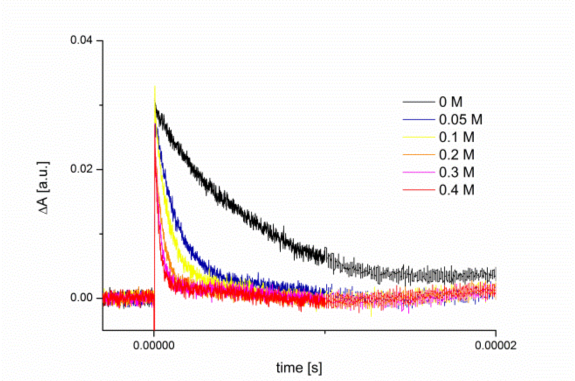

Figure 52. Transient absorbance decay of *R'2* in the presence of various butyl acrylate concentrations.

With LFP it is possible to observe the decay of the transient absorbance and often the decay can be fitted with a single exponential function. Quenching the formed radicals with defined amounts of butyl acrylate or oxygen results in the determination of addition rate constants of pseudo first order reactions.[130]

The addition rate constant for the phosphinoyl radical ***R'2*** in toluene is k_{butyl}= 7.42 x 10^6 M^{-1} s^{-1}. This is lower, than the published rate constant k_{butyl}= 1.10 10^7 M^{-1} s^{-1}, which was measured also via LFP but in acetonitrile.[35] The rate k_{butyl}= 7.6 x 10^6 M^{-1} s^{-1} ± 0.2 determined in toluene via TR-EPR fits excellent to my LFP result.[56]

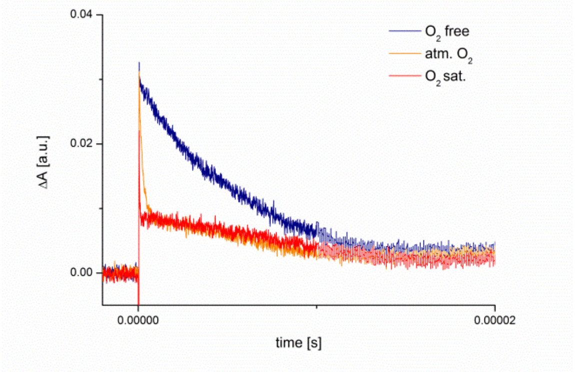

Figure 53. Transient absorbance decay of *R'2* in the presence of various oxygen concentrations.

To resolve the addition rate of oxygen to BAPO only oxygen concentrations between 0 and 0.5 mM are suitable. At higher oxygen concentrations first the exponential decay of the transient absorbance is very fast and then a further slow linear decay occurs. **Figure 53** displays this effect.

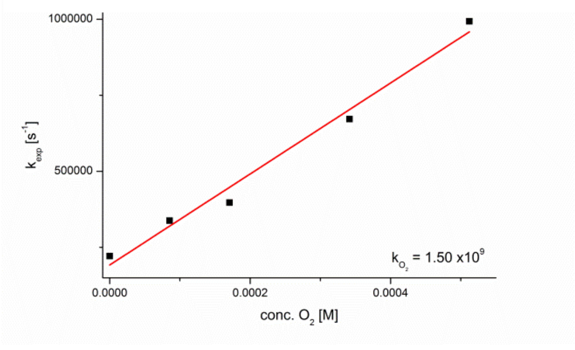

Figure 54. Stern-Volmer plot to obtain the addition rate constant of *R'2* to oxygen.

The addition rate constant for oxygen should be considerably higher and I expect it to be in the range between 10^9 and 10^{10} M^{-1} s^{-1}.[35,56] The addition rate for oxygen to ***R'2*** is k_{O_2} = 1.50 x 10^9 M^{-1} s^{-1}. This is considerably lower than the published rate in acetonitrile of k_{O_2} = 2.70 x 10^9 M^{-1} s^{-1} but within the same order of magnitude.[59] The rate constant obtained from TR-EPR measurements is published with the value of k_{O_2} = 4.3 x 10^{10} M^{-1} s^{-1} and therefore more than one order of magnitude bigger than my via LFP obtained addition rate constant.

5.1.10 Kinetic Simulations with Copasi®

With available kinetic data it was possible to simulate the first steps of a simplified reaction pathway of BAPO. In the absence of oxygen I focused on the formation of ***R'1*** and ***R'2*** and their recombination products. This model is based on complete cleavage of the initiator and the cleavage of all mesitoyl groups.

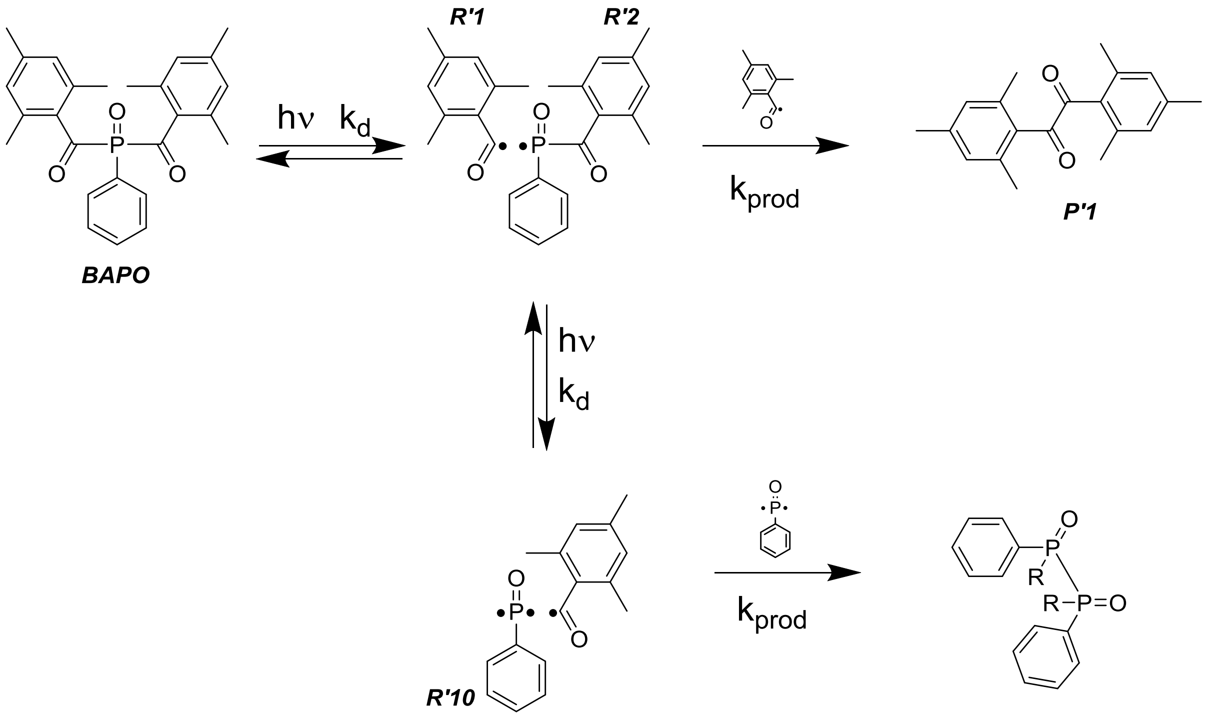

Scheme 42. First reactions of BAPO in the absence of oxygen. Radicals are formed upon irradiation. The phosphinoyl radical *R'2* can form additional radicals after second excitation with light.

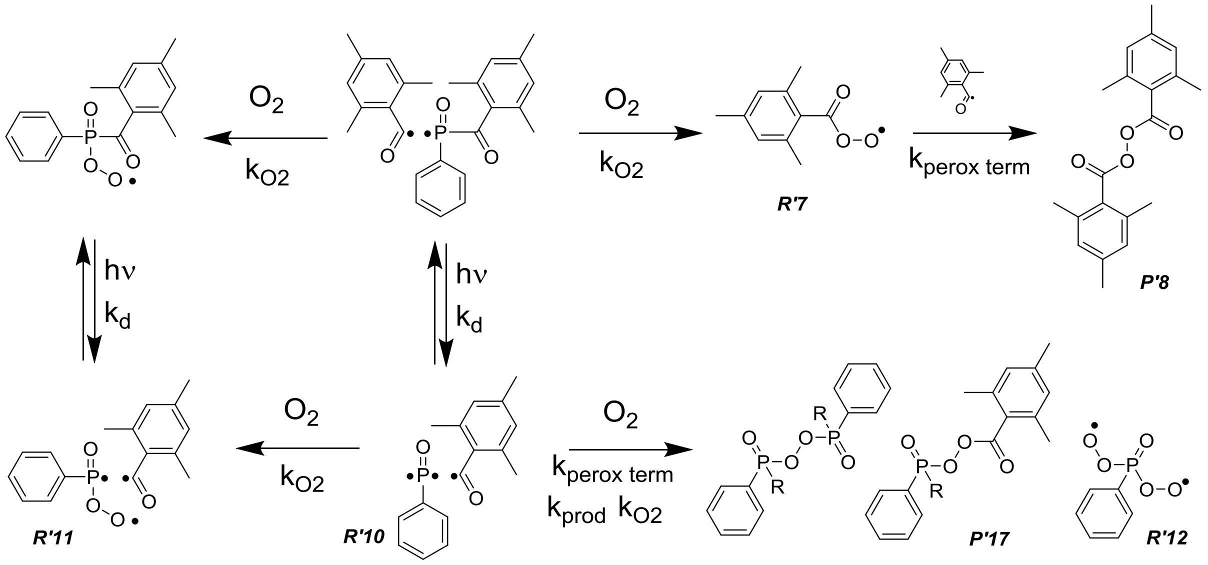

Scheme 43. Overview of simulated reactions of BAPO in the presence of oxygen.

In the presence of oxygen multiple side reactions can take place, therefore the simulations included radical peroxide formation and termination reactions. In this simulation it is determined that the phosphorus centered radicals are both able to react with oxygen and form further intermediates.

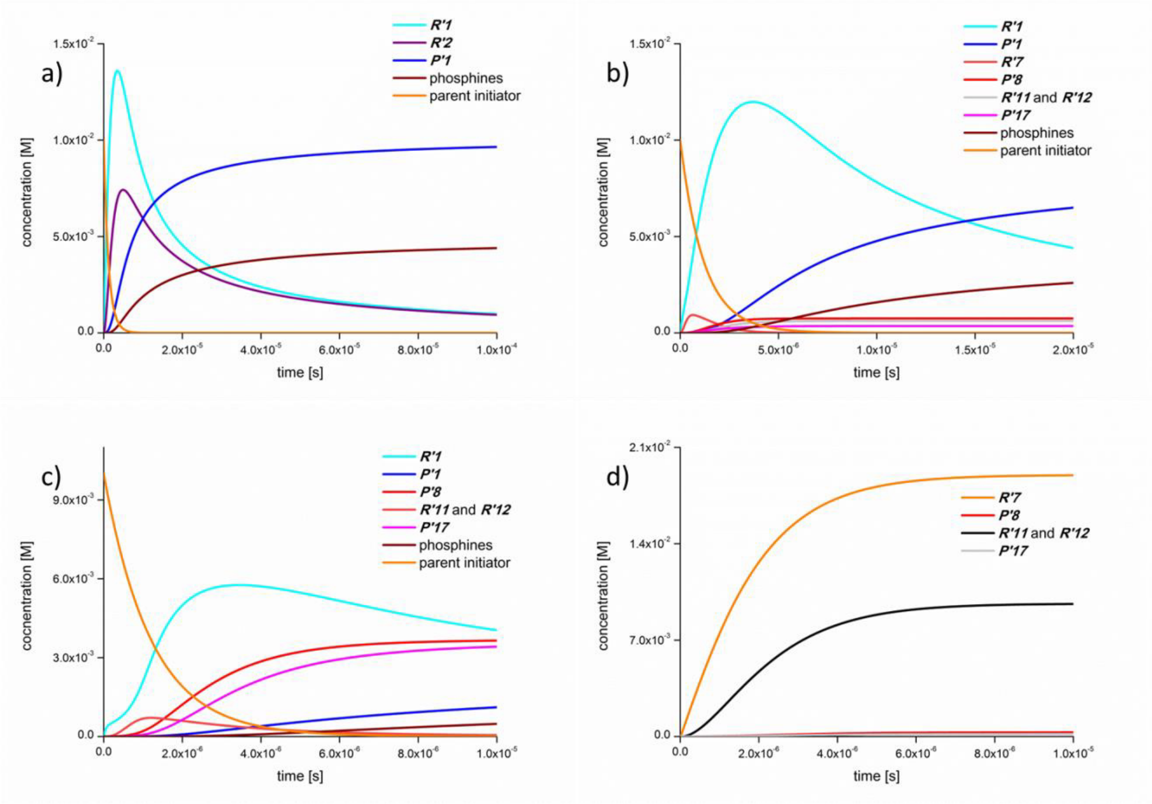

Figure 55. Kinetic simulations of BAPO 10 mM reacting upon irradiation in the presence of various oxygen concentrations. Time versus concentration plots of selected species. a) simulation in the absence of oxygen. Decomposition of the initiator, intermediate radicals and products are observed. b) under atmospheric conditions (1.75 mM oxygen). Similar behavior as in the absence of oxygen. Additional peroxides are found. c) Simulation with 10 mM oxygen. Increase of peroxides and less initiator radicals. Products are still detected d) with 50 mM oxygen. Only phosphinoyl peroxide radicals *R'12* and mesitoyl peroxide radicals *R'7* are found.

Graphs **a** and **b** represent the simulation in the absence of oxygen and the simulation under atmospheric conditions (1.75 mM oxygen), which are similar. High amounts of mesitoyl ***R'1*** and phosphinoyl ***R'2*** as radical intermediates appear. Dimesitoyl ***P'1*** and phosphines are the main products. Under atmospheric conditions small amounts of peroxides are formed, which fits to my NMR results, where oxygen-free samples and those under atmospheric conditions led to equivalent results.

The composition of products and intermediates changes tremendously, when the oxygen concentration increases to 10 mM and 50 mM respectively. With 10 mM oxygen ***R'1*** still is observed but the new main products are peroxides ***P'8*** and ***P'17***. On the other hand I obtain only about 10 % of the possible dimesitoyl concentration. Mesitoyl peroxide radicals ***R'7*** and phosphinoyl peroxide radicals ***R'11*** are only intermediates in this simulation.

With 50 mM oxygen, ***R'7*** and ***R'12*** are the main products and all other compounds are detected only in traces. Through the high oxygen concentration and the high addition rate constant towards oxygen mesitoyl radicals ***R'1*** and phosphinoyl radicals ***R'2*** react dominantly with oxygen. Also with 50 mM the oxygen concentration is higher than the maximum radical concentration. Therefore not all oxygen is consumed, while with 10 mM the whole oxygen is consumed.

Polymerization simulations contain the same data set as before and reactions of the radicals with monomers were added. The starting concentrations were for BAPO 10 mM, for butyl acrylate 100 mM and for oxygen 0 M, 1.75 mM, 10 mM and 50 mM.

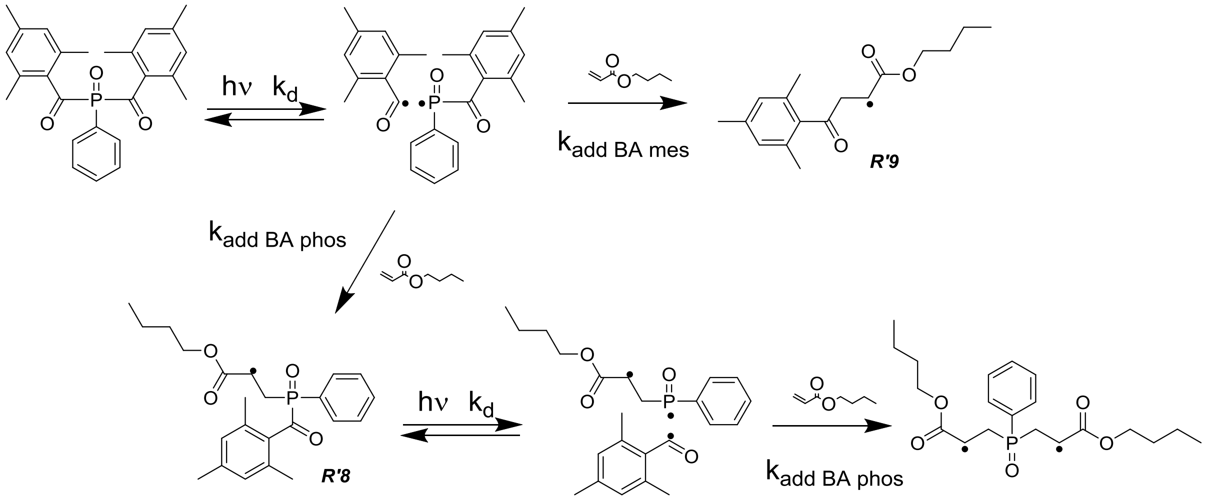

Scheme 44. First addition reactions of radicals to butyl acrylate.

The simulations show the first addition products and they contain a propagation step to obtain polymers. For simplification the initiating radicals do not influence the rate of the propagation step and chain termination reactions were not included.

In the absence of oxygen first the fast formation of ***R'1*** and ***R'2*** occurs. Due to the higher amount of ***R'1*** and the lower addition rate towards butyl acrylate, the concentration of ***R'1*** decreases slower than the concentration ***R'2***.

In the meantime, the first radical addition forms intermediate main products. The concentration of the first radical addition products decreases and polymer concentrations rise when the time scale is increased. In the absence of oxygen the polymerization is completed after ~0.2 s. The most dominant side product is dimesitoyl ***P'1***.

Figure 56 a and **b** displays the simulations in the absence of oxygen.

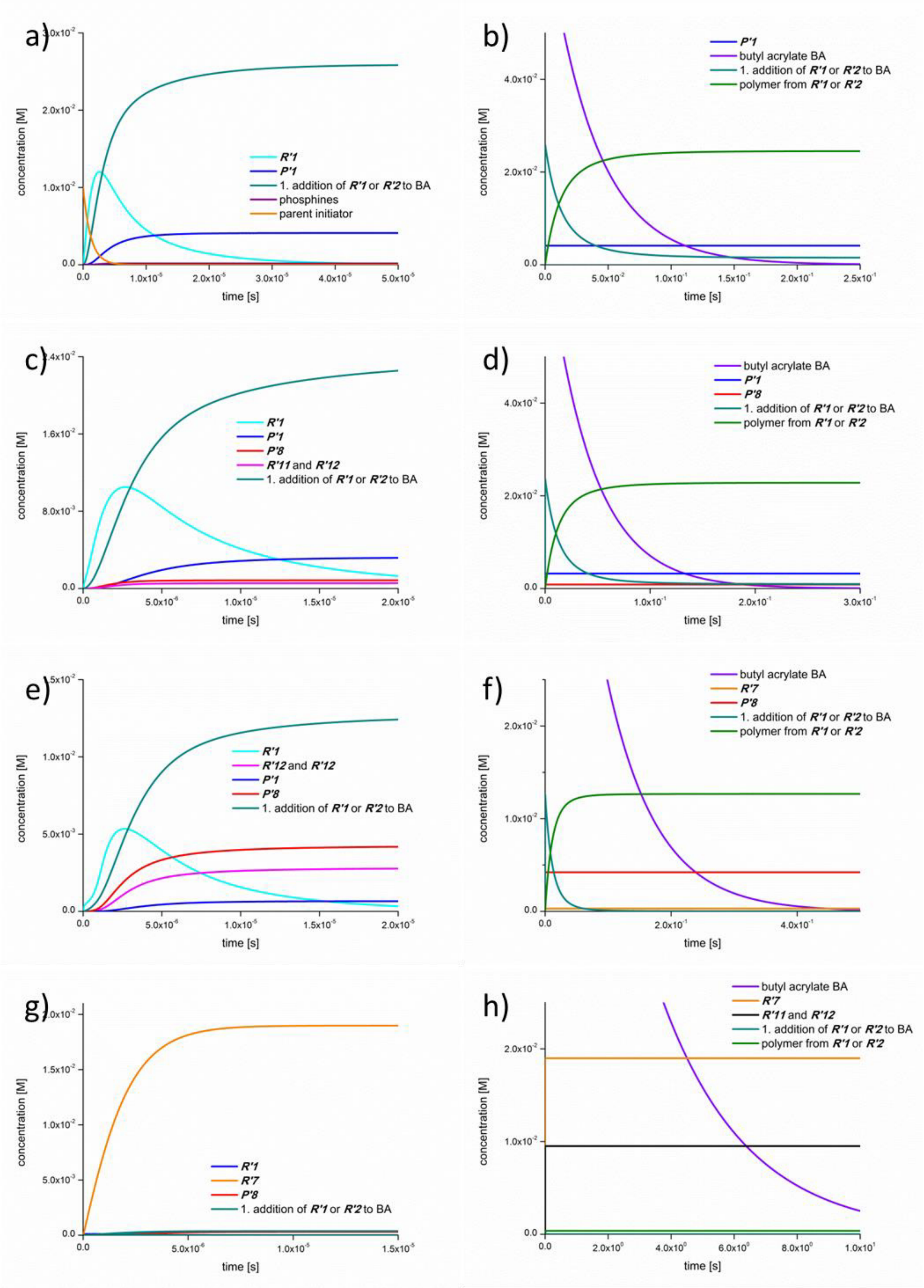

Figure 56. Kinetic simulations of BAPO 10 mM with butyl acrylate and various oxygen concentrations. The left graphs (a,c,e,g) represent short timescales 10^{-5} s while the right graphs (b,d,f,h) show the long timescale ~1 s. a & b) oxygen-free simulation. c & d) atmospheric condition O_2 1.75 mM. e & f) 10 mM oxygen. and g & h) 50 mM oxygen.

The simulation under atmospheric conditions shows comparable results as the oxygen-free sample. Efficient addition and polymer formation occurs and peroxide side products are detected. The polymerization speed is slightly reduced as the reaction is complete after 0.22 seconds compared to 0.2 s in the oxygen-free simulation.

In the presence of 10 mM oxygen dimesitoyl peroxide ***P'8*** and phosphinoyl peroxide radicals ***R'12*** appear in high amounts. Nevertheless still sufficient amounts of reactive radicals are available for a first addition. The maximum concentration of the first addition product is here ~12 mM compared to ~25 mM in the absence of oxygen. In other words about 50 % of reactive radicals are consumed by oxygen. Through the lower concentration of first addition products also the polymerization takes a proximately twice as long as in the absence of oxygen.

With 50 mM oxygen I observe in the short timescale only mesitoyl peroxide radicals ***R'7*** and phosphinoyl peroxide radicals (***R'11*** and ***R'12***). Minor amounts of radicals attack the monomer. As these simulations do not include further oxygen based termination reactions, slow polymerization in form of butyl acrylate consumption is still observed. Through the very low concentration of first addition products, the polymerization requires more time. After 20 s the monomer is consumed. In the absence of oxygen this process takes only 0.2 s.

The simulation results correlate well with my experimental findings. Samples with atmospheric oxygen concentrations and oxygen-free samples behave similar. There it is possible to observe polymerization. Oxygen-saturated samples mainly led to peroxides and polymerization or any double bond conversion did not occur.

Table 2. rate constants used for kinetic simulations.

rate constant	value	unit	reference	rate constant	value	unit	reference
k_d	8.3×10^5	s^{-1}	96,34,97	$k_{add\,BA\,mes}$	1.8×10^5	$M^{-1}\,s^{-1}$	121
k_{prod}	$\sim 2 \times 10^7$	$M^{-1}\,s^{-1}$	34,97,53	$k_{add\,BA\,phosph}$	7.4×10^6	$M^{-1}\,s^{-1}$	own work
$k_{add\,O_2\,benz}$	1.8×10^9	$M^{-1}\,s^{-1}$	35	$k_{perox\,term}$	$\sim 6 \times 10^7$	$M^{-1}\,s^{-1}$	101,60,61
$k_{add\,O_2\,phosph}$	1.5×10^9	$M^{-1}\,s^{-1}$	own work	k_{prop}	1000	$M^{-1}\,s^{-1}$	108,45,60,61

5.1.11 Thermal Imaging

It was possible to study thermal polymerization effects with a live view thermal imaging camera. The differentiation between bulk effects, thermal diffusion and oxygen inhibition was successful. In contrast to previous experiments, i.e. NMR and ESI-MS experiments worked in diluted, here the focus is put on bulk reactions and concentrated butyl acrylate samples are cured.

The results are described in detail in the attached paper while here I highlight a few findings.[8]

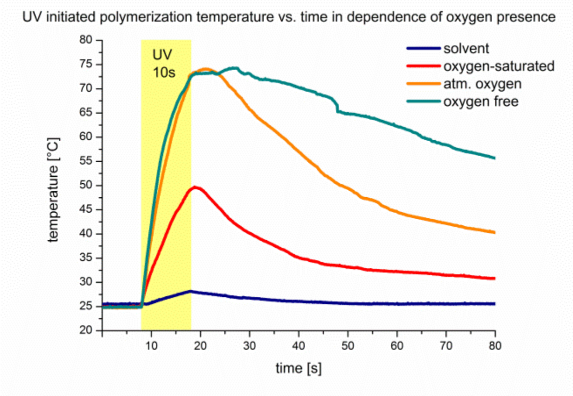

Figure 57. Time versus temperature plots of BAPO in bulk butyl acrylate at various oxygen concentrations. Irradiation time 10 s.

A high resolution thermal camera recorded spatially resolved the surface temperature during the polymerization. The observed heat is produced dominantly through the double bond conversion. Therefore it is possible to follow the polymerization process. The results for the oxygen-free sample and the sample under atmospheric conditions are similar and correspond with our previous findings.

Upon irradiation of those samples the temperature increases rapidly, with reaching a maximum at ~ 75 °C. The atmospheric sample keeps this temperature after irradiation stopped for about 10 s an then the temperature decreases slowly. The oxygen-free probe stays around 75 °C for about 15 s and the temperature decrease afterwards is slower than under atmospheric conditions.

The polymerization spreads out through the whole sample tube and at the end the probes are cured.

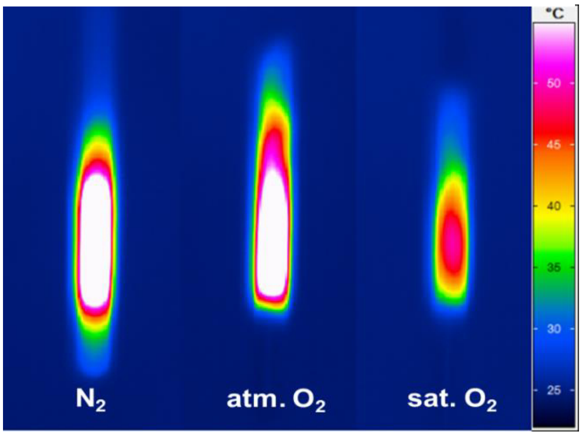

Figure 58. Thermal images of BAPO in bulk butyl acrylate 10 s after irradiation started. The oxygen-saturated sample shows minor heat development.

The oxygen-saturated sample behaves different, as the temperature increases during irradiation to a maximum of 50 °C and immediately after the irradiation stopped the temperature rapidly decreases. Heat development is restricted to the irradiated area, and the sample did not cure and therefore stayed liquid.

Simple bulk polymerizations seem to work also in the presence of atmospheric oxygen. Irradiation times and photo initiator concentrations might be adopted.

Polymer Chemistry

PAPER

View Article Online
View Journal | View Issue

Cite this: *Polym. Chem.*, 2015, **6**, 2488

Thermal effects in polymerisations – a live view differentiating between bulk effects, thermal diffusion, and oxygen inhibition

Roman Geier,[a] Christina Wappl,[a] Hilde Freiszmuth,[a] Christian Slugovc[b] and Georg Gescheidt*[a]

Received 15th December 2014,
Accepted 23rd January 2015

DOI: 10.1039/c4py01739k

www.rsc.org/polymers

Thermography has been shown to be an efficient tool for the screening of the efficiency of exothermic reactions. Here we show that the use of a thermal IR camera reveals effects of heat transfer in polymerising mixtures if appropriately designed reaction vessels are used. We report on case studies illustrated by photo-induced radical polymerisation of butyl acrylate and thermally triggered ring-opening metathesis polymerisation of dicyclopentadiene.

Introduction

Generally, polymerisation reactions are exothermic. It is well established that bulk effects lead to rather high temperatures in polymerising mixtures. These thermal effects have been investigated by a variety of methods, in particular DSC or *in situ* with thermal sensors. Another important aspect in real systems is that heat is dissipated at the interfaces between the reaction mixture and its environment, *i.e.*, the vessel and the atmosphere. This obviously causes a rather inhomogeneous heat distribution, which may substantially alter the homogeneity and the properties of the final polymeric product. This feature is well established and has been addressed particularly using simulations.[1–4] A related aspect is the inhibition of radical polymerisations by oxygen, which also appears at the interface between the polymerising formulation and air.[5] A detailed analysis of these above-mentioned phenomena requires a corresponding technique, which provides information offering spatial and time resolution appropriate for polymerisation reactions.

It has been shown that the use of a thermal sensor[6] and, particularly, a thermal camera provides valuable insights for assessing the efficiency of (preferably) exothermic events.[7–9] Although thermal images exclusively display the temperature at the surface of the sample and disturbing reflections may occur, an image representing a two-dimensional spatial heat distribution offers useful insights into environmental effects of chemical reactions.[10]

We have, therefore, evaluated the use of a high-resolution thermal camera for simultaneously following the temperature and its dissipation depending on various reaction conditions. Moreover we have developed and tested reaction vessels for this type of study. Here we report our initial results, which indicate the scope (and caveats) of this experimental approach.

Results and discussion

As a first example, we have chosen a photo-initiated radical polymerisation for our investigations.[11–14] Such a procedure provides a clearly defined trigger for starting the polymerisation. In a thin-walled NMR tube, a mixture of the phosphine oxide based photoinitiator Irgacure 819 and butyl acrylate (Fig. 1A) in benzene was irradiated using a Hg/Xe high-pressure lamp for 10 s (shutter). The corresponding setup is shown in Fig. 1B. The Hg/Xe lamp is oriented perpendicular toward the NMR tube. This allows following the development of heat in a cross section below and above the centre of the irradiating light. The dissipation of heat together with the corresponding thermographic curves is displayed in Fig. 1C and D. Fig. 1C shows that a hot spot is immediately created at the position where the sample is irradiated. The temperature gradually decreases at larger distances. Upon stopping irradiation after 10 s, the temperature rises to its maximum, then gradually cools down but still being above room temperature after 140 s. In Fig. 1D, the influence of oxygen is illustrated. The three samples shown contain identical mixtures of the initiator and butyl acrylate. The sample on the left side is degassed on a vacuum line and sealed under N_2 (identical to the sample in the middle of Fig. 1C), the one in the middle reflects atmospheric conditions, whereas that on the right is saturated with O_2. All three images are obtained immediately

---

[a] *Institute of Physical and Theoretical Chemistry, Graz University of Technology, NAWI Graz, Stremayrgasse 9, 8010 Graz, Austria*
[b] *Institute for Chemistry and Technology of Materials, Graz University of Technology, NAWI Graz, Stremayrgasse 9, 8010 Graz, Austria. E-mail: g.gescheidt-demner@tugraz.at*

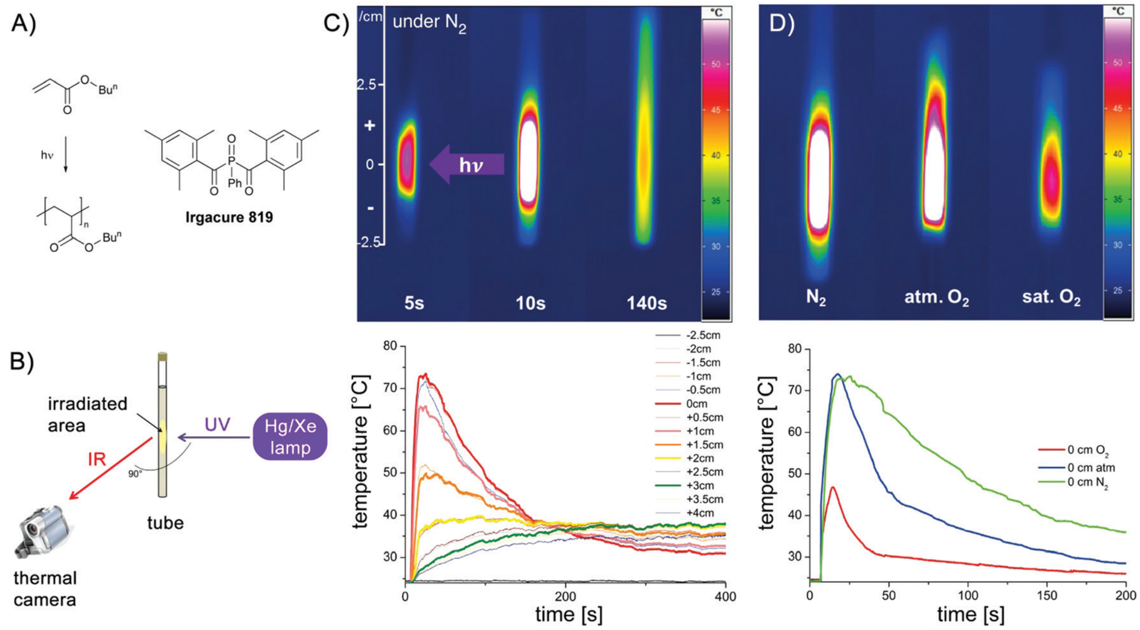

Fig. 1 Polymerisation under investigation (A), experimental setup for the recording of thermal images (B), thermal images of formulations irradiated for 10 s at 5, 10, and 140 s after irradiation was stopped (under N_2) (C, above) and time/temperature profiles for the same experiment at selected distances from the position of irradiation (C, below) as well as thermal images of samples at different oxygen concentrations recorded 10 s after irradiation was stopped (D, above) and time/temperature profiles at the centre of irradiation of these samples (D, below).

after the irradiation ended. In the sample under an inert atmosphere, the heat is evenly distributed above and below the centre of irradiation. Although the highest temperature is essentially identical in the image in the middle, the heat distribution becomes inhomogeneous. The substantial inhibiting effect of oxygen can be clearly distinguished in the right sample: the temperature is much lower (less than half compared to the degassed case), clearly showing a substantially hampered polymerisation. This is shown in Fig. 1D (lower part) comparing the rise and decrease of the temperature in these three samples over 200 s at the centre of the irradiation. Whereas the green curve recorded under inert conditions (N_2 saturated sample) reaches the highest temperature ($T_{\max}$) and decreases only slowly indicating a rather long period of polymerisation, the blue curve recorded under atmospheric atmosphere has an identical $T_{\max}$ but a substantially faster decay. When the solution is saturated with oxygen, $T_{\max}$ is markedly lower and the decay is even more pronounced. Fig. 1C reveals that particularly at later stages of the polymerisation, the dissipation of heat is not uniform, but systematically depends on convection and, possibly on the thermal properties of the environment. This is mirrored by the fact that the temperature above the centre of irradiation (positive values in Fig. 1C) is higher than that at the corresponding distance below.

The spatially-resolved images shown in Fig. 1C reveal that under an inert atmosphere, a maximum number of active initiating radicals is produced. Accordingly many polymer chains start to grow. Moreover, since chain growth is not quenched by oxygen, recombination and disproportionation reactions appear as side reactions of the radical-chain reaction. A substantial portion of the heat is produced by the formation of novel C–C bonds. As soon as oxygen is present, the formation of active initiating radicals is hindered by the deactivation of the initiating radicals by oxygen. Since the photo-induced α cleavage is rather fast and the quenching of the initiating radicals by O_2 is a second-order diffusion-controlled reaction, this reaction is not dominating in the very first phase of polymerisation under atmospheric conditions. However, this becomes much more pronounced in the O_2 saturated sample where the initiating radicals are attacked by oxygen at a higher rate. The oxygen quenching of the C-centred radicals of the growing chain is evident in both oxygen-containing samples showing a much faster decrease of the temperature relative to the degassed one.

Not all effects discussed above are exclusively caused by the role of oxygen. Heat transfer to the interfaces between the sample and the glass walls and the atmosphere definitely contribute to the efficacy of the polymerisation reaction. We have therefore specifically addressed the influence of the bulk and the interface area in a second series of experiments. To this end, we have chosen ROMP (ring-opening metathesis polymerisation, Fig. 2) since the progress of ROMP (initiated with the particular class of ruthenium compounds used) is hardly affected by the presence of oxygen and starts after an induction period of a few minutes allowing a proper mixing of the solutions and placing them in appropriate vessels.[15]

In a first set of measurements, four vials were filled with differing volumes of the same polymerising mixture (0.5–3.7 mL) and immediately, the thermal development of the samples was monitored with the thermal camera (Fig. 2). After an induction period of *ca.* 4 min, the sample with the highest

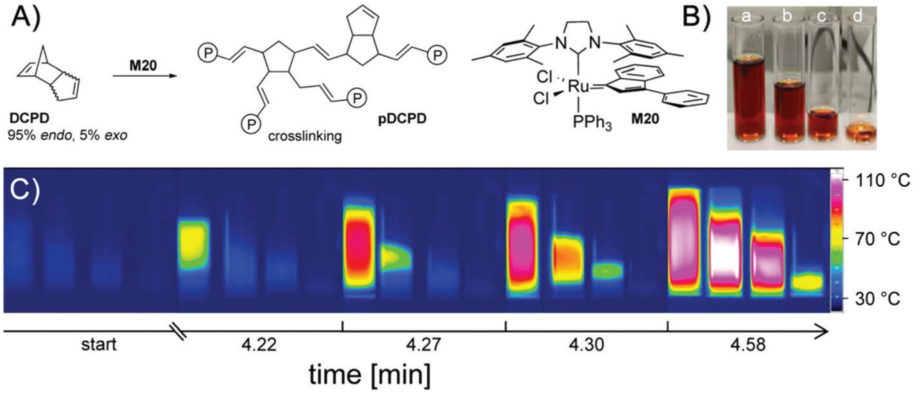

Fig. 2 ROMP of dicyclopentadiene initiated with **M20** (A), photographs of reaction vessels ((a) 3.7, (b) 2.6, (c) 1.2 and (d) 0.5 mL)) containing the formulation for ROMP (B) and thermal images showing the heat evolvement during polymerisation depending on the volume (C).

volume starts to polymerise, consecutively followed by the samples with decreasing volumes of the formulation. The starting area of the reaction is always the (*a priori*) warmest region of the samples. This can be additionally perceived by the fact that even a slight heat transfer from one sample to another (if they are in close vicinity) creates a "hot spot" becoming the starting area for the polymerisation in the adjacent vessel. The lower the volume of the sample, the longer it takes for the start of the polymerisation and the lower the highest temperature achieved. Clearly these effects can be traced back to bulk effects counterbalanced by heat transfer across interfaces. To assess the influence of the overall volume and the interface area in a systematic way (walls of the sample vessel and atmosphere), we have constructed reaction chambers (Teflon) providing specific volume/interface area ratios. To avoid heat transfer between the samples, the reaction chambers were positioned well apart from each other (Fig. 3A and B). The measurement of the reaction temperature at the surface of the samples was achieved by positioning the camera above the reaction chambers. Selected results are displayed in Fig. 3C. In analogy with the measurements shown in Fig. 2, an induction period of *ca.* 3 min was observed. Polymerisation started first in the sample with the highest volume. This can be seen in Fig. 3C and D, where column a, corresponding to the reaction chamber with the highest volume (Table 1), reveals the first detection of heat after 211 s.

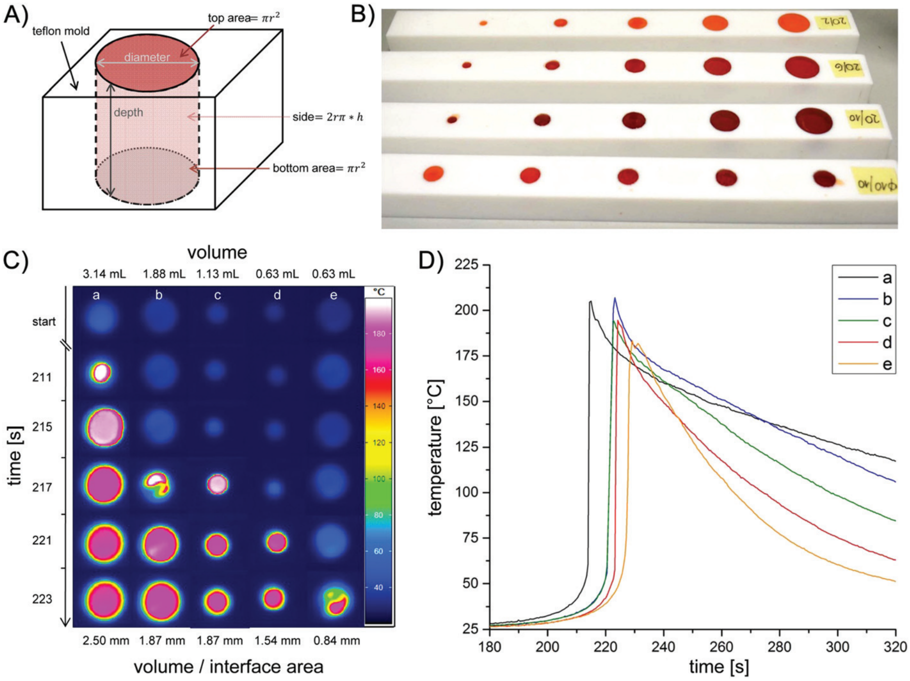

Fig. 3 General shape of the reaction chambers (A), photograph of the reaction chambers made of Teflon (B), thermal image showing the heat evolvement during ROMP in dependence of the dimensions of the reaction chambers (*cf.* Table 1) (C) and time/temperature profiles of the reaction chambers a–e (D).

Table 1 Dimensions of reaction chambers

Reaction chamber	a	b	c	d	e
Diameter [mm]	20	20	12	10	20
Depth [mm]	10	6	10	8	2
Volume [mL]	3.14	1.88	1.13	0.63	0.63
Volume–interface area ratio [mm]	2.50	1.87	1.87	1.54	0.84

Columns b–d in Fig. 3C then follow in the order of their gradually smaller volumes.

In addition to this 'volume effect', also the volume/interface ratio appears to play a major role. The polymerisation in chambers b and c starts almost simultaneously (see 4th line in Fig. 3C) although the volume of chamber c is only 60% of that of b. Remarkably, b and c have the same volume/interface area ratio. This implies that the heat is evenly dissipated across the interfaces between the sample and Teflon/atmosphere. Comparing the reaction in chambers d and e underpins the influence of the volume/interface area ratio. These chambers have identical volumes (0.63 mL) but different interface areas (volume/interface area ratio 1.54 and 0.84 mm, respectively). Significantly, in sample e with a lower volume/interface area ratio, the polymerisation starts later and reaches a lower maximum temperature (Fig. 3D). Here, a larger amount of the reaction heat is transferred from the bulk to the surrounding. Generally Fig. 3D indicates that the samples with higher volume and bigger volume/interface ratio polymerise earlier and reach higher temperatures. Moreover the observation that the decay of the maximum temperature is substantially less pronounced in a, b than in d, e (Fig. 3D) is in line with the higher volume/surface ratio of the former samples.

Experimental section

For the temperature measurements, we have used an InfraTec VarioCam hr M83072 thermography system providing a 640 × 480 dpi resolution at a frequency of 60 Hz. We used 10 Hz and 2 Hz for photoinitiated and ring opening metathesis polymerisation reactions, respectively.

Since thermal camera images exclusively present surface temperatures, our measurements were either performed in thin-walled glass tubes (NMR) or in specifically produced reaction vessels (Teflon). The specific shapes of the latter were designed to account for the effects of the overall reaction volume and the ratio of volume *vs.* the interfacing area with the atmosphere and the contact area of the polymerising mixture with the Teflon surface.

For the photoinitiated reactions benzene solutions of butyl acrylate and Irgacure 819 (phenylbisacylphosphine oxide, BASF, Germany) were used. For the measurements 0.8 mL of a prepared stock solution consisting of 9.8 wt% benzene, 0.1 wt% Irgacure 819 and 90.1 wt% of butyl acrylate was filled in thin-walled 5 mm NMR tubes. The NMR tubes were sealed with septa and either degassed (N_2 bubbling for 3 min) or enriched with oxygen under light exclusion (wrapped in aluminium foil). Samples representing atmospheric oxygen levels were kept untreated. Every sample was freshly prepared before the experiment. A Hg/Xe lamp (Hamamatsu LC4, L8252 lamp, max at 365 nm) equipped with a light guide (diameter 5 mm) was used. This setup yielded 2200 ± 300 mW cm^{-2}. A cross section of 15 mm was irradiated for 10 s (shutter). The recording of the thermal response was started 7 s before irradiation.

For the ring opening metathesis polymerisation in bulk, dicyclopentadiene (97%, a mixture of *endo* and *exo* isomer (95 : 5), ABCR; 7.84 g and 14.7 g for measurements in glass vials and Teflon moulds, respectively) was molten and mixed with dichloromethane (30 μL per mL DCPD) to keep it in the liquid state. A stock solution of the initiator M20 (Umicore)[16] in dichloromethane (34.5 mg mL^{-1}) was prepared. For the thermal measurements, the polymerisation was initiated by the addition of initiator-solution (240 and 450 μL; equal to 150 ppm M20 in respect of DCPD) to the monomer. Subsequently, the formulation was filled in the respective moulds and the heat evolvement was measured.

Conclusions

Although thermal measurements were reported for several cases as a (semi)quantitative tool for describing the efficiency of chemical reactions,[17] our results illustrate pretty well the power of thermography to visualize, study and quantify the polymerisation progress under different conditions. The aim of our investigation was testing whether the use of a thermal camera provides new and useful insights into polymerisation phenomena. The images and the curves shown in Fig. 1 and 3 illustrate that we have been capable of systematically establishing and distinguishing bulk effects, heat transfer, the influence of interfaces, and the impact of oxygen. Although the recorded images provide only information on the temperature of the surface of the investigated samples, the non-isotopic heat flow can be followed rather precisely and reproducibly.

In these terms, the use of a high-resolution thermal camera is very useful for investigating the efficiency of the formation of polymers on a convenient time scale (1/60 s) and an appropriate resolution (sub mm), which is likely to be useful for studying rather subtle details during the curing of photo-polymerisable coatings in addition to standard IR procedures monitoring the conversion of double bonds.[18] Such investigations require custom-made reaction chambers that allow following the desired phenomena, always bearing in mind that the surface temperature is monitored exclusively. It is also crucial to control the environmental conditions very precisely to achieve a perfect reproducibility of the results.

We are currently expanding our studies toward frontal polymerisation, non-homogeneous systems, *etc.* and developing specific vials for enhancing the scope of this approach. A detailed look on thermographic images seems to be valuable and should also enhance the development of theoretical models.[19]

Acknowledgements

We are indebted to Herbert Lang (Workshop Physical and Theoretical Chemistry TU Graz) for preparing the Teflon-based reaction vessels.

Notes and references

1 G. L. Batch and C. W. Macosko, *J. Appl. Polym. Sci.*, 1992, **44**, 1711–1729.

2 A. Boddapati, S. B. Rahane, R. P. Slopek, V. Breedveld, C. L. Henderson and M. A. Grover, *Polymer*, 2011, **52**, 866–873.

3 C. E. Corcione, A. Greco and A. Maffezzoli, *Polym. Eng. Sci.*, 2006, **46**, 493–502.

4 P. M. Johnson, J. W. Stansbury and C. N. Bowman, *Macromolecules*, 2008, **41**, 230–237.

5 S. C. Ligon, B. Husar, H. Wutzel, R. Holman and R. Liska, *Chem. Rev.*, 2014, **114**, 557–589.

6 B. J. Falk, S. M. Vallinas and J. V. Crivello, *J. Polym. Sci., Part A: Polym. Chem.*, 2003, **41**, 579–596.

7 A. Holzwarth, H.-W. Schmidt and W. F. Maier, *Angew. Chem., Int. Ed.*, 1998, **37**, 2644–2647.

8 M. T. Reetz, M. H. Becker, K. M. Kühling and A. Holzwarth, *Angew. Chem., Int. Ed.*, 1998, **37**, 2647–2649.

9 Y. M. Kim, L. K. Kostanski, J. F. MacGregor and A. E. Hamielec, *J. Therm. Anal. Calorim.*, 2004, **78**, 153–164.

10 T. Nagasawa, B. Ochiai and T. Endo, *J. Polym. Sci., Part A: Polym. Chem.*, 2006, **44**, 5519–5524.

11 K. Dietliker, T. Jung, J. Benkhoff, H. Kura, A. Matsumoto, H. Oka, D. Hristova, G. Gescheidt and G. Rist, *Macromol. Symp.*, 2004, **217**, 77–97.

12 I. Gatlik, P. Rzadek, G. Gescheidt, G. Rist, B. Hellrung, J. Wirz, K. Dietliker, G. Hug, M. Kunz and J.-P. Wolf, *J. Am. Chem. Soc.*, 1999, **121**, 8332–8336.

13 S. Jockusch and N. J. Turro, *J. Am. Chem. Soc.*, 1998, **120**, 11773–11777.

14 Y. Yagci, S. Jockusch and N. J. Turro, *Macromolecules*, 2010, **43**, 6245–6260.

15 A. Leitgeb, J. Wappel, C. A. Urbina-Blanco, S. Strasser, C. Wappl, C. S. J. Cazin and C. Slugovc, *Monatsh. Chem.*, 2014, **145**, 1513–1517.

16 J. Broggi, C. A. Urbina-Blanco, H. Clavier, A. Leitgeb, C. Slugovc, A. M. Z. Slawin and S. P. Nolan, *Chem. – Eur. J.*, 2010, **16**, 9215–9225.

17 J. Loskyll, K. Stoewe and W. F. Maier, *ACS Comb. Sci.*, 2012, **14**, 295–303.

18 K. Taki, Y. Watanabe, H. Ito and M. Ohshima, *Macromolecules*, 2014, **47**, 1906–1913.

19 M. D. Goodner and C. N. Bowman, *Chem. Eng. Sci.*, 2002, **57**, 887–900.

5.2 Discussion

The results for the oxygen dependent reactivity of BAPO and the α-hydroxy ketone ***A1*** are comparable. In both cases in the presence of oxygen, peroxide formation and reduced double bond conversion of butyl acrylate were observed. Additionally to ^{1}H- and ^{13}C-NMR techniques, BAPO invites to use ^{31}P-NMR experiments.

In the absence of oxygen it was possible to detect and assign the main reaction products of BAPO upon irradiation. The in this work presented results match perfectly with published data.[125,118]

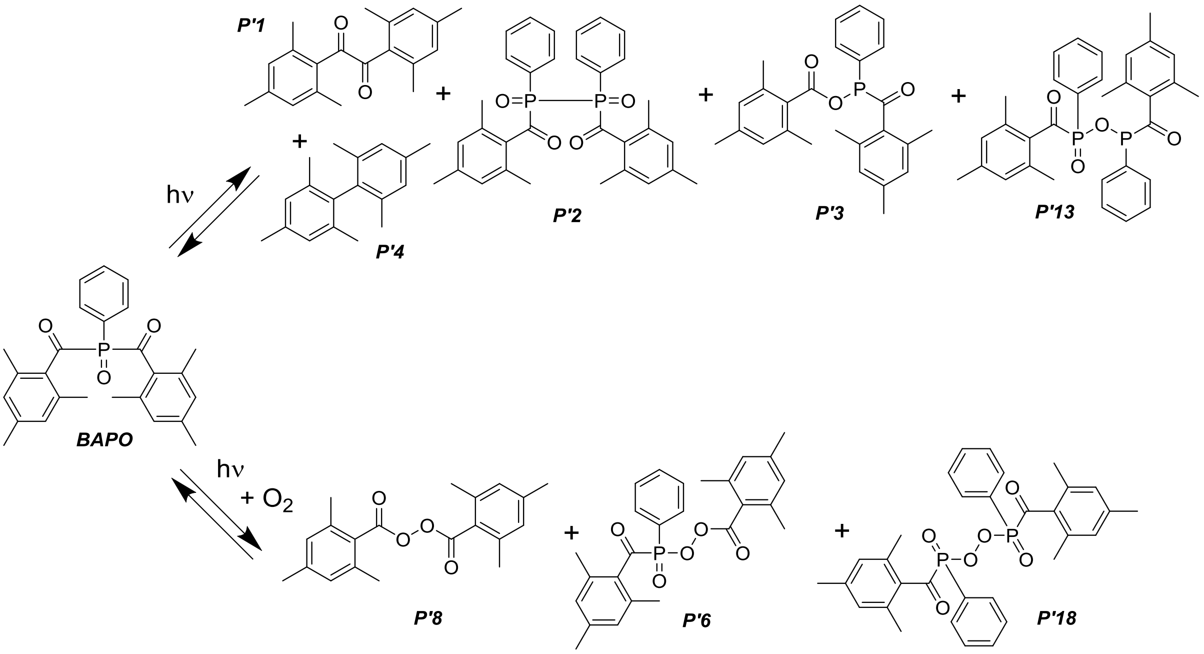

Scheme 45. Compounds detected with various NMR techniques (NMR and CIDNP of different nuclei) in the presence and absence of oxygen. In the presence of oxygen the displayed compounds are formed additionally.

Longer irradiation times cause further follow-up products. One of these products is 2,2',4,4',6,6'-hexamethyl-1,1'-biphenyl ***P'4***, which is of particular interest, as it appears in the absence and presence of oxygen, but the signal intensities are in the absence of oxygen higher. The α-hydroxy ketone ***A1*** leads to comparable compounds. There a decarboxylation step preferably takes place in the presence of oxygen.

Opposite to ***A1***, the decarboxylation of BAPO is preferred in the absence of oxygen, which is caused by a different mechanism. With ***A1*** first a peroxide needs to be formed, which can then decompose and subsequently decarboxylates. For BAPO an additional possibility exists.

The first step is the reduction to compound ***P'3***, which is followed by the light induced cleavage and formation of ***R'4***. ***R'4*** can undergo fast decarboxylation, which leads to the mesityl radical ***R'6***. It is possible to detect ***P'4***, but further recombination products with ***R'1***,

R'2 or other intermediates are feasible. ESI-MS results support this as mesityl substituted compounds are found.

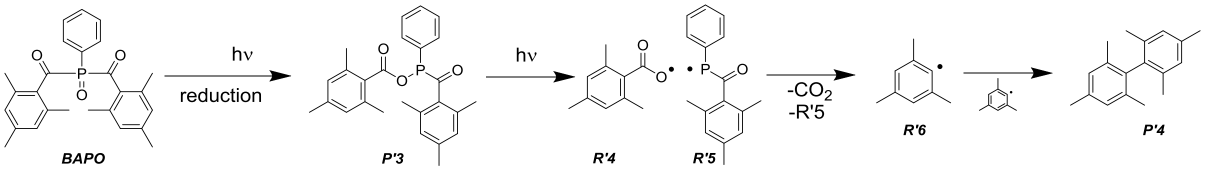

Scheme 46. Suggested reactions for the formation of *P'4*.

Decarbonylation of ***R'1*** is an additional possibility to obtain ***R'6***, but as I discussed already for ***A1*** decarbonlyations of benzoyl radicals and its derivatives are about four orders of magnitudes slower than corresponding decarboxylations.[109,110,111]

NMR experiments with butyl acrylate showed that polymerization only occurs in the absence of oxygen and under atmospheric conditions. The oxygen-saturated samples showed no double bond conversion. It was also possible to detected addition products of ***R'1*** and ***R'2*** to the acrylate. Both mesitoyl groups of BAPO can cleave and the resulting phosphinoyl radical can react with two acrylates, but the direct observation was not achievable.

Therefore experiments included TEMPO. It can trap radical intermediates and ^{31}P-NMR experiments revealed compound ***P'15***, which is ***R'10*** with two attached TEMPO units.

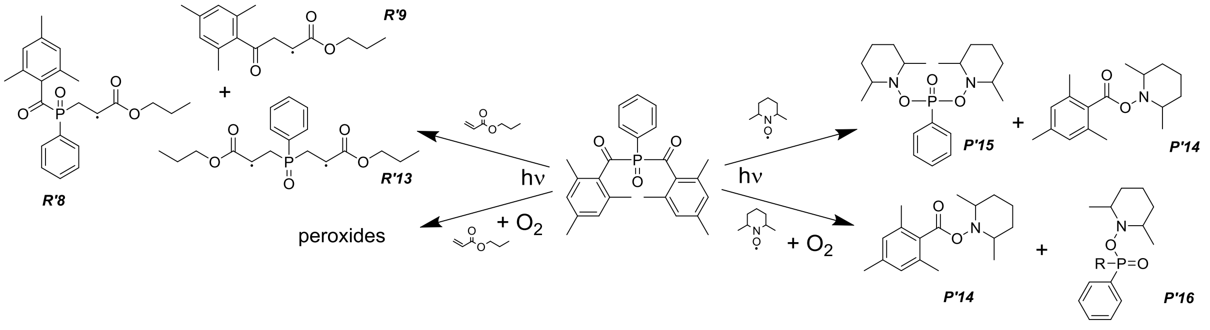

Scheme 47. Determined products formed of BAPO and TEMPO or butyl acrylate in the absence and presence of oxygen.

The experiments with TEMPO showed, that the addition of two butyl acrylate units to one BAPO derived phosphinoyl is plausible. This is in line with end group analysis.[131–133] My working group performed also successful experiments with wavelength selective cleavage of BAPOs mesitoyl groups and further selective diblock copolymerization.[134]

The determined addition rate constants for phosphinoyl radical ***R'2*** to butyl acrylate and for ***R'2*** to oxygen are k_{butyl}= 7.42 x 10^6 M^{-1} s^{-1} in toluene, which fits well to the published value of k_{butyl}= 7.6 x 10^6 M^{-1} s^{-1} ± 0.2 in toluene[135,136] and k_{O_2}= 1.50 x 10^9 M^{-1} s^{-1}, which is considerably lower than published rates.[34,56,102,136] The Turro group i.e. published the addition rate constant k_{O_2} = 2.70 x 10^9 M^{-1} s^{-1} measured with LFP in acetonitrile. The difference in the addition rate constants might be caused by solvent effects. The addition of ***R'2*** to oxygen is about 2-3 orders of magnitudes faster than the addition of ***R'2*** to butyl acrylate. For the mesitoyl radical ***R'1*** it is the same.

The fast reaction of oxygen with ***R'1*** and ***R'2*** is one reason for oxygen inhibition. With kinetic simulations it was possible to visualize the inhibiting effect. When the oxygen concentration increases, the amounts of peroxides rise and the desired product concentrations of i.e. polymers decrease. The used kinetic models are in line with my experimental results. In the presence of oxygen different peroxide species and reduced amounts of products are detected. Further it is not possible to observe double bond conversion and polymerization in oxygen-saturated samples. Additionally the quantification of the oxygen consumption with optical oxygen sensors is feasible

Thermal imaging provided information of the bulk behavior, which mainly corresponds with observations in diluted systems. Inhibition in the presence of high oxygen concentrations occurred and the observed effects are exclusively caused by oxygen. Heat transfer from the center to the glass surface, diffusion and changed gas solubility's through temperature increase also play an important role. It was possible to differentiate between those effects with oxygen independent ROMP reactions.[8] This technique was a useful additional tool to visualize oxygen effects on bulk samples. These results contribute to a better understanding of oxygen reactivity and follow-up products in photo-induced radical polymerization.

Tetramesitoylgermane

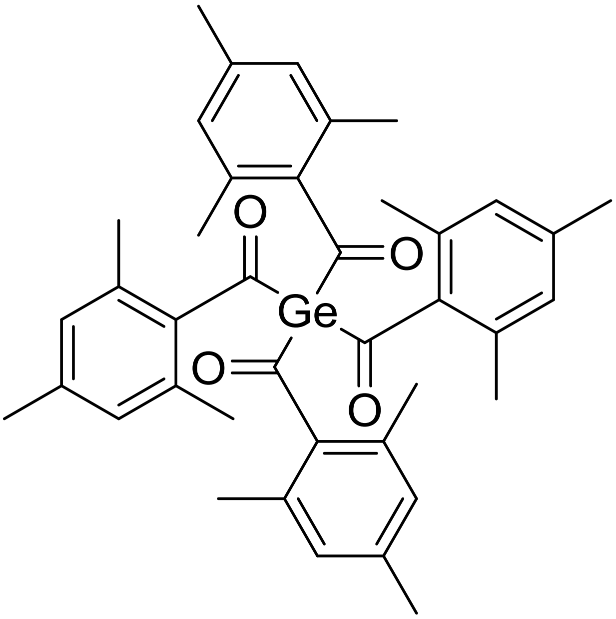

6 Tetramesitoylgermane

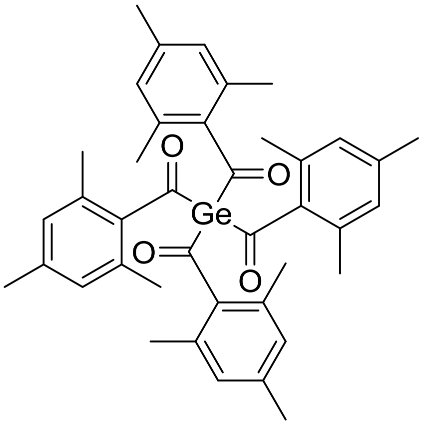

Scheme 48. Tetramesiotylgermane ($GeAc_4$)

Tetramesitoylgermane ($GeAc_4$) is a new compound, which was first synthesized by Michael Haas from the Stüger group of the Institute of Inorganic Chemistry at Graz University of Technology. This new compound is related to dibenzoydiethylgermane and the commercially available bisacylgermane (BAG) (diethylgermanediyl)bis ((4-methoxyphenyl)methanone). My group studied the photo initiating ability of dibenzoyldiethylgermane and based on this I characterized $GeAc_4$.

The next section presents results gained from EPR, NMR and LFP experiments as well as polymerization tests.

6.1 Results

Time resolved EPR experiments determined the homolytic cleavage upon irradiation of tetramesitoylgermane. ^{1}H- and ^{13}C-NMR experiments before and after irradiation, which correspond to the experiments carried out with the α-hydroxy ketone ***A1*** and BAPO, provide oxygen dependent structural information. ^{1}H-CIDNP experiments revealed interesting properties of this new compound and LFP measurements were performed to determine the addition rate constants of the germyl radical to butyl acrylate and to oxygen. Here I will also show results of polymerization experiments. Various formulations, with either $GeAc_4$ or dimesitoyldiethylgermane as initiator, were cured.

6.1.1 Time Resolved EPR

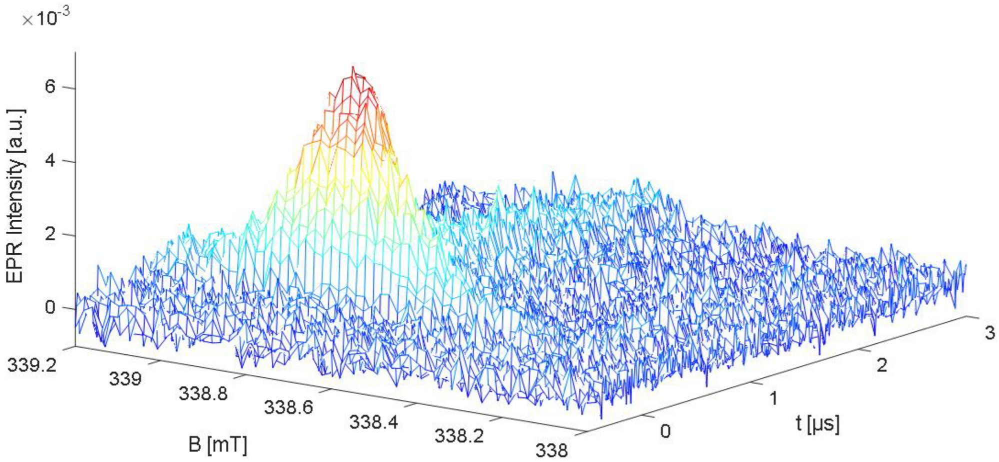

Figure 59 TR-EPR spectrum of GeAc$_4$ in toluene

With TR-EPR primary formed radicals can be observed. **Figure 59** displays the TR-EPR spectrum of GeAc$_4$. Upon irradiation, a signal in absorption between 339.2 and 338.2 mT appears. From previous studies it is known that mesitoyl and germyl radicals are detected within this magnetic field.[137] The signal in absorption indicates that most of the polarization is obtained through the radical pair mechanism RPM. The spectrum is not well resolved and therefore both signals overlap. After 3 µs the signal disappeared. The light induced cleavage of the parent compound and the formation of radicals are proven.

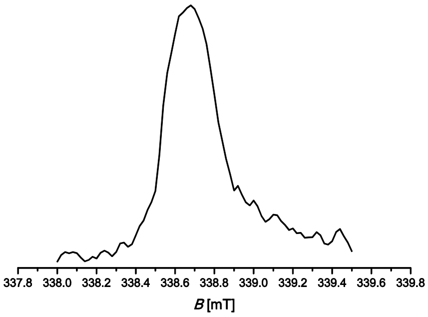

Figure 60. EPR spectrum derived from GeAc$_4$ 200 ns after the laser pulse.

Figure 60 displays the EPR spectrum recorded after 200 ns. Here the broad signal is clearly visible.

The scheme below is based on previous research and shows the most likely formed radicals upon irradiation.

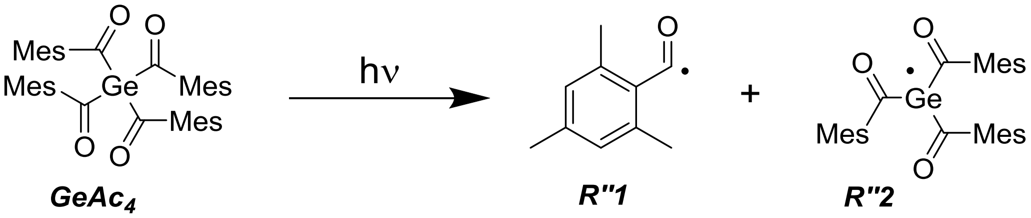

Scheme 49. Formation of mesitoyl *R"1* and germyl *R"2* radicals after irradiation of GeAc$_4$ with UV light.

6.1.2 ^{1}H-NMR Experiments

The ^{1}H-NMR spectrum of $GeAc_4$ in toluene confirmed the purity of the analyte as no additional signals beside the solvent peaks are detected. It is possible to assign the signals belonging to the protons of the methyl groups and the protons on the mesitoyl substituent of the parent compound in the displayed spectrum **Figure 61**. The aromatic protons ***1*** at 6.35 ppm represent the meta position. The ortho methyl groups' protons ***2*** are found at 2.22 ppm and the para methyl groups' protons ***3*** at 2.05 ppm. The signal intensities integral ratio of ortho and para methyl groups is 2:1. This matches perfectly the structure of the compound.

After 3 minutes of irradiation with UV light in the absence of oxygen, additional peaks appear. Peak ***4*** in the aromatic region of the NMR spectrum corresponds to the aromatic protons of dimesitoyl ***P"2***. Further proofs for the formation of ***P"2*** are the signals obtained from the ortho methyl groups protons ***5*** at 2.34 ppm and the para methyl group protons ***6*** at 2.15 ppm. The results of the ^{1}H-CIDNP experiments, which are described in the next section, support the formation of ***P"2***. After irradiation signals belonging to the parent compound are still detected, but with reduced intensity.[138]

After irradiation broad and additional signals in the aromatic and aliphatic range arise. The assignment of these peaks is currently not possible. One of the difficulties for signal assignment occurs from germanium. Germanium has a huge impact on the chemical shift, but only few references exist and the current prediction tools are not able to handle germanium containing compounds properly.

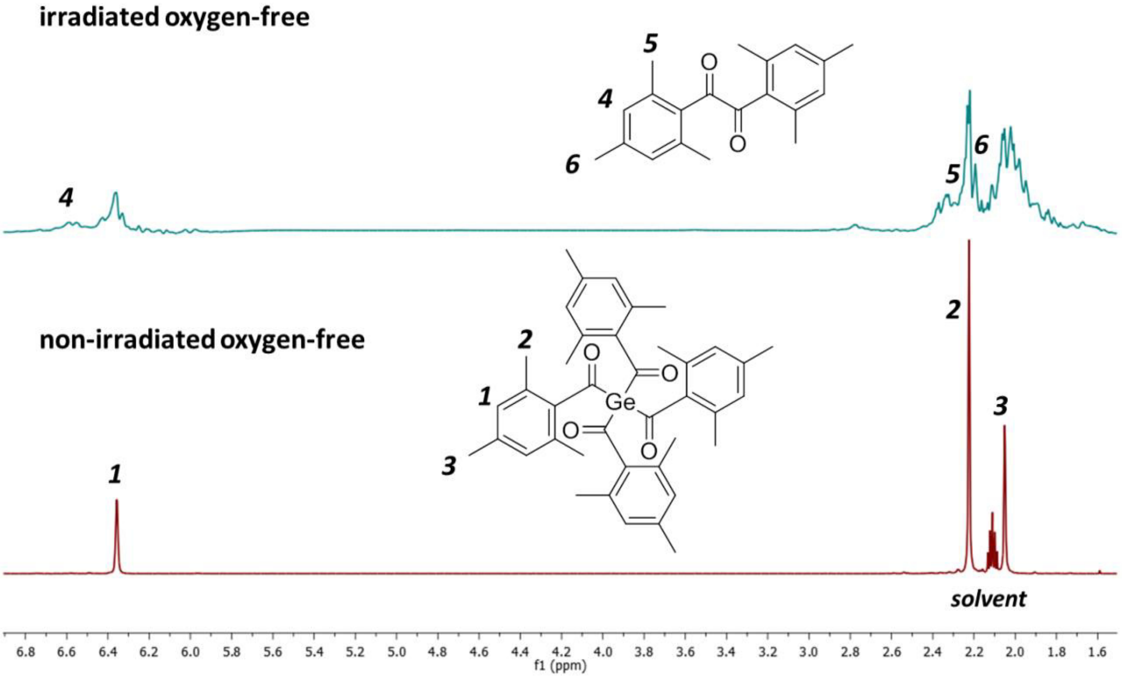

Figure 61. ^{1}H-NMR of $GeAc_4$ (10 mM) before and after irradiation (3 min) (16 scans in toluene). Bottom trace non-irradiated reference spectrum and on top the spectrum after irradiation in the absence of oxygen.

Another difficulty of the signal assignment is the long irradiation time, as a mix of follow-up products is obtained. The recombination of germyl radicals can lead to follow-up products containing Ge-Ge bonds. An indication for this, are the additional signals, which appear next to the peaks of the parent compound. Haas observed with GC-MS products of similar germanium based initiators, which indicated Ge-Ge bonds.

The signal of an additional follow-up product at 2.76 ppm might belong to 2,2',4,4',6,6'-hexamethyl-1,1'-biphenyl ***P"3***, which can be formed after decarbonylation.

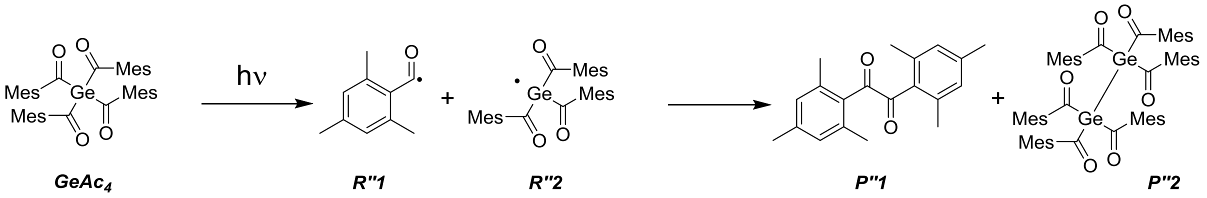

Scheme 50. Expected follow up products of GeAc$_4$ upon irradiation.

Irradiation of samples, containing 50 mM or more GeAc$_4$ in the absence of oxygen for 3 minutes leads to the formation of a white sediment. Through the long irradiation additional mesitoyl substituents cleave and the formation of germanium particles is possible. This process includes electron transfers, but with these experiments it was not feasible to obtain additional information about it.[137,139]

The oxygen dependence is better observable and the amount of follow-up products decrease, when the irradiation time is reduced. I combined these requirements with the CIDNP experiments and recorded additional ^{1}H-NMR spectra after the CIDNP measurements. One CIDNP spectrum consists out of 32 scans; this means that the sample is hit by 32 1 µs laser pulses. The previous samples were irradiated for 3 minutes with the Hamamatsu UV-lamp.

Through the reduced irradiation time, I expect fewer light induced products and therefore less signals in the NMR spectra. 32 ^{1}H-CIDNP scans are usually not sufficient to degrade the sample. For example with BAPO or with ***A1*** it is not possible to detect sample degradation after 32 scans. In the case of GeAc$_4$ the ^{1}H-NMR spectra, which were recorded after the CIDNP experiments show changes.

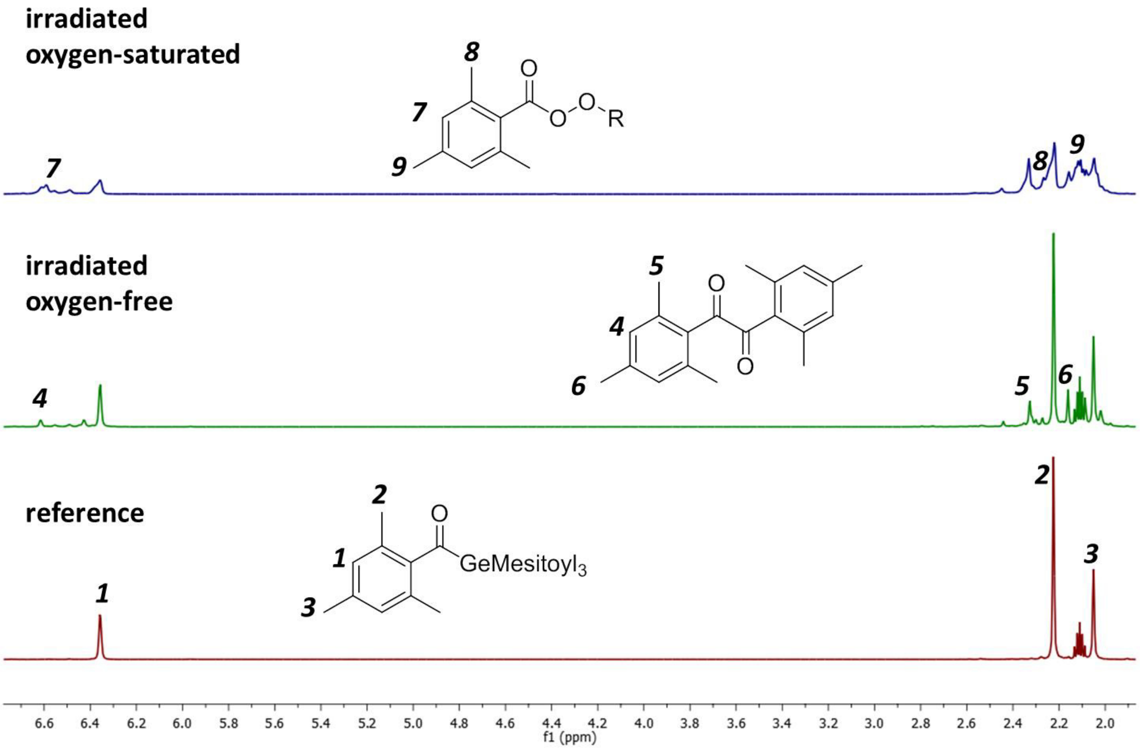

Figure 62. ^{1}H-NMR of GeAc$_4$ after CIDNP experiment with 32 1 µs laser pulses in the dependence of oxygen (16 scans in toluene). The spectrum on the bottom shows the non-irradiated compound and serves as reference. In the middle the spectrum of the oxygen-free irradiated sample is displayed and on top is the spectrum of the oxygen-saturated irradiated sample.

The bottom trace of **Figure 62** displays the reference spectrum of the non-irradiated GeAc$_4$. After the irradiation with 32 laser pulses through the CIDNP experiment, additional peaks caused by sample degradation appear. In the absence of oxygen the formation of the dimesitoyl ***P"1*** occurs. The signals for ***P"1*** are less pronounced here, than in the spectrum obtained after 3 minutes of irradiation with the UV lamp, but they are better resolved, as less additional products are formed. Its aromatic protons ***4*** have a peak at 6.61 ppm. The signals of the methyl groups' protons ***5*** and ***6*** are again recorded at 2.34 and 2.15 ppm.

I detect additional signals at 6.49, 6.43 and 2.44 ppm but currently proper assignment is not possible. It is likely that these signals belong to species with a Ge-Ge bond.

There are two effects in the presence of oxygen. First a general line broadening and second the appearance of new signals. In the aromatic range the high field shifted peak ***7*** at 6.59 ppm next to the proton signal of ***P"1*** belongs to the protons of a peroxide derivative of mesitoyl ***P"4***, indicated in the spectrum above. The substituent ***R*** could be either another mesitoyl group or a germanium based fragment. This signal is not suitable to distinguish, what the substituent ***R*** is but the addition of oxygen to ***R"1*** can be assured. The addition of oxygen causes expected high field shifts of the peaks.

In the aliphatic region of the NMR spectrum line broadening is a problem. However, signals ***8*** and ***9*** at 2.28 and 2.12 ppm correspond to the protons of the methyl groups of the mesitoyl peroxide ***P"4***. In the presence of oxygen proton signals for ***P"3*** are found too.

Worth to mention are the signal intensities of the parent initiator. In the absence of oxygen the signals for $GeAc_4$ are clearly visible and the signal intensities ratios are corresponding to the non-irradiated sample. When oxygen is present these signals are far less pronounced and overlap with additional signals. The appearance of multiple new signals in the aliphatic range indicates oxygen addition to germanium. ***R"1*** derived signals are the same as ***R'1*** based product signals from BAPO, but so far it is not exactly known how the addition of oxygen to ***R"2*** influences the shifts of the methyl protons of ***R"2***.

Additional proton spectra included samples containing butyl acrylate. After CIDNP experiments double bond conversion was observed only in traces. The irradiation with UV light (3 minutes) led to double bond conversion in the absence of oxygen. The results are comparable to the experiments of α-hydroxy ketone ***A1*** with butyl acrylate displayed in **Figure 13**, where double bond conversion in the absence of oxygen and no double bond conversion in the presence of oxygen is described.

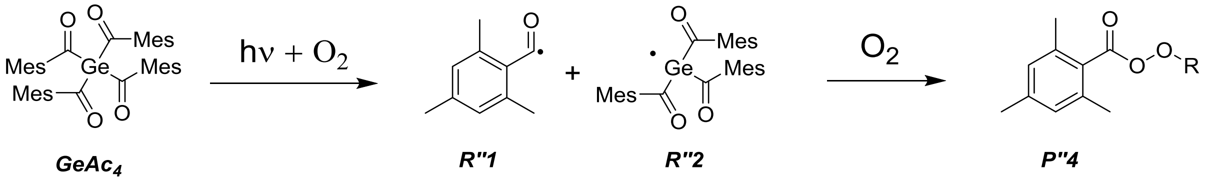

Scheme 51. Overview of products formed by irradiating $GeAc_4$ in the presence of oxygen. Mesitoyl peroxide species are the only confirmed additional products.

The detected products, which are formed upon irradiation in the absence of oxygen, met the expectations (see **Scheme 50**). Dimesitoyl ***P"1*** and Ge-Ge species are formed. In the presence of oxygen it is only possible to confirm the formation of mesitoyl peroxides ***P"4***. The formation of Ge-O-Ge or Ge-O-O-Ge species is probable, but ^{1}H-NMR experiments are not feasible for their determination.

6.1.3 ^{13}C-NMR Experiments

Similar to the ^{1}H-NMR experiments I recorded ^{13}C-NMR spectra of $GeAc_4$ before and after irradiation. To obtain reasonable spectra 4096 scans were required. **Figure 63** displays the spectra of the non-irradiated reference and the irradiated sample in the absence of oxygen.

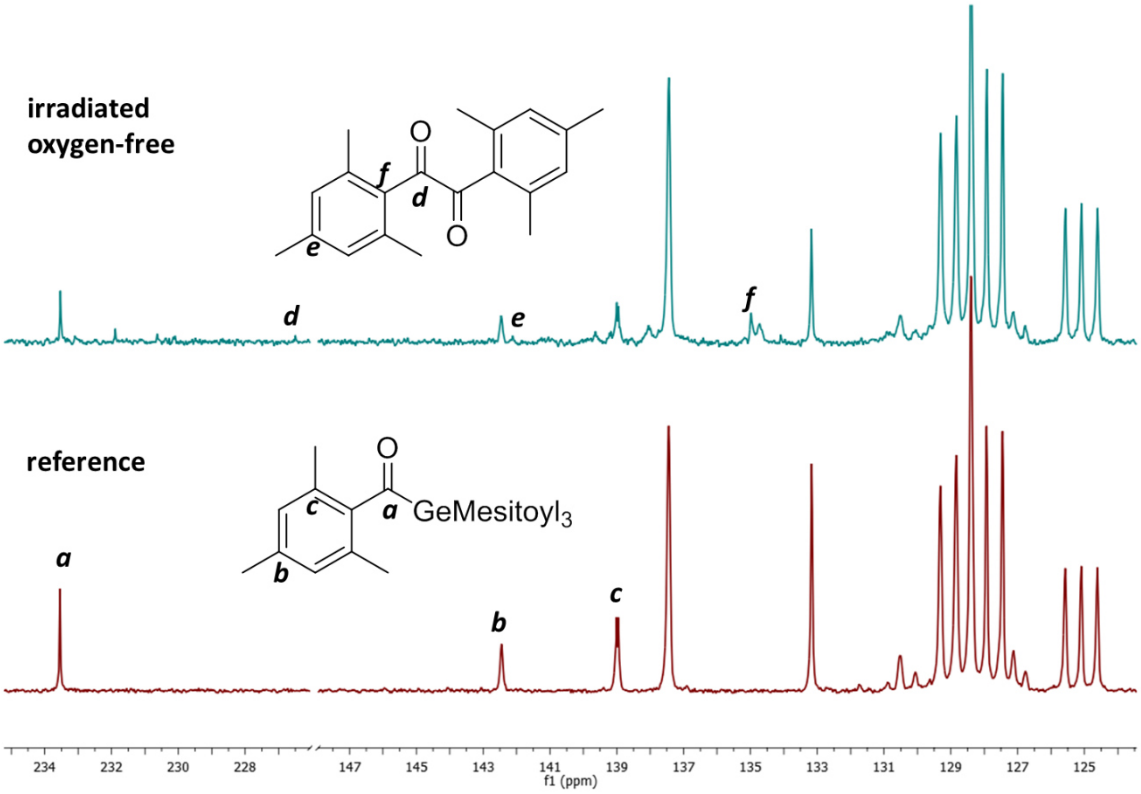

Figure 63. ^{13}C-NMR spectra of $GeAc_4$ in the absence of oxygen before (bottom trace) and after irradiation (spectrum on top) (4096 scans in toluene).

The solvent peaks dominate the spectra and overlap with the carbon signals of the methyl groups. In the aromatic region of the NMR spectrum the signals ***a***, ***b*** and ***c*** belong to $GeAc_4$. Signal ***a*** at 233.95 is characteristic for the carbonyl next to the germanium. This signal is used for quality control in the synthesis of $GeAc_4$. ***b*** and ***c*** correspond to the para and ortho carbon of the mesitoyl.

After irradiation the new signal ***d*** at 226.91 ppm is a hint for compound ***P"1***. ***d*** represents the carbonyl group of the newly formed dimesitoyl ***P"1***. Further evidence, for the formation of ***P"1*** is provided by the signals ***e*** and ***f***.

An additional peak at 138.05 ppm possibly belongs to ***P"3***. Further expected peaks of ***P"3*** would overlap with the solvent. ^{13}C-NMR experiments cannot confirm the formation of ***P"3*** but the results do not contradict with the outcomes of the ^{1}H-NMR measurements.

In the spectrum below we can see next to the parent compounds carbonyl peak two additional high field shifted signals.

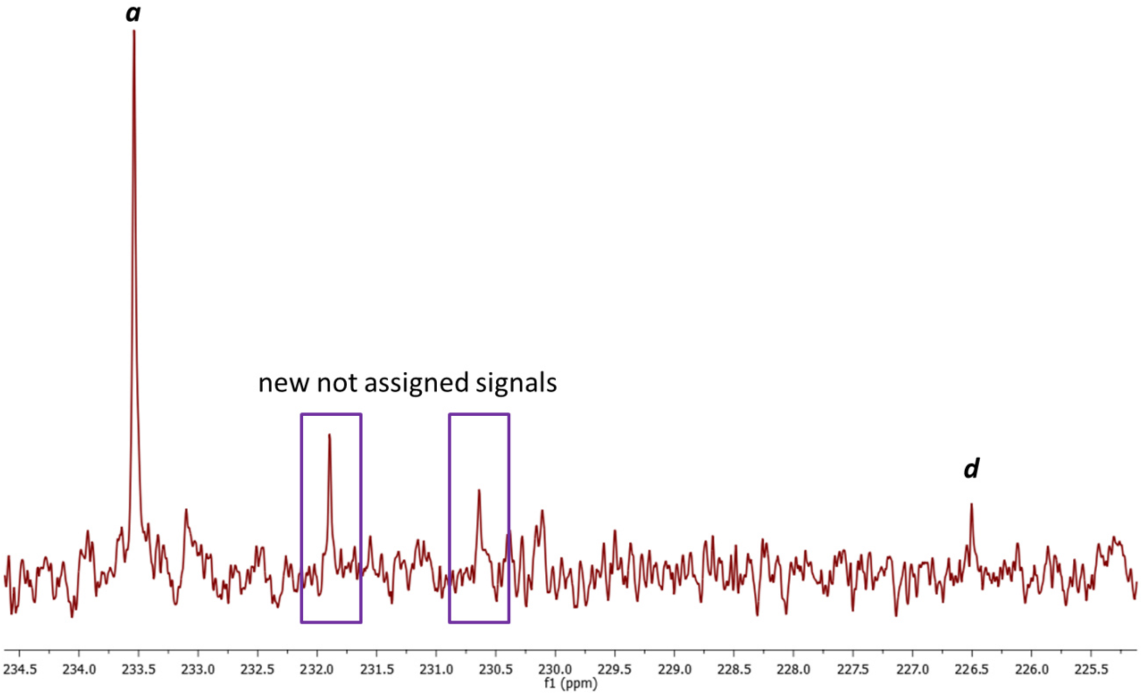

Figure 64. ^{13}C-NMR spectrum of GeAc$_4$ in the absence of oxygen and after irradiation. Additional, not assigned carbonyl carbon signals are detected after irradiation of GeAc$_4$ in the absence of oxygen (4096 scans in toluene)

Figure 64 shows the enlarged part of the irradiated GeAc$_4$ ^{13}C-NMR spectrum in the absence of oxygen. New signals appear at 231.88 and 230.63 ppm. Due to their relative high shift it is possible that they belong to a carbonyl next to a germanium atom.

^{13}C-NMR measurements confirm the decomposition of GeAc$_4$ after UV irradiation and the formation of dimesitoyl ***P"1*** is a proof of it. The additionally found carbonyl carbon signals indicate germanium based follow-up products. The shift of these signals could be a hint for Ge-Ge bond formation.

6.1.4 ^{1}H-CIDNP Experiments

Time resolved EPR experiments revealed the formation of radicals. To follow the products, which are formed via a radical mechanism, CIDNP experiments were performed. **Figure 65** shows a comparison of ^{1}H-CIDNP spectra obtained from samples containing different oxygen concentrations.

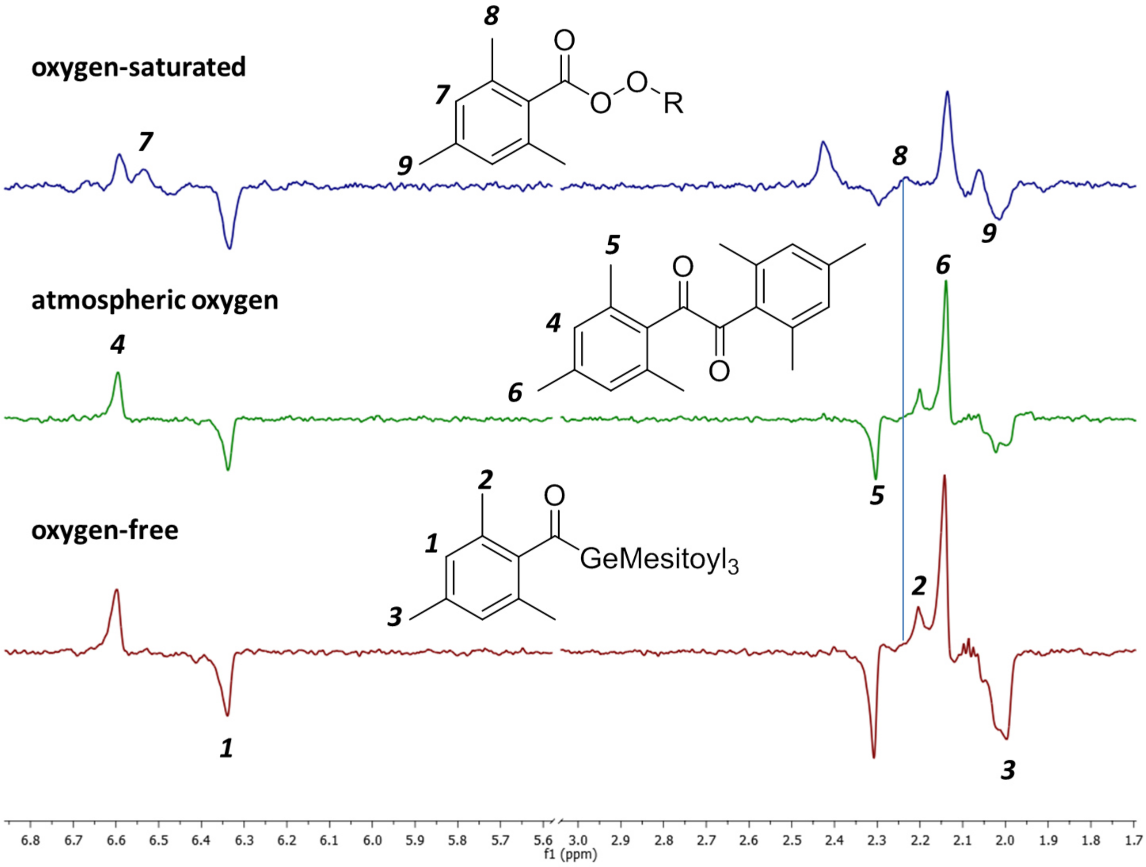

Figure 65. ^{1}H-CIDNP spectra of GeAc$_4$ containing different oxygen concentrations (32 scans in toluene).The bottom trace displays the spectrum recorded with the oxygen-free sample. The middle spectrum was recorded under atmospheric conditions and the sample represented by the top spectrum is oxygen-saturated.

The oxygen-free sample and the sample containing oxygen in atmospheric concentrations behave similar. In both cases the cage reaction occurs. Peaks ***1***, ***2*** and ***3*** correspond with the formation of the initial compound. Peak ***2*** is less pronounced, while peak ***3*** seems to overlap with other signals. Comparable to ^{1}H-NMR results signals correspond to dimesitoyl ***P"1***. Peaks ***4***, ***5*** and ***6*** belong to ***P"1*** and are in accordance with the ^{1}H-NMR measurements. The enhanced signal intensity of the ortho methyl group protons of ***P"1*** compared to the ortho methyl group protons of the parent compound is of interest. The probable high amount of free ***R"1*** could lead to enhanced intensities of ***P"1***. But quantitative interpretation of data obtained by CIDNP experiments is not feasible, due to the non-Boltzmann distribution of the spin states.

The oxygen-saturated sample faces significant line broadening and the aliphatic signals are slightly shifted to lower fields. Additional resonances belong to the peroxide form of mesitoyl ***P"4***, which are indicated in the spectrum above and are in accordance with the results from the ^{1}H-NMR measurements. Signal ***7***, corresponding to the aromatic protons of the ***P"4***, is here much better resolved than in the ^{1}H-NMR spectrum. Here it is possible to detect the protons of the ortho methyl group of the peroxide ***8*** as an independent signal. In the ^{1}H-NMR spectra this signal overlaps with the signal from the parent compound and it is only recognized as a shoulder in the peak.

As described before the signal at 2.44 ppm could belong to ***P"3***. ^{1}H- and ^{13}C-NMR experiments support this finding.

Irradiation creates mesitoyl radicals ***R"1*** and the formation of the corresponding aldehyde is expectable, like in the reaction of the α-hydroxy ketone ***A1***. The formation of the corresponding 2,4,6-trimethylbenzaldehyde ***P"5*** was not observed, as GeAc$_4$ like BAPO has no abstractable hydrogen-atoms, which are necessary to form the aldehyde. When butyl acrylate is present, hydrogen-atom abstraction of the growing polymer chain takes place and the aldehyde is detected.

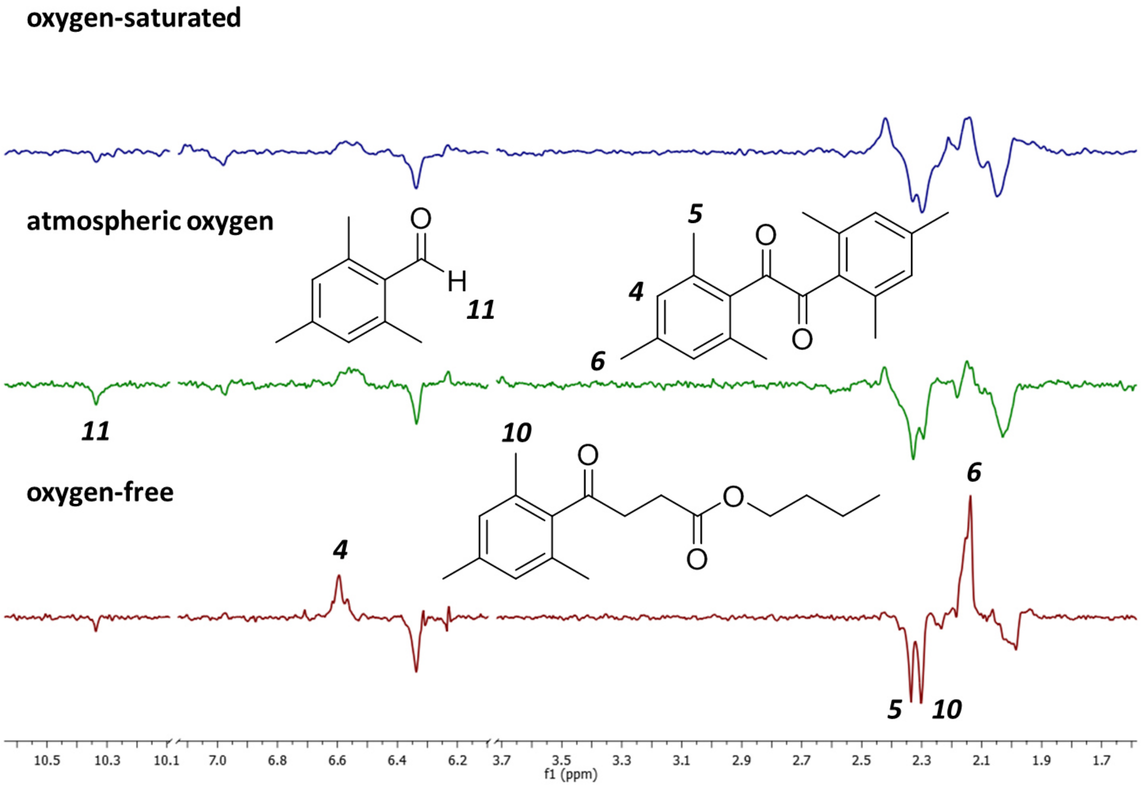

Figure 66. ^{1}H-CIDNP spectra of GeAc$_4$ with butyl acrylate in dependence of the oxygen concentration (32 scans in toluene). On the bottom trace the spectrum of the oxygen-free sample is displayed. The spectrum in the middle shows the sample prepared under atmospheric conditions and the spectrum on top represents the oxygen-saturated sample.

I detect a signal, which belongs to 2,4,6-trimethylbenzaldehyde ***P"5*** in the presence of monomer in all three samples with different oxygen concentrations. Peak ***11*** is assigned to the aldehydes proton, which is indicated in the figure above. The spectra of all samples contain the additional signal ***10***, with the best resolution of it in the spectrum of the oxygen-free sample. This signal ***10*** belongs to the addition product ***P"6*** of the mesitoyl radical ***R"1*** to butyl acrylate.

Here it is not possible to observe the addition of the germyl radical ***R"2*** to butyl acrylate. Further the signal of the parent compounds ortho methyl group protons ***2*** is not detected. This signal should be visible at 2.22 ppm, but in the presence of a monomer the cage reaction is less likely as further reaction pathways exist.

In the presence of oxygen the spectra indicate the formation of a plateau from 6.5 to 6.6 ppm. The signals representing ***P"1*** and ***P"4*** are expected in this range. Taking the results from the α-hydroxy ketone ***A1*** into account, I can additionally expect mesitoyl peroxide attached to butyl acrylate. Solely from this data it is not possible confirm this addition product.

The signal intensities at 2.44 ppm, which represent ***P"3***, rise with the increase of the oxygen concentration. Oxygen induced line broadening is a problem preventing further assignments.

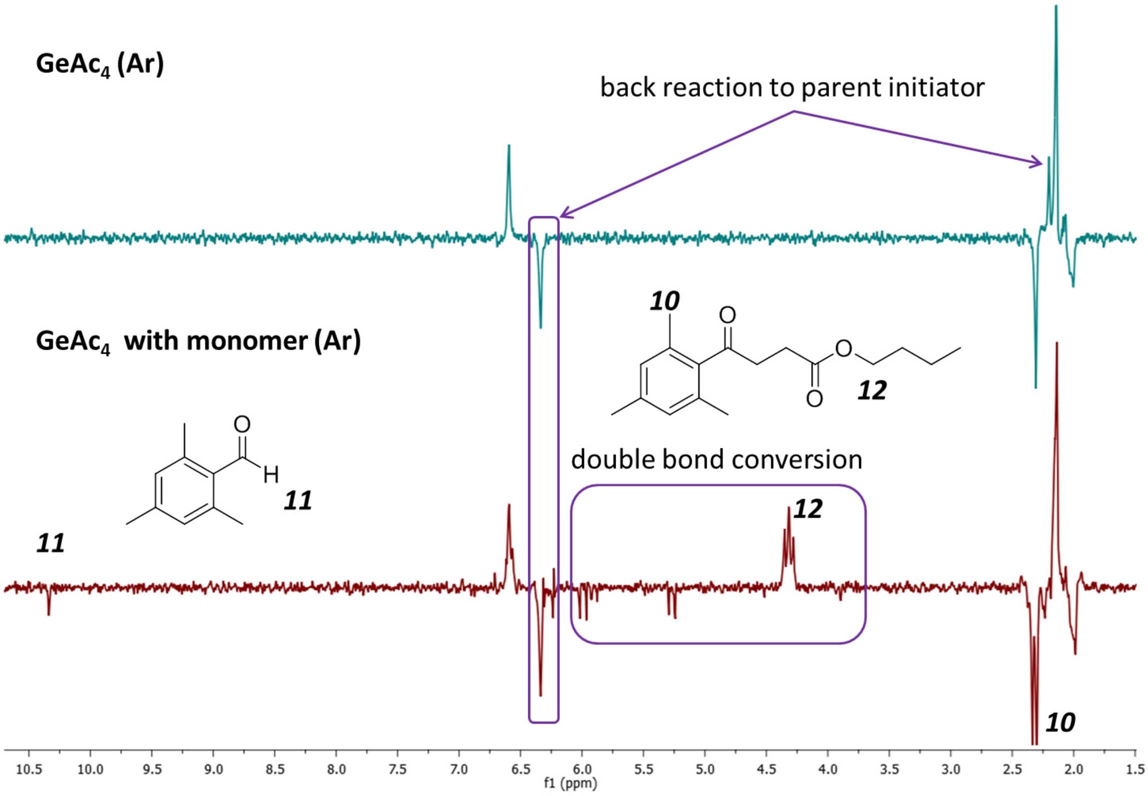

Figure 67. **^{1}H-CIDNP spectra of GeAc$_4$ in the presence and absence of butyl acrylate indicating double bond conversation and cage reactions (32 scans in toluene). The sample of the bottom spectrum contains butyl acrylate, while the top trace shows the spectrum of the monomer-free sample.**

Figure 67 displays the direct comparison of the ^{1}H-CIDNP spectra of $GeAc_4$ in the presence and absence of monomer. As described before only in the presence of monomer it is possible to observe the aldehyde ***P"5***, which is represented by signal ***11*** in the bottom trace.

There is evidence for the addition of ***R"1*** to butyl acrylate. In this comparison I marked a further indication for double bond conversion. The signals around 5.2 ppm belong to protons attached to the double bond and around 4.2 ppm the α-protons of the butyl chain are detected. Those polarized signals indicate an addition of a radical. Some polarization of these signals can be seen in the dummy scan through not efficient presaturation. The dummy scans were subtracted from the CIDNP spectra.

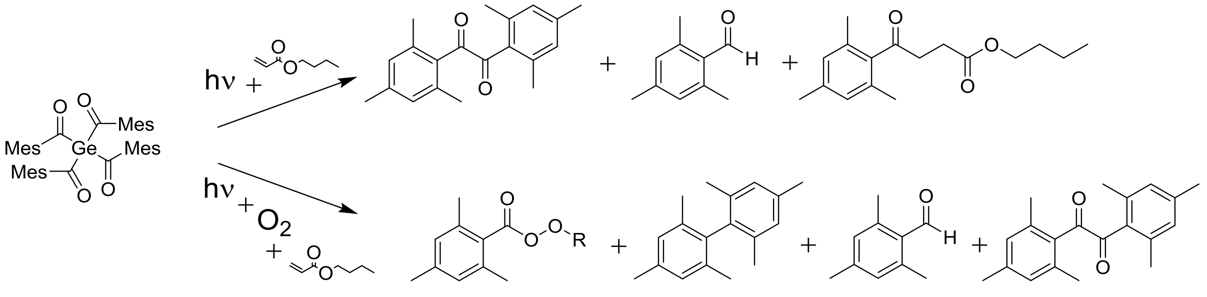

Scheme 52. Reaction products of $GeAc_4$ and butyl acrylate upon irradiation in the absence and presence of oxygen.

$GeAc_4$ shows similar behavior like the α-hydroxy ketone ***A1*** and BAPO. In the absence of oxygen and under atmospheric conditions the mesitoyl radical attacks butyl acrylate and double bond conversion occurs. Increasing the oxygen concentration causes lower signal intensities from ***P"6***, on the other hand the signal intensities for ***P"4*** rise. With $GeAc_4$ and BAPO I detect traces of 2,2',4,4',6,6'-hexamethyl-1,1'-biphenyl ***P"3***.

6.1.5 Laser Flash Photolysis

The results of the NMR experiments confirmed the addition of mesitoyl radicals ***R"1*** to butyl acrylate. However, these experiments showed no hints for the addition of germyl radicals ***R"2*** to the monomer. Laser flash photolysis experiments helped to obtain the desired information.[130]

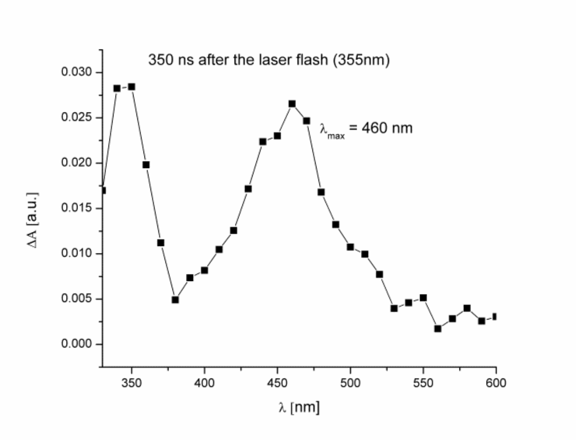

Figure 68. Transient absorbance spectrum of *R"2* obtained through excitation with a 355 nm laser pulse

The transient absorbance spectrum of the germyl radical ***R"2*** reveals a λ_{max} of 460 nm. The excitation was obtained by a 355 nm laser pulse.

Figure 69 shows the time dependence of the transient absorbance in presence and absence of monomer. When no monomer is present the decay is slower compared to the sample where monomer is present. The monomer is used as a quencher and pseudo first order reaction kinetics can be derived.

The decays are fitted to obtain the exponential coefficients k_{exp}. With those it is possible to obtain the Stern-Volmer plot displayed in **Figure 70**. The addition rate constant of ***R"2*** to butyl acrylate is k_{butyl}= 1.75 x 10^7 M^{-1} s^{-1}.

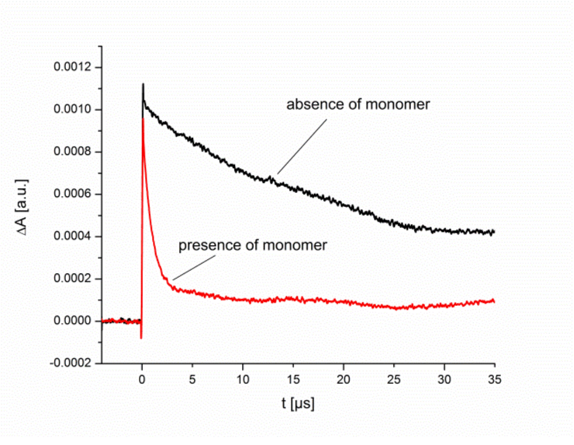

Figure 69. Comparison of the transient state quenching in presence and absence of monomer

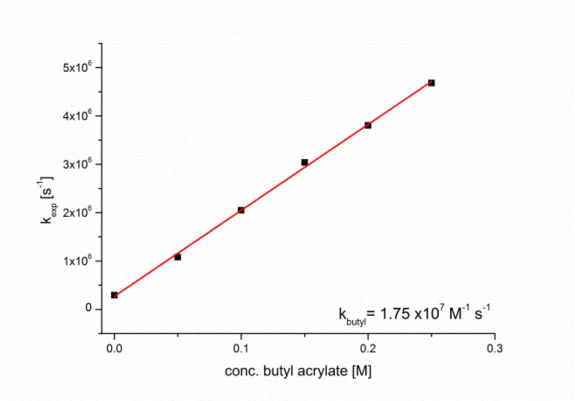

Figure 70. Stern-Volmer plot to obtain the addition rate constant of *R"2* to butyl acrylate

6.1.6 UV-Vis

$GeAc_4$ has in acetonitrile a broad absorption band from approximately 350 to 440 nm with a maximum at 375.5 nm.

The compound has four mesitoyl groups attached to the germanium and as I showed already irradiation leads to mesitoyl ***R"1*** and germyl ***R"2*** radicals. In principle it should be possible to cleave all four mesitoyl groups. Cleaving one group should cause a change in the absorption spectrum. Based on this a wavelength selective cleavage might be achievable, which was tested by irradiating $GeAc_4$ with different wavelengths and recording time resolved UV-Vis spectra. I started with 450 nm but this energy is not sufficient to excite the sample. Wavelengths lower than 435 nm are required. The results of irradiating the sample with 435 and 420 nm are similar. In both cases $GeAc_4$ is decomposed and the absorption bands disappear, which is displayed in **Figure 72**.

The plot of the absorbance versus the irradiation time visualizes an exponential decay.

The addition of methyl methacrylate causes an enhanced decay of the absorption band.

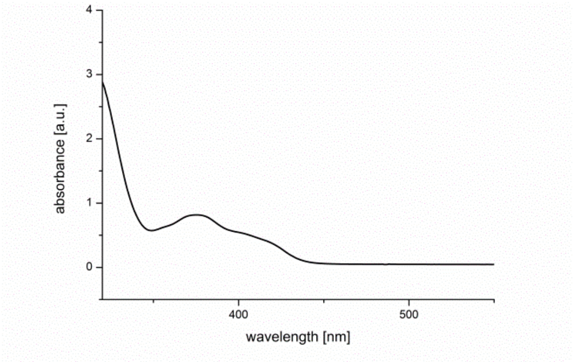

Figure 71. UV-Vis spectrum of $GeAc_4$ in acetonitrile

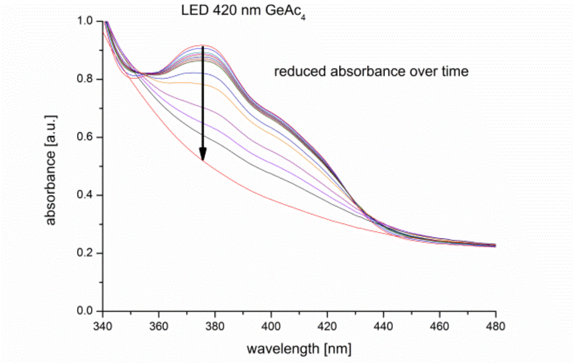

Figure 72. Time dependent absorption spectra of $GeAc_4$ in acetonitrile

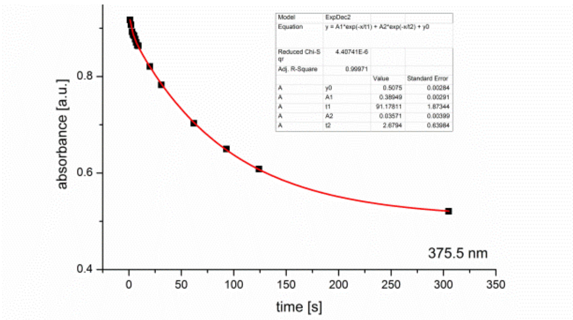

Model	ExpDec2		
Equation	y = A1*exp(-x/t1) + A2*exp(-x/t2) + y0		
Reduced Chi-Sqr	4.40741E-6		
Adj. R-Square	0.99971		
		Value	Standard Error
A	y0	0.5075	0.00284
A	A1	0.38949	0.00291
A	t1	91.17811	1.87344
A	A2	0.03571	0.00399
A	t2	2.6794	0.63984

Figure 73. Time dependent absorption decay upon irradiation of $GeAc_4$.

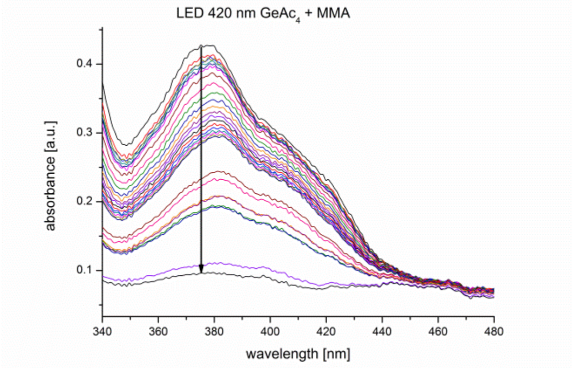

Figure 74. Time dependent absorption spectra of $GeAc_4$ and MMA in acetonitrile.

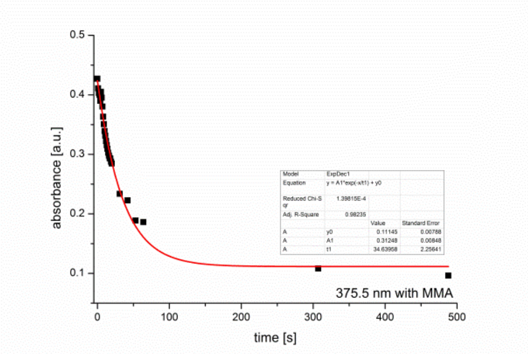

Model	ExpDec1		
Equation	y = A1*exp(-x/t1) + y0		
Reduced Chi-Sqr	1.39815E-4		
Adj. R-Square	0.98235		
		Value	Standard Error
A	y0	0.11145	0.00788
A	A1	0.31248	0.00848
A	t1	34.63958	2.25641

Figure 75. Time dependent absorption decay upon irradiation of $GeAc_4$ in the presence of MMA.

6.1.7 Polymerization Experiments

I produced polymer pellets using $GeAc_4$ as photoinitiator and compared it with the similar and published initiator K-42. Details for the production of the tablet shaped polymers are given in the experimental section. These results discuss the curing ability of $GeAc_4$ for different monomer formulations. The standard monomer of choice was butyl acrylate, as NMR and LFP experiments showed the possible curing ability of $GeAc_4$. It was possible to follow double bond conversion by NMR techniques and to determine the addition rate constant of the germyl radical ***R"2*** to the acrylate.

Here I performed polymerization experiments with methyl methacrylate, styrene, triethylene glycol dimethacrylat (TEGDMA), diurethane dimethacrylat (UDMA), a mixture of TEGDMA and UDMA in the ratio 1:4 wt. as well as mixtures of TEGDMA with methyl methacrylate, butyl acrylate and styrene in a 1:1 wt. ratio. The mixture TEGDMA and UDMA is used in the same ratio by Ivoclar Vivadent AG for their dental application.[140]

$GeAc_4$ is insufficiently soluble in the monomers itself, but to obtain a defined initiator concentration, it was dissolved first in toluene. This set of experiments used initiator concentrations of 0.1 0.5 1 and 2 wt. %.

I irradiated the monomer mixtures for defined amounts of time and checked the curing process by sticking the probe with a spatula. The Bluephase™ dental lamp from Ivoclar Vivadent AG initiated the curing process. The lamp was arranged in a distance of 1.5 cm, which allowed irradiating the whole surface of the formulation. These specifications result in 650 W cm^{-2} for the low power mode and 1200 W cm^{-2} for the high power option.

6.1.7.1 Styrene

Styrene samples contained 1 wt. % initiator dissolved directly in the monomer and the irradiation was started in 10 s steps at the low power mode. After 10 respectively 20 s no change of the samples or polymerization was observed. To check the ability of the initiators to cure styrene, both samples were irradiated for 3 min, with the lamp in the high power mode. It was not possible to obtain cured pellets. After irradiation the sample containing $GeAc_4$ bleached almost completely and became colorless. The mixture containing K-42 also bleached but the yellow color was still clearly visible.

6.1.7.2 Methyl methacrylate

These samples required the initiator to be previously dissolved in toluene. Initiator concentration was 1 wt. % and the curing settings were the same as for the styrene samples. Again it was not possible to observe sufficient curing. I increased the irradiation time to 3 min and the intensity by using the high power mode. Also with these settings polymerization was not observed. 2 hours after the irradiation both samples became sticky. It is likely that parts of the monomer polymerized and formed longer chains and that the free monomer evaporated through its high volatility. The sufficient curing of methyl methacrylate was also not possible.

6.1.7.3 Butyl acrylate

The same preparation and sample treatment as with methyl methacrylate was applied. 20 s after irradiation in the low power mode smoke appeared. Within this time the monomer cured and the sample heated up. The huge heat development caused smoke. 15 to 20 s after the irradiation started small bubbles within the pellets were observed. The increased temperature changes the solubility of gases in liquids and the bubbles were the result of released dissolved gas. The cured monomers remain sticky and oily on the surface, but they form transparent pellets. Both initiators led to the same results; they are able to cure butyl acrylate within a short amount of time (20 s).

6.1.7.4 TEGDMA

Dental filling compositions contain TEGDMA (triethylene glycol dimethacrylat) as a curable monomer.[141] Ivoclar Vivadent AG i.e. described test compositions containing TEGDMA as monomer and K-42 as initiator. They used different initiator concentrations starting with 0.1 wt. % as the lowest.[140] I performed the first test polymerization with a photoinitiator concentration of 1 wt. %. To obtain this concentration the initiator was dissolved before in toluene. The dental lamp irradiated the samples in the low power mode for 20 s. After 10 s the samples were already cured and smoke was detected. As the samples were already cured I stopped the irradiation after 20 s. It was not possible to observe a difference in the curing abilities between K-42 and $GeAc_4$.

As 1 wt. % of initiator was more than efficient to cure the monomer, I reduced the amount to 0.1 wt. %. Again the samples were irradiated in the low power mode for total 40 s. 10 s after the irradiation started the sample containing $GeAc_4$ had the consistency of a soft gel with a skin on top. 5 s later it became jelly like and more rigid. Another 5 s later the sample is on top rigid, while the bottom is still a bit softer, from this point on the temperature increased significantly. 5 s after this the polymer pellet is fully cured and hot. 5 and 10 s of additional irradiation did not change the properties of the pellet.

The sample containing 0.1 wt. % of K-42 as initiator behaved similarly. 10s after the irradiation started the observed structure was jelly like. 5 s later the sample became rigid on top but was still soft on the bottom. 5s after this the pellet was rigid and hot. After 10 and 20 s of additional irradiation no further changes were observed.

I performed these experiments also in the high power mode of the UV lamp. The sample containing 0.1 wt. % of $GeAc_4$ was jelly like after 10 s of irradiation. 5 s later it became rigid with smeary edges. 5 s later it was fully cured and hot. Longer irradiation times did not change the properties of the test pellets.

The sample containing 0.1 wt. % K-42, which was irradiated in the high power mode, was 10 s after irradiation start also jelly like. 5 s later it was rigid and had smeary edges. After additional 5 s it was fully cured, rigid and hot.

These results show that $GeAc_4$ and K-42 have comparable polymerization abilities for TEGDMA. In the high power mode both initiators behave the same, but in the low power mode it is possible to observe slight differences. K-42 reacts slightly faster with TEGDMA. The sample containing K-42 is completely cured after 20s, while it takes 25 s for the sample containing $GeAc_4$. In the low power mode maybe only one mesitoyl group cleaves. This would lead in case of $GeAc_4$ to the bulky and sterically hindered germyl radical ***R”2***. The K-42 derived germyl radical is not as bulky as ***R”2*** and therefore more likely to add to the monomer. When the light intensity increases more cleavages are possible and $GeAc_4$ can in principle form more radicals than K-42.

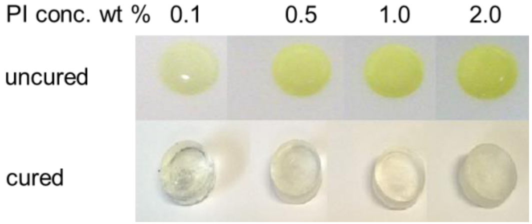

Figure 76. Example of observed photobleaching, for $GeAc_4$ curing TEGDMA. The pictures in the upper trace show the liquid monomer with the photoinitiator before irradiation at various initiator concentrations. The lower trace displays the cured TEGDMA pellets. The samples become almost colorless and transparent; only the sample with 2 wt. % initiator shows slight yellow coloring.

6.1.7.5 UDMA

UDMA (diurethane dimethacrylat) is another compound used in dental fillings and I tested it with our initiators using a concentration of 0.1 wt. %. Irradiation was done in the low power mode with the dental lamp. 10s after irradiation start the sample containing $GeAc_4$ was jelly like rigid. 10s later it was completely cured hot and smoke appeared.

The probe with K-42 behaved in the same way. 10 s after irradiation start the sample was jelly like rigid and another 10 s later it was completely rigid and smoke developed.

UDMA showed no differences of the two initiators polymerization abilities.

6.1.7.6 Mixtures with TEGDMA

As the polymerization experiments with TEGDMA were very efficient I tested mixtures of it with other monomers. The initiator concentration of K-42 and $GeAc_4$ for these experiments was always 0.1 wt. %

It was not possible to cure the 1:1 mixture of TEGDMA and styrene, neither with K-42 nor with $GeAc_4$ as initiator.

The curing of 1:1 mixtures of TEGDMA and methyl methacrylate were sufficient and both initiators behaved similar. In contrast to pure TEGDMA the required irradiation time was much longer. The samples were irradiated for 160 s in the high power mode. After this time pellets cured completely. The pellets were brittle and could be crushed with a spatula.

TEGDMA 1:1 mixed with butyl acrylate behaves similar compared to the formulation containing methyl methacrylate. 140 s of irradiation in the high power mode were required to obtain a pellet. The pellet was first like rigid jelly and after a few minutes it became brittle. These brittle pellets were easily crumbled with a spatula.

The mixture of TEGDMA and UDMA in the wt. ratio 1:4 was a huge contrast to the mixtures containing acrylates. For curing the low power mode of the lamp is sufficient and also the required time is significantly lower. The TEGDMA UDMA mixtures were completely cured after 10s of irradiation. It was not possible to observe a difference in the polymerization behavior of the two initiators. I was even able to cure these mixtures with a standard visible light LED used for bike lighting.

6.2 Discussion

$GeAc_4$ is a new compound and I tested its photoinitiating abilities. Time resolved EPR experiments proved the formation of two different radicals (a germanium centered radical ***R”2*** and a mesitoyl radical ***R”1***). This is in accordance with previous studies for the similar bisacyl-germanes.[142]

My continuing studies focused on NMR techniques, to observe follow-up products and to study the impact of oxygen on $GeAc_4$ based radicals. It was possible to detect ***R”1*** based products. Through the influence of germanium on the proton shifts and few existing references, the structure elucidation of germanium based follow-up products was not feasible. ^{1}H- and ^{13}C-NMR experiments provided hints for the formation of Ge-Ge bonds. There are also indications that germanium particles are formed, as sediments in concentrated and oxygen-free samples occur.

After irradiation the NMR proton signal intensities of $GeAc_4$ decrease stronger than those of the α-hydroxy ketone ***A1*** and BAPO. For $GeAc_4$ 32 1 µs laser pulses were sufficient to observe sample degradation and to determine follow-up products. Longer irradiation times led to overlapping signals. For BAPO and the ***A1*** irradiation times around 3 minutes were ideal.

The CIDNP studies support radical mechanisms. Polarized signals of the parent compound, which indicates the cage reaction, appear. Further these experiments reveal products like dimesitoyl ***P”1*** in the absence and peroxide ***P”4*** in the presence of oxygen.

The cage reaction is, similar to BAPO and ***A1***, more pronounced in the absence of oxygen. When oxygen is present the intensities of additional follow-up products increase. Mesitoyl peroxides (i.e. ***P”4***) are the main species. It was not feasible to assign further germanium based products.

NMR experiments indicate the addition of ***R”1*** to butyl acrylate. The signals for this step are more pronounced in the absence of oxygen. Samples prepared under atmospheric condition showed double bond conversion too but the spectra from oxygen-saturated samples showed no indications for monomer addition. The NMR results confirm the formation of ***P”6*** through the addition of ***R”1*** to butyl acrylate. Comparable to BAPO 2,4,6-trimethylbenzaldehyde ***P”5*** is only formed in the presence of a monomer with abstractable hydrogen-atoms.

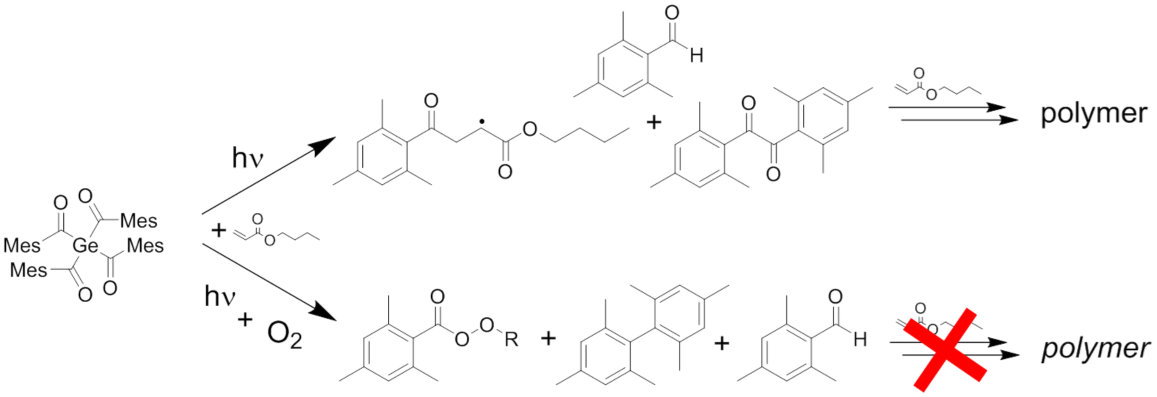

Scheme 53. With NMR techniques observed intermediates and products, through the reaction of GeAc$_4$ with butyl acrylate in the presence and absence of oxygen detected. In the absence of oxygen *R"1* adds to the monomer and induces a radical chain reaction. The aldehyde *P"5* is formed in the absence and presence of oxygen through hydrogen-atom abstraction. *P"4* is the main and *P"3* is an additional product in the presence of oxygen. Oxygen-saturated samples show no signs for polymerization.

The addition of ***R"2*** to butyl acrylate happens, as I know from LFP experiments, but with NMR it is possible to confirm it. Laser flash photolysis experiments proved the first addition of ***R"2*** to the monomer and the addition rate constant $k_{butyl}= 1.75 \times 10^{7}\ M^{-1}\ s^{-1}$ was determined. The addition rate constant of the bisacylgermane K-42 derived germyl radical is $k_{butyl}= 1.2 \times 10^{8}\ M^{-1}\ s^{-1}$. This is approximately one order of magnitude higher, but it is essential to take sterical effects in account. As mentioned before the germanium center of ***R"2*** is sterically shielded. The monomer needs to have a certain orientation to react with the radical. Therefore the first addition should be slower. Also solvent effects need to be taken into account. I used toluene, while the addition rate of K-42 was determined in acetonitrile.

Through sterical hindrance the first addition of ***R"2*** to butyl acrylate is slower than the first addition of the K-42 derived germyl radical. Upon further cleavages of mesitoyl groups the sterical hindrance should decrease and the addition rate of the new GeAc$_4$ derived germyl radicals to the monomer should increase.

There are several hints for the cleavage of further mesitoyl groups from GeAc$_4$. When no monomer is present, Ge-Ge bonds are probable to be formed and upon long irradiation a precipitation, which most likely consists out of germanium derived particles, occurs. These particles can be formed only if the mesitoyl groups split off. Further the UV-Vis spectra are important. Mono-, bis-, tris-, and tetraacylgermanes have similar UV-Vis absorption properties. They have an absorption maximum around 375 nm. Upon irradiation of GeAc$_4$ the absorption bands decay and no substantial batho- or hypsochromic shift is observed.

It is possible to follow the decay of the absorption maximum in the absence and in the presence of monomer. In the absence of monomer ***P"1*** and Ge-Ge bonds are formed. In the presence of monomer, polymerization starts through the addition of ***R"1*** and ***R"2*** to butyl acrylate.

$GeAc_4$ is able to split off up to 4 mesitoyl groups and therefore leading step by step to 4 germyl radicals. In total up to 8 different radicals can be formed, which indicates a high polymerization potential.

I brought this theoretical idea to a practical approach and tested the polymerization abilities of $GeAc_4$ by curing different monomer formulations and compared the results with the bisacylgermane K-42.

Both of them behave very similar. It was possible to polymerize butyl acrylate, TEGDMA, UDMA and mixtures of them with both initiators. K-42 seems to polymerize butyl acrylate slightly faster, but the polymerization times for the other monomers are the same. Both initiators are not able to cure methyl methacrylate, and styrene.

An outstanding result is that $GeAc_4$ is a new and promising photoinitiator. It has comparable abilities to commercially available initiators. First tests showed that $GeAc_4$ cures monomers, which are of interest in dental applications.[140,141] Polymerization under atmospheric conditions is possible. The main effects from oxygen are observed in oxygen-saturated samples. For practical applications the impact of oxygen seems neglect able.

In principle $GeAc_4$ and its derivatives could be potential initiators for star shaped polymers, but wavelength selective cleavage of the mesitoyl groups did not work in these first experiments and more work needs to be done. By substitutions on the acyl groups wavelength selective cleavage could be achieved. An additional approach would be dose dependent polymerization, where defined light intensities are applied. The following scheme visualizes a germanium centered star shaped polymer with 4 different monomers.

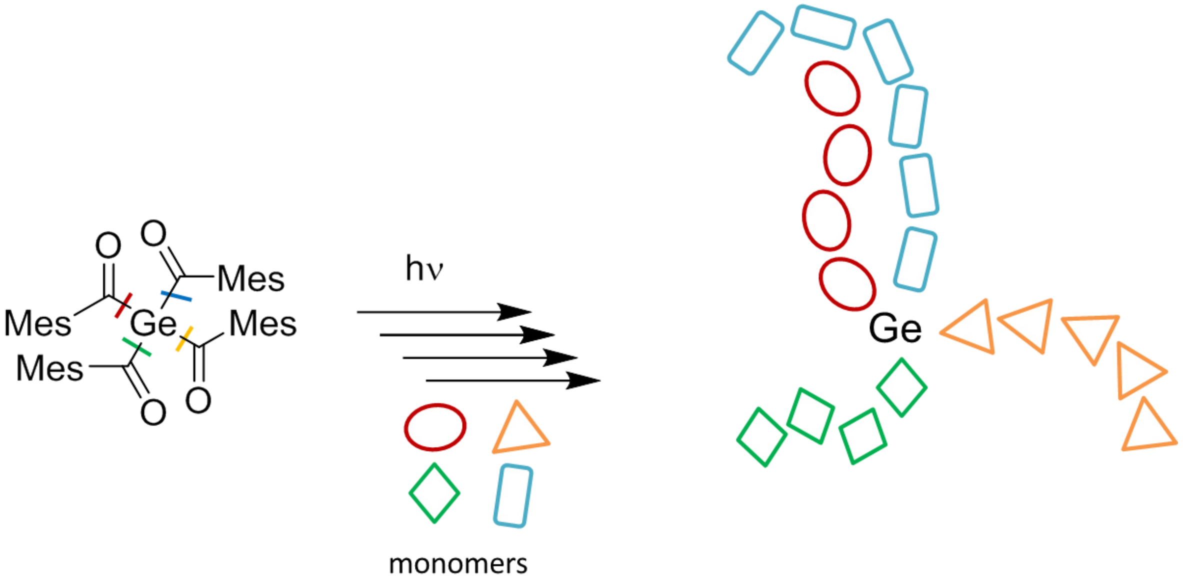

Scheme 54. Schematic approach to obtain star shaped tetra block copolymers. Either wavelength selective or dose dependent initiation.

7 Conclusions

This study shows that tetramesiotylgermane $GeAc_4$ is photo active and can be used as a photo initiator. Through its mesitoyl groups, it shows similar reaction patterns like BAPO. The addition rate constant of the formed germyl radical ***R"2*** towards butyl acrylate were determined and various monomer formulations were cured. The characterization shows that tetraacylgermanes are excellent photoinitiators.

The main work focused on oxygen inhibition and all three studied initiators showed similar oxygen concertation dependent behavior. It was possible to follow the oxygen addition to the radicals and to determine follow-up products. In case of the α-hydroxy ketone ***A1*** the decarboxylation increased in the presence of oxygen and therefore the formation of 2-phenylpropan-2-ol ***P9*** rose. Interestingly the decarboxylation process of BAPO is more efficient in the absence of oxygen. I can explain this effect by two different mechanisms. ***A1*** decarboxylizes mainly via a peroxide intermediate, while BAPO's phosphorus can be reduced and then the resulting product decarboxylizes.

Concerning photo-induced radical polymerization it was possible to follow double bond conversion in the presence of oxygen. Only the oxygen-saturated systems did not show any evidence for sufficient double bond conversion. Experiments with ***A1*** even revealed minor peroxyl radical addition to the monomer.

It was possible to measure the oxygen consumption upon irradiation. BAPO experiments showed linear dependent oxygen consumption.

Determination of follow-up products and intermediates is supported by ESI-MS experiments and by radical trapping.

Oxygen addition rate constants were obtained for BAPO's ***R'2*** and addition rate constants towards butyl acrylate were determined for ***R'2*** and $GeAc_4$'s ***R"2***. These results correspond with published data and based on them I performed kinetic simulations on the suggested reaction mechanisms. The simulations support the suggestions for the formation of follow-up products. Polymerization experiments indicate lower polymer concentrations in the presence of oxygen, this fits to the simulations, where fewer polymers are formed in an increased time span.

Additionally it was possible to study thermal effects and differentiate between bulk effects, thermal diffusion and oxygen inhibition.

8 List of Publications

Publications in scientific journals

Geier, R.; Wappl, C.; Freiszmuth, H.; Slugovc, C.; Gescheidt, G. *Polym. Chem.* **2015**, *6* (13), 2488.

Schweinfurth, D.; Mazzolini, M.; Neshchadin, D.; Hoyer, C.; Geier, R.; Gatterer, K.; Trapp, N.; Gescheidt, G.; Diederich, F. *Chem. - A Eur. J.* **2016**, *22* (21), 7152.

Presentations at scientific conferences

Geier, R.; Neshchadin, D.; Gescheidt, G. In *Photopolymerization Fundamentals 2015*; Boulder, CO, **2015**.

Wappl, C.; Geier, R.; Freiszmuth, H.; Slugovc, C.; Gescheidt, G. *Abstracts of Papers, 249th ACS National Meeting & Exposition*; Denver CO, **2015**; p Poly – 30.

Geier, R.; Neshchadin, D.; Gescheidt, G. In *XXVI International EPR Seminar 2015*; Graz Austria, **2015.**

Geier, R.; Neshchadin, D.; Gescheidt, G. In *4. GÖCH-Symposium 2014 “Physikalische Chemie in Österreich”;* Leoben Austria, **2014**.

9 List of Figures

10 List of Schemes

11 List of Tables

12 References

(1) Turro, N. J.; Ramamurthy, V.; Scaiano, J. C. *Modern Molecular Photochemistry of Organic Molecules*; University Science Books, **2010**.

(2) Pape, M. *Pure Appl. Chem.* **1975**, *41* (4), 535.

(3) Cambié, D.; Bottecchia, C.; Straathof, N. J. W.; Hessel, V.; Noël, T.; Cambie, D.; Bottecchia, C.; Straathof, N. J. W.; Hessel, V.; Noe, T. *Chem. Rev.* **2016**, *116* (17), 10276.

(4) *Encyclopedia of Radicals in Chemistry, Biology and Materials*, Vol. 4.; Chatgilialoglu, C., Studer, A., Eds.; John Wiley & Sons: New York, **2012**.

(5) Fouassier, J.-P. *Photoinitiation, Photopolymerization, and Photocuring: Fundamentals and Applications*; Hanser Gardner Publications: Munich-Vienna New York, **1995**.

(6) Fouassier, J. P.; Allonas, X.; Laleve, J.; Dietlin, C. In *Photochemistry and Photophysics of Polymer Materials*; John Wiley & Sons: Hoboken, NJ, USA, **2010**; pp 351–419.

(7) Yagci, Y.; Jockusch, S.; Turro, N. J. *Macromolecules* **2010**, *43* (15), 6245.

(8) Geier, R.; Wappl, C.; Freiszmuth, H.; Slugovc, C.; Gescheidt, G. *Polym. Chem.* **2015**, *6* (13), 2488.

(9) Dietliker, K. *A compilation of photoinitiators commercially available for UV today*; SITA Technology Limited: Edinburgh: London, **2002**.

(10) Green, A. W. *Industrial Photoinitiators: A Technical Guide*; CRC: London, **2010**.

(11) Cai, X.; Sakamoto, M.; Yamaji, M.; Fujitsuka, M.; Majima, T. *J. Phys. Chem. A* **2005**, *109* (27), 5989.

(12) Yamaji, M.; Suzuki, A.; Ito, F.; Tero-Kubota, S.; Tobita, S.; Marciniak, B. *J. Photochem. Photobiol. A Chem.* **2005**, *170* (3), 253.

(13) Cohen, S. G.; Parola, A.; Parsons, G. H. *Chem. Rev.* **1973**, *73* (2), 141.

(14) Lalevee, J.; Fouassier, J. P. *Encycl. Radicals Chem., Biol. Mater.*; John Wiley & Sons: New York, **2012**.

(15) Allen, N. S.; Lam, E.; Kotecha, J. L.; Green, W. A.; Timms, A.; Navaratnam, S.; Parsons, B. J. *J. Photochem. Photobiol. A Chem.* **1990**, *54* (3), 367.

(16) Shanks, R. A.; Clarke, S. R. *Polym. Photochem.* **1984**, *4* (6), 451.

(17) Peters, K. S.; Kim, G. *J. Phys. Chem. A* **2004**, *108* (14), 2598.

(18) Moad, G.; Solomon, D. H. *The Chemistry of Radical Polymerization*, 2nd ed.; Elsevier, **2006**.

(19) Griesser, M.; Neshchadin, D.; Dietliker, K.; Moszner, N.; Liska, R.; Gescheidt, G. *Angew.*

Chemie Int. Ed. **2009**, *48* (49), 9359.

(20) Benkhoff, J.; Dietliker, K.; Powell, K.; Jung, T.; Studer, K.; Sitzmann, E. V. *JCT coatingsTech (Blue Bell, Pa.)* **2007**, *4* (4), 40.

(21) Briguglio, J. J.; Keil, C. R.; Tara, V. M.; Reardon, E. J., Jr.; Kautz, R. W. Polymers and Use in Photoimageable Compositions. US 5609991, **1997**.

(22) Hoyle, C. E.; Bowman, C. N. *Angew. Chemie Int. Ed.* **2010**, *49* (9), 1540.

(23) Crivello, J. V.; Ma, J.; Jiang, F.; Hua, H.; Ahn, J.; Acosta Ortiz, R. *Macromol. Symp.* **2004**, *215* (1), 165.

(24) Campo, A. del; Greiner, C. *J. Micromechanics Microengineering* **2007**, *17* (6), R81.

(25) Liu, J.; Cai, B.; Zhu, J.; Ding, G.; Zhao, X.; Yang, C.; Chen, D. *Microsyst. Technol.* **2004**, *10* (4), 265.

(26) Madou, M. J. *Fundamentals of Microfabrication: The Science of Miniaturization, Second Edition*; CRC, **2002**.

(27) Odian, G. *Principle of Polymerization*; John Wiley & Sons, **1991**.

(28) Rabek, J. F. *Experimental and analytical methods for the investigation of radiation curing. In Radiation Curing in Polymer Science and Technology*, 1st ed.; Fouassier, J. P., Rabek, J. F., Ed.; Elsevier: London, **1993**.

(29) Ligon, S. C.; Husár, B.; Wutzel, H.; Holman, R.; Liska, R. *Chem. Rev.* **2014**, *114* (1), 557.

(30) Husár, B.; Ligon, S. C.; Wutzel, H.; Hoffmann, H.; Liska, R. *Prog. Org. Coatings* **2014**, *77* (11), 1789.

(31) McKean, D. R.; Schaedeli, U.; MacDonald, S. A. *J. Polym. Sci. Part A Polym. Chem.* **1989**, *27* (12), 3927.

(32) Puiu, M.; Istrate, O.; Rotariu, L.; Bala, C. *Anal. Biochem.* **2012**, *421* (2), 587.

(33) Decker, C. *Macromol. Rapid Commun.* **2002**, *23* (18), 1067.

(34) Da Silva, J. P.; Jockusch, S.; Turro, N. J. *Photochem. Photobiol. Sci.* **2009**, *8* (2), 210.

(35) Jockusch, S.; Turro, N. J. *J. Am. Chem. Soc.* **1998**, *120* (45), 11773.

(36) Dietliker, K. *Chemistry and Technology of UV and EB Formulation for Coatings, Inks & Paints, Volume 3: Photoinitiators for Free Radical and Cationic Polymerisation*; SITA Technology Ltd.: London, **1991**.

(37) Scherzer, T. *J. Polym. Sci. Part A Polym. Chem.* **2004**, *42* (4), 894.

(38) Decker, C.; Jenkins, A. D. *Macromolecules* **1985**, *18* (6), 1241.

(39) Lalevée, J.; Allonas, X.; Fouassier, J. P. *Chem. Phys. Lett.* **2005**, *415* (4–6), 287.

(40) Cook, W. D. *J. Polym. Sci. Part A Polym. Chem.* **1993**, *31* (4), 1053.

(41) Lovell, L. G.; Lu, H.; Elliott, J. E.; Stansbury, J. W.; Bowman, C. N. *Dent. Mater.* **2001**, *17* (6), 504.

(42) Andrzejewska, E.; Andrzejewski, M. *J. Polym. Sci. Part A Polym. Chem.* **1998**, *36* (4), 665.

(43) Russell, G. A. *J. Am. Chem. Soc.* **1957**, *79* (14), 3871.

(44) O'Brien, A. K.; Bowman, C. N. *Macromolecules* **2006**, *39* (7), 2501.

(45) Scott, T. F.; Cook, W. D.; Forsythe, J. S.; Bowman, C. N.; Berchtold, K. A. *Macromolecules* **2003**, *36* (16), 6066.

(46) Goodner, M. D.; Bowman, C. N. *Chem. Eng. Sci.* **2002**, *57* (5), 887.

(47) Gou, L.; Opheim, B.; Scranton, A. B. *Methods to overcome oxygen inhibition in free radical photopolymerizations. In Photo- chemistry and UV Curing: New Trends*; Fouassier, J. P., Ed.; Research Signpost: Trivandrum: India, **2006**.

(48) Hou, H.; Gan, Y.; Yin, J.; Jiang, X. *Adv. Mater. Interfaces* **2014**, *1* (9), 1400385.

(49) Taki, K.; Watanabe, Y.; Ito, H.; Ohshima, M. *Macromolecules* **2014**, *47* (6), 1906.

(50) Corcione, C. E.; Striani, R.; Frigione, M. *Thermochim. Acta* **2014**, *576* (1), 47.

(51) Structure, P. R.; Sluggett, G. W.; Mcgarry, P. F.; Koptyug, I. V; Turro, N. J. **1996**, *7863* (96), 7367.

(52) Colley, C. S.; Grills, D. C.; Besley, N. A.; Jockusch, S.; Matousek, P.; Parker, A. W.; Towrie, M.; Turro, N. J.; Gill, P. M. W.; George, M. W. *J. Am. Chem. Soc.* **2002**, *124* (50), 14952.

(53) Weber, M.; Turro, N. J. *J. Phys. Chem. A* **2003**, *107* (18), 3326.

(54) Karatekin, E.; O'Shaughnessy, B.; Turro, N. J. *Macromolecules* **1998**, *31* (22), 7992.

(55) Moscatelli, A.; Chen, T. K.; Jockusch, S.; Forbes, M. D. E.; Turro, N. J.; Ottaviani, M. F. *J. Phys. Chem. B* **2006**, *110* (14), 7574.

(56) Hristova-Neeley, D.; Neshchadin, D.; Gescheidt, G. *J. Phys. Chem. B* **2015**, *119* (43), 13883.

(57) Sivaguru, J.; Solomon, M. R.; Poon, T.; Jockusch, S.; Bosio, S. G.; Adam, W.; Turro, N. J. *Acc. Chem. Res.* **2008**, *41* (3), 387.

(58) Cerkovnik, J.; Plesničar, B.; Koller, J.; Tuttle, T. *J. Org. Chem.* **2009**, *74* (1), 96.

(59) Harding, L. B.; Goddard, W. A. *J. Am. Chem. Soc.* **1980**, *102* (2), 439.

(60) Andrzejewska, E.; Bogacki, M. B.; Andrzejewski, M.; Janaszczyk, M. *Phys. Chem. Chem. Phys.* **2003**, *5* (12), 2635.

(61) Kurochkin, S. A.; Silant'ev, M. A.; Perepelitsyna, E. O.; Grachev, V. P. *Polymer (Guildf).* **2013**, *54* (1), 31.

(62) Tanaka, S.; Kon, Y.; Uesaka, Y.; Morioka, R.; Tamura, M.; Sato, K. *Chem. Lett.* **2016**, *45* (2), 188.

(63) Ward, H. R.; Lawler, R. G. *J. Am. Chem. Soc.* **1967**, *89*, 5518.

(64) Bargon, J.; Fischer, H.; Johnsen, U. *Zeitschrift für Naturforsch. A* **1967**, *22* (10), 1551.

(65) Goez, M. *Concepts Magn. Reson.* **1995**, *7* (1), 69.

(66) Pine, S. H. *J. Chem. Educ.* **1972**, *49* (10), 664.

(67) Kaptein, R. *J. Chem. Soc. D Chem. Commun.* **1971**, *1* (14), 732.

(68) Kaptein, R.; Oosterhoff, L. J. *Chem. Phys. Lett.* **1969**, *4* (1), 195.

(69) Kaptein, R.; Oosterhoff, L. J. *Chem. Phys. Lett.* **1969**, *4* (1), 214.

(70) Lawler, R. G. *Acc. Chem. Res.* **1972**, *5* (1), 25.

(71) Goez, M. Neckers, D. C., Volman, D. H., von Bünau, G., Eds.; John Wiley & Sons, **1997**; Vol. 23, pp 63–163.

(72) Kaptein, R. *Adv. Free. Chem.* **1975**, *5* (1), 319.

(73) Lepley, A. R.; Closs, G. L. *Chemically Induced Magnetic Polarization*; John Wiley & Sons: New York, **1973**.

(74) Pedersen, J. B. *Theories of Chemically Induced Magnetic Polarization*; Odense University, **1979**.

(75) Roth, H. D. In *Encyclopedia of Magnetic Resonance*; John Wiley & Sons: Chichester, UK, **2011**.

(76) Muus, L. T.; Atkins, P. W.; McLauchlan, K. A.; Pederson, J. B. *Chemically Induced Magnetic Polarization*; Reidel Publication Company: Dordrecht, **1977**.

(77) Neshchadin, D. Quantitative Application of ^{1}H and ^{31}P Chemically Induced Nuclear Polarization, PhD Thesis, Basel, **2003**.

(78) Goez, M. In *Annu. Rep. NMR Spectrosc.*; Elsevier, **2009**; Vol. 66, pp 77–147.

(79) Höfer, P. *Electron Paramagnetic Resonance*; Brustolon, M., Giamello, E., Eds.; John Wiley & Sons: Hoboken, NJ, USA, **2009**.

(80) Rutsch, W.; Dietliker, K.; Leppard, D.; Köhler, M.; Misev, L.; Kolczak, U.; Rist, G. *Prog. Org. Coatings* **1996**, *27* (1–4), 227.

(81) Dietliker, K.; Broillet, S.; Hellrung, B.; Rzadek, P.; Rist, G.; Wirz, J.; Neshchadin, D.; Gescheidt, G. *Helv. Chim. Acta* **2006**, *89* (10), 2211.

(82) Dietliker, K.; Jung, T.; Benkhoff, J.; Kura, H.; Matsumoto, A.; Oka, H.; Hristova, D.; Gescheidt, G.; Rist, G. *Macromol. Symp.* **2004**, *217* (1), 77.

(83) *CRC Handbook of Photochemistry and Photobiology*, 2nd ed.; Horspool, W., Lenci, F., Eds.; London, **2004**.

(84) Wagner, P. J.; Zhang, Y.; Puchalski, A. E. *J. Phys. Chem.* **1993**, *97* (50), 13368.

(85) Neckers, D. C.; Schaap, A. P.; Hardy, J. *J. Am. Chem. Soc.* **1966**, *88* (6), 1265.

(86) Fried, A.; McKeen, S.; Sewell, S.; Harder, J.; Henry, B.; Goldan, P.; Kuster, W.; Williams, E.; Baumann, K.; Shetter, R.; Cantrell, C. *J. Geophys. Res. Atmos.* **1997**, *102* (D5), 6283.

(87) Sankar, M.; Nowicka, E.; Carter, E.; Murphy, D. M.; Knight, D. W.; Bethell, D.; Hutchings, G. J. *Nat. Commun.* **2014**, *5* (2), 3332.

(88) Criqui, A.; Lalevée, J.; Allonas, X.; Fouassier, J.-P. *Macromol. Chem. Phys.* **2008**, *209* (21), 2223.

(89) Cataldo, L.; Dutan, C.; Misra, S. K.; Loss, S.; Grützmacher, H.; Geoffroy, M. *Chem. - A Eur. J.* **2005**, *11* (11), 3463.

(90) Ruzzi, M.; Sartori, E.; Moscatelli, A.; Khudyakov, I. V; Turro, N. J. *J. Phys. Chem. A* **2013**, *117* (25), 5232.

(91) Brunton, G.; Gilbert, B. C.; Mawby, R. J. *J. Chem. Soc. Perkin Trans. 2* **1976**, *1* (6), 650.

(92) Marriott, P. R.; Perkins, M. J.; Griller, D. *Can. J. Chem.* **1980**, *58* (8), 803.

(93) Cosgrove, J. P.; Borish, E. T.; Church, D. F. *Biochem. Biophys. Res. Commun.* **1985**, *132* (1), 390.

(94) Xiang, Z. *J. Mol. Struct.* **2012**, *1029* (1), 15.

(95) Sohn, C. H.; Yin, S.; Peng, I.; Loo, J. A.; Beauchamp, J. L. *Int. J. Mass Spectrom.* **2015**, *390* (1), 49.

(96) Fouassier, J.; Merlin, A. *Can. J. Chem.* **1979**, *57* (21), 2812.

(97) Jockusch, S.; Landis, M. S.; Freiermuth, B.; Turro, N. J. *Macromolecules* **2001**, *34* (6), 1619.

(98) Woodward, J. R.; Sakaguchi, Y. *J. Phys. Chem. A* **2001**, *105* (16), 4010.

(99) Friedline, R. A. The Reaction Kinetics of Neutral Free Radicals and Radical Ions Studied by Laser Flash Photolysis, PhD Thesis, Virginia Polytechnic State University, **2004**.

(100) Walbiner, M.; Wu, J. Q.; Fischer, H. *Helv. Chim. Acta* **1995**, *78* (4), 910.

(101) Sideridou, I. D.; Achilias, D. S.; Karava, O. *Macromolecules* **2006**, *39* (6), 2072.

(102) Jockusch, S.; Turro, N. J. *J. Am. Chem. Soc.* **1999**, *121* (16), 3921.

(103) Zaman, F.; Beezer, A. E.; Mitchell, J. C.; Clarkson, Q.; Elliot, J.; Davis, A. F.; Willson, R. J. *Int. J. Pharm.* **2001**, *227* (1–2), 133.

(104) Ng, S. C.; Chee, K. K. *J. Polym. Sci. Polym. Chem. Ed.* **1982**, *20* (2), 409.

(105) Harman, D. G.; Ramachandran, A.; Gracanin, M.; Blanksby, S. J. *J. Org. Chem.* **2006**, *71* (21), 7996.

(106) Lamrini, R.; Lacan, P.; Francina, A.; Guilluy, R.; Desage, M.; Michon, J.; Becchi, M.; Brazier, J. . *Free Radic. Biol. Med.* **1998**, *24* (2), 280.

(107) Capla, M.; Rado, R.; Borsig, E. *Chem. zveali* **1975**, *29* (1), 92.

(108) Williams, R. M.; Khudyakov, I. V.; Purvis, M. B.; Overton, B. J.; Turro, N. J. *J. Phys. Chem. B* **2000**, *104* (44), 10437.

(109) Tauster, S. J. *Acc. Chem. Res.* **1987**, *20* (11), 389.

(110) Urry, W. H.; Trecker, D. J.; Hartzler, H. D. *J. Org. Chem.* **1964**, *29* (7), 1663.

(111) Wilzbach, K. E.; Kaplan, L. *J. Am. Chem. Soc.* **1965**, *87* (17), 4004.

(112) Melorose, J.; Perroy, R.; Careas, S. In *Climate Change 2013 - The Physical Science Basis*; Intergovernmental Panel on Climate Change, Ed.; Cambridge University, **2015**; Vol. 1, pp 1–30.

(113) Batchelor, S. N.; Fischer, H. *J. Phys. Chem.* **1996**, *100* (23), 9794.

(114) Sander, R. *Atmos. Chem. Phys.* **2015**, *15* (8), 4399.

(115) Achord, J. M.; Hussey, C. L. *Anal. Chem.* **1980**, *52* (3), 601.

(116) Horstmann, S.; Grybat, A.; Kato, R. *J. Chem. Thermodyn.* **2004**, *36* (11), 1015.

(117) Franco, C.; Olmsted III, J. *Talanta* **1990**, *37* (9), 905.

(118) Kolczak, U.; Rist, G.; Dietliker, K.; Wirz, J. *J. Am. Chem. Soc.* **1996**, *118* (27), 6477.

(119) Mackay, D.; Marx, U. F.; Waters, W. A. *J. Chem. Soc.* **1964**, 4793.

(120) Sluggett, G. W.; Turro, C.; George, M. W.; Koptyug, I. V.; Turro, N. J. *J. Am. Chem. Soc.* **1995**, *117* (18), 5148.

(121) Weber, M.; Khudyakov, I. V.; Turro, N. J. *J. Phys. Chem. A* **2002**, *106* (10), 1938.

(122) Khudyakov, I. V.; Arsu, N.; Jockusch, S.; Turro, N. J. *Des. Monomers Polym.* **2003**, *6* (1), 91.

(123) Spichty, M.; Turro, N. J.; Rist, G.; Birbaum, J.; Dietliker, K.; Wolf, J.; Gescheidt, G. *J. Photochem. Photobiol. A Chem.* **2001**, *142* (2–3), 209.

(124) Gatlik, I.; Rzadek, P.; Gescheidt, G.; Rist, G.; Hellrung, B.; Wirz, J.; Dietliker, K.; Hug, G.; Kunz, M.; Wolf, J. *J. Am. Chem. Soc.* **1999**, *121* (36), 8332.

(125) Kolczak, U. CIDNP. NMR and ESR Investigation of New Radical Photoinitiators and New Antioxidants, PhD Thesis, Basel, **1995**.

(126) Li, A.; Tang, S.; Tan, P.; Liu, C.; Liang, B. *J. Chem. Eng. Data* **2007**, *52* (6), 2339.

(127) Battino, R.; Rettich, T. R.; Tominaga, T. *J. Phys. Chem. Ref. Data* **1983**, *12* (2), 163.

(128) Field, L. R.; Wilhelm, E.; Battino, R. *J. Chem. Thermodyn.* **1974**, *6* (3), 237.

(129) Sumiyoshi, T.; Schnabel, W.; Henne, A.; Lechtken, P. *Polymer (Guildf).* **1985**, *26* (1), 141.

(130) *Reactive Intermediate Chemistry*; Moss, R. A., Platz, M. S., Jones, M., Eds.; John Wiley & Sons: Hoboken, NJ, USA, **2003**.

(131) Voll, D.; Neshchadin, D.; Hiltebrandt, K.; Gescheidt, G.; Barner-Kowollik, C. *Macromolecules* **2012**, *45* (15), 5850.

(132) Shanmugam, S.; Xu, J.; Boyer, C. *Macromolecules* **2014**, *47* (15), 4930.

(133) Jockusch, S.; Koptyug, I. V.; McGarry, P. F.; Sluggett, G. W.; Turro, N. J.; Watkins, D. M. *J. Am. Chem. Soc.* **1997**, *119* (47), 11495.

(134) Eibel, A. Toward Enhancing the Scope of Photoinitiating Compounds, Master Thesis, Graz University of Technology, **2016**.

(135) Hristova, D.; Gatlik, I.; Rist, G.; Dietliker, K.; Wolf, J.-P.; Birbaum, J.-L.; Savitsky, A.; Möbius, K.; Gescheidt, G. *Macromolecules* **2005**, *38* (18), 7714.

(136) Hristova, D. Kinetic Studies of Radical Reactions using time-resolved EPR Kinetic Studies of Radical Reactions using time-resolved EPR, PhD Thesis, Basel, ***2005***.

(137) Neshchadin, D.; Rosspeintner, A.; Griesser, M.; Lang, B.; Mosquera-Vazquez, S.; Vauthey, E.; Gorelik, V.; Liska, R.; Hametner, C.; Ganster, B.; Saf, R.; Moszner, N.; Gescheidt, G. *J. Am. Chem. Soc.* **2013**, *135* (46), 17314.

(138) Durmaz, Y. Y.; Kukut, M.; Monszner, N.; Yagci, Y. *Macromolecules* **2009**, *42* (8), 2899.

(139) Takahashi, M.; Ichii, K.; Tokuda, Y.; Uchino, T.; Yoko, T.; Nishii, J.; Fujiwara, T. *J. Appl. Phys.* **2002**, *92* (7), 3442.

(140) Moszner, N.; Zeuner, F.; Lamparth, I.; Fischer, U. K. *Macromol. Mater. Eng.* **2009**, *294* (12), 877.

(141) Van Landuyt, K. L.; Snauwaert, J.; De Munck, J.; Peumans, M.; Yoshida, Y.; Poitevin, A.; Coutinho, E.; Suzuki, K.; Lambrechts, P.; Van Meerbeek, B. *Biomaterials* **2007**, *28* (26), 3757.

(142) El-Roz, M.; Lalevée, J.; Allonas, X.; Fouassier, J. P. *Macromolecules* **2009**, *42* (22), 8725.